Title
Histone variant H2A.Z coordinates the processes of transcription and pre-mRNA splicing.

Author
Neves, Lauren

Publication Date
2018

Peer reviewed|Thesis/dissertation

UNIVERSITY OF CALIFORNIA

Los Angeles

Histone variant H2A.Z coordinates the processes of transcription and pre-mRNA splicing.

A dissertation submitted in partial satisfaction

of the requirements for the degree Doctor of Philosophy

in Molecular Biology

by

Lauren Taylor Neves

2018

ABSTRACT OF THE DISSERTATION

Histone variant H2A.Z coordinates the processes of transcription and pre-mRNA splicing.

by

Lauren Taylor Neves

Doctor of Philosophy in Molecular Biology

University of California, Los Angeles, 2018

Professor Tracy L Johnson, Chair

Because RNA-synthesis and RNA-processing are spatially and temporally coordinated, RNA splicing takes place in the context of chromatin. H2A.Z is a highly conserved histone variant of the canonical histone H2A. In *Saccharomyces cerevisiae*, the SWR-C complex deposits H2A.Z into chromatin near the beginning of protein-coding genes where it helps regulate transcription. In this dissertation we elucidate a role for H2A.Z in coordinating the processes of RNA transcription and pre-mRNA splicing.

H2A.Z is required for optimal splicing of intron-containing genes, particularly under suboptimal splicing conditions. H2A.Z genetically interacts with the, particularly with U2 snRNP complex, and is required for efficient spliceosome rearrangements. Loss of H2A.Z results in defective spliceosome rearrangements, particularly those involving the U2 snRNP. H2A.Z loss impairs transcription elongation, suggesting that spliceosome rearrangements are tied to the role of H2A.Z in elongation. Depletion of disassembly factor Prp43 suppresses H2A.Z-mediated splice defects, indicating that, in the absence of H2A.Z, stalled spliceosomes are disassembled and unspliced RNAs are released. These data demonstrate that H2A.Z is required for efficient

pre-mRNA splicing and indicate a role for H2A.Z in coordinating the kinetics of transcription elongation and splicing.

Chromatin not only affects splicing locally but also globally. We demonstrate that a chromatin remodeler regulates respiration through modulation spliceosome availability. Nutrient-responsive decrease in the Snf2 chromatin remodeler leads to ribosomal protein gene (RPG) down-regulation. Because RPGs are intron-enriched and highly transcribed, this relieves competition for limiting spliceosomes and allows for increased splicing of weaker substrates, such as *PTC7*. The spliced *PTC7* isoform encodes a mitochondrial protein that promotes Coenzyme Q_6 biosynthesis during respiration. These findings establish a role for the SWI/SNF complex in yeast in transition to respiratory metabolism through global regulation of splicing.

Furthermore, we show that disruption of transcription elongation kinetics can effect splicing both locally and globally, resulting in multi-faceted changes in splicing outcomes. While loss of the elongation factor Dst1 exacerbates transcription and splicing defects in cells lacking H2A.Z, it can also improve splicing of many intron-containing genes. In the absence of both Dst1 and H2A.Z, RPGs are down-regulated, allowing for spliceosome redistribution to and increased splicing of weaker substrates.

Additionally, we show that H2A.Z is required for growth in alkaline pH and expression of phosphate-starvation response genes. However, we find that, when H2A.Z is lost, deletion of Swr1 suppresses alkaline sensitivity, relieves aberrant RNA polymerase II (RNAPII) phosphorylation, and restores appropriate phosphate-gene. Therefore, stress sensitivity and transcription misregulation may be due to deleterious effects of an incomplete SWR-C complex, demonstrating the need for precise control of chromatin remodeling activity in the coordination of gene expression processes.

The dissertation of Lauren Taylor Neves is approved.

John S Adams

Steven Erik Jacobsen

Siavash K Kurdistani

Guillaume Chanfreau

Tracy L Johnson, Committee Chair

University of California, Los Angeles

2018

For my parents and for my husband,
without their love, support and faith in me
none of this would have been possible.

TABLE OF CONTENTS **PAGE**

LIST OF FIGURES **PAGE**

LIST OF TABLES **PAGE**

LIST OF SUPPLEMENTARY FIGURES **PAGE**

LIST OF ABBREVIATIONS

S. cerevisiae	*Saccharomyces cerevisiae*
DNA	deoxyribonucleic acid
RNA	ribonucleic acid
mRNA	messenger RNA
pre-mRNA	precursor mRNA
snRNA	small nuclear RNA
snRNP	small nuclear ribonucleoprotein
TSS	transcription start site
5'SS	5' splice site
BP	branch point
3'SS	3' splice site
ICG	intron-containing gene
RPG	ribosomal protein gene
ORF	open reading frame
gDNA	genomic DNA
SWR-C	SWi2/snf2-related complex
RNAPII	RNA polymerase II
CTD	C-terminal domain
Ser2-P	serine 2 phosphorylation

Thr4-P	threonine 4 phosphorylation
SWI/SNF	SWItch/Sucrose Non-Fermentable
CoQ_6	Coenzyme Q_6

ACKNOWLEDGEMENTS

The pursuit of a Ph.D is a very personal endeavor and yet, in many ways, it is also a team effort. The work presented here would not have been possible without the support of so many people in my life.

First and foremost, I would like to thank my supervisor and mentor, Dr. Tracy Johnson, who has given me both the creative freedom and constructive direction throughout my graduate career to bring this work to fruition. She has helped shape not just my dissertation work, but also has shaped me as a scientist, a writer and a person. I am so thankful for her guidance and advice, as well as her endless encouragement and enthusiasm that have taught me to believe in myself and trust in my science. I am truly fortunate to have trained with her mentorship and will always be grateful for my time spent in her lab. I would also like to thank the members of my committee, Dr. Guillaume Chanfreau, Dr. John Adams, Dr. Steve Jacobsen, and Dr. Siavash Kurdistani for their insightful discussions, thoughtful suggestions, and continuous support throughout my time at UCLA. I am grateful to Dr. Debra Pires and Dr. Tama Hassen for fostereing my growth as a writer and teacher.

I would also like to thank all members of the Johnson lab, past and present. The have provided me with a wealth of both intellectual and moral support, as well as productive advice, stimulating conversation, and constructive criticism. I must make special acknowledgement of Dr. Azad Hossain, who first mentored me in the lab and has been a constant source of help (and often humor) ever since. Additionally I would like to thank graduate students Samantha Edwards and Calvin Leung, not only for their technical help, but also for their friendship and willingness to listen to my struggles.

Chapter 2 of this dissertation benefited greatly from the work of two additional laboratories. I am grateful for the opportunity to collaborate with Dr. Tracy Kress, whose work is presented in this text. Her contributions and insight have been invaluable to the success of this story. I must also thank Dr. Stephen Douglass and Dr. Roberto Spreafico for their assistance with bioinformatics analyses. Additionally, I would like to thank the laboratory of Dr. Christine Guthrie and especially her graduate student Dr. Kelly Nissen, whose work was published in parallel with our own. The countless insightful scientific discussions have served to immeasurably strengthen our work.

I am also sincerely thankful for the community at UCLA, faculty, staff and students alike, for all their support and assistance through the years.

I am thankful to Sriranjini Venkataramanan and Venkataramanan Ramani for unreservedly welcoming me into their family.

I am deeply grateful to my parents, Karen Delaney and Richard Neves, for the love and encouragement they have given me through my life. They have instilled in me a love of learning and drive to always finish what I begin. They have always been there to offer their support and advice, or simply patiently listen when I need it. I cannot thank them enough for all they have done for me.

Most importantly, I would like to thank my husband Srivats Venkataramanan. He is not only my best friend, but has also been, at times, my scientific mentor, my drinking buddy, my sous chef, my travel companion, my shoulder to cry on, and my confidant. He has offered his love and support through life's highs and lows unconditionally and without reserve. I truly could not have completed this dissertation work without him and I cannot thank him enough for being with me every step of the way.

As a graduate student, I received financial support from a Ruth L. Kirschstein National Research Service Award GM007185, the Philip J. Whitcome Graduate Fellowship from the Molecular Biology Interdepartmental Ph.D. Program at UCLA, as well as a UCLA Graduate Division Dissertation Year Fellowship. Funding from the National Institutes of Health Grant GM085474 to Tracy Johnson supported the research presented in this work.

Reprint of publications

Neves, L. T., Douglass, S., Spreafico, R., Venkataramanan, S., Kress, T. L. and Johnson, T. L. (2017) "The histone variant H2A.Z promotes efficient cotranscriptional splicing in S. cerevisiae", ***Genes & Development***, 31(7), pp. 702–717. doi: 10.1101/gad.295188.116.

Chapter 2 is a reprint of this publication. I am grateful to Dr. Tracy Kress for her collaboration on this work and all of the authors on this paper. I am also grateful to Cold Spring Harbor Lab Press for allowing me to include a reprint of this chapter.

Awad, A.*, Venkataramanan, S.*, Nag, A., Galivanche, A.R., Bradley, M., Neves, L.T., Douglass, S., Clarke, C. & Johnson, T.L. "The SWI/SNF complex regulates Coenzyme Q6 (CoQ6) synthesis and the metabolic shift to respiration in *Saccharomyces cerevisiae* via regulation of splicing." ***Journal of Biological Chemistry*****,** 292**,** 14851-14866. doi: 10.1074/jbc.M117.798397. * - indicates co-first authorship.

Chapter 3 is a reprint of this publication. I contributed to the *PTC7* splicing analysis in Figures 1, 4, 5, and 7. I am grateful acknowledge all authors on this paper, and the American Society for Biochemistry and Molecular Biology for allowing me to include a reprint of this chapter.

VITA

EDUCATION

Bachelors of Science in Molecular, Cell, and Developmental Biology
University of California at Santa Cruz, 2007-2011
Summa Cum Laude

PUBLICATIONS

Neves, L. T., Douglass, S., Spreafico, R., Venkataramanan, S., Kress, T. L. and Johnson, T. L. (2017) "The histone variant H2A.Z promotes efficient cotranscriptional splicing in S. cerevisiae", ***Genes & Development***, 31(7), pp. 702–717. doi: 10.1101/gad.295188.116.

Awad, A.*, Venkataramanan, S.*, Nag, A., Galivanche, A.R., Bradley, M., Neves, L.T., Douglass, S., Clarke, C. & Johnson, T.L. (2017) "The SWI/SNF complex regulates Coenzyme Q6 (CoQ6) synthesis and the metabolic shift to respiration in *Saccharomyces cerevisiae* via regulation of splicing." ***Journal of Biological Chemistry*****,** 292**,** 14851-14866. doi:10.1074/jbc.M117.798397.

AWARDS AND HONORS

Dissertation Year Fellowship, 2017 – 2018, Graduate Department, University of California, Los Angeles

Whitcome Fellowship, 2016 – 2017, Molecular Biology Institute, University of California, Los Angeles

Cellular and Molecular Biology Training Program, 2014 – 2016, Molecular Biology Institute, University of California, Los Angeles

Poster award, November 2016, Molecular Cellular and Developmental Biology Departmental Retreat and Research Conference

Travel award: ASBMB Annual Meeting, April 2016, Federation of American Societies for Experimental Biology Annual Research Conference

CONFERENCE PRESENTATIONS

Molecular Biology Interdepartamental Program Retreat and Research Conference 2017, Talk: "Histone variant H2A.Z promotes efficient co-transcriptional splicing"

Molecular Cellular and Developmental Biology Departmental Retreat and Research Conference 2016, Poster: "Histone variant H2A.Z promotes efficient co-transcriptional splicing"

Molecular Biology Interdepartamental Program Retreat and Research Conference 2016, Poster: "The role of histone variant H2A.Z in co-transcriptional splicing"

Federation of American Societies for Experimental Biology Annual Research Conference 2016, Poster: "The role of histone variant H2A.Z in co-transcriptional splicing"

Molecular Cellular and Developmental Biology Departmental Retreat and Research Conference 2015, Talk: "The role of histone variant H2A.Z in co-transcriptional splicing"

CHAPTER 1

Introduction – Splicing in the context of transcription and chromatin

Spliceosome assembly and pre-mRNA splicing.

Pre-messenger RNAs (pre-mRNAs) are transcribed by RNA polymerase II and often contain intervening non-coding regions known as introns. These introns are typically excised from the pre-mRNA, and the coding regions, or exons, are ligated together in a process known as pre-mRNA splicing. The process of splicing is highly conserved and, while metazoans have a number of additional splicing factors (Fabrizio et al. 2009), the majority of the machinery is also conserved across eukaryotes. Appropriate splicing is critical for proper gene expression and changes in splicing can alter the downstream products, stability of the RNA and/or protein products. It has become clear that splicing is precisely regulated, as improper splicing is associated with many human diseases (Faustino and Cooper 2003; Fredericks et al. 2015).

The process of splicing is carried out by the spliceosome, a complex and dynamic biological machine composed five highly structured small nuclear RNAs (snRNAs) and over one hundred associated proteins. The spliceosome recognizes conserved sites within the intron and, through a series of rearrangements of the five small ribonucleoprotein complexes (snRNPs), catalyzes the removal of introns and the ligation of exons in two sequential, highly coordinated transesterification steps. Spliceosome assembly and catalysis rely on recognition of specific sequences within the pre-mRNA: the 5' splice site (5'SS), the branch point (BP), and the 3' splice site (3'SS). Recruitment and assembly of the snRNPs on the pre-mRNA occurs in a stepwise manner (Reviewed in Matera and Wang 2014). First the A complex forms in which the U1 snRNP binds the pre-mRNA through base pairing between its core snRNA and the 5'SS. Additionally, the U2 snRNP binds the BP sequence, forming the bulged branch helix and priming the branch point for the first catalytic step (Krummel et al. 2010). Next, the U4/U5.U6 tri-snRNP is recruited to the RNA, forming the B complex. At this stage the spliceosome is fully

assembled, yet catalytically inactive (Plaschka et al. 2017). During B^{act} complex formation, a series of ATP-driven rearrangements occur as the U4/U6 duplex unwinds, U6 replaces U1, and U1 and U4 are released from the spliceosome (Raghunathan and Guthrie 1998). Finally, the 5'SS and BP are brought in close proximity to form the B* complex and carry out the catalytic steps of splicing (Galej et al. 2013; Nguyen et al. 2013). In the first of two transesterification reactions, the 2'OH of the BP adenosine attacks the 5'SS, forming an intron lariat, releasing the 5' exon, and forming complex C (Fica et al. 2017). The 5' exon remains tethered to the spliceosome, poised for the second step. The C* complex then forms through U5 snRNP dependent rearrangements and brings the 5' and 3' exon in close proximity, which allows the free 3'OH of the 5'exon attacks the 3'SS, releasing the intron lariat and ligating the two exons (Fica et al. 2017). The spliced RNA is released from the spliceosome and the excised intron remains associated with the intron-lariat complex (ILS) (Wilkinson et al. 2017). In the final step, the spliceosome is disassembled by RNA DEAH-box helicase Prp43, releasing the lariat for degradation and freeing the spliceosome components for further rounds of splicing (Reviewed in Matera and Wang 2014) (Figure 1.1).

Intron recognition and splicing fidelity in yeast

While pre-mRNA splicing is a process that is highly conserved across eukaryotic organisms, the functional role of introns is often debated. It has been proposed that introns help increase proteome diversity both in individual organisms through alternative splicing, and on an evolutionary time scale by promoting exon shuffling through recombination in introns (Dibb 1993). Additionally, splicing can be an important checkpoint for regulation of gene expression. Multiple surveillance mechanisms, such as spliceosome-mediated decay (SMD) (Volanakis et al.

2013), intron-mediated enhancement (IME) (Shaul 2017), and alteration of RNA stability, nuclear export and/or translation efficiency (Braunschweig et al. 2013), can alter downstream translation and modulate final protein output. Precise regulation of splicing is therefore crucial to maintenance of organismal health and, in fact, improper splicing has been associated with many human diseases (Faustino and Cooper 2003; Padgett 2012; Singh and Cooper 2012).

Although the components and process of pre-mRNA splicing are conserved across eukaryotes, there are only about 300 introns present in the approximately 6500 genes of the *Saccharomyces cerevisiae* (budding yeast) genome. It has been proposed that *S. cerevisiae* have experienced evolutionary pressures that select for intronless genes and have therefore undergone extensive intron loss (Jeffares et al. 2006; Hooks et al. 2014). However, despite the fact that only about 5% of yeast genes contain introns, intron-containing genes (ICGs) are highly expressed and typically make up about 30% of all transcripts in the cell (Ares et al. 1999; Warner 1999). It has been shown that deletion of many of these introns leads to impaired growth or ability to respond to environmental changes (Hooks et al. 2014). Curiously, it has recently been shown that a small number of excised introns not only escape degradation and are maintained in the cell, but also contribute to the cell's ability to respond to environmental stress (Hooks et al. 2016). Not only does this suggest that introns that have been retained in yeast convey a fitness advantage, but this also indicates that the mechanisms for intron recognition and splicing fidelity must be well regulated.

There are a number of factors that can affect how well the spliceosome is able to recognize and excise a given intron from a transcript. Specific intronic sequences demarcate the intron boundaries and are recognized by the spliceosome. While these sequences can be quite degenerate in metazoans, they are highly conserved in *S. cerevisiae* with consensus sequences

5'SS (GUAUGU), BP (UACUAAC), and 3'SS (YAG). In contrast to yeast, in which splicing is almost entirely dependent on intron definition, there are a number of additional signals to define the small exons of metazoan genes, perhaps allowing for less stringent conservation of intronic splice sites (Berget 1995) (Figure 1.2). The 5'SS and the BP sequences are largely constrained by base pairing with the U1/U6 or U2 snRNA, respectively (Lamond 1993). In fission yeast the 3'SS is constrained by $U2AF^{35}$ proteins (Webb and Wise 2004), but in budding yeast may be partially constrained by Prp8, as no $U2AF^{35}$ homologues have been found (Collins and Guthrie 1999; Galej et al. 2016; Fica et al. 2017). There does exist a subset of introns with non-consensus splice sites, however, even among these non-consensus introns, splice sites rarely vary more than one nucleotide from the consensus sequence (Grate and Ares 2002). In general, ICGs containing introns with non-consensus or 'weak' splice sites are less efficiently spliced than those with consensus introns (Figure 1.3). Interestingly, although *S. cerevisiae* lack $U2AF^{35}$, which is required for poly-U tract recognition in eukaryotes, many introns contain a prominent poly-U tract upstream of the 3'SS (Ma and Xia 2011). This poly-U tract has been shown to increase splicing efficiency, particularly of ICGs with a short BP-to-3'SS distance (Patterson and Guthrie 1991). Introns with strong splicing signals are expected to promote efficient splicing and, satisfyingly, spliceosome assembly and subsequent catalysis have been shown to occur more slowly on genes containing weak introns (Oesterreich et al. 2016).

In some cases splicing of ICGs, particularly those with non-consensus introns, is regulated by additional spliceosomal factors. For example, *YRA1* is autoregulated by its own protein product. Yra1 inhibits splicing of *YRA1* pre-mRNA, which contains a large intron with extensive secondary structure and a non-consensus BP sequence (Rodriguez-Navarro et al. 2002; Dong et al. 2007). In contrast to the Yra1 negative autoregulation, meiotic ICGs require an

additional factor for efficient splicing. Mer1, a meiosis-specific splicing factor, activates splicing of four ICGs whose protein products are critically important for meiosis progression. *MER1* is expressed during meiosis and promotes splicing of *MER2, MER3, SPO22* and *AMA1* through interaction with a conserved intronic enhancer sequence (Spingola and Ares 2000; Munding et al. 2010; Qiu et al. 2011). Meiotic genes are unusual as this class of genes is enriched in introns, and these introns are highly enriched in non-consensus splice sites (Venkataramanan et al. 2017). In fact, meiotic genes are the third largest class of ICGs in *S. cerevisiae* after ribosomal protein genes and secretory genes (Venkataramanan et al. 2017).

In budding yeast, there exists a strong correlation between high expression, efficient splicing, and strong splice sites in ICGs (Pleiss et al. 2007b; Ma and Xia 2011). This is not unexpected as there is likely greater selective pressure on highly transcribed genes to maintain strong splice sites (Ma and Xia 2011). Introns help regulate expression and, indeed, deletion of introns from highly expressed genes reduces RNA abundance of that gene and, in some cases, leads to growth defects (Juneau et al. 2006; Parenteau et al. 2011). Ribosomal protein genes (RPGs) are the most highly expressed class of ICGs, and not only are they enriched in introns but they also make up the largest class of ICGs. Although RPGs make up only about a third of all ICGs, due to their high expression, they account for 90% of all spliced transcripts (Manuel Ares et al. 1999; Warner 1999). Despite the heavy load intron-containing RPGs pose on spliceosomes, they are remarkably well spliced, typically with greater that 90% efficiency (mature mRNA/total mRNA) (Neves et al. 2017; Venkataramanan et al. 2017). However, splicing of RPGs is sensitive to mutations to many splicing factors, suggesting that RPG splice sites are very well adapted to the spliceosome machinery (Pleiss et al. 2007b). Additionally, both expression and splicing of RPGs are sensitive to environmental changes. Upon amino acid starvation, not only is RPG

expression rapidly down-regulated, but splicing of these transcripts is also inhibited, although the mechanism by which specific inhibition of RPG splicing occurs is yet unknown (Pleiss et al. 2007a). It is possible that, due to the rapid synthesis of new ribosomal pre-mRNA, there exists a pool of spliceosome components around these loci: as one spliceosome completes catalysis and is disassembled, it quickly reassembles on a nearby nascent transcript (Hicks et al. 2006). Thus, high levels of transcription could ensure high splicing efficiency.

In fact, it has been demonstrated that the spliceosomes are limiting in the cell and are redistributed under certain conditions. For example, rapamycin-induced RPG downregulation leads to globally increased splicing of non-RPGs (Munding et al. 2013). Interestingly, splicing of ICGs with non-consensus splice sites benefits the most from this decreased RPG expression (Venkataramanan et al. 2017), suggesting that increased spliceosome availability can promote splicing of weak introns. In *S. cerevisiae,* spliceosome redistribution is also critically important for sexual reproduction. During the onset of meiosis, as meiotic genes are turned on, RPGs are rapidly downregulated and spliceosome components become available to splice new intron-containing meiotic transcripts (Munding et al. 2013; Venkataramanan et al. 2017). Notably, as mentioned above, these meiotic ICGs are typically poorly spliced due to weak splice sites and, possibly, very low expression under non-meiotic conditions. Thus, not only are *cis* elements, such as splice sites, powerful determinants of intron recognition, but *trans* factors, such as global and local spliceosome viability, can also affect how efficiently ICGs are spliced.

Co-transcriptional splicing

While RNA synthesis and RNA splicing have traditionally been analyzed as biochemically distinct reactions, many studies have demonstrated that these processes are

spatially and temporally coordinated. Some of the earliest studies to hint at this come from *in vivo* immunofluorescent visualization of splicing factor recruitment to chromatin in bloodworms (Bauren et al. 1996). There is ample evidence to show that the spliceosome recognizes splice sites within nascent pre-mRNA while the RNA polymerase II (RNAPII) is actively transcribing the DNA template (Beyer and Osheim 1988; Beyer and Osheim 1991; Bauren and Wieslander 1994; Huang and Spector 1996; Maniatis and Reed 2002). Recently, it has been shown that not only spliceosome recruitment, but also catalysis and completion of splicing occurs while the nascent RNA is associated with actively transcribing polymerase (Oesterreich et al. 2016). Chromatin immunoprecipitation studies (in yeast and metazoans) show that spliceosome components accumulate around splice sites in a step-wise manner while the RNA is still associated with the polymerase (Kotovic et al. 2003; Gornemann et al. 2005; Lacadie and Rosbash 2005; Listerman et al. 2006; Gunderson and Johnson 2009; Gunderson et al. 2011). The U1 snRNP is recruited first to the nascent pre-mRNA and binds the 5'SS soon after it leaves the polymerase RNA exit channel (Gornemann et al. 2005). As transcription proceeds, U2 binds the newly synthesized BP sequence (Gornemann et al. 2005). Finally, the U4/U5.U6 tri-snRNP binds the pre-mRNA followed by a decrease in U1 snRNP occupancy as RNA-RNA conformational rearrangements occur (Gornemann et al. 2005).

Because the spliceosome binds to RNA while it is still associated with the RNAPII, polymerase dynamics and physical conformation may influence the assembly of the spliceosome and/or kinetics of splicing catalysis. There is evidence that dynamic RNAPII phosphorylation and splicing are linked. RNA polymerase II contains a unique C-terminal domain (CTD) consisting of amino acid sequence repeats of Tyr1-Ser2-Pro3-Thr4-Ser5-Pro6-Ser7 (26 repeats in yeast and 52 in humans) (Allison et al. 1985; Corden et al. 1985) . The CTD is dynamically

phosphorylated in a predictable and conserved manner during transcription elongation. At the promoter, RNAPII is hypo-phosphorylated and, during early transcription, becomes phosphorylated at serines 5 and 7 (Ser5-P and Ser7-P) (Komarnitsky et al. 2000; Alexander et al. 2010; Kim et al. 2010). Ser5-P declines near the 3' end of the transcript in favor of serine 2 phosphorylation (Ser2-P) (Komarnitsky et al. 2000; Alexander et al. 2010). While Ser2-P is a hallmark of the elongating polymerase, it has been unclear whether phosphorylation of Ser2 drives elongation or if RNAPII engagement with the DNA promotes phosphorylation. In yeast, RNAPII is more heavily phosphorylated at Ser2 over long transcripts than shorter transcripts and increased RNAPII pausing correlates with increased Ser2-P (Kim et al. 2010; Davidson et al. 2014). Additionally, a recent study proposes a "dwell time in the target zone" model for Ser2 phosphorylation. In both yeast and human cells, polymerase mutations that slow the rate of elongation result in increased Ser2-P, particularly near the 5' end of genes (Fong et al. 2017), suggesting that Ser2-P levels correlate with the amount of time RNAPII remains engaged with the DNA template. Although serine phosphorylation profiles have been most extensively studied, recent reports show that phosphorylation of threonine 4 and tyrosine 1 (Thr4-P and Tyr1-P) also occurs during mid- to late-elongation (Milligan et al. 2016). Interestingly, RNAPII CTD phosphorylation patterns not only correlate and influence the phases of transcription but also appear to be coupled with splicing signals, particularly around intron boundaries (Harlen et al. 2016; Milligan et al. 2016). In mammals, although Ser5-P levels are highest near the transcriptional start sites, Ser5-P also peaks near the 5'SS of alternatively included exons (Nojima et al. 2015). Phosphorylation pattern transitions are frequently observed around the 3'SS as the polymerase passes the intron-exon boundary (Harlen et al. 2016; Milligan et al. 2016). Several studies in yeast suggest that the polymerase pausing around the 3'SS can be a

"checkpoint" for spliceosome assembly (Alexander et al. 2010; Carrillo Oesterreich et al. 2011; Chathoth et al. 2014). In addition to influencing RNAPII pausing, the phosphorylated CTD may act as a 'scaffold' for the spliceosome by recruiting processing factors and, in mammals, U1-associated protein Prp40 and 3'SS recognition factor U2AF bind directly to the CTD (Morris and Greenleaf 2000), although these findings have been disputed (Gornemann et al. 2011) . In yeast, it has recently been show that Ser5-P and Ser2-P interact extensively with U1 and U2 components, respectively (Harlen et al. 2016).

Additional support for temporal coordination of these two processes also comes from evidence showing changes in transcription elongation rate can alter splicing efficiency and splice site selection (de la Mata et al. 2003; Howe et al. 2003; Oesterreich et al. 2016). Although the average elongation rate of RNA synthesis is 1-4kb per minute, there are localized differences in polymerase kinetics (Kwak and Lis 2013; Jonkers and Lis 2015). RNAPII elongation rate has been shown to be variable between, and even within, genes (Jonkers and Lis 2015) and, in metazoans, elongation rates appear to be faster over introns than over exons (Jonkers et al. 2014). It has been proposed that changes in polymerase elongation affect the "window of opportunity" available for nascent transcripts to be spliced, and slower elongation increases this available window (Braberg et al. 2013; Dujardin et al. 2014a; Oesterreich et al. 2016). However, studies in mammalian cells demonstrate that an optimal elongation rate is required for proper pre-mRNA splicing, and both increased and decreased elongation rate alter splicing outcomes, indicating that transcription and splicing are coupled in a "Goldilocks-like phenomenon" (Fong et al. 2014). In particular, slow elongation enhanced exon skipping and, in some cases, intron retention in many mammalian genes (Fong et al. 2014). The rate of transcription elongation is known to affect RNA folding, which may in turn affect access to processing and regulatory signals (Buratti

and Baralle 2004). Association of accessory proteins to the nascent RNA may also be affected by transcription changes. In human cells, slow elongation leads to increased exclusion the well-characterized alternative exon 9 of CTFR due to enhanced binding of the silencer protein ETR-3 in the upstream intron (Dujardin et al. 2014b). Interestingly, similar findings have been made in yeast, in which the majority of yeast genes do not require enhancers/silencers for splicing. Observations of polymerase trigger-loop mutants in yeast show that, while splicing of some genes benefit from slowed elongation, a number of genes are more poorly spliced when the polymerase is slow (Braberg et al. 2013). Together this suggests that the mechanisms by which the kinetic relationship between splicing and transcription affect splicing outcomes may be diverse and gene specific.

Because the rates of spliceosome rearrangements are finely tuned, slow rearrangements may provide the opportunity for recognition by 'proofreading' machinery and subsequent spliceosome disassembly and release of unspliced RNAs (Koodathingal et al. 2010; Koodathingal and Staley 2013a). A subset of DEAD- and DEAH-box proteins hydrolyze ATP to drive spliceosomal rearrangements and disassembly and function as 'proofreaders' of splice sites to ensure splicing fidelity (Koodathingal et al. 2010; Semlow et al. 2016). In particular, five helicases, Prp5, Prp28, Prp16, Prp22, and Prp43, help to ensure fidelity by rejecting suboptimal splicing substrates (Xu and Query 2007; Mayas et al. 2010; Yang et al. 2013). Specifically, Prp16 and Prp22 promote sampling of candidate splice sites by remodeling the RNP while it is engaged with the spliceosome in a winching mechanism. These two DEAH-box helicases are capable of pulling on pre-mRNA to destabilize RNA-RNA interactions between the spliceosome and substrate mRNA and, therefore, promote splicing fidelity by disengaging suboptimal splice sites from the spliceosome (Semlow et al. 2016). Upon splice site rejection, the pre-mRNA is

then resampled for a stronger splice site or, if no acceptable sequence can be found, the spliceosome is targeted for disassembly (Koodathingal et al. 2010; Mayas et al. 2010).

Prp16, which helps ensure both 5'SS and BP selection fidelity has been proposed to act as a 'molecular clock' (Koodathingal and Staley 2013a). Together with the disassembly factor Prp43, Prp16 helps determine the fate of weak intron substrates when splicing is stalled. Through the winching mechanism described above, Prp16 can recognize and reversibly reject suboptimal, slowly spliced substrates for further sampling of splice sites or trigger spliceosome disassembly and subsequent degradation of unspliced transcripts (Koodathingal et al. 2010; Koodathingal and Staley 2013a; Semlow et al. 2016). When the rate of 5' splice site cleavage is slow, Prp16 rejects the pre-mRNA substrate through a Prp43 dependent pathway (Koodathingal et al. 2010; Mayas et al. 2010). Prp22, which helps ensure the fidelity of exon ligation, is closely related to Prp16 and likely functions in a similar manner during the second step of splicing to determine the fate of suboptimal splice sites (Koodathingal and Staley 2013b; Semlow et al. 2016).

Prp16 and Prp22 likely act as intrinsic timing mechanisms for the completion of splicing. Interestingly, the presence of Prp16 or Prp22 at the catalytic center precludes binding of the NTR complex, which recruits the disassembly factor Prp43 to the spliceosome, and prevents NTR-mediated spliceosome disassembly (Chen et al. 2013). After lariat formation, the ATPase activity of Prp16 is required to eject two first-step factors, Yju2 and Cwc25, to allow for binding of second-step factors Prp22 and Slu7. In the case that the pre-mRNA substrate is rejected prior to the first catalytic step, Prp16 ejection of Cwc25 is required to allow for binding of the NTR complex protein Ntr2. Similarly, Prp22 is required to eject Slu7 to allow for disassembly after splicing is complete or prior to exon ligation, in the case of substrate rejection. In the absence of first-step factors Prp16/Cwc25 or second-step factors Prp22/Slu7, stalled spliceosomes become

highly susceptible to NTR-mediated disassembly (Chen et al. 2013). Curiously, when the pre-mRNA branchpoint is mutated, Prp16 stabilizes the interaction of Cwc25 with the spliceosome, possibly to facilitate resampling for optimal splice sites (Tseng et al. 2011). In sum, Prp16 and Prp22 not only antagonize slow spliceosomes and target them for Prp43-mediated disassembly but also enable alternative splice site selection by protecting the nascent RNA by outcompeting disassembly factors and, thus, promoting substrate resampling. Therefore, the balance of the 'molecular clock' proteins Prp16 and Prp22 with the disassembly helicase Prp43 helps determine the fate of nascent mRNA.

Role of chromatin in splicing

Because pre-mRNA splicing occurs on transcripts as they are actively synthesized, the spliceosome and RNA-synthesis machinery act in close proximity. Splicing, therefore, not only takes place within the context of transcription, but also within the context of chromatin, the array of nucleosomes made up of DNA wrapped around eight histone proteins. Ample evidence indicates that the chromatin environment is capable of regulating both the processes and coordination of transcription and splicing.

Similar to the dynamic phosphorylation of the RNAPII CTD, the chromatin environment may influence splicing outcomes through various mechanisms that can be categorized into two broad models. In the recruitment model, specific chromatin features, such as histone modifications, recruit and maintain splicing factors in the vicinity of the transcription machinery. Alternatively, in a "kinetic model", the chromatin structure can influence transcription elongation, altering the rate at which the pre-mRNA becomes available to the spliceosome, and can therefore, coordinate the kinetic coupling of transcription and splicing. It is important to note

that the recruitment and kinetic models are not mutually exclusive, and the chromatin likely influences splicing in a manner that includes a combination of mechanisms from the overlapping models.

The chromatin architecture is not uniform across genes, and variation in chromatin state may help mark and differentiate gene features. Nucleosomes are well positioned within genes and nucleosome density is typically higher across exons than introns (Schwartz et al. 2009; Amit et al. 2012) and have been found to more stably positioned over constitutive exons than alternatively spliced exons (Huang et al. 2012). In addition to differential density, exonic nucleosomes are enriched for a distinguishable set of histone post-translational modifications (PTMs) (H3K27me1, me2, and me3, H3K36me3, H3K79me1, H4K20me1) (Andersson et al. 2009; Hon et al. 2009; Kolasinska-Zwierz et al. 2009; Nahkuri et al. 2009; Spies et al. 2009; Dhami et al. 2010; Huff et al. 2010) than intronic nucleosomes (which are enriched in H2BK5me1, H2Bub1, H3K4me1, and me2, H3K9me1, H3K79me1, me2, and me3) (Dhami et al. 2010; Huff et al. 2010). These findings strongly suggests that nucleosomes help demarcate exons at the DNA level.

While the precise roles of nucleosome density and many histone modifications in splicing have not been well-characterized, perturbations to chromatin organization have been linked to widespread changes in splicing, and PTMs of individual histone proteins can influence splicing outcomes (Reviewed in Naftelberg et al. 2015). Changes in chromatin structure have been shown to alter nuclear localization and recruitment of splicing factors (Schor et al. 2012). Additionally, roles for specific histone marks in splicing regulation have been demonstrated. H3K4me3, for example, has been shown to recruit the U2 snRNP through interactions with the chromo domain-containing CHD1(Sims et al. 2007). In yeast, monoubiquitylation of histone H2B and

methylation of H3K36 by Set2 each promote efficient splicing and are required for efficient co-transcriptional recruitment of splicing factors to the nascent mRNA (Moehle et al. 2012; Sorenson et al. 2016). In human cells, MRG15, a component of the H3K4 demethylase complex, has been implicated in alternative splicing by bridging methylated H3K36 and the splicing regulator PTB (Luco et al. 2010). Furthermore, we have shown that acetylation of H3 by Gcn5 is important for spliceosome assembly and downstream rearrangements (Gunderson and Johnson 2009; Gunderson et al. 2011).

In addition to the core histone proteins, H2A, H2B, H3, and H4, a number of variant histones, such as H2A.Z, H3.3, and macroH2A, have also been characterized. The chromatin reader, BS69, preferentially recognizes H3.3K36me3 on lysine 36 and physically interacts with the U5 snRNP (Guo et al. 2014), forming a physical link between the chromatin and the spliceosome, and suggesting that both histones and histone variants may influence spliceosome recruitment.

Not only can nucleosome composition affect splicing by influencing spliceosome recruitment, but it can also influence RNA transcription, which is kinetically coupled to splicing. The presence of nucleosomes provides a substantial barrier to transcribing polymerase complexes and RNAPII must overcome this barrier to access the DNA and efficiently transcribe mRNA (Reviewed in Petesch and Lis 2012). In colon carcinoma cells, general histone depletion alters transcription rates and leads to diverse splicing defects (Jimeno-Gonzalez et al. 2015). Nucleosomes may also provide localized barriers to transcription elongation and act as 'speedbumps' to promote RNAPII pausing that, in turn, facilitates splicing (Reviewed in Naftelberg et al. 2015). In addition to recruitment of splicing factors, specific histone modifications can influence elongation in such a manner to affect splicing outcomes. In neuronal

cells, the balance between acetylation and methylation of H3K9 modulates transcription elongation, leading to functional changes in splicing that determine neuron depolarization or activation (Schor et al. 2013).

Additionally, the chromatin environment can also affect splicing indirectly by altering spliceosome availability. For example, deletion of the chromatin-remodeling factor Snf2 decreases RPG expression to 30-40% of wild-type levels and leads to increased splicing efficiency of many non-RPGs (Venkataramanan et al. 2017). It has been demonstrated that global modulation of splicing via regulation of Swr1 protein expression is important several adaptive programs. During meiosis, Snf2, and subsequent RPG, down-regulation promotes splicing of weak meiotic transcripts (Venkataramanan et al. 2017) and, during diauxic shift, such down-regulation allows for splicing of the two-isoform gene *PTC7* (Awad et al. 2017). The spliced *PTC7* transcript encodes a mitochondrial phosphatase regulator of Coenzyme Q_6 (CoQ_6) biosynthesis, a mitochondrial redox-active lipid essential for respiration, and the nonspliced *PTC7* isoform encodes a protein capable of repressing CoQ_6 biosynthesis (Awad et al. 2017). Therefore, the role of Snf2 in global splicing regulation is an important factor in CoQ_6 production during the shift from fermentative to respiratory conditions in yeast.

While the nuances of how regulation of splicing by the chromatin occurs, it is clear that nucleosome density, positioning and composition play an important role in coordinating the crosstalk among chromatin, transcription, and splicing on a local and global scale.

Histone variant H2A.Z

In addition to the core histone proteins, H2A, H2B, H3, and H4, a number of variant histones, including H2A.Z, H3.3, and macroH2A, have also been characterized. H2A.Z, encoded

by *HTZ1* in *S. cerevisiae*, is the only histone variant found across all eukaryotes and is highly conserved. While H2A.Z and H2A share about 60% sequence similarity, H2A.Z is almost 90% conserved across species from yeast to humans (Reviewed in Zlatanova and Thakar 2008), suggesting that the variant carries out an important and conserved function in the cell, distinct from H2A. Several features distinguish H2A.Z from H2A: (1) a unique C-terminus region, (2) an extended surface charge patch, and (3) a small internal loop (Zhang et al. 2005). Among H2A histone family variants, the C-terminus domain is the most highly divergent region indicating that this region may be important for specific roles of each variant. In the case of H2A.Z, this region is required for stable association with the chromatin after deposition (Wratting et al. 2012). Similar to canonical histones, the N-terminal tail of H2A.Z is subject to PTMs, such as acetylation by the NuA4 or SAGA complexes (Millar et al. 2006). Additionally, H2A.Z occupancy within nucleosomes is strongly correlated with several canonical histone marks as H2A.Z-containing nucleosomes most often consist of H4K12ac and H3K4me3, but, strikingly, not H3K36me3 (Chen et al. 2012). These histone marks may help determine H2A.Z deposition and vice versa, but as of now, their functional relationships remains unclear.

Unlike the four canonical histones, which are incorporated into chromatin at the time of DNA replication, H2A.Z can be inserted throughout the cell cycle (Reviewed in Zlatanova and Thakar 2008). H2A.Z is well positioned in the chromatin as, though it is found in only 5% of nucleosomes, it is present in approximately 65% of all *S. cerevisiae* genes, typically at the +1 and -1 nucleosomes around the transcription start site (TSS) (Guillemette et al. 2005; Raisner et al. 2005). The SWR-C remodeling complex catalyzes the displacement of the H2A/H2B dimer in the chromatin in exchange for an H2A.Z/H2B dimer (Mizuguchi et al. 2004). SWR-C recognizes the nucleosome-free region (NFR) surrounding the TSS of genes and deposits H2A.Z in

nucleosomes flanking the NFR (Ranjan et al. 2013) (Figure 1.4). SWR-C is a multisubunit complex made up of the catalytic core protein Swr1, a Swi2/Snf2-related ATPase, and 12 additional subunits (Mizuguchi et al. 2004). Of these additional proteins, Swc2 is responsible for binding the H2A.Z/H2B dimer, while Bdf1, which contains a bromodomain, helps target SWR-C to the chromatin via interactions with acetylated H3 and H4 (Luk et al. 2010). It has been proposed that acetylation of H2A.Z N-terminal lysines 12 or 14 promote deposition in to the chromatin (Millar et al. 2006; Chen et al. 2012). However, this has been disputed, as mutation to either of these lysine residues does not alter H2A.Z localization and H2A.Z appears to be acetylated only after incorporation (Babiarz et al. 2006; Keogh et al. 2006).

H2A.Z has been shown to play an important role in the regulation of transcription initiation and gene expression (Reviewed in Subramanian et al. 2015). In yeast, H2A.Z genetically interacts with a number of transcription factors (TFs) (Wan et al. 2009) and, in mammals, H2A.Z is necessary for recruitment of pioneer TFs (Li et al. 2012). In general, H2A.Z appears to promote transcription, however, the effects of H2A.Z gene expression are dynamic as we and others have observed both up- and down-regulation of genes upon H2A.Z loss (Zhang et al. 2005; Santisteban et al. 2011; Rosonina et al. 2014). The presence of nucleosomes provides a substantial barrier to transcribing polymerase complexes and RNAPII must overcome this barrier to access the DNA and efficiently transcribe mRNA (Reviewed in Petesch and Lis 2012). *In vitro* experiments demonstrate that H2A.Z is less stably associated with DNA and, therefore, more susceptible to release from the chromatin (Zhang et al. 2005). Thus, H2A.Z likely promotes transcription initiation by decreasing the transcriptional barrier of the +1 nucleosome and promoting RNAPII progression (Zhang et al. 2005; Weber et al. 2014).

The mechanism by which H2A.Z is evicted from the chromatin has been widely debated and it remains unclear whether H2A.Z is actively and specifically removed from the chromatin or if the histone is displaced by general mechanisms that displace the entire nucleosome. *In vitro* studies have shown that the INO80 chromatin-remodeling complex is capable of exchanging nucleosomal H2A.Z/H2B dimers for H2A/H2B (Papamichos-Chronakis et al. 2011; Watanabe et al. 2013). However, later reports have disputed these findings, as specific exchange of H2A.Z for H2A-containing dimers by INO80 could not be replicated (Wang et al. 2016). Therefore, eviction of H2A.Z from the chromatin may occur in a more generalized manner. Recently it has been shown that the pre-initiation complex is required for H2A.Z eviction from the chromatin during active transcription (Tramantano et al. 2016) (Figure 1.2). Interestingly, while, in yeast, RPGs are typically deplete of H2A.Z-containing nucleosomes (Raisner et al. 2005; Zhang et al. 2005; Ranjan et al. 2013; Gu et al. 2015), depletion of components of the transcription machinery lead to H2A.Z accumulation in RPGs (Tramantano et al. 2016), indicating that the polymerase itself displaces H2A.Z and high levels of RNAPII prevent accumulation of H2A.Z-containing nucleosomes. Satisfyingly, a recent study found that the INO80 complex evicts H2A.Z by translocation along the DNA (Brahma et al. 2017), suggesting that INO80 and the polymerase remove H2A.Z from the chromatin in a similar way.

Studies in yeast also indicate a role in regulation of transcription elongation, as H2A.Z genetically interacts with elongation factors Spt5 and Dst1 and deletion of H2A.Z renders cell susceptible to 6-azauracil, a transcription elongation inhibitor (Malagon et al. 2004; Santisteban et al. 2011). Additionally, genetic studies of polymerase trigger-loop mutants that display slowed rates of elongation have strong negative interactions with both H2A.Z and Swr1 (Braberg et al. 2013). Moreover, H2A.Z has been found to promote transcription elongation in both yeast and

mammalian cells. In mammalian systems, runoff assays demonstrate that RNAPII is slower along chromatin substrates lacking H2A.Z *in vitro* (Rudnizky et al. 2016), while in yeast, H2A.Z deletion leads to slow RNAPII clearance in runoff studies performed *in vivo* (Santisteban et al. 2011). Together these findings indicate that H2A.Z is not only important for the initiation of transcription but also for maintenance of appropriate elongation kinetics. It should be noted that while one study observed decreased phosphorylation of RNAPII CTD Ser2 upon deletion of H2A.Z (Santisteban et al. 2011), we have observed increased Ser2 phosphorylation, as described in Chapter 2. This discrepancy is likely because the observed Ser2-P levels in the previous study are not normalized to total RNAPII. We find that RNAPII occupancy is considerably reduced across the gene body of tested genes and, therefore, levels of Ser2-P per polymerase are increased in cells lacking H2A.Z, consistent with the "dwell time" model of serine 2 phosphorylation describe above (Fong et al. 2017).

H2A.Z and splicing

H2A.Z and components of the SWR-C complex have been reported to interact with spliceosome machinery. In yeast, a high-throughput genetic screen revealed negative interactions between *HTZ1* and genes encoding several splicing factors, including the U2 snRNP-associated protein Lea1 (Wilmes et al. 2008) and loss of SWR-C component Vps72 was found to result in modest splicing defects of a subset of ICGs (Albulescu et al. 2012). Additionally, in mammals, H2A.Z may bind SF3B1, a component of the U2 snRNP (Fujimoto et al. 2012).

In chapter 2, we demonstrate that H2A.Z is required for efficient pre-mRNA splicing and promotes the splicing of weak introns, and does so by coordinating the kinetics of transcription elongation and co-transcriptional spliceosome rearrangements (Neves et al. 2017). In chapter 3,

we show that, during respiratory conditions, down-regulation of Snf2, a chromatin remodeling protein, leads to global down-regulation of a subset of highly expressed ICGs which, in turn, relieves competition for a limiting spliceosome to allow for increased splicing of a transcript necessary for optimal mitochondrial activity. Chapter 4 demonstrates that the local effects H2A.Z on splicing outcomes and global effects of spliceosome abundance are not mutually exclusive and can account for gene-specific splicing outcomes. Finally, Chapter 5 provides evidence that H2A.Z is important for environmental stress responses and highlights the importance of tight control of chromatin assembly by remodeling complexes.

In sum, the work presented in this dissertation establishes a novel relationship between chromatin and the regulation of pre-mRNA splicing. I demonstrate that a variant histone affects the splicing of intron-containing genes by coordinating the relative kinetics of RNA synthesis with spliceosome rearrangements and disassembly.

Figure 1.1

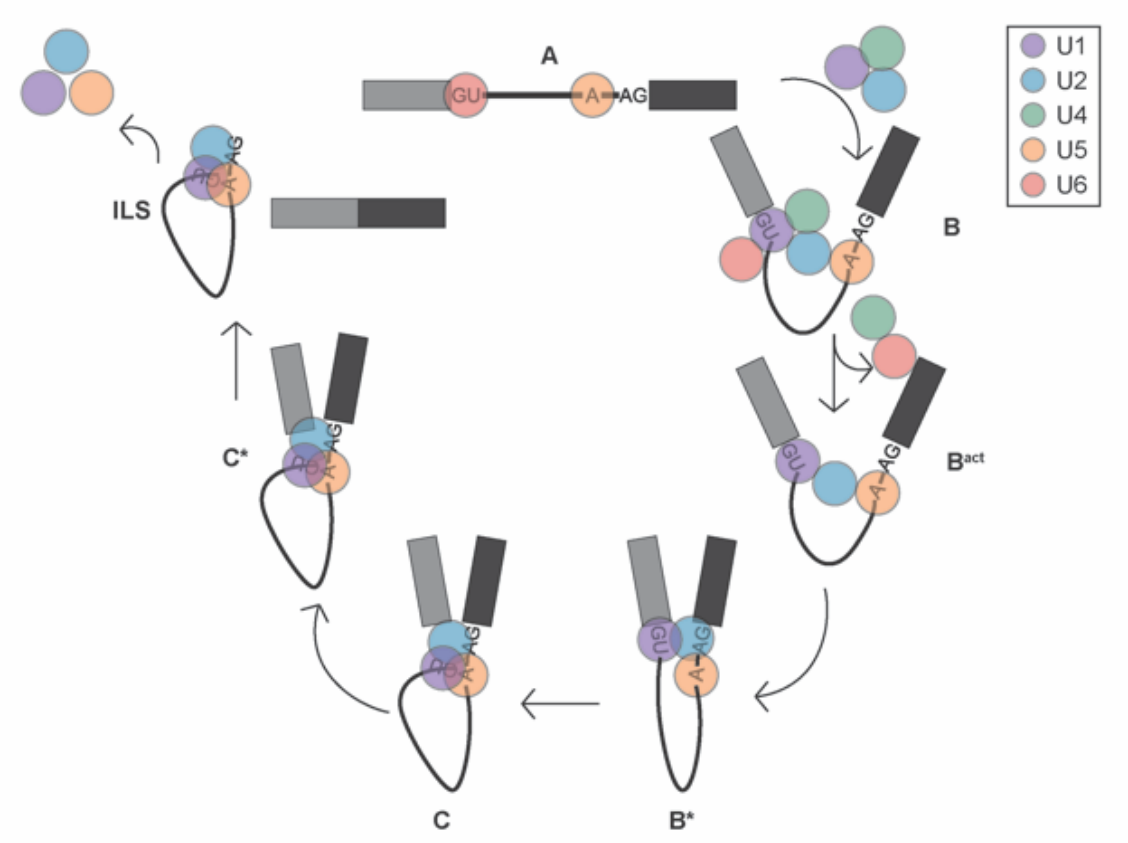

Figure 1.1 Spliceosome rearrangements. U1 and U2 assemble co-transcriptionally by binding to the 5' SS and BP, respectively, forming the A complex. They recruit the tri-snRNP, forming the B complex. U1 and U4 then leave the spliceosome, and U6 replaces U1 at binding the 5' SS, forming the B^{act} complex. The B* complex has rearrangements that promote the first transesterification reaction (complex C). The C* complex then has rearrangements that promote the second transesterification reaction. The resulting products are the ligated exons and the ILS, from which the spliceosome is disassembled. Figure courtesy of Dr. Srivats Venkataramanan and Dr. Erin Wissink.

Figure 1.2

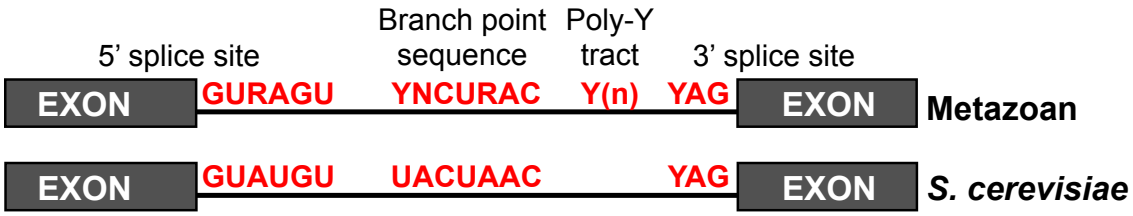

Figure 1.2 Comparison of metazoan and yeast intron sequences

Conserved sequences found at the 5′ and 3′ splice sites and branch point sequence of pre-mRNA introns in metazoans and budding yeast. Y = pyrimidine and R = purine. The polypyrimidine tract is indicated by (Yn). Figure adapted from (Will and Luhrmann 2011).

Figure 1.3

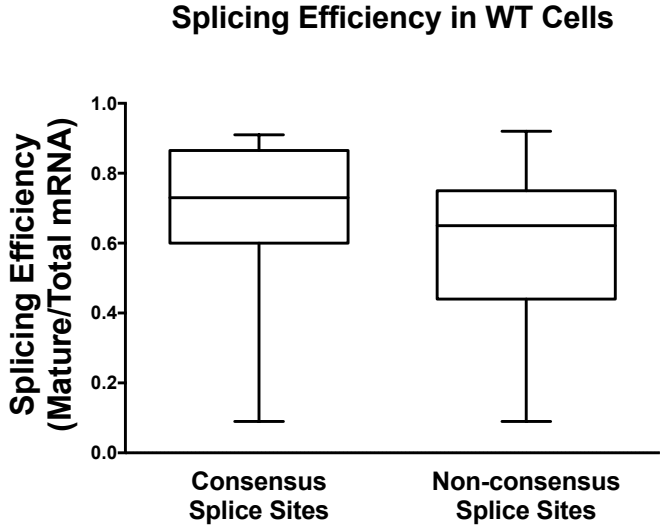

Figure 1.3 Introns containing non-consensus splice sites are poorly spliced.

On average intron-containing genes containing all consensus splice sites have higher splicing efficiency than those containing a non-consensus 5' splice site or branchpoint sequence. Analysis of RNA-seq data of wild type yeast cells (Neves et al. 2017).

Figure 1.4

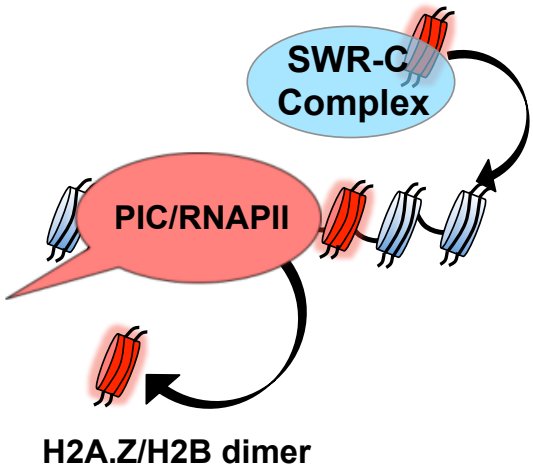

Figure 1.4 H2A.Z is dynamically inserted into and evicted from the chromatin.

The SWR-C complex, driven by the catalytic protein Swr1, inserts H2A.Z in to the chromatin by exchanging H2A/H2B dimers for H2A.Z/H2B (Mizuguchi et al. 2004). H2A.Z is evicted from the chromatin by the pre-initiation complex (PIC) containing RNA polymerase II (RNAPII) (Tramantano et al. 2016) but can also be displaced by the INO80 complex as it translocates along the DNA (Brahma et al. 2017).

REFERENCES

Albulescu LO, Sabet N, Gudipati M, Stepankiw N, Bergman ZJ, Huffaker TC, Pleiss JA. 2012. A quantitative, high-throughput reverse genetic screen reveals novel connections between Pre-mRNA splicing and 5' and 3' end transcript determinants. *PLoS Genet* **8**: e1002530.

Alexander RD, Innocente SA, Barrass JD, Beggs JD. 2010. Splicing-Dependent RNA Polymerase Pausing in Yeast. *Mol Cell* **40**: 582-593.

Allison LA, Moyle M, Shales M, Ingles CJ. 1985. Extensive homology among the largest subunits of eukaryotic and prokaryotic RNA polymerases. *Cell* **42**: 599-610.

Amit M, Donyo M, Hollander D, Goren A, Kim E, Gelfman S, Lev-Maor G, Burstein D, Schwartz S, Postolsky B et al. 2012. Differential GC Content between Exons and Introns Establishes Distinct Strategies of Splice-Site Recognition. *Cell Reports* **1**: 543-556.

Andersson R, Enroth S, Rada-Iglesias A, Wadelius C, Komorowski J. 2009. Nucleosomes are well positioned in exons and carry characteristic histone modifications. *Genome Res* **19**: 1732-1741.

Ares M, Jr., Grate L, Pauling MH. 1999. A handful of intron-containing genes produces the lion's share of yeast mRNA. *RNA* **5**: 1138-1139.

Awad AM, Venkataramanan S, Nag A, Galivanche AR, Bradley MC, Neves L, Douglass S, Clarke CF, Johnson TL. 2017. Chromatin-remodeling SWI/SNF complex regulates coenzyme Q6 synthesis and a metabolic shift to respiration in yeast. *J Biol Chem*.

Babiarz JE, Halley JE, Rine J. 2006. Telomeric heterochromatin boundaries require NuA4-dependent acetylation of histone variant H2A.Z in Saccharomyces cerevisiae. *Genes Dev* **20**: 700-710.

Bauren G, Jiang WQ, Bernholm K, Gu F, Wieslander L. 1996. Demonstration of a dynamic, transcription-dependent organization of pre-mRNA splicing factors in polytene nuclei. *J Cell Biol* **133**: 929-941.

Bauren G, Wieslander L. 1994. Splicing of Balbiani ring 1 gene pre-mRNA occurs simultaneously with transcription. *Cell* **76**: 183-192.

Berget SM. 1995. Exon recognition in vertebrate splicing. *J Biol Chem* **270**: 2411-2414.

Beyer AL, Osheim YN. 1988. Splice Site Selection, Rate of Splicing, and Alternative Splicing on Nascent Transcripts. *Gene Dev* **2**: 754-765.

-. 1991. Visualization of RNA transcription and processing. *Semin Cell Biol* **2**: 131-140.

Braberg H, Jin H, Moehle EA, Chan YA, Wang S, Shales M, Benschop JJ, Morris JH, Qiu C, Hu F et al. 2013. From structure to systems: high-resolution, quantitative genetic analysis of RNA polymerase II. *Cell* **154**: 775-788.

Brahma S, Udugama MI, Kim J, Hada A, Bhardwaj SK, Hailu SG, Lee TH, Bartholomew B. 2017. INO80 exchanges H2A.Z for H2A by translocating on DNA proximal to histone dimers. *Nature Communications* **8**.

Braunschweig U, Gueroussov S, Plocik AM, Graveley BR, Blencowe BJ. 2013. Dynamic Integration of Splicing within Gene Regulatory Pathways. *Cell* **152**: 1252-1269.

Buratti E, Baralle FE. 2004. Influence of RNA secondary structure on the pre-mRNA splicing process. *Mol Cell Biol* **24**: 10505-10514.

Carrillo Oesterreich F, Bieberstein N, Neugebauer KM. 2011. Pause locally, splice globally. *Trends Cell Biol* **21**: 328-335.

Chathoth KT, Barrass JD, Webb S, Beggs JD. 2014. A splicing-dependent transcriptional checkpoint associated with prespliceosome formation. *Mol Cell* **53**: 779-790.

Chen HC, Tseng CK, Tsai RT, Chung CS, Cheng SC. 2013. Link of NTR-mediated spliceosome disassembly with DEAH-box ATPases Prp2, Prp16, and Prp22. *Mol Cell Biol* **33**: 514-525.

Chen J, Miller A, Kirchmaier AL, Irudayaraj JM. 2012. Single-molecule tools elucidate H2A.Z nucleosome composition. *J Cell Sci* **125**: 2954-2964.

Collins CA, Guthrie C. 1999. Allele-specific genetic interactions between Prp8 and RNA active site residues suggest a function for Prp8 at the catalytic core of the spliceosome. *Gene Dev* **13**: 1970-1982.

Corden JL, Cadena DL, Ahearn JM, Jr., Dahmus ME. 1985. A unique structure at the carboxyl terminus of the largest subunit of eukaryotic RNA polymerase II. *Proc Natl Acad Sci U S A* **82**: 7934-7938.

Davidson L, Muniz L, West S. 2014. 3' end formation of pre-mRNA and phosphorylation of Ser2 on the RNA polymerase II CTD are reciprocally coupled in human cells. *Genes Dev* **28**: 342-356.

de la Mata M, Alonso CR, Kadener S, Fededa JP, Blaustein M, Pelisch F, Cramer P, Bentley D, Kornblihtt AR. 2003. A slow RNA polymerase II affects alternative splicing in vivo. *Mol Cell* **12**: 525-532.

Dhami P, Saffrey P, Bruce AW, Dillon SC, Chiang K, Bonhoure N, Koch CM, Bye J, James K, Foad NS et al. 2010. Complex exon-intron marking by histone modifications is not determined solely by nucleosome distribution. *PLoS One* **5**: e12339.

Dibb NJ. 1993. Why do genes have introns? *FEBS Lett* **325**: 135-139.

Dong S, Li C, Zenklusen D, Singer RH, Jacobson A, He F. 2007. YRA1 autoregulation requires nuclear export and cytoplasmic Edc3p-mediated degradation of its pre-mRNA. *Mol Cell* **25**: 559-573.

Dujardin G, Kornblihtt AR, Corcos L. 2014a. [Kinetic regulation of pre-messenger RNA alternative splicing]. *Med Sci (Paris)* **30**: 940-943.

Dujardin G, Lafaille C, de la Mata M, Marasco LE, Munoz MJ, Le Jossic-Corcos C, Corcos L, Kornblihtt AR. 2014b. How slow RNA polymerase II elongation favors alternative exon skipping. *Mol Cell* **54**: 683-690.

Fabrizio P, Dannenberg J, Dube P, Kastner B, Stark H, Urlaub H, Luhrmann R. 2009. The evolutionarily conserved core design of the catalytic activation step of the yeast spliceosome. *Mol Cell* **36**: 593-608.

Faustino NA, Cooper TA. 2003. Pre-mRNA splicing and human disease. *Genes Dev* **17**: 419-437.

Fica SM, Oubridge C, Galej WP, Wilkinson ME, Bai XC, Newman AJ, Nagai K. 2017. Structure of a spliceosome remodelled for exon ligation. *Nature* **542**: 377-380.

Fong N, Kim H, Zhou Y, Ji X, Qiu J, Saldi T, Diener K, Jones K, Fu XD, Bentley DL. 2014. Pre-mRNA splicing is facilitated by an optimal RNA polymerase II elongation rate. *Genes Dev* **28**: 2663-2676.

Fong N, Saldi T, Sheridan RM, Cortazar MA, Bentley DL. 2017. RNA Pol II Dynamics Modulate Co-transcriptional Chromatin Modification, CTD Phosphorylation, and Transcriptional Direction. *Mol Cell* **66**: 546-557 e543.

Fredericks AM, Cygan KJ, Brown BA, Fairbrother WG. 2015. RNA-Binding Proteins: Splicing Factors and Disease. *Biomolecules* **5**: 893-909.

Fujimoto S, Seebart C, Guastafierro T, Prenni J, Caiafa P, Zlatanova J. 2012. Proteome analysis of protein partners to nucleosomes containing canonical H2A or the variant histones H2A.Z or H2A.X. *Biol Chem* **393**: 47-61.

Galej WP, Oubridge C, Newman AJ, Nagai K. 2013. Crystal structure of Prp8 reveals active site cavity of the spliceosome. *Nature* **493**: 638-643.

Galej WP, Wilkinson ME, Fica SM, Oubridge C, Newman AJ, Nagai K. 2016. Cryo-EM structure of the spliceosome immediately after branching. *Nature* **537**: 197-+.

Gornemann J, Barrandon C, Hujer K, Rutz B, Rigaut G, Kotovic KM, Faux C, Neugebauer KM, Seraphin B. 2011. Cotranscriptional spliceosome assembly and splicing are independent of the Prp40p WW domain. *RNA* **17**: 2119-2129.

Gornemann J, Kotovic KM, Hujer K, Neugebauer KM. 2005. Cotranscriptional spliceosome assembly occurs in a stepwise fashion and requires the cap binding complex. *Mol Cell* **19**: 53-63.

Grate L, Ares M, Jr. 2002. Searching yeast intron data at Ares lab Web site. *Methods Enzymol* **350**: 380-392.

Gu M, Naiyachit Y, Wood TJ, Millar CB. 2015. H2A.Z marks antisense promoters and has positive effects on antisense transcript levels in budding yeast. *BMC Genomics* **16**: 99.

Guillemette B, Bataille AR, Gevry N, Adam M, Blanchette M, Robert F, Gaudreau L. 2005. Variant histone H2A.Z is globally localized to the promoters of inactive yeast genes and regulates nucleosome positioning. *PLoS Biol* **3**: e384.

Gunderson FQ, Johnson TL. 2009. Acetylation by the transcriptional coactivator Gcn5 plays a novel role in co-transcriptional spliceosome assembly. *PLoS Genet* **5**: e1000682.

Gunderson FQ, Merkhofer EC, Johnson TL. 2011. Dynamic histone acetylation is critical for cotranscriptional spliceosome assembly and spliceosomal rearrangements. *Proc Natl Acad Sci U S A* **108**: 2004-2009.

Guo R, Zheng L, Park JW, Lv R, Chen H, Jiao F, Xu W, Mu S, Wen H, Qiu J et al. 2014. BS69/ZMYND11 reads and connects histone H3.3 lysine 36 trimethylation-decorated chromatin to regulated pre-mRNA processing. *Mol Cell* **56**: 298-310.

Harlen KM, Trotta KL, Smith EE, Mosaheb MM, Fuchs SM, Churchman LS. 2016. Comprehensive RNA Polymerase II Interactomes Reveal Distinct and Varied Roles for Each Phospho-CTD Residue. *Cell Rep* **15**: 2147-2158.

Hicks MJ, Yang CR, Kotlajich MV, Hertel KJ. 2006. Linking splicing to Pol II transcription stabilizes pre-mRNAs and influences splicing patterns. *PLoS Biol* **4**: e147.

Hon G, Wang W, Ren B. 2009. Discovery and annotation of functional chromatin signatures in the human genome. *PLoS Comput Biol* **5**: e1000566.

Hooks KB, Delneri D, Griffiths-Jones S. 2014. Intron evolution in Saccharomycetaceae. *Genome Biol Evol* **6**: 2543-2556.

Hooks KB, Naseeb S, Parker S, Griffiths-Jones S, Delneri D. 2016. Novel Intronic RNA Structures Contribute to Maintenance of Phenotype in Saccharomyces cerevisiae. *Genetics* **203**: 1469-1481.

Howe KJ, Kane CM, Ares M, Jr. 2003. Perturbation of transcription elongation influences the fidelity of internal exon inclusion in Saccharomyces cerevisiae. *RNA* **9**: 993-1006.

Huang H, Yu S, Liu H, Sun X. 2012. Nucleosome organization in sequences of alternative events in human genome. *Biosystems* **109**: 214-219.

Huang S, Spector DL. 1996. Intron-dependent recruitment of pre-mRNA splicing factors to sites of transcription. *J Cell Biol* **133**: 719-732.

Huff JT, Plocik AM, Guthrie C, Yamamoto KR. 2010. Reciprocal intronic and exonic histone modification regions in humans. *Nat Struct Mol Biol* **17**: 1495-1499.

Jeffares DC, Mourier T, Penny D. 2006. The biology of intron gain and loss. *Trends Genet* **22**: 16-22.

Jimeno-Gonzalez S, Payan-Bravo L, Munoz-Cabello AM, Guijo M, Gutierrez G, Prado F, Reyes JC. 2015. Defective histone supply causes changes in RNA polymerase II elongation rate and cotranscriptional pre-mRNA splicing. *Proc Natl Acad Sci U S A* **112**: 14840-14845.

Jonkers I, Kwak H, Lis JT. 2014. Genome-wide dynamics of Pol II elongation and its interplay with promoter proximal pausing, chromatin, and exons. *Elife* **3**: e02407.

Jonkers I, Lis JT. 2015. Getting up to speed with transcription elongation by RNA polymerase II. *Nat Rev Mol Cell Biol* **16**: 167-177.

Juneau K, Miranda M, Hillenmeyer ME, Nislow C, Davis RW. 2006. Introns regulate RNA and protein abundance in yeast. *Genetics* **174**: 511-518.

Keogh MC, Mennella TA, Sawa C, Berthelet S, Krogan NJ, Wolek A, Podolny V, Carpenter LR, Greenblatt JF, Baetz K et al. 2006. The Saccharomyces cerevisiae histone H2A variant Htz1 is acetylated by NuA4. *Genes Dev* **20**: 660-665.

Kim H, Erickson B, Luo W, Seward D, Graber JH, Pollock DD, Megee PC, Bentley DL. 2010. Gene-specific RNA polymerase II phosphorylation and the CTD code. *Nat Struct Mol Biol* **17**: 1279-1286.

Kolasinska-Zwierz P, Down T, Latorre I, Liu T, Liu XS, Ahringer J. 2009. Differential chromatin marking of introns and expressed exons by H3K36me3. *Nat Genet* **41**: 376-381.

Komarnitsky P, Cho EJ, Buratowski S. 2000. Different phosphorylated forms of RNA polymerase II and associated mRNA processing factors during transcription. *Gene Dev* **14**: 2452-2460.

Koodathingal P, Novak T, Piccirilli JA, Staley JP. 2010. The DEAH Box ATPases Prp16 and Prp43 Cooperate to Proofread 5 ' Splice Site Cleavage during Pre-mRNA Splicing. *Mol Cell* **39**: 385-395.

Koodathingal P, Staley JP. 2013a. Splicing fidelity DEAD/H-box ATPases as molecular clocks. *Rna Biol* **10**: 1073-1079.

-. 2013b. Splicing fidelity: DEAD/H-box ATPases as molecular clocks. *RNA Biol* **10**: 1073-1079.

Kotovic KM, Lockshon D, Boric L, Neugebauer KM. 2003. Cotranscriptional recruitment of the U1 snRNP to intron-containing genes in yeast. *Mol Cell Biol* **23**: 5768-5779.

Krummel DA, Nagai K, Oubridge C. 2010. Structure of spliceosomal ribonucleoproteins. *F1000 Biol Rep* **2**.

Kwak H, Lis JT. 2013. Control of Transcriptional Elongation. *Annu Rev Genet* **47**: 483-508.

Lacadie SA, Rosbash M. 2005. Cotranscriptional spliceosome assembly dynamics and the role of U1 snRNA:5'ss base pairing in yeast. *Mol Cell* **19**: 65-75.

Lamond AI. 1993. The Spliceosome. *Bioessays* **15**: 595-603.

Li Z, Gadue P, Chen K, Jiao Y, Tuteja G, Schug J, Li W, Kaestner KH. 2012. Foxa2 and H2A.Z mediate nucleosome depletion during embryonic stem cell differentiation. *Cell* **151**: 1608-1616.

Listerman I, Sapra AK, Neugebauer KM. 2006. Cotranscriptional coupling of splicing factor recruitment and precursor messenger RNA splicing in mammalian cells. *Nat Struct Mol Biol* **13**: 815-822.

Luco RF, Pan Q, Tominaga K, Blencowe BJ, Pereira-Smith OM, Misteli T. 2010. Regulation of alternative splicing by histone modifications. *Science* **327**: 996-1000.

Luk E, Ranjan A, Fitzgerald PC, Mizuguchi G, Huang Y, Wei D, Wu C. 2010. Stepwise histone replacement by SWR1 requires dual activation with histone H2A.Z and canonical nucleosome. *Cell* **143**: 725-736.

Ma P, Xia X. 2011. Factors affecting splicing strength of yeast genes. *Comp Funct Genomics* **2011**: 212146.

Malagon F, Tong AH, Shafer BK, Strathern JN. 2004. Genetic interactions of DST1 in Saccharomyces cerevisiae suggest a role of TFIIS in the initiation-elongation transition. *Genetics* **166**: 1215-1227.

Maniatis T, Reed R. 2002. An extensive network of coupling among gene expression machines. *Nature* **416**: 499-506.

Manuel Ares J, Grate L, Pauling MH. 1999. An handful of intron-containing genes produces the lion's share of yeast mRNA. *RNA* **5**: 1138-1139.

Matera AG, Wang Z. 2014. A day in the life of the spliceosome. *Nat Rev Mol Cell Biol* **15**: 108-121.

Mayas RM, Maita H, Semlow DR, Staley JP. 2010. Spliceosome discards intermediates via the DEAH box ATPase Prp43p. *P Natl Acad Sci USA* **107**: 10020-10025.

Millar CB, Xu F, Zhang K, Grunstein M. 2006. Acetylation of H2AZ Lys 14 is associated with genome-wide gene activity in yeast. *Genes Dev* **20**: 711-722.

Milligan L, Huynh-Thu VA, Delan-Forino C, Tuck A, Petfalski E, Lombrana R, Sanguinetti G, Kudla G, Tollervey D. 2016. Strand-specific, high-resolution mapping of modified RNA polymerase II. *Mol Syst Biol* **12**: 874.

Mizuguchi G, Shen X, Landry J, Wu WH, Sen S, Wu C. 2004. ATP-driven exchange of histone H2AZ variant catalyzed by SWR1 chromatin remodeling complex. *Science* **303**: 343-348.

Moehle EA, Ryan CJ, Krogan NJ, Kress TL, Guthrie C. 2012. The yeast SR-like protein Npl3 links chromatin modification to mRNA processing. *PLoS Genet* **8**: e1003101.

Morris DP, Greenleaf AL. 2000. The splicing factor, Prp40, binds the phosphorylated carboxyl-terminal domain of RNA polymerase II. *J Biol Chem* **275**: 39935-39943.

Munding EM, Igel AH, Shiue L, Dorighi KM, Trevino LR, Ares M, Jr. 2010. Integration of a splicing regulatory network within the meiotic gene expression program of Saccharomyces cerevisiae. *Genes Dev* **24**: 2693-2704.

Munding EM, Shiue L, Katzman S, Donohue JP, Ares M, Jr. 2013. Competition between pre-mRNAs for the splicing machinery drives global regulation of splicing. *Mol Cell* **51**: 338-348.

Naftelberg S, Schor IE, Ast G, Kornblihtt AR. 2015. Regulation of alternative splicing through coupling with transcription and chromatin structure. *Annu Rev Biochem* **84**: 165-198.

Nahkuri S, Taft RJ, Mattick JS. 2009. Nucleosomes are preferentially positioned at exons in somatic and sperm cells. *Cell Cycle* **8**: 3420-3424.

Neves LT, Douglass S, Spreafico R, Venkataramanan S, Kress TL, Johnson TL. 2017. The histone variant H2A.Z promotes efficient cotranscriptional splicing in S. cerevisiae. *Genes Dev* **31**: 702-717.

Nguyen TH, Li J, Galej WP, Oshikane H, Newman AJ, Nagai K. 2013. Structural basis of Brr2-Prp8 interactions and implications for U5 snRNP biogenesis and the spliceosome active site. *Structure* **21**: 910-919.

Nojima T, Gomes T, Grosso AR, Kimura H, Dye MJ, Dhir S, Carmo-Fonseca M, Proudfoot NJ. 2015. Mammalian NET-Seq Reveals Genome-wide Nascent Transcription Coupled to RNA Processing. *Cell* **161**: 526-540.

Oesterreich FC, Herzel L, Straube K, Hujer K, Howard J, Neugebauer KM. 2016. Splicing of Nascent RNA Coincides with Intron Exit from RNA Polymerase II. *Cell* **165**: 372-381.

Padgett RA. 2012. New connections between splicing and human disease. *Trends Genet* **28**: 147-154.

Papamichos-Chronakis M, Watanabe S, Rando OJ, Peterson CL. 2011. Global regulation of H2A.Z localization by the INO80 chromatin-remodeling enzyme is essential for genome integrity. *Cell* **144**: 200-213.

Parenteau J, Durand M, Morin G, Gagnon J, Lucier JF, Wellinger RJ, Chabot B, Elela SA. 2011. Introns within ribosomal protein genes regulate the production and function of yeast ribosomes. *Cell* **147**: 320-331.

Patterson B, Guthrie C. 1991. A U-rich tract enhances usage of an alternative 3' splice site in yeast. *Cell* **64**: 181-187.

Petesch SJ, Lis JT. 2012. Overcoming the nucleosome barrier during transcript elongation. *Trends in Genetics* **28**: 285-294.

Plaschka C, Lin PC, Nagai K. 2017. Structure of a pre-catalytic spliceosome. *Nature* **546**: 617-621.

Pleiss JA, Whitworth GB, Bergkessel M, Guthrie C. 2007a. Rapid, transcript-specific changes in splicing in response to environmental stress. *Mol Cell* **27**: 928-937.

-. 2007b. Transcript specificity in yeast pre-mRNA splicing revealed by mutations in core spliceosomal components. *PLoS Biol* **5**: e90.

Qiu ZR, Schwer B, Shuman S. 2011. Determinants of Nam8-dependent splicing of meiotic pre-mRNAs. *Nucleic Acids Res* **39**: 3427-3445.

Raghunathan PL, Guthrie C. 1998. RNA unwinding in U4/U6 snRNPs requires ATP hydrolysis and the DEIH-box splicing factor Brr2. *Curr Biol* **8**: 847-855.

Raisner RM, Hartley PD, Meneghini MD, Bao MZ, Liu CL, Schreiber SL, Rando OJ, Madhani HD. 2005. Histone variant H2A.Z marks the 5' ends of both active and inactive genes in euchromatin. *Cell* **123**: 233-248.

Ranjan A, Mizuguchi G, FitzGerald PC, Wei D, Wang F, Huang Y, Luk E, Woodcock CL, Wu C. 2013. Nucleosome-free region dominates histone acetylation in targeting SWR1 to promoters for H2A.Z replacement. *Cell* **154**: 1232-1245.

Rodriguez-Navarro S, Strasser K, Hurt E. 2002. An intron in the YRA1 gene is required to control Yra1 protein expression and mRNA export in yeast. *EMBO Rep* **3**: 438-442.

Rosonina E, Yurko N, Li WC, Hoque M, Tian B, Manley JL. 2014. Threonine-4 of the budding yeast RNAP II CTD couples transcription with Htz1-mediated chromatin remodeling. *P Natl Acad Sci USA* **111**: 11924-11931.

Rudnizky S, Bavly A, Malik O, Pnueli L, Melamed P, Kaplan A. 2016. H2A.Z controls the stability and mobility of nucleosomes to regulate expression of the LH genes. *Nat Commun* **7**: 12958.

Santisteban MS, Hang M, Smith MM. 2011. Histone variant H2A.Z and RNA polymerase II transcription elongation. *Mol Cell Biol* **31**: 1848-1860.

Schor IE, Fiszbein A, Petrillo E, Kornblihtt AR. 2013. Intragenic epigenetic changes modulate NCAM alternative splicing in neuronal differentiation. *EMBO J* **32**: 2264-2274.

Schor IE, Lleres D, Risso GJ, Pawellek A, Ule J, Lamond AI, Kornblihtt AR. 2012. Perturbation of chromatin structure globally affects localization and recruitment of splicing factors. *PLoS One* **7**: e48084.

Schwartz S, Meshorer E, Ast G. 2009. Chromatin organization marks exon-intron structure. *Nature Structural & Molecular Biology* **16**: 990-U117.

Semlow DR, Blanco MR, Walter NG, Staley JP. 2016. Spliceosomal DEAH-Box ATPases Remodel Pre-mRNA to Activate Alternative Splice Sites. *Cell* **164**: 985-998.

Shaul O. 2017. How introns enhance gene expression. *Int J Biochem Cell Biol*.

Sims RJ, 3rd, Millhouse S, Chen CF, Lewis BA, Erdjument-Bromage H, Tempst P, Manley JL, Reinberg D. 2007. Recognition of trimethylated histone H3 lysine 4 facilitates the recruitment of transcription postinitiation factors and pre-mRNA splicing. *Mol Cell* **28**: 665-676.

Singh RK, Cooper TA. 2012. Pre-mRNA splicing in disease and therapeutics. *Trends Mol Med* **18**: 472-482.

Sorenson MR, Jha DK, Ucles SA, Flood DM, Strahl BD, Stevens SW, Kress TL. 2016. Histone H3K36 methylation regulates pre-mRNA splicing in Saccharomyces cerevisiae. *Rna Biol* **13**: 412-426.

Spies N, Nielsen CB, Padgett RA, Burge CB. 2009. Biased chromatin signatures around polyadenylation sites and exons. *Mol Cell* **36**: 245-254.

Spingola M, Ares M, Jr. 2000. A yeast intronic splicing enhancer and Nam8p are required for Mer1p-activated splicing. *Mol Cell* **6**: 329-338.

Subramanian V, Fields PA, Boyer LA. 2015. H2A.Z: a molecular rheostat for transcriptional control. *F1000Prime Rep* **7**: 01.

Tramantano M, Sun L, Au C, Labuz D, Liu Z, Chou M, Shen C, Luk E. 2016. Constitutive turnover of histone H2A.Z at yeast promoters requires the preinitiation complex. *Elife* **5**.

Tseng CK, Liu HL, Cheng SC. 2011. DEAH-box ATPase Prp16 has dual roles in remodeling of the spliceosome in catalytic steps. *RNA* **17**: 145-154.

Venkataramanan S, Douglass S, Galivanche AR, Johnson TL. 2017. The chromatin remodeling complex Swi/Snf regulates splicing of meiotic transcripts in Saccharomyces cerevisiae. *Nucleic Acids Res*.

Volanakis A, Passoni M, Hector RD, Shah S, Kilchert C, Granneman S, Vasiljeva L. 2013. Spliceosome-mediated decay (SMD) regulates expression of nonintronic genes in budding yeast. *Genes Dev* **27**: 2025-2038.

Wan Y, Saleem RA, Ratushny AV, Roda O, Smith JJ, Lin CH, Chiang JH, Aitchison JD. 2009. Role of the histone variant H2A.Z/Htz1p in TBP recruitment, chromatin dynamics, and regulated expression of oleate-responsive genes. *Mol Cell Biol* **29**: 2346-2358.

Wang F, Ranjan A, Wei D, Wu C. 2016. Comment on "A histone acetylation switch regulates H2A.Z deposition by the SWR-C remodeling enzyme". *Science* **353**: 358.

Warner JR. 1999. The economics of ribosome biosynthesis in yeast. *Trends Biochem Sci* **24**: 437-440.

Watanabe S, Radman-Livaja M, Rando OJ, Peterson CL. 2013. A histone acetylation switch regulates H2A.Z deposition by the SWR-C remodeling enzyme. *Science* **340**: 195-199.

Webb CJ, Wise JA. 2004. The splicing factor U2AF small subunit is functionally conserved between, fission yeast and, humans. *Mol Cell Biol* **24**: 4229-4240.

Weber CM, Ramachandran S, Henikoff S. 2014. Nucleosomes are context-specific, H2A.Z-modulated barriers to RNA polymerase. *Mol Cell* **53**: 819-830.

Wilkinson ME, Fica SM, Galej WP, Norman CM, Newman AJ, Nagai K. 2017. Postcatalytic spliceosome structure reveals mechanism of 3'-splice site selection. *Science* **358**: 1283-1288.

Will CL, Luhrmann R. 2011. Spliceosome structure and function. *Cold Spring Harb Perspect Biol* **3**.

Wilmes GM, Bergkessel M, Bandyopadhyay S, Shales M, Braberg H, Cagney G, Collins SR, Whitworth GB, Kress TL, Weissman JS et al. 2008. A genetic interaction map of RNA-processing factors reveals links between Sem1/Dss1-containing complexes and mRNA export and splicing. *Mol Cell* **32**: 735-746.

Wratting D, Thistlethwaite A, Harris M, Zeef LA, Millar CB. 2012. A conserved function for the H2A.Z C terminus. *J Biol Chem* **287**: 19148-19157.

Xu YZ, Query CC. 2007. Competition between the ATPase prp5 and branch region-U2 snRNA pairing modulates the fidelity of spliceosome assembly. *Mol Cell* **28**: 838-849.

Yang F, Wang XY, Zhang ZM, Pu J, Fan YJ, Zhou JH, Query CC, Xu YZ. 2013. Splicing proofreading at 5' splice sites by ATPase Prp28p. *Nucleic Acids Research* **41**: 4660-4670.

Zhang H, Roberts DN, Cairns BR. 2005. Genome-wide dynamics of Htz1, a histone H2A variant that poises repressed/basal promoters for activation through histone loss. *Cell* **123**: 219-231.

Zlatanova J, Thakar A. 2008. H2A.Z: view from the top. *Structure* **16**: 166-179.

CHAPTER 2

The histone variant H2A.Z promotes efficient co-transcriptional splicing in *Saccharomyces cerevisiae.*

The histone variant H2A.Z promotes efficient cotranscriptional splicing in *S. cerevisiae*

Lauren T. Neves,[1,2] Stephen Douglass,[1] Roberto Spreafico,[3] Srivats Venkataramanan,[1] Tracy L. Kress,[4] and Tracy L. Johnson[1,5]

[1]Department of Molecular, Cell, and Developmental Biology, University of California at Los Angeles, Los Angeles, California, 90095 USA; [2]Graduate Program in Molecular Biology Interdepartmental Program, University of California at Los Angeles, Los Angeles, California 90095, USA; [3]Institute for Quantitative and Computational Biosciences, University of California at Los Angeles, Los Angeles, California 90095, USA; [4]Department of Biology, The College of New Jersey, Ewing, New Jersey 08628, USA; [5]Molecular Biology Institute, University of California at Los Angeles, Los Angeles, California 90095, USA

In eukaryotes, a dynamic ribonucleic protein machine known as the spliceosome catalyzes the removal of introns from premessenger RNA (pre-mRNA). Recent studies show the processes of RNA synthesis and RNA processing to be spatio–temporally coordinated, indicating that RNA splicing takes place in the context of chromatin. H2A.Z is a highly conserved histone variant of the canonical histone H2A. In *Saccharomyces cerevisiae*, H2A.Z is deposited into chromatin by the SWR-C complex, is found near the 5′ ends of protein-coding genes, and has been implicated in transcription regulation. Here we show that splicing of intron-containing genes in cells lacking H2A.Z is impaired, particularly under suboptimal splicing conditions. Cells lacking H2A.Z are especially dependent on a functional U2 snRNP (small nuclear RNA [snRNA] plus associated proteins), as H2A.Z shows extensive genetic interactions with U2 snRNP-associated proteins, and RNA sequencing (RNA-seq) reveals that introns with nonconsensus branch points are particularly sensitive to H2A.Z loss. Consistently, H2A.Z promotes efficient spliceosomal rearrangements involving the U2 snRNP, as H2A.Z loss results in persistent U2 snRNP association and decreased recruitment of downstream snRNPs to nascent RNA. H2A.Z impairs transcription elongation, suggesting that spliceosome rearrangements are tied to H2A.Z's role in elongation. Depletion of disassembly factor Prp43 suppresses H2A.Z-mediated splice defects, indicating that, in the absence of H2A.Z, stalled spliceosomes are disassembled, and unspliced RNAs are released. Together, these data demonstrate that H2A.Z is required for efficient pre-mRNA splicing and indicate a role for H2A.Z in coordinating the kinetics of transcription elongation and splicing.

[*Keywords*: H2A.Z; HTZ1; RNA processing; Swr1; budding yeast; chromatin; pre-mRNA splicing]

Supplemental material is available for this article.

Received December 19, 2016; revised version accepted March 27, 2017.

Eukaryotic genes are comprised of coding sequences (exons) interrupted by intervening sequences (introns). Introns are removed from the newly synthesized RNA by a large macromolecular machine known as the spliceosome. The spliceosome is a dynamic ribonucleoprotein complex made up of five highly structured small nuclear RNAs (snRNAs) and over a hundred associated proteins and catalyzes intron removal through a series of precisely coordinated rearrangements of its five snRNPs (snRNA plus associated proteins).

While RNA synthesis and RNA splicing have been traditionally analyzed as biochemically distinct reactions, many studies have demonstrated that these processes are spatially and temporally coordinated. There is ample evidence to show that the spliceosome recognizes splice sites within nascent premessenger RNA (pre-mRNA) while the RNA polymerase II (RNAPII) is actively transcribing the DNA template (Beyer and Osheim 1988, 1991; Bauren and Wieslander 1994; Bauren et al. 1996; Huang and Spector 1996; Maniatis and Reed 2002). Chromatin immunoprecipitation (ChIP) studies (in yeast and metazoans) show that spliceosome components are recruited to specific sequence signals (splice sites) in the pre-mRNA while still associated with the transcription complex (Kotovic et al. 2003; Gornemann et al. 2005; Lacadie and Rosbash 2005; Listerman et al. 2006).

Corresponding author: tljohnson@ucla.edu
Article is online at http://www.genesdev.org/cgi/doi/10.1101/gad.295188.116.

Recently, it has been shown that not only spliceosome recruitment but also catalysis and completion of splicing occur while the nascent RNA is associated with actively transcribing polymerase (Oesterreich et al. 2016). Support for temporal coordination of these two processes also comes from evidence showing that changes in transcription elongation rate can alter splicing efficiency and splice site selection (de la Mata et al. 2003; Howe et al. 2003; Fong et al. 2014; Oesterreich et al. 2016).

Due to the proximity of the splicing complex to the DNA synthesis machinery, splicing takes place within the context of not only transcription but also chromatin, the array of nucleosomes made up of DNA wrapped around eight histone proteins. Nucleosomes are well positioned within genes and have been found to occupy exons more frequently than introns (Schwartz et al. 2009; Amit et al. 2012), suggesting that nucleosomes help demarcate exons at the DNA level. Perturbations to chromatin organization have been linked to widespread changes in splicing, and post-translational modifications of individual histone proteins can influence splicing (for review, see Naftelberg et al. 2015). Particularly in budding yeast, monoubiquitylation of histone H2B and methylation of H3K36 by Set2 each promotes efficient splicing and is required for efficient cotranscriptional recruitment of splicing factors to the nascent mRNA (Moehle et al. 2012; Sorenson et al. 2016). Additionally, we showed that acetylation of H3 by Gcn5 is important for spliceosome assembly and downstream rearrangements (Gunderson and Johnson 2009; Gunderson et al. 2011).

In addition to the core histone proteins H2A, H2B, H3, and H4, a number of variant histones, such as H2A.Z, H3.3, and macroH2A, have also been characterized. A recent study identified a chromatin reader, BS69, that preferentially recognizes trimethylation of the histone variant H3.3 on Lys36 and physically interacts with the U5 snRNP (Guo et al. 2014), forming a physical link between the chromatin and the spliceosome, suggesting that both histones and histone variants may influence splicing. H2A.Z, encoded by *HTZ1* in *Saccharomyces cerevisiae*, is the only histone variant found across all eukaryotes. While H2A.Z and H2A share ~60% sequence similarity, H2A.Z is almost 90% conserved across species from yeast to humans (for review, see Zlatanova and Thakar 2008), suggesting that the variant carries out an important and conserved function in the cell, distinct from H2A. Unlike the four canonical histones, which are incorporated into chromatin at the time of DNA replication, H2A.Z can be inserted throughout the cell cycle (for review, see Zlatanova and Thakar 2008). The SWR-C remodeling complex catalyzes the displacement of the H2A/H2B dimer in the chromatin in exchange for an H2A.Z/H2B dimer. SWR-C recognizes the nucleosome-free region (NFR) surrounding the transcription start site (TSS) of genes and deposits H2A.Z in nucleosomes flanking the NFR (Ranjan et al. 2013). H2A.Z is well positioned in the chromatin as, although it is found in only 5% of nucleosomes, it is present in ~65% of all *S. cerevisiae* genes, typically at the +1 and −1 nucleosomes around the TSS (Guillemette et al. 2005; Raisner et al. 2005).

H2A.Z has been shown to play an important role in the regulation of transcription initiation and gene expression (Subramanian et al. 2015). In yeast, H2A.Z interacts genetically with a number of transcription factors (TFs) (Wan et al. 2009), and, in mammals, H2A.Z is necessary for recruitment of pioneer TFs (Li et al. 2012). In vitro experiments demonstrate that H2A.Z is less stably associated with DNA and therefore is more susceptible to release from the chromatin (Zhang et al. 2005). As the +1 nucleosome poses a transcriptional barrier to RNAPII, H2A.Z may promote transcription initiation by decreasing the nucleosome barrier and promoting RNAPII progression (Zhang et al. 2005; Weber et al. 2014). Studies in yeast also indicate a role in the regulation of transcription elongation, as H2A.Z genetically interacts with elongation factors Spt5 and Dst1 (Malagon et al. 2004; Santisteban et al. 2011). Moreover, H2A.Z has been found to promote transcription elongation in both yeast and mammalian cells (Santisteban et al. 2011; Rudnizky et al. 2016).

Based on the connections between transcription and pre-mRNA splicing as well as H2A.Z's role in transcriptional regulation, we performed genetic analysis of interactions between *HTZ1* and genes encoding nonessential splicing factors and showed that when any major component of the spliceosome, particularly the U2 snRNP, is compromised, the cell becomes dependent on the presence of H2A.Z. Furthermore, H2A.Z is required for efficient splicing of a subset of intron-containing genes (ICGs). This pool of genes is enriched in introns containing a branch point (BP) sequence that deviates from the highly conserved consensus sequence. Interestingly, although H2A.Z is found primarily in close proximity to the TSS, we observed H2A.Z enrichment near the BP of many ICGs. When H2A.Z is deleted, proper spliceosome rearrangements are compromised, and this is coincident with altered RNA polymerase elongation that occurs in the absence of H2A.Z. Depletion of the spliceosome disassembly factor Prp43 in cells lacking H2A.Z enhances splicing of introns, particularly of introns with nonconsensus BP sequences. These results reveal an important role for the highly conserved H2A.Z histone variant in coordinating elongation with spliceosome assembly.

Results

Cells with mutant spliceosomes are dependent on H2A.Z

In order to characterize interactions between H2A.Z and genes encoding factors involved in splicing, a targeted genetic screen was performed to identify interactions between *htz1*Δ and null alleles of nonessential splicing factors. Deletion of the genes encoding the U2 snRNP factors Msl1, Lea1, or Snu17 combined with deletion of *HTZ1* confers synthetic lethality (Fig. 1A). Msl1 and Lea1 are yeast homologs of the human proteins U2A′/B″ and bind a conserved stem–loop in the U2 snRNA (Tang et al. 1996). Snu17, which has been shown to associate with the U2 snRNP, is required for the release of the U1 snRNP after the addition of the U4/U6.U5 tri-snRNP and progression through the first catalytic step of splicing

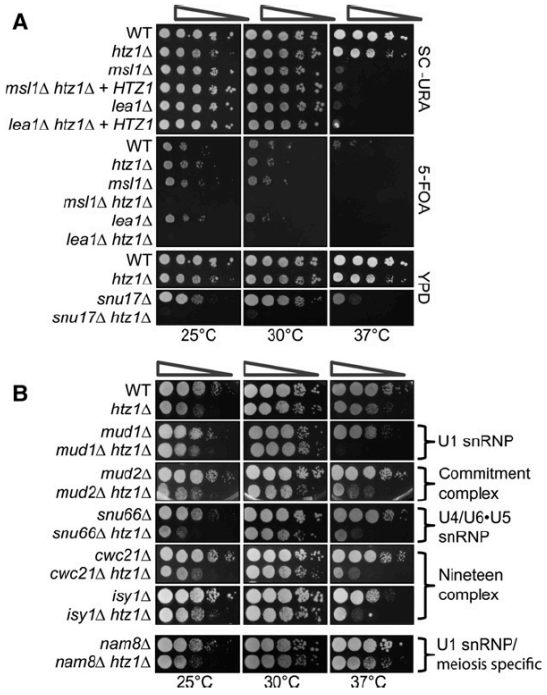

Figure 1. The histone variant H2A.Z is necessary for an optimal splicing environment. (*A*) Serial dilution assay of U2 snRNP double mutants *msl1Δ htz1Δ*, *lea1Δ htz1Δ*, and *snu17Δ htz1Δ*. For the *msl1Δ* and *lea1Δ* growth assay, cells were transformed with empty pRS316 *URA* plasmid (wild type [WT], *htz1Δ*, *msl1Δ*, and *lea1Δ*) or pRS316 containing *HTZ1* (*msl1Δ htz1Δ* and *lea1Δ htz1Δ*). Cells were grown at 30°C in SC–URA selective liquid medium until the desired OD_{600} was obtained. Cells were spotted as a 10-fold dilution onto SC–URA plates or 5-FOA plates to select for loss of the plasmid. Plates were incubated for 2 d for SC–URA plates or 4 d for 5-FOA plates at 25°C, 30°C, or 37°C. For *snu17Δ*, cells were grown at 30°C in YPD liquid medium until the desired OD_{600} was obtained. Cells were spotted as a 10-fold dilution onto YPD plates and incubated for 2 d at 25°C, 30°C, or 37°C. (*B*) Serial dilution assay of double mutants, *mud1Δ htz1Δ*, *mud2Δ htz1Δ*, *snu17Δ htz1Δ*, *snu66Δ htz1Δ*, *cwc21Δ htz1Δ*, *isy1Δ htz1Δ*, and *nam8Δ htz1Δ*. Cells were grown at 30°C in YPD liquid medium until the desired OD_{600} was obtained. Cells were spotted as a 10-fold dilution onto YPD plates and incubated for 2 d at 25°C, 30°C, or 37°C.

(Gottschalk et al. 2001). Snu17 is also a component of the retention and splicing (RES) complex, which is important for nuclear retention of unspliced pre-mRNA. This indicates that cells lacking H2A.Z are dependent on intact U2 snRNP.

Splicing is a highly dynamic process with thermal-sensitive RNA–RNA and RNA–protein interactions. We suspected that if H2A.Z affects splicing factor recruitment and/or rearrangements of the spliceosome, then perturbations in temperature could reveal additional genetic interactions between *HTZ1* and genes encoding splicing factors. To identify these interactions, we repeated our targeted genetic screen under growth temperatures that are suboptimal (37°C and 25°C). This analysis revealed genetic interactions between *HTZ1* and genes encoding components of every major spliceosomal complex (Fig. 1B). Slow growth phenotypes in many of the double mutants are exacerbated at higher temperatures, indicating that H2A.Z may be important for stabilizing spliceosomal complexes and/or rearrangements, especially in destabilizing conditions such as thermal stress. A notable exception is Nam8, a U1-associated factor that is particularly important for meiosis-specific splicing (Fig. 1B, bottom; Spingola and Ares 2000). Together, these genetic interactions indicate that a mutant spliceosome—and especially a compromised U2 snRNP—is particularly sensitive to the absence of H2A.Z in the chromatin.

H2A.Z is required for optimal splicing of a subset of ICGs

In order to determine whether deletion of H2A.Z affects splicing, we used RNA sequencing (RNA-seq) to analyze the effect of *HTZ1* deletion genome-wide. We compared the splicing efficiency of ICGs in wild-type and *htz1Δ* cells (Fig. 2A, left). Ribosomal protein genes (RPGs), which account for roughly one-third of all ICGs, show little to no change in splicing efficiency upon deletion of H2A.Z (Fig. 2A). However, H2A.Z is required for optimal splicing of a subset of ICGs with distinct properties. Notably, among non-RPGs, introns with nonconsensus BP sequences have a significantly stronger splicing defect than those with consensus BP sequences ($P = 0.018$) (Fig. 2A, right). In yeast, the highly conserved canonical BP sequence is UACUAAC, while the sequences most affected by *HTZ1* deletion contain the sequences that differ at the +1 position of the BP sequence: GACUAAC (5), AACUAAC (5), and CACUAAC (4). Neither nonconsensus 5′ splice site (5′SS) nor 3′ splice site (3′SS) sequences show this significantly enhanced dependence on H2A.Z for optimal splicing compared with non-RPG introns with consensus splice sites (Supplemental Fig. S1A, left), reinforcing the connection between H2A.Z and the U2 snRNP, which directly base-pairs with the BP sequence.

We and others have shown previously that defects in splicing are often masked by the rapid turnover of misspliced and unspliced transcripts (Hossain et al. 2011; Kawashima et al. 2014). To determine whether rapid turnover of misspliced transcripts masks splicing defects that occur in *htz1Δ* cells, we performed RNA-seq analysis in cells lacking *HTZ1* in combination with deletion of genes encoding cytoplasmic degradation pathway proteins Xrn1 or Upf1. Xrn1 is a 3′–5′ exonuclease (Larimer and Stevens 1990), and Upf1 is an ATP-dependent RNA helicase involved in nonsense-mediated decay (Ono et al. 2005). Genome-wide profiles of splicing efficiency in *htz1Δ* cells in the degradation mutant background are similar to the wild-type background profile (Fig. 2A,B, left). However, the subset of genes whose splicing is most strongly affected by deletion of *HTZ1* is larger, and splicing defects are often stronger in the degradation mutant backgrounds than the wild-type background, likely because unspliced transcripts are stabilized in the absence of Xrn1 or Upf1 (Fig. 2B). In both the *xrn1Δ* and *upf1Δ* mutant backgrounds, a

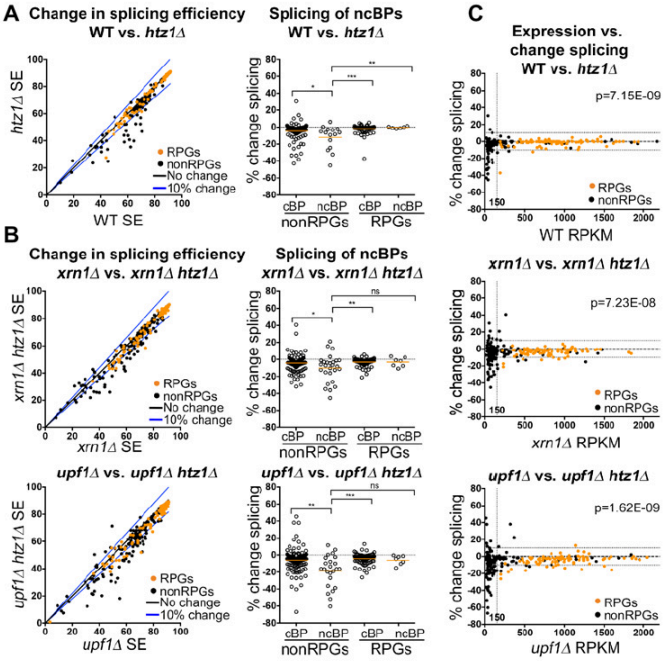

Figure 2. H2A.Z is required for optimal splicing of a subset of ICGs. (*A*, *left*) Distribution in splicing efficiencies of all ICGs upon deletion of *HTZ1*, represented as an *X*–*Y* plot. RPGs are denoted in orange. (*Right*) Distribution of changes in splicing in groups of ICGs characterized by RPGs or non-RPGs and consensus or nonconsensus BPs. (*B*, *left*) Distribution in splicing efficiencies of all ICGs upon deletion of *HTZ1* in either *xrn1*Δ (*top*) or *upf1*Δ (*bottom*) cells, represented as an *X*–*Y* plot. RPGs are denoted in orange. (*Right*) Distribution of changes in splicing in groups of ICGs characterized by RPGs or non-RPGs and consensus or nonconsensus BPs. *P*-values were determined by Mann-Whitney. (*C*) Distribution of changes in splicing efficiency upon deletion of *HTZ1* compared with reads per kilobase per million mapped reads (RPKM) in wild-type (*top*), *xrn1*Δ (*middle*), and *upf1*Δ (*bottom*) cells. The vertical dotted line represents RPKM of 150. The horizontal lines represent 10% change in splicing efficiency. Genes with an RPKM ≤150 are enriched in genes with ≥10% splicing defect (χ^2 test; *P*-values are indicated). (cBP) Consensus BP; (ncBP) nonconsensus BP; (ns) not significant; (*) *P*-value < 0.05; (**) *P*-value < 0.01; (***) *P*-value < 0.001.

significant majority of RPGs exhibits a <5% change in splicing when *HTZ1* is deleted ($P = 0.023$ and $P = 0.032$, respectively). Similar to the wild-type background, the subset of genes whose splicing is most strongly affected in *htz1*Δ is characterized by non-RPGs with nonconsensus BP sequences (Fig. 2B, right; Supplemental Fig. S1A).

RNA-seq analysis revealed 91 ICGs with a splice defect (≥10%) upon deletion of *HTZ1* in at least one background (wild type, *xrn1*Δ, or *upf1*Δ) (Supplemental Fig. S1B). This pool of genes is enriched in introns containing nonconsensus BPs (24 of 91 introns; $P = 0.003$). Of these 91 genes, 23 genes showed decreased splicing in both degradation mutant backgrounds, and 52 genes showed decreased splicing in only the *xrn1*Δ or *upf1*Δ background. It is clear that these degradation pathways can overlap, but there may be additional signals that help determine which pathway is used to remove specific unspliced transcripts.

H2A.Z is deposited in the chromatin in place of the canonical histone H2A. Swr1, a Swi2/Snf2-related ATPase, catalyzes this exchange (Krogan et al. 2003; Kobor et al. 2004; Mizuguchi et al. 2004). Similarly to *HTZ1*, *SWR1* interacts with genes encoding early splicing factors (Supplemental Fig. S2A). Loss of Swr1 leads to a global decrease in H2A.Z occupancy and loss of H2A.Z enrichment at promoters (Mizuguchi et al. 2004; Zhang et al. 2005; Sadeghi et al. 2011). We therefore asked whether Swr1 has effects on splicing similar to those of H2A.Z. To address this question, splicing efficiency of ICGs was analyzed in *swr1*Δ, *swr1*Δ *xrn1*Δ, and *swr1*Δ *upf1*Δ background cells (Supplemental Fig. S2B). Similar to H2A.Z, Swr1 appears to be important for optimal splicing of a subset of genes. Additionally, there is considerable overlap between the splicing efficiency in *swr1*Δ and *htz1*Δ cells (Supplemental Fig. S2C). While a number of genes display better splicing in *swr1*Δ cells as compared with *htz1*Δ cells, these affected genes are, for the most part, the same genes affected by H2A.Z loss (Supplemental Fig. S2D). While loss of Swr1 leads to decreased H2A.Z occupancy at promoters, it does not completely eliminate the H2A.Z in the chromatin, as Swr1-independent H2A.Z incorporation has been observed (Sadeghi et al. 2011). Residual H2A.Z in the chromatin likely accounts for the moderated splice defect in *swr1*Δ as compared with *htz1*Δ cells. Together, these results suggest that the effect of Swr1 on splicing is likely due to its role in H2A.Z exchange.

H2A.Z occupancy is reported to be negatively correlated to transcription and has been implicated in regulating gene expression (Santisteban et al. 2000; Zhang et al. 2005). We therefore asked whether defects in splicing correlate with gene expression. ICGs with strong splicing defects also have relatively low expression (reads per kilobase per million mapped reads [RPKM] <150) in the wild-type or degradation mutant background (Fig. 2C). We considered the possibility that this correlation was due to a bias in our sequencing results or filtering process. To ensure that the results are not due to an artifact of the sequencing data, we analyzed genes that did not pass the minimum-read filter threshold (Supplemental Fig. S3A). We found that changes in splicing of these genes are evenly distributed between increased and decreased splicing efficiency, demonstrating that our filters effectively removed noise and that there was no significant selection bias (Supplemental Fig. S3B). If splicing defects observed in ICGs with low expression are due to stochastic variation, we would expect the distribution of genes with

increased or decreased splicing efficiency to be the same in our filtered data and in the noise. However, we found that lowly expressed ICGs are significantly enriched in genes that have ≥10% decrease in splicing upon loss of H2A.Z as compared with the noise ($P << 0.01$ in all backgrounds) (Fig. 2C).

RT–PCR analysis confirms that genes with nonconsensus splice sites are particularly sensitive to loss of H2A.Z

In order to verify the RNA-seq results, RT–PCR was used to assess the splicing of a pool of candidate genes. Since unspliced pre-mRNA is targeted by both Xrn1 and Upf1 in ways that mask H2A.Z's effect on splicing, we decided to focus on two groups of genes: (1) genes that show intron accumulation in the wild-type, *xrn1*Δ, and *upf1*Δ backgrounds (eight genes) (Supplemental Fig. S1B) and (2) genes that show intron accumulation in both the *xrn1*Δ and *upf1*Δ cell backgrounds (15 genes) (Supplemental Fig. S1B). Of these 23 genes, nine contain introns with at least one nonconsensus splice site (Fig. 3A, in orange).

RT–PCR confirmed the decreased splicing of all eight genes in group 1 in the presence and absence of H2A.Z in wild-type, *xrn1*Δ, and *upf1*Δ cells (Fig. 3B,C). We examined the splicing intermediates of the two-intron gene *SUS1*, whose splicing has been well characterized (Hossain et al. 2009, 2011). *SUS1* is unique not only because it is one of the 10 yeast genes that contain multiple introns but also because its first intron contains both a nonconsensus 5′SS and BP sequence (Fig. 3A). Upon deletion of *HTZ1*, there is modest accumulation of *SUS1* pre-

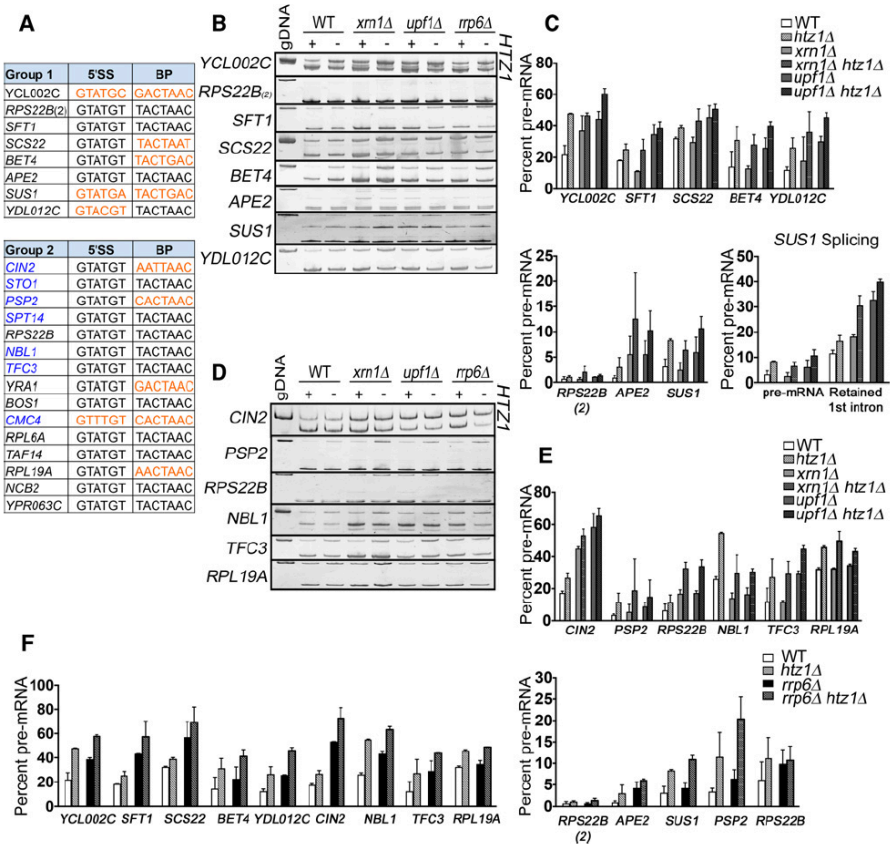

Figure 3. RT–PCR analysis confirms that genes with nonconsensus splice sites are particularly sensitive to loss of H2A.Z. (*A*) Group 1 consists of ICGs whose splicing decreases by ≥10% in the wild-type, *xrn1*Δ, and *upf1*Δ backgrounds. Group 2 consists of ICGs whose splicing decreases by ≥10% in the *xrn1*Δ and *upf1*Δ backgrounds. Genes that did not pass the minimum-read filter in the wild-type background are denoted in blue. Nonconsensus splice sites are denoted in orange. (*RPS22B*) 5′ untranslated region (UTR) intron; (*RPS22B_2*) coding region intron. (*B*) Analysis of group 1 genes by RT–PCR in wild-type, *xrn1*Δ, and *upf1*Δ cells ±*HTZ1*. Products were analyzed on 6% PAGE gels (8% for *SUS1*). Pre-mRNA size is indicated by genomic DNA size. (*C*) Quantification of group 1 RT–PCR unspliced (pre-mRNA) products. (*Bottom right*) Quantification of *SUS1* pre-mRNA and splicing intermediate containing only the second *SUS1* intron. (*D*) Analysis of group 2 genes by RT–PCR in wild-type, *xrn1*Δ, and *upf1*Δ cells ±*HTZ1*. Products were analyzed on 6% PAGE gels. Pre-mRNA size is indicated by genomic DNA size. (*E*) Quantification of group 2 RT–PCR unspliced products. (*F*) Quantification of group 1 and group 2 RT–PCR unspliced products in *rrp6*Δ cells ±*HTZ1*. Quantification graphs represent the average of two independent experiments, and error bars represent the standard deviation (SD). (gDNA) Genomic DNA.

mRNA and strong accumulation of partially spliced (first intron retained) mRNA (Fig. 3C, bottom right). Due to its weak splice sites, the first intron of *SUS1* is more susceptible to H2A.Z loss.

Of the 15 genes in group 2, seven genes did not pass our minimum-read filter in the wild-type cells and were not included in the RNA-seq analysis (Fig. 3A, in blue). It is possible that deletion of *HTZ1* causes decreased splicing of these introns in the wild-type background as well. We therefore used RT–PCR to confirm *htz1*Δ-related splicing defects in group 2 genes in wild-type, *xrn1*Δ, and *upf1*Δ cells (Fig. 3D,E). As expected, upon *HTZ1* deletion, these genes have decreased splicing in not only the degradation mutant background but also the wild-type background.

In a recent report, H2A.Z has been shown to act coordinately with the nuclear exosome, particularly the Rrp6 subunit, to control RNA expression and turnover (Rege et al. 2015). Rrp6 is a 3′–5′ exonuclease that has been implicated in the turnover of unspliced transcripts (Bousquet-Antonelli et al. 2000; Sayani and Chanfreau 2012). To determine whether the nuclear exosome is important for clearing the cell of unspliced transcripts that arise in *htz1*Δ cells, we used RT–PCR to analyze the splicing of our candidate genes in the presence and absence of H2A.Z in *rrp6*Δ cells (Fig. 3F). Deletion of *RRP6* alone results in increased pre-mRNA and, similar to *XRN1* and *UPF1* deletion, stabilizes many unspliced transcripts in *htz1*Δ cells, indicating that the nuclear exosome is important for clearing erroneous unspliced transcripts that arise in *htz1*Δ cells.

Because we found interactions between H2A.Z and components of every major spliceosome complex (Fig. 1A,B), we also examined splicing of our candidate genes in viable double mutants lacking H2A.Z and U1 snRNP factor Mud1 or nineteen complex (NTC) factor Isy1. Consistent with our genetic analyses, deletion of *HTZ1* enhances splicing defects of *mud1*Δ and *isy1*Δ cells (Supplemental Fig. S4A). Intriguingly, while splicing of most intron-containing RPGs is unaffected by *HTZ1* deletion alone, when H2A.Z loss is combined with deletion of splicing factor components, RPG splicing is defective (Supplemental Fig. S4B,C). Most intron-containing RPGs have consensus BP sequences (93%) and are efficiently spliced (Fig. 2A). Thus, it appears that, in general, H2A.Z deletion negatively affects splicing, but this effect is less obvious when splicing is robust. Moreover, these data indicate that H2A.Z generally affects the process of splicing, but BP recognition is particularly susceptible to changes in the splicing environment such that splicing of introns containing nonconsensus BP sequences is inefficient in *htz1*Δ cells even under otherwise optimal conditions.

H2A.Z-mediated splicing defects are not due to changes in spliceosome availability

H2A.Z is reported to be involved in transcriptional regulation and gene expression (Santisteban et al. 2000; Zhang et al. 2005). We therefore considered the possibility that the splicing effect of *HTZ1* deletion was due to altered transcription of a gene involved in splicing. However, RNA-seq analysis shows no significant change in the expression of genes encoding general splicing factors (Chen and Cheng 2012) or spliceosomal snRNAs (Supplemental Table S1; Supplemental Fig. S5A).

It also has been shown that competition between RNAs for spliceosome components alters splicing efficiency. Specifically in *S. cerevisiae*, due to the large number of intron-containing RPGs, perturbations to RPG expression alter the availability of the spliceosome to non-RPG pre-mRNAs (Munding et al. 2013). Therefore, up-regulation of RPG expression could lead to a decrease in splicing of non-RPGs. However, this is not the case, as the RNA-seq results show no significant change in expression of RPGs (Supplemental Fig. S5B).

H2A.Z is enriched around splice sites

H2A.Z is enriched around the TSS of the majority of yeast genes, typically in the +1 and −1 nucleosome flanking the NFR (Ranjan et al. 2013; Gu et al. 2015). However, recent reports indicate that, in *Drosophila*, H2A.Z also demarcates exon boundaries (Weber et al. 2010), while, in humans, a histone variant highly related to H2A.Z is enriched near BPs of introns (Tolstorukov et al. 2012). This suggested to us that H2A.Z's effects on splicing may be a direct result of H2A.Z's positioning relative to splicing-specific gene features in yeast. Using previously published ChIP-seq (ChIP combined with high-throughput sequencing) data (Gu et al. 2015), we confirmed that H2A.Z occupies the nucleosomes flanking the TSS of most ICGs (Fig. 4A,B, left). Additionally, H2A.Z is well positioned over, or just upstream of, the BP sequence and the 3′SS of many ICGs (Fig. 4B). At this point, it is unclear what the mechanism of this increased occupancy of H2A.Z is at particular intron sequences, but it follows a trend similar to other histone enrichment patterns within introns (for review, see Brown et al. 2012; Saldi et al. 2016). In parallel studies in *Schizosaccharomyces pombe*, this pattern of H2A.Z enrichment around splicing signals is also observed (Nissen et al. 2017).

A number of studies found that RPGs are deplete of H2A.Z-containing nucleosomes (Raisner et al. 2005; Zhang et al. 2005; Ranjan et al. 2013; Gu et al. 2015). Consistent with these studies, we observed low H2A.Z occupancy at the TSS, BP sequence, and 3′SS of intron-containing RPGs (Fig. 4A,C). Recently, it has been shown that the preinitiation complex is required for H2A.Z eviction from the chromatin during active transcription (Tramantano et al. 2016). Because RPGs are highly transcribed genes, it is possible that ChIP-seq experiments cannot capture H2A.Z occupancy in these genes due to rapid nucleosome turnover. In fact, depletion of components of the transcription machinery leads to H2A.Z accumulation in RPGs (Tramantano et al. 2016), demonstrating that, although steady-state levels are low, H2A.Z is present in RPGs and could contribute to their efficient splicing (Supplemental Fig. S4).

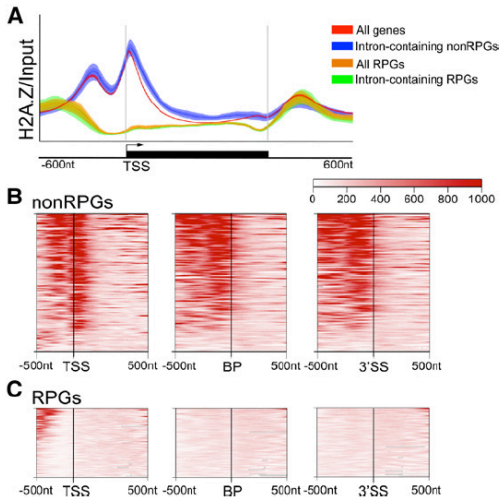

Figure 4. H2A.Z is well positioned near splice sites in non-RPGs. (*A*) H2A.Z ChIP-seq occupancy over input across the transcribed region and 600 nucleotides (nt) upstream of and downstream from the TSS and transcription stop site of all genes, all ICGs, all RPGs, intron-containing RPGs, and intron-containing non-RPGs. Lines represent the average fold enrichment of two biological replicates and 95% CI. The *Y*-axis represents 0–1000 mapped ChIP reads normalized to input. Analysis of data from Gu et al. (2015). (*B*) Hierarchical clustering of H2A.Z-binding profiles of intron-containing non-RPGs around TSSs or splice sites, oriented gene-directionality. (*Left*) Five-hundred nucleotides upstream of and 1000 nt downstream from the TSS. The vertical line indicates the TSS. Five-hundred nucleotides upstream of and 500 nt downstream from the BP sequence (*middle*) or 3′SS (*right*). $n = 147$. Introns found in the 5′ UTR were excluded. (*C*) Hierarchical clustering of H2A.Z-binding profiles of intron-containing RPGs around TSSs or splice sites, oriented gene-directionality. (*Left*) Five-hundred nucleotides upstream of and 1000 nt downstream from the TSS. The vertical line indicates the TSS. Five-hundred nucleotides upstream of and 500 nt downstream from the BP sequence (*middle*) or 3′SS (*right*). $n = 88$. Introns found in the 5′ UTR were excluded. Analysis of data by Gu et al. (2015), including an average of two biological replicates.

Cotranscriptional U2 snRNP rearrangement and downstream recruitment profiles are defective in the absence of H2A.Z

Cotranscriptional recruitment of the spliceosome to the nascent pre-mRNA has been shown to occur in a predictable and stepwise fashion (Kotovic et al. 2003; Gornemann et al. 2005; Lacadie and Rosbash 2005; Tardiff and Rosbash 2006). When spliceosomal rearrangements are perturbed, a lag in snRNP disengagement can be observed (Gornemann et al. 2005; Lacadie and Rosbash 2005; Tardiff and Rosbash 2006). Our previous studies demonstrated that histone acetylation patterns affect the recruitment of the U2 snRNP and alter spliceosomal rearrangements (Gunderson and Johnson 2009; Gunderson et al. 2011). Because ICGs containing nonconsensus BPs were enriched in our RNA-seq analysis and because we observed genetic interactions between *HTZ1* and several components of the U2 snRNP, we first analyzed U2 snRNP recruitment to nascent mRNA. We specifically examined the recruitment of Msl1, the U2B homolog, to two genes with H2A.Z occupancy upstream of the ORF (*ECM33* and *YCL002C)* and one gene deplete of H2A.Z occupancy (*RPL13A)* (Fig. 5A; Gu et al. 2015). The pattern of splicing factor recruitment to *ECM33* has been reported previously (Gornemann et al. 2005; Gunderson and Johnson 2009; Gunderson et al. 2011). *YCL002C* has a nonconsensus 5′SS and BP, and deletion of *HTZ1* leads to a splicing defect in this gene (Figs. 3B, 5B). While deletion of *HTZ1* results in no significant change in the recruitment of Msl1 to the selected genes, there is increased Msl1 enrichment at primer set 4 of *ECM33* and primer set 5 of *YCL002C* (Fig. 5D). This persistent U2 snRNP association suggests decreased U2 snRNP dissociation, and similar occupancy profiles have been interpreted as a defect in spliceosomal rearrangements (Gunderson et al. 2011). Surprisingly, *RPL13A* shows no significant increase in Msl1 in the gene body (Fig. 5D, right). Total protein levels of Msl1 or its interaction partner, Lea1, are unaffected by deletion of *HTZ1* (Supplemental Fig. S6A). This result indicates that H2A.Z's presence in the chromatin is important for the spliceosomal rearrangements that involve the U2 snRNP.

The observed Msl1 recruitment profiles, along with the results from our targeted genetic screen and RNA-seq analysis, suggest a specific role for H2A.Z in U2 snRNP function and/or rearrangements involving the U2 snRNP. However, it is possible that deletion of *HTZ1* acts more generally upon cotranscriptional recruitment or rearrangements of all snRNPs. To determine whether H2A.Z affects events upstream of U2 snRNP recruitment, we examined the recruitment of the U1 snRNP component Prp42 to *ECM33*, *YCL002C*, and *RPL13A*. Deletion of *HTZ1* does not affect Prp42 recruitment profiles to any of our candidate genes (Fig. 5E), suggesting that H2A.Z likely affects spliceosomal rearrangements that occur after U1 snRNP release. Total protein levels of Prp42 are unchanged by loss of H2A.Z (Supplemental Fig. S6B).

We predicted that, because of the stepwise cotranscriptional recruitment of splicing factors, association of splicing factors recruited to the nascent mRNA after U2 snRNP would be negatively impacted by loss of H2A.Z. In fact, there is decreased association of the U5 snRNP representative protein Snu114 with all candidate genes in the absence of *HTZ1* (Fig. 5F). While we observed no change in U2 snRNP occupancy at *RPL13A*, U5 snRNP occupancy is markedly decreased (Fig. 5F). This is consistent with our RT–PCR results in which H2A.Z loss exacerbates RPG splicing defects when the spliceosome is compromised (Supplemental Fig. S4C). H2A.Z likely affects spliceosome dynamics at all ICGs, but, because splicing of RPGs is particularly robust, spliceosome rearrangements do not rely as heavily on H2A.Z's presence in healthy cells. Decreased Snu114 occupancy cannot be attributed to changes in protein expression (Supplemental Fig. S6C). These results suggest that loss of H2A.Z increases the association of the U2 snRNP and reduces the

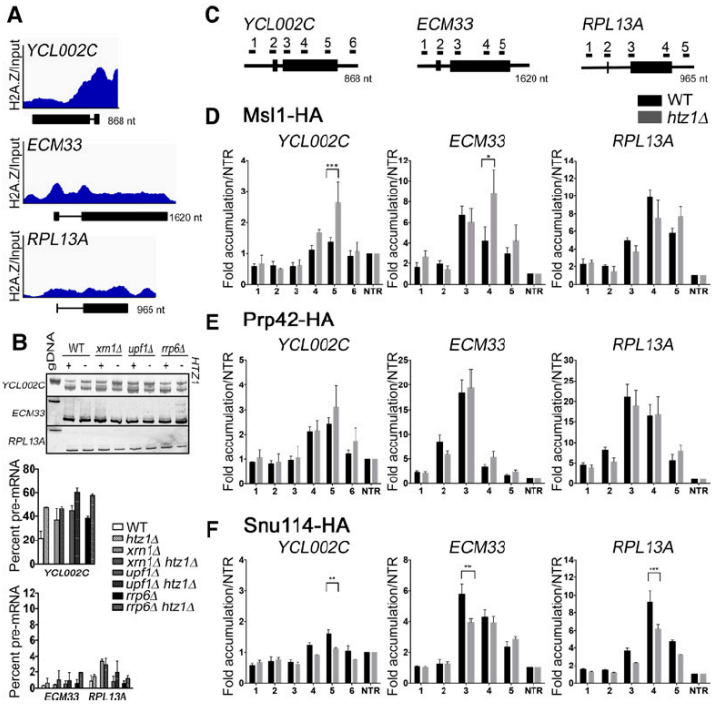

Figure 5. Cotranscriptional U2 snRNP recruitment is defective in the absence of H2A.Z. (*A*) Integrative Genome Viewer track view of H2A.Z occupancy over input by ChIP-seq across the ORF of *YCL002C* (*top*), *ECM33* (*middle*), and *RPL13A* (*bottom*). The *Y*-axis represents 0–1000 mapped ChIP reads normalized to input. A schematic of each gene is included *below* each occupancy profile. Analysis of data from Gu et al. (2015). (*B*, *top*) Analysis of *YCL002C*, *ECM33*, and *RPL13A* genes by RT–PCR in the presence and absence of *HTZ1*. Products were analyzed on 6% PAGE gels. Pre-mRNA size is indicated by genomic DNA size. (*Bottom*) Quantification of RT–PCR products. Graphs represent the average of two independent experiments, and error bars represent the SD. (*C*) Schematic of ICGs *YCL002C*, *ECM33*, and *RPL13A*. Underlined numbers represent amplicons generated by each primer set used in this experiment. (*D*) Occupancy of Msl1 at each region of *YCL002C* (*left*), *ECM33* (*middle*), or *RPL13A* (*right*) relative to the nontranscribed region in wild type or *htz1*Δ. Graphs represent the average of six (wild type) or three (*htz1*Δ) independent experiments, and error bars represent the standard error of the means (SEM). *P*-values for each primer set were determined by Student's *t*-test. Significant values are indicated. (*E*) Occupancy of Prp42 at each region candidate gene relative to the nontranscribed region in wild type or *htz1*Δ. Graphs represent the average of four independent experiments, and error bars represent the SEM. *P*-values for each primer set were determined by Student's *t*-test. No significant values were found. (*F*) Occupancy of Snu114 at each region of candidate genes relative to the nontranscribed region in wild type or *htz1*Δ. Graphs represent the average of three independent experiments, and error bars represent the SEM. *P*-values for each primer set were determined by Student's *t*-test. Significant values are indicated. (gDNA) Genomic DNA. (*) *P*-value < 0.01; (**) *P*-value < 0.001; (***) *P*-value < 0.0001.

association of downstream splicing factors. These results are consistent with a role for H2A.Z in efficient spliceosomal rearrangements.

RNAPII kinetics are altered upon loss of H2A.Z

Because we found that H2A.Z is enriched around splice sites of many ICGs, it is possible that H2A.Z promotes splicing through physical interactions with the spliceosome, perhaps through a chromatin-associated adaptor protein. Indeed, such physical interactions between splicing factors and histones have been reported (Sims et al. 2007; Luco et al. 2010), and, in humans, it has been reported that H2A.Z weakly binds the SF3B complex (Tolstorukov et al. 2012). However, we found no direct interactions between H2A.Z and tested splicing factors (Prp43, Snu66, Prp4, Lea1, Msl1, Snu114, and Cus1) (data not shown).

Cotranscriptional splicing is spatially and temporally linked to transcription, and therefore changes in RNAPII elongation rates and pausing can perturb the precisely timed rearrangements of the spliceosome and alter splicing outcomes (de la Mata et al. 2003; Howe et al. 2003; Carrillo Oesterreich et al. 2010). As H2A.Z has roles in the regulation of both transcription initiation and elongation, we considered the possibility that H2A.Z helps coordinate the processes of transcription and splicing (Santisteban et al. 2000, 2011; Zhang et al. 2005; Wan et al. 2009; Li et al. 2012; Weber et al. 2014; Subramanian et al. 2015; Rudnizky et al. 2016).

In order to determine whether loss of H2A.Z affects RNAPII kinetics in such a way that it could alter spliceosome rearrangements, we first examined the recruitment of Rpb3, the large subunit of RNAPII, to *YCL002C*, *ECM33*, and *RPL13A*. While Rpb3 recruitment to the promoter is unchanged in *htz1*Δ cells, Rpb3 occupancy through the gene body of *ECM33* and *RPL13A* is decreased in *htz1*Δ cells compared with wild-type cells (25%–31% decrease for locations 2–5) (Fig. 6B). We observed a small but consistent decrease of Rpb3 occupancy in *YCL002C* (11%–16% decrease for all locations) (Fig. 6B, left). *YCL002C* is a lowly expressed gene with generally low Rpb3 occupancy, and we believe that this makes it difficult to resolve the differences in polymerase enrichment. In order to determine whether changes in RNAPII occupancy are specific to ICGs or are a general outcome of *HTZ1* deletion, we examined Rpb3 recruitment to an intronless gene, *PMA1*. We found that, similar to the candidate ICGs, Rpb3 occupancy is reduced in *PMA1* upon *HTZ1* deletion (17%–36% decrease for all locations) (Fig. 6B, right). Unlike *ECM33* and *RPL13A*, Rpb3 occupancy is decreased at primer set 1 of *PMA1*. This could be due to primer set 1 amplifying a region just downstream from the TSS. However, this may also indicate decreased Rpb3 recruitment to the promoter of *PMA1* in

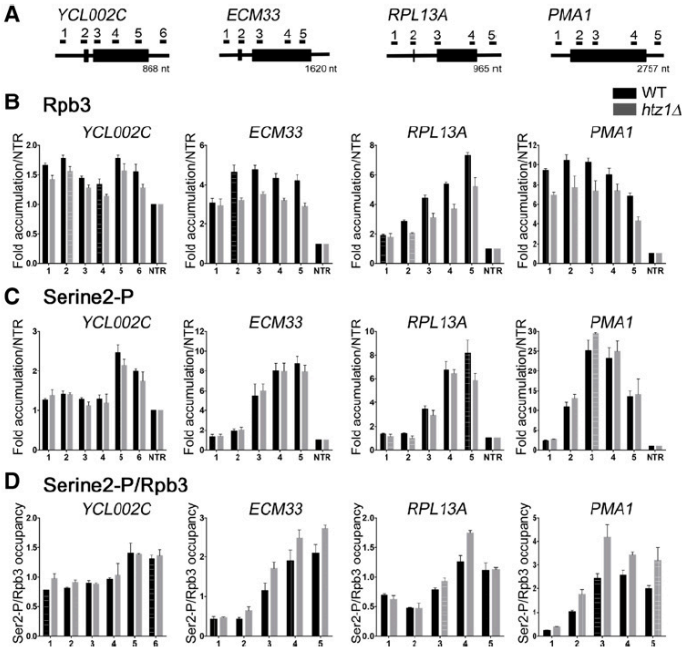

Figure 6. RNAPII elongation kinetics are altered in the absence of H2A.Z. (*A*) Schematic of ICGs *YCL002C*, *ECM33*, and *RPL13A* and intronless gene *PMA1*. (*B*) Occupancy of Rpb3 at each region of *YCL002C* (*left*), *ECM33* (*middle left*), *RPL13A* (*middle right*), or *PMA1* (*right*) relative to the nontranscribed region in wild type or *htz1*Δ. Graphs represent the average of three independent experiments, and error bars represent the SEM. (*C*) Ser2 phosphorylation state of the RNAPII C-terminal domain at each region of candidate genes relative to the nontranscribed region in wild type or *htz1*Δ. Graphs represent the average of three independent experiments, and error bars represent the SEM. (*D*) Ser2 phosphorylation state (from *C*) normalized to Rpb3 (from *B*) occupancy at each region of candidate genes.

*htz1*Δ cells. Total protein levels of Rpb3 are unchanged by loss of H2A.Z (Supplemental Fig. S6D). These results indicate that loss of H2A.Z reduces RNAPII occupancy and influences transcription elongation. While additional changes such as polymerase pausing or processivity cannot be ruled out, decreased RNAPII occupancy in *htz1*Δ cells likely reflects slowed transcription elongation. Not only does slow elongation correlate with decreased RNAPII occupancy (Mason and Struhl 2005; Garcia et al. 2010, 2012; Malik et al. 2017), but H2A.Z deletion has been shown previously to lead to a decreased rate of elongation in both yeast and mammalian cells (Santisteban et al. 2011; Rudnizky et al. 2016). Therefore, our results are consistent with past findings that H2A.Z promotes efficient transcription elongation and that H2A.Z deletion leads to changes likely including, but not limited to, slow elongation rate.

RNAPII contains a unique C-terminal domain (CTD) consisting of sequence repeats that are phosphorylated in a predictable manner during transcription elongation. Typically, the polymerase is hypophosphorylated at the promoter and, upon initiation, becomes phosphorylated at Ser5. Ser5 phosphorylation (Ser5-P) declines near the 3′ end of the transcript in favor of Ser2-P (Komarnitsky et al. 2000; Alexander et al. 2010). This dynamic phosphorylation has been implicated in regulating transcription elongation kinetics, and Ser2-P in particular is a hallmark of the elongating polymerase (for review, see Hsin and Manley 2012). Because perturbations to CTD phosphorylation reflect changes in active elongation (Garcia et al. 2010; Allepuz-Fuster et al. 2014; Davidson et al. 2014), we analyzed Ser2-P states on our candidate genes. Although *HTZ1* deletion results in decreased RNAPII occupancy across candidate genes, there is increased Ser2-P on polymerases bound to the 3′ ends of *ECM33*, *RPL13A*, and *PMA1* in *htz1*Δ cells (Fig. 6C,D). Because polymerase occupancy of *YCL002C* is low compared with other candidate genes, we were not able to observe small changes in Ser2-P on this gene (Fig. 6C,D, left). We found that Ser2-P begins to accumulate earlier toward the 5′ end in the gene bodies of *YCL002C*, *ECM33*, and *PMA1* in *htz1*Δ cells as compared with wild-type cells (Supplemental Fig. S7B). These findings are similar to past studies that have shown that transcription elongation defects correlate with increased Ser2-P (Garcia et al. 2010, 2012), Hence, it appears that increased pausing or slower elongation in cells lacking H2A.Z may allow Ser2-P accumulation earlier in transcription.

Deletion of a general elongation factor exacerbates H2A.Z-mediated splice defects and affects U2 snRNP recruitment profiles

We suspected that if H2A.Z affects splicing via its role in transcription elongation, we might be able to observe functional interactions between H2A.Z and elongation factors. Consistent with this, we observed slow growth in cells lacking both H2A.Z and the general elongation factor Dst1 (TFIIS) (Supplemental Fig. S8A). Dst1 promotes elongation and prevents backtracking of stalled polymerase elongation complexes (for review, see Freedman et al. 2013). In the absence of Dst1, RNAPII elongation is compromised, and polymerase pause sites are altered, particularly under transcriptional stress (Mason and Struhl 2005; Churchman and Weissman 2011). Intriguingly, deletion of Dst1 can also negatively affect splicing and

lead to aberrant intron retention (Lacadie et al. 2006; Carey 2015). While loss of Dst1 alone does not decrease splicing of our candidate genes, deletion of *DST1* in *htz1*Δ cells exacerbates H2A.Z-mediated splice defects, and we observed increased pre-mRNA levels in double mutants (Supplemental Fig. S8B). The *SUS1* splicing intermediate that retains the nonconsensus first intron, but not the unspliced pre-mRNA, accumulates in *dst1Δ htz1*Δ cells, suggesting that, similar to *htz1*Δ, splicing of introns with nonconsensus BP sequences is particularly affected in the double mutant (Supplemental Fig. S8B, right).

Deletion of Dst1 not only decreases polymerase processivity (Mason and Struhl 2005) but was also found, in a genome-wide study, to decrease RNAPII occupancy by 1.6-fold, on average, compared with wild-type cells (Ghavi-Helm et al. 2008). Because Dst1 loss exacerbates splicing defects in *htz1*Δ cells and generally decreases RNAPII occupancy, we asked whether Dst1 could affect spliceosome rearrangements similar to H2A.Z. Consistent with our observations in *htz1*Δ cells, enrichment of the U2 snRNP factor Msl1 is increased at *YCL002C* in *dst1*Δ cells (Supplemental Fig. S8D, left). While Dst1 and H2A.Z likely affect transcription elongation in different ways, this supports a model in which elongation defects can lead to changes in U2 snRNP occupancy patterns.

Depletion of disassembly factor Prp43 can suppress H2A.Z-mediated splice defects

Our findings that H2A.Z affects spliceosome rearrangements and transcription elongation suggest that the kinetics of transcription and splicing are well coordinated. We suspect that, in the absence of H2A.Z, spliceosome kinetics are disrupted by changes in transcription elongation, and stalled spliceosomes are disassembled while pre-mRNA is released. Prp43 is a DEAH-box helicase that has functions in ribosome biogenesis as well as spliceosome disassembly (Arenas and Abelson 1997; Leeds et al. 2006). Prp43 not only catalyzes disassembly upon completion of splicing (Arenas and Abelson 1997) but can also disassemble spliceosomes when splicing is slowed (Koodathingal et al. 2010; Koodathingal and Staley 2013). Intriguingly, deletion of *HTZ1* suppresses the growth defect of *prp43*^{DAmP} cells (Fig. 7A). In this strain, the 3′ untranslated region (UTR) of *PRP43* is disrupted with an antibiotic resistance cassette, which leads to decreased RNA expression (Supplemental Fig. S9A). Surprisingly, despite the severe growth defect, we did not observe a significant splicing defect for our candidate genes when Prp43 expression was decreased (Fig. 7B). This suggests that the Prp43 functions outside of splicing are significant contributors to the growth defect of *prp43*^{DAmP} cells. Interestingly, decreased Prp43 partially suppresses the splicing defect observed in *htz1*Δ cells, indicating that spliceosome disassembly is at least partially responsible for pre-mRNA accumulation in cells lacking H2A.Z (Fig. 7B; Supplemental Fig. S9B). We next analyzed splicing genome-wide to determine to what extent Prp43 depletion suppresses H2A.Z-mediated splice defects. Splicing is largely unaffected by Prp43 depletion alone; however,

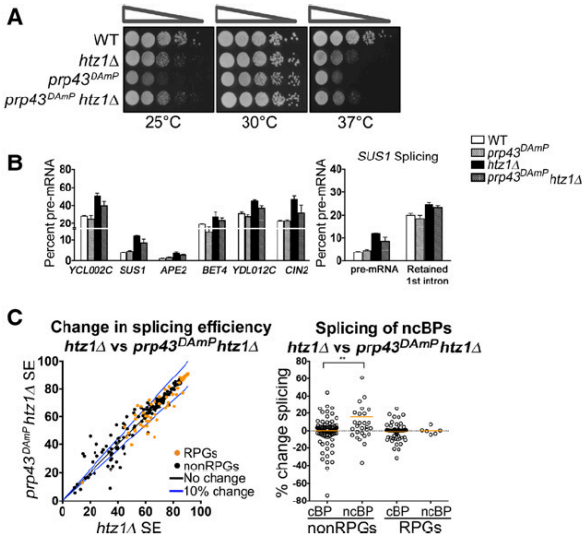

Figure 7. Decreased spliceosome disassembly can suppress H2A.Z-mediated splice defects. (*A*) Serial dilution assay of double mutant *prp43*^{DAmP} *htz1Δ*. Cells were grown at 30°C in YPD + G418 liquid medium until the desired OD_{600} was obtained. Cells were spotted as a 10-fold dilution onto YPD + G418 plates and incubated for 2 d at 25°C, 30°C, or 37°C. (*B*, *left*) Quantification of pre-mRNA of candidate genes by RT–PCR in wild-type and *prp43*^{DAmP} cells ±*HTZ1*. (*Right*) Quantification of *SUS1* RT–PCR pre-mRNA and splicing intermediate containing only the second *SUS1* intron. Quantification graphs represent the average of two to three independent experiments, and error bars represent the SD. (*C*, *left*) Distribution in splicing efficiencies of all ICGs upon deletion of *HTZ1* in *prp43*^{DAmP} cells, represented as an *X*–*Y* plot. RPGs are denoted in orange. (*Right*) Distribution of changes in splicing in groups of ICGs characterized by RPGs or non-RPGs and consensus or nonconsensus BPs. (cBP) Consensus BP; (ncBP) nonconsensus BP. (**) *P*-value < 0.01.

there are subsets of ICGs whose splicing efficiency increases or decreases in *prp43*^{DAmP} cells, suggesting gene-specific sensitivity to Prp43 depletion (Supplemental Fig. S9C). Consistent with the results shown in Figure 7B, we found that Prp43 depletion in *htz1*Δ cells improves splicing in a subset of ICGs (Fig. 7C left). The pool of genes in which splicing is most improved by Prp43 depletion (≥10%) is significantly enriched with introns containing a nonconsensus BP ($P = 0.005$). Additionally, among non-RPGs, splicing of introns containing a nonconsensus BP sequence is significantly more improved by Prp43 depletion than splicing of those with consensus BP sequences ($P = 0.01$) (Fig. 7C right). Consistent with our observations in *htz1*Δ cells, introns with nonconsensus BPs are more sensitive to Prp43 depletion than those with nonconsensus 5′SSs or 3′SSs (Supplemental Fig. S9D). Together, these data suggest that when rearrangements involving the U2 snRNP are defective or slowed in *htz1*Δ cells, decreased disassembly may allow more time for spliceosome rearrangements to occur.

Overall, these results are consistent with a model in which compromised elongation leads to a splicing defect.

In the case of *htz1*Δ, this defect contributes to defects in U2 snRNP rearrangements and downstream snRNP recruitment. Prp43 is able to recognize and disassemble spliceosomes with defective rearrangement, leading to the release of unspliced pre-mRNA in *htz1*Δ cells. While genes with robust splicing are refractory to these changes in the kinetics of spliceosome rearrangements, those with weak splice sites are unable to splice efficiently. These results highlight an important, albeit underappreciated, feature of cotranscriptional splicing: Compromised transcription elongation does not necessarily provide a "window of opportunity" to resolve splicing defects, but rather, kinetics of transcription elongation and splicing are optimally coordinated to promote splicing. Specific factors such as H2A.Z appear to ensure the appropriate tuning of this coordination to promote splicing for subsets of introns.

Discussion

An ever-growing body of work has established that transcription and RNA processing are spatially and temporally coordinated. Because the spliceosome acts upon nascent mRNA while the transcript is associated with the elongating polymerase, the process of splicing takes place in the context of the transcription machinery and the chromatin it engages. Here we demonstrate that the histone variant H2A.Z plays a novel role in the process of cotranscriptional splicing. Consistent with published studies from the Pleiss and Stevens laboratories (Albulescu et al. 2012; Sorenson and Stevens 2014), we found many genetic interactions between *HTZ1* and genes encoding splicing factors. In particular, mutations to U2 snRNP components render cells reliant on H2A.Z for viability. Additionally, H2A.Z is necessary for optimal splicing of many endogenous ICGs, particularly when introns contain weak splice sites. Furthermore H2A.Z facilitates polymerase elongation and ensures appropriate cotranscriptional spliceosome rearrangements. Finally, decreased expression of an elongation factor or a spliceosome disassembly factor modulates the cells sensitivity to the presence of H2A.Z. Our studies support a role for H2A.Z in coordinating the processes of transcription and splicing: H2A.Z regulates transcription elongation, thereby affecting downstream spliceosome dynamics on ICGs.

H2A.Z affects kinetics of polymerase elongation

Our experiments reveal that loss of H2A.Z results in decreased polymerase occupancy across our candidate genes, suggesting that H2A.Z normally promotes RNAPII elongation (Fig. 6; Supplemental Figs. S7, S8). Although our experiments do not directly measure elongation rate, there are several lines of evidence to support a role for H2A.Z in facilitating efficient elongation. The presence of nucleosomes provides a substantial barrier to transcribing polymerase complexes, and RNAPII must overcome this barrier to access the DNA and efficiently transcribe mRNA (for review, see Petesch and Lis 2012). Because H2A.Z is less stably associated with DNA, exchange of canonical histone H2A with variant H2A.Z facilitates nucleosome eviction and helps lower this transcriptional barrier (Zhang et al. 2005; Weber et al. 2014). In fact, using an in vivo run-off assay, Santisteban et al. (2011) show that H2A.Z loss decreases the rate of elongation across the ORF of a representative gene. Similar decreases in elongation rate have been observed in mammalian systems (Rudnizky et al. 2016). Additionally, we found that CTD Ser2-P accumulates closer to the TSS and remains high throughout the body of candidate genes in *htz1*Δ cells (Fig. 6D; Supplemental Fig. S7B). These findings are similar to past studies that have shown transcription elongation defects correlate with increased Ser2-P. In yeast, deletion of transcription coactivator Sub1 decreases elongation rate and increases total Ser2-P (Garcia et al. 2010, 2012), while, in human cells, increased polymerase pausing leads to Ser2-P accumulation (Davidson et al. 2014), suggesting that Ser2-P levels correlate with the time RNAPII is engaged with the DNA. Therefore, increased and premature Ser2-P in *htz1*Δ cells may reflect polymerase elongation defects. While our results are consistent with past findings that H2A.Z loss results in slowed elongation, we cannot rule out the possibility that H2A.Z influences polymerase kinetics in additional ways, such as altered pausing, backtracking, and/or processivity. Although we did not observe physical interactions, we also cannot rule out that contact between H2A.Z and components of the splicing machinery may contribute to H2A.Z's effects on splicing. In any case, the evidence described here and elsewhere that deletion of H2A.Z negatively impacts elongation and that further compromising elongation (as in *dst1*Δ *htz1*Δ cells) further impairs splicing suggests that the kinetics of transcription and splicing are intimately coordinated and that H2A.Z is important for this coordination.

How do changes in polymerase elongation affect spliceosome dynamics?

Growing evidence supports a model in which splicing is kinetically coupled to transcription (Merkhofer et al. 2014). Several studies in yeast suggest that the polymerase pausing can be a "checkpoint" for spliceosome assembly, and splicing catalysis coincides with polymerase elongation (Alexander et al. 2010; Carrillo Oesterreich et al. 2011; Chathoth et al. 2014; Oesterreich et al. 2016). It has also been proposed that changes in polymerase elongation affect the "window of opportunity" available for nascent transcripts to be spliced, and slower elongation increases this available window (Braberg et al. 2013; Dujardin et al. 2014; Oesterreich et al. 2016). Nonetheless, the rates of spliceosome rearrangements are also finely tuned, and slow rearrangements provide the opportunity for spliceosome disassembly and release of unspliced RNAs (Koodathingal et al. 2010; Koodathingal and Staley 2013). Recent mammalian studies demonstrate that an optimal elongation rate is required for proper pre-mRNA splicing. Both increased and decreased elongation rates

can alter alternative splicing and intron retention, indicating that transcription and splicing are coupled in a "Goldilocks-like phenomenon" (Fong et al. 2014). In yeast, results from splicing analyses in polymerase trigger-loop mutants show that, while splicing of some genes benefit from slowed elongation, numerous genes are more poorly spliced when the polymerase is slow (Braberg et al. 2013). Intriguingly, the combination of "slow polymerase" RNAPII mutations with deletion of H2A.Z or Swr1 renders cells very sick (Braberg et al. 2013). Additionally, we found that deletion of the general elongation factor Dst1, which can negatively impact splicing outcomes (Lacadie et al. 2006; Carey 2015), results in increased U2 association with nascent pre-mRNA, indicating that elongation defects may lead to aberrant spliceosomal rearrangements (Supplemental Fig. S8D). These observations suggest that the timing of polymerase elongation and pausing can have important implications for the fate of the RNA. H2A.Z-mediated splice defects do not entirely mimic those observed in slow polymerase mutants, suggesting that H2A.Z likely influences transcription elongation in more nuanced ways than altering rate alone. Our data suggest a model in which deletion of H2A.Z alters elongation such that the combined effects of poor splice site recognition and RNAPII elongation defects have a deleterious impact on splicing. As a result, spliceosomes are disassembled, leading to release of unspliced products and, ultimately, RNA degradation by nuclear and cytoplasmic machineries. H2A.Z helps coordinate the kinetics of transcription and splicing to ensure proper splicing outcomes.

A subset of DEAD-box and DEAH-box helicases hydrolyzes ATP to drive spliceosomal rearrangements and disassembly and has been proposed to act as "molecular clocks" (Koodathingal and Staley 2013). In particular, DEAH-box helicases Prp16, a factor that ensures splicing fidelity, and Prp43, a disassembly factor, help determine the fate of weak intron substrates when splicing is stalled. Prp16 can recognize and reversibly reject suboptimal slowly spliced substrates to either facilitate proofreading of splice sites or trigger spliceosome disassembly and subsequent degradation of unspliced transcripts (Koodathingal et al. 2010; Koodathingal and Staley 2013). Interestingly, the presence of Prp16 prevents binding of the NTR complex (Chen et al. 2013), which recruits the disassembly factor Prp43 to help mediate spliceosome disassembly. The balance of Prp16 and Prp43 therefore helps determine the fate of the nascent mRNA. Unexpectedly, despite the strong growth defect, splicing of the majority of ICGs in cells containing a hypomorphic Prp43 allele is unaffected, suggesting that decreased Prp43 expression disproportionately affects nonspliceosomal functions of Prp43 (Fig. 7B; Supplemental Fig. S9C). Indeed, Prp43 largely localizes to the nucleolus, where it has functions in ribosome biogenesis (Combs et al. 2006). However, decreased Prp43 expression partially suppresses splicing defects and preferentially improves splicing of introns containing nonconsensus BP sequences in *htz1*Δ cells, suggesting that decreased spliceosome disassembly allows more time for spliceosome rearrangements to occur before RNA is released (Fig. 7B,C). Consistent with these results, the Guthrie laboratory (Nissen et al. 2017) recently found that Prp43 overexpression in *htz1*Δ cells leads to a synthetic growth defect in *S. pombe*. Additionally, they show that Prp16 overexpression suppresses defective splicing caused by H2A.Z deletion (Nissen et al. 2017). It has been shown that Prp16 enables alternative branch site selection; thus, although Prp16 normally antagonizes stalled spliceosomes, excess Prp16 may protect the nascent mRNA by outcompeting disassembly factors and promoting resampling of weak splice sites (Chen et al. 2013; Semlow et al. 2016). Therefore, Prp16 overexpression is expected to have an outcome similar to that of decreased Prp43 expression, favoring splice site resampling over the discard pathway.

We propose that H2A.Z functions to coordinate the kinetics of transcription elongation and spliceosome rearrangements to promote efficient splicing. In the absence of H2A.Z, polymerase elongation is defective and therefore alters the availability of the nascent mRNA to the spliceosome, ultimately altering splicing kinetics. Prp16 and Prp43 may act as intrinsic timing mechanisms that recognize slowed or stalled spliceosomes and target them for splice site resampling or disassembly and the subsequent release of unspliced pre-mRNA. Decreased Prp43 or increased Prp16 allows for decreased reliance on H2A.Z to provide precise coordination of splicing with transcription elongation.

Materials and methods

Yeast strains, media, and DNA constructs

All *S. cerevisiae* strains used in this study are listed in Supplemental Table S2. Strains described in Supplemental Table S2 are in the BY4743 strain background with the exception of the Lea1-HA, Msl1-HA, and Snu114-HA strains used for ChIP, which were provided by Karla Neugebauer. All strains were propagated according to standard procedures in either YPD (1% yeast extract, 2% peptone, 2% dextrose) or the appropriate selective medium.

For deletion of *HTZ1* in *rrp6*Δ and LG1 strains, deletion of genes at their endogenous loci was performed using standard PCR-based homologous recombination while preserving the endogenous promoters (Longtine et al. 1998; Goldstein and McCusker 1999). Deletions were confirmed by whole-cell extract and immunoblot with anti-HTZ1 (Abcam, ab4626).

For all other strains, standard methods for mating, sporulation, transformations, and tetrad analysis were used as described in Amberg et al. (2005). The genotype of each viable spore was confirmed via PCR. Plasmids used in this study are listed in Supplemental Table S3.

Generation of HTZ1 *backup plasmid*

The *HTZ1* gene along with 450 base pairs upstream of and downstream from *HTZ1* was PCR-amplified from *S. cerevisiae* genomics using the primers Htz1InFusion-F and Htz1InFusion-R (Supplemental Table S2). Restriction enzyme cleavage sites for HinDIII were introduced into both primers. PCR products were digested with HinDIII and cloned into pRS316 (*URA3*) using the InFusion Cloning HD Plus system (Clontech). Selected clones were verified by sequencing. Plasmids were transformed into

*htz1*Δ cells, and expression of Htz1 was verified by whole-cell extract and immunoblot with anti-HTZ1 (Abcam, ab4626).

Viability assay/dilution series

For growth analysis of *msl1*Δ and *lea1*Δ strains containing a centromeric pRS316 (*URA3*) plasmid, strains were grown overnight in SC−URA liquid medium at 30°C. Cells were diluted to an OD_{600} of 0.1 in 5 mL of SC−URA medium and incubated at 30°C until all strains reached early log phase. A 10-fold serial dilution of each strain was spotted onto SC−URA plates or 5-FOA plates to select for plasmid loss and incubated at 25°C, 30°C, or 37°C. The SC−URA plates were incubated for 2 d. The 5-FOA plates were incubated for 4 d.

For growth analysis of viable double mutants, strains were grown overnight in YPD liquid medium at 30°C. Cells were diluted to an OD_{600} of 0.1 in 5 mL of YPD and incubated at 30°C until all strains reached early log phase. A 10-fold serial dilution of each strain was spotted onto YPD plates and incubated for 2 d at 25°C, 30°C, or 37°C. For $prp43^{DAmP}$ strains, cells were grown in liquid YPD + G418 and plated on YPD + G418 for growth.

RNA-seq library preparation and alignment

RNA-seq libraries were prepared using an Illumina Truseq V3 kit and ribosomal RNA depletion. Sequence reads were aligned to SacCer3 and spliced transcripts from the Ares Lab Yeast Intron Database version 3 (Grate and Ares 2002) in a single step using STAR (Dobin et al. 2013). Only the highest-scoring alignments for each read were kept, allowing for a single tie at most. Gene Expression Omnibus accession numbers are as follows: GSE97416 and GSE94404:GSM2474880 (for wild-type replicate #2).

RNA-seq RPKM and splicing efficiency calculation

RPKMs were computed for each gene by dividing the total number of reads that aligned entirely within the gene's exon boundaries by the gene's total exon length in kilobase pairs per million mapped reads. Reads within ICGs were categorized as exonic, spliced, or unspliced. Exonic reads were those that mapped entirely within a single exon, as defined by the Ares Lab Yeast Intron Database. Spliced reads were those that aligned with a gap that corresponded to an annotated intron, and unspliced reads mapped partially within an exon and partially within an intron with no gap. Spliced and unspliced read counts were normalized by dividing each count value by the number of unique alignment positions that were able to contribute to the total. For spliced reads, this normalization value was the length of the read minus 1 for every intron. For unspliced read counts, this was the length of the intron plus the read length minus 1. Splicing efficiency for each intron was calculated as normalized spliced counts divided by the sum of the normalized spliced and normalized unspliced counts.

RT–PCR analysis and quantification

Cells were grown in YPD medium to an OD_{600} between 0.4 and 0.7. For $prp43^{DAmP}$ strains, cells were grown in YPD + G418. Total RNA was isolated from 10 mL of cells using a hot phenol extraction method and dissolved in 100 µL of diethylpyrocarbonate (DEPC)-treated water. Ten micrograms to 20 µg of RNA was DNase-treated (Roche), and treated RNA concentration was measured by spectrophotometer. Two micrograms to 4 µg of RNA was used to make cDNA using the Maxima first strand cDNA synthesis kit (Fermentas). cDNA was diluted 1:20 and used for PCR. To detect splicing isoforms, primers flanking the intronic sequences were used for 27-cycle PCR using 1 µL of diluted cDNA. PCR products were diluted 1:5 and run on a 6% TBE polyacrylamide gel. *SUS1* products were run on an 8% TBE polyacrylamide gel. Gels were stained with SYBR Green (Sigma), and images were captured using Image Lab (Bio-Rad). Bands were quantified as percent total of band intensity using Image Lab software.

ChIP-seq analysis

ChIP-seq reads were obtained from Gu et al. (2015) and converted to FastQ format using the NCBI Sequence Read Archive (SRA) toolkit. Contaminating adapter sequences were trimmed, and Bowtie2 was used to align the FastQ reads of two replicates to sacCer3 with only one reported alignment (-k 1). Genomic track files from immunoprecipitation and input alignments were created using SAMTools, BEDTools, and the University of California at Santa Cruz bedgraphToBigWig utility. After the input and immunoprecipitation pileup tracks were normalized for differential read count, a ratio track was created by dividing the normalized immunoprecipitation track by the normalized input track.

Metagenes and heat maps were plotted using the R package seqPlots (http://github.com/przemol/seqplots). For metagenes, transcripts were scaled to 1000 nucleotides (nt) between the TSS and transcription termination site (TTS). For metagenes across ORFs, transcripts were scaled to 1000 nt between the TSS and TTS. Metagenes were also plotted for 600 nt upstream of the TSS as well as 600 nt downstream from the TTS and scaled 1:1. Heat maps were plotted of fixed distances upstream of and downstream from TSS, BP, and 3′SS sequences, separately for intron-containing RPGs and non-RPGs.

ChIP and quantitative PCR

Cells were grown in YPD to an OD_{600} between 0.5 and 0.7 and then cross-linked for 15 min at room temperature with formaldehyde to a final concentration of 1%. Cross-linking was quenched for 5 min at room temperature with glycine to a final concentration of 125 mM. Cells were disrupted with 0.5-mm glass beads for 40 min at 4°C. To shear chromatin for Msl1 samples, lysates were sonicated for a total of 3 min and 20 sec at 15% intensity (10 sec on and 15 sec off on ice). For all other samples, lysates were sonicated for a total of 2 min and 30 sec. After sonication, lysates were cleared by centrifugation. For Msl1, Prp42, and Snu114, samples were then used for immunoprecipitation with anti-HA Y11 (Santa Cruz Biotechnology). For Rpb3 and Ser2 samples, samples were used for immunoprecipitation with anti-Rpb3 (BioLegend) and anti-phospho-S2 (Abcam), respectively. After immunoprecipitation, samples were washed and incubated overnight at 65°C to reverse cross-linking.

All samples were incubated with Proteinase K (Sigma) and RNase A (Ambion) followed by purification using a PCR product purification kit (Qiagen).

DNA samples were then analyzed by real-time PCR. Input DNA was diluted 1:10, and 1 µL of this was used in a 20-µL (for Msl1 and Prp42) or 10-µL (for Snu114, Ser-2, and Rpb3) reaction volume. For ChIP DNA, samples were diluted 1:2, and 1 µL of this was used in a 20- or 10-µL reaction volume. Reactions consisted of 1× Perfecta SYBR Green master mix (Quanta Biosciences) and 0.5 µL of primers. Real-time PCR was performed using a CFX96 touch system (Bio-Rad). All samples were run in technical duplicate for each independent experiment.

For quantification, standard curves were generated for each primer set, and DNA concentration for each input and ChIP sample

was calculated. ChIP values were divided by the input, and these values were divided by the nontranscribed control and expressed as fold accumulation over the nontranscribed control. Reported values are averages of three or more independent experiments, and error bars represent the standard error of the mean.

Acknowledgments

This work was supported by grants to T.L.J. from the National Institute of General Medical Sciences (GM-085474 and U01 HG007912), and grants to T.L.K. from the Research Corporation for the Advancement of Science (Cottrell College Science award no. 20186) and the National Institutes of Health (R15GM122026). This work was also supported by the Cellular and Molecular Biology Training Program Ruth L. Kirschstein National Research Service Award (GM007185) (awarded to L.T.N.) and the Whitcome Predoctoral Fellowship in Molecular Biology (awarded to L.T.N. and S.V.). We also acknowledge support from a Quantitative and Computational Biosciences (QCB) Collaboratory Post-doctoral Fellowship (awarded to R.S.) and the OCB Collaborator community, directed by Matteo Pellegrini. We acknowledge Dr. Alexander Hoffmann for providing mentorship to R.S.

References

Albulescu LO, Sabet N, Gudipati M, Stepankiw N, Bergman ZJ, Huffaker TC, Pleiss JA. 2012. A quantitative, high-throughput reverse genetic screen reveals novel connections between Pre-mRNA splicing and 5′ and 3′ end transcript determinants. *PLoS Genet* **8:** e1002530.

Alexander RD, Innocente SA, Barrass JD, Beggs JD. 2010. Splicing-dependent RNA polymerase pausing in yeast. *Mol Cell* **40:** 582–593.

Allepuz-Fuster P, Martinez-Fernandez V, Garrido-Godino AI, Alonso-Aguado S, Hanes SD, Navarro F, Calvo O. 2014. Rpb4/7 facilitates RNA polymerase II CTD dephosphorylation. *Nucleic Acids Res* **42:** 13674–13688.

Amberg DC, Burke D, Strathern J. 2005. *Methods in yeast genetics: a Cold Spring Harbor Laboratory course manual.* Cold Spring Harbor Laboratory Press, Cold Spring Harbor, NY.

Amit M, Donyo M, Hollander D, Goren A, Kim E, Gelfman S, Lev-Maor G, Burstein D, Schwartz S, Postolsky B, et al. 2012. Differential GC content between exons and introns establishes distinct strategies of splice-site recognition. *Cell Rep* **1:** 543–556.

Arenas JE, Abelson JN. 1997. Prp43: an RNA helicase-like factor involved in spliceosome disassembly. *Proc Natl Acad Sci* **94:** 11798–11802.

Bauren G, Wieslander L. 1994. Splicing of Balbiani ring 1 gene pre-mRNA occurs simultaneously with transcription. *Cell* **76:** 183–192.

Bauren G, Jiang WQ, Bernholm K, Gu F, Wieslander L. 1996. Demonstration of a dynamic, transcription-dependent organization of pre-mRNA splicing factors in polytene nuclei. *J Cell Biol* **133:** 929–941.

Beyer AL, Osheim YN. 1988. Splice site selection, rate of splicing, and alternative splicing on nascent transcripts. *Genes Dev* **2:** 754–765.

Beyer AL, Osheim YN. 1991. Visualization of RNA transcription and processing. *Semin Cell Biol* **2:** 131–140.

Bousquet-Antonelli C, Presutti C, Tollervey D. 2000. Identification of a regulated pathway for nuclear pre-mRNA turnover. *Cell* **102:** 765–775.

Braberg H, Jin H, Moehle EA, Chan YA, Wang S, Shales M, Benschop JJ, Morris JH, Qiu C, Hu F, et al. 2013. From structure to systems: high-resolution, quantitative genetic analysis of RNA polymerase II. *Cell* **154:** 775–788.

Brown SJ, Stoilov P, Xing Y. 2012. Chromatin and epigenetic regulation of pre-mRNA processing. *Hum Mol Genet* **21:** R90–R96.

Carey LB. 2015. RNA polymerase errors cause splicing defects and can be regulated by differential expression of RNA polymerase subunits. *Elife* **4:** e09945.

Carrillo Oesterreich F, Preibisch S, Neugebauer KM. 2010. Global analysis of nascent RNA reveals transcriptional pausing in terminal exons. *Mol Cell* **40:** 571–581.

Carrillo Oesterreich F, Bieberstein N, Neugebauer KM. 2011. Pause locally, splice globally. *Trends Cell Biol* **21:** 328–335.

Chathoth KT, Barrass JD, Webb S, Beggs JD. 2014. A splicing-dependent transcriptional checkpoint associated with prespliceosome formation. *Mol Cell* **53:** 779–790.

Chen HC, Cheng SC. 2012. Functional roles of protein splicing factors. *Biosci Rep* **32:** 345–359.

Chen HC, Tseng CK, Tsai RT, Chung CS, Cheng SC. 2013. Link of NTR-mediated spliceosome disassembly with DEAH-box ATPases Prp2, Prp16, and Prp22. *Mol Cell Biol* **33:** 514–525.

Churchman LS, Weissman JS. 2011. Nascent transcript sequencing visualizes transcription at nucleotide resolution. *Nature* **469:** 368–373.

Combs DJ, Nagel RJ, Ares M Jr, Stevens SW. 2006. Prp43p is a DEAH-box spliceosome disassembly factor essential for ribosome biogenesis. *Mol Cell Biol* **26:** 523–534.

Davidson L, Muniz L, West S. 2014. 3′ end formation of pre-mRNA and phosphorylation of Ser2 on the RNA polymerase II CTD are reciprocally coupled in human cells. *Genes Dev* **28:** 342–356.

de la Mata M, Alonso CR, Kadener S, Fededa JP, Blaustein M, Pelisch F, Cramer P, Bentley D, Kornblihtt AR. 2003. A slow RNA polymerase II affects alternative splicing in vivo. *Mol Cell* **12:** 525–532.

Dobin A, Davis CA, Schlesinger F, Drenkow J, Zaleski C, Jha S, Batut P, Chaisson M, Gingeras TR. 2013. STAR: ultrafast universal RNA-seq aligner. *Bioinformatics* **29:** 15–21.

Dujardin G, Kornblihtt AR, Corcos L. 2014. [Kinetic regulation of pre-messenger RNA alternative splicing]. *Med Sci (Paris)* **30:** 940–943.

Fong N, Kim H, Zhou Y, Ji X, Qiu J, Saldi T, Diener K, Jones K, Fu XD, Bentley DL. 2014. Pre-mRNA splicing is facilitated by an optimal RNA polymerase II elongation rate. *Genes Dev* **28:** 2663–2676.

Freedman MS, Kaplan JM, Markovic-Plese S. 2013. Insights into the mechanisms of the therapeutic efficacy of alemtuzumab in multiple sclerosis. *J Clin Cell Immunol* **4:** 1000152.

Garcia A, Rosonina E, Manley JL, Calvo O. 2010. Sub1 globally regulates RNA polymerase II C-terminal domain phosphorylation. *Mol Cell Biol* **30:** 5180–5193.

Garcia A, Collin A, Calvo O. 2012. Sub1 associates with Spt5 and influences RNA polymerase II transcription elongation rate. *Mol Biol Cell* **23:** 4297–4312.

Ghavi-Helm Y, Michaut M, Acker J, Aude JC, Thuriaux P, Werner M, Soutourina J. 2008. Genome-wide location analysis reveals a role of TFIIS in RNA polymerase III transcription. *Genes Dev* **22:** 1934–1947.

Goldstein AL, McCusker JH. 1999. Three new dominant drug resistance cassettes for gene disruption in *Saccharomyces cerevisiae*. *Yeast (Chichester, England)* **15:** 1541–1553.

Gornemann J, Kotovic KM, Hujer K, Neugebauer KM. 2005. Cotranscriptional spliceosome assembly occurs in a stepwise

fashion and requires the cap binding complex. *Mol Cell* **19:** 53–63.

Gottschalk A, Bartels C, Neubauer G, Luhrmann R, Fabrizio P. 2001. A novel yeast U2 snRNP protein, Snu17p, is required for the first catalytic step of splicing and for progression of spliceosome assembly. *Mol Cell Biol* **21:** 3037–3046.

Grate L, Ares M Jr. 2002. Searching yeast intron data at Ares lab Web site. *Methods Enzymol* **350:** 380–392.

Gu M, Naiyachit Y, Wood TJ, Millar CB. 2015. H2A.Z marks antisense promoters and has positive effects on antisense transcript levels in budding yeast. *BMC Genomics* **16:** 99.

Guillemette B, Bataille AR, Gevry N, Adam M, Blanchette M, Robert F, Gaudreau L. 2005. Variant histone H2A.Z is globally localized to the promoters of inactive yeast genes and regulates nucleosome positioning. *PLoS Biol* **3:** e384.

Gunderson FQ, Johnson TL. 2009. Acetylation by the transcriptional coactivator Gcn5 plays a novel role in co-transcriptional spliceosome assembly. *PLoS Genet* **5:** e1000682.

Gunderson FQ, Merkhofer EC, Johnson TL. 2011. Dynamic histone acetylation is critical for cotranscriptional spliceosome assembly and spliceosomal rearrangements. *Proc Natl Acad Sci* **108:** 2004–2009.

Guo R, Zheng L, Park JW, Lv R, Chen H, Jiao F, Xu W, Mu S, Wen H, Qiu J, et al. 2014. BS69/ZMYND11 reads and connects histone H3.3 lysine 36 trimethylation-decorated chromatin to regulated pre-mRNA processing. *Mol Cell* **56:** 298–310.

Hossain MA, Claggett JM, Nguyen T, Johnson TL. 2009. The cap binding complex influences H2B ubiquitination by facilitating splicing of the SUS1 pre-mRNA. *RNA* **15:** 1515–1527.

Hossain MA, Rodriguez CM, Johnson TL. 2011. Key features of the two-intron *Saccharomyces cerevisiae* gene *SUS1* contribute to its alternative splicing. *Nucleic Acids Res* **39:** 8612–8627.

Howe KJ, Kane CM, Ares M Jr. 2003. Perturbation of transcription elongation influences the fidelity of internal exon inclusion in *Saccharomyces cerevisiae*. *RNA* **9:** 993–1006.

Hsin JP, Manley JL. 2012. The RNA polymerase II CTD coordinates transcription and RNA processing. *Genes Dev* **26:** 2119–2137.

Huang S, Spector DL. 1996. Intron-dependent recruitment of pre-mRNA splicing factors to sites of transcription. *J Cell Biol* **133:** 719–732.

Kawashima T, Douglass S, Gabunilas J, Pellegrini M, Chanfreau GF. 2014. Widespread use of non-productive alternative splice sites in *Saccharomyces cerevisiae*. *PLoS Genet* **10:** e1004249.

Kobor MS, Venkatasubrahmanyam S, Meneghini MD, Gin JW, Jennings JL, Link AJ, Madhani HD, Rine J. 2004. A protein complex containing the conserved Swi2/Snf2-related ATPase Swr1p deposits histone variant H2A.Z into euchromatin. *PLoS Biol* **2:** E131.

Komarnitsky P, Cho EJ, Buratowski S. 2000. Different phosphorylated forms of RNA polymerase II and associated mRNA processing factors during transcription. *Gene Dev* **14:** 2452–2460.

Koodathingal P, Staley JP. 2013. Splicing fidelity DEAD/H-box ATPases as molecular clocks. *RNA Biol* **10:** 1073–1079.

Koodathingal P, Novak T, Piccirilli JA, Staley JP. 2010. The DEAH box ATPases Prp16 and Prp43 cooperate to proofread 5′ splice site cleavage during pre-mRNA splicing. *Mol Cell* **39:** 385–395.

Kotovic KM, Lockshon D, Boric L, Neugebauer KM. 2003. Cotranscriptional recruitment of the U1 snRNP to intron-containing genes in yeast. *Mol Cell Biol* **23:** 5768–5779.

Krogan NJ, Keogh MC, Datta N, Sawa C, Ryan OW, Ding H, Haw RA, Pootoolal J, Tong A, Canadien V, et al. 2003. A Snf2 family ATPase complex required for recruitment of the histone H2A variant Htz1. *Mol Cell* **12:** 1565–1576.

Lacadie SA, Rosbash M. 2005. Cotranscriptional spliceosome assembly dynamics and the role of U1 snRNA:5′ss base pairing in yeast. *Mol Cell* **19:** 65–75.

Lacadie SA, Tardiff DF, Kadener S, Rosbash M. 2006. In vivo commitment to yeast cotranscriptional splicing is sensitive to transcription elongation mutants. *Genes Dev* **20:** 2055–2066.

Larimer FW, Stevens A. 1990. Disruption of the gene *XRN1*, coding for a 5′ → 3′ exoribonuclease, restricts yeast cell growth. *Gene* **95:** 85–90.

Leeds NB, Small EC, Hiley SL, Hughes TR, Staley JP. 2006. The splicing factor Prp43p, a DEAH box ATPase, functions in ribosome biogenesis. *Mol Cell Biol* **26:** 513–522.

Li Z, Gadue P, Chen K, Jiao Y, Tuteja G, Schug J, Li W, Kaestner KH. 2012. Foxa2 and H2A.Z mediate nucleosome depletion during embryonic stem cell differentiation. *Cell* **151:** 1608–1616.

Listerman I, Sapra AK, Neugebauer KM. 2006. Cotranscriptional coupling of splicing factor recruitment and precursor messenger RNA splicing in mammalian cells. *Nat Struct Mol Biol* **13:** 815–822.

Longtine MS, McKenzie A III, Demarini DJ, Shah NG, Wach A, Brachat A, Philippsen P, Pringle JR. 1998. Additional modules for versatile and economical PCR-based gene deletion and modification in *Saccharomyces cerevisiae*. *Yeast (Chichester, England)* **14:** 953–961.

Luco RF, Pan Q, Tominaga K, Blencowe BJ, Pereira-Smith OM, Misteli T. 2010. Regulation of alternative splicing by histone modifications. *Science* **327:** 996–1000.

Malagon F, Tong AH, Shafer BK, Strathern JN. 2004. Genetic interactions of DST1 in *Saccharomyces cerevisiae* suggest a role of TFIIS in the initiation-elongation transition. *Genetics* **166:** 1215–1227.

Malik I, Qiu C, Snavely T, Kaplan CD. 2017. Wide-ranging and unexpected consequences of altered Pol II catalytic activity in vivo. *Nucleic Acids Res* doi: 10.1093/nar/gkx037.

Maniatis T, Reed R. 2002. An extensive network of coupling among gene expression machines. *Nature* **416:** 499–506.

Mason PB, Struhl K. 2005. Distinction and relationship between elongation rate and processivity of RNA polymerase II in vivo. *Mol Cell* **17:** 831–840.

Merkhofer EC, Hu P, Johnson TL. 2014. Introduction to cotranscriptional RNA splicing. *Methods Mol Biology* **1126:** 83–96.

Mizuguchi G, Shen X, Landry J, Wu WH, Sen S, Wu C. 2004. ATP-driven exchange of histone H2AZ variant catalyzed by SWR1 chromatin remodeling complex. *Science* **303:** 343–348.

Moehle EA, Ryan CJ, Krogan NJ, Kress TL, Guthrie C. 2012. The yeast SR-like protein Npl3 links chromatin modification to mRNA processing. *PLoS Genet* **8:** e1003101.

Munding EM, Shiue L, Katzman S, Donohue JP, Ares M Jr. 2013. Competition between pre-mRNAs for the splicing machinery drives global regulation of splicing. *Mol Cell* **51:** 338–348.

Naftelberg S, Schor IE, Ast G, Kornblihtt AR. 2015. Regulation of alternative splicing through coupling with transcription and chromatin structure. *Annu Rev Biochem* **84:** 165–198.

Nissen KE, Homer CM, Ryan CJ, Shales M, Krogan NJ, Patrick KL, Guthrie C. 2017. The histone variant H2A.Z promotes splicing of weak introns. *Genes Dev* (this issue). doi: 10.1101/gad.295287.116.

Oesterreich FC, Herzel L, Straube K, Hujer K, Howard J, Neugebauer KM. 2016. Splicing of nascent RNA coincides with intron exit from RNA polymerase II. *Cell* **165:** 372–381.

Ono B, Yoshida R, Kamiya K, Sugimoto T. 2005. Suppression of termination mutations caused by defects of the NMD

machinery in *Saccharomyces cerevisiae*. *Genes Genet Syst* **80:** 311–316.

Petesch SJ, Lis JT. 2012. Overcoming the nucleosome barrier during transcript elongation. *Trends Genet* **28:** 285–294.

Raisner RM, Hartley PD, Meneghini MD, Bao MZ, Liu CL, Schreiber SL, Rando OJ, Madhani HD. 2005. Histone variant H2A.Z marks the 5′ ends of both active and inactive genes in euchromatin. *Cell* **123:** 233–248.

Ranjan A, Mizuguchi G, FitzGerald PC, Wei D, Wang F, Huang Y, Luk E, Woodcock CL, Wu C. 2013. Nucleosome-free region dominates histone acetylation in targeting SWR1 to promoters for H2A.Z replacement. *Cell* **154:** 1232–1245.

Rege M, Subramanian V, Zhu C, Hsieh TH, Weiner A, Friedman N, Clauder-Munster S, Steinmetz LM, Rando OJ, Boyer LA, et al. 2015. Chromatin dynamics and the RNA exosome function in concert to regulate transcriptional homeostasis. *Cell Rep* **13:** 1610–1622.

Rudnizky S, Bavly A, Malik O, Pnueli L, Melamed P, Kaplan A. 2016. H2A.Z controls the stability and mobility of nucleosomes to regulate expression of the LH genes. *Nat Commun* **7:** 12958.

Sadeghi L, Bonilla C, Stralfors A, Ekwall K, Svensson JP. 2011. Podbat: a novel genomic tool reveals Swr1-independent H2A.Z incorporation at gene coding sequences through epigenetic meta-analysis. *PLoS Comput Biol* **7:** e1002163.

Saldi T, Cortazar MA, Sheridan RM, Bentley DL. 2016. Coupling of RNA Polymerase II Transcription Elongation with Pre-mRNA Splicing. *J Mol Biol* **428:** 2623–2635.

Santisteban MS, Kalashnikova T, Smith MM. 2000. Histone H2A.Z regulates transcription and is partially redundant with nucleosome remodeling complexes. *Cell* **103:** 411–422.

Santisteban MS, Hang M, Smith MM. 2011. Histone variant H2A.Z and RNA polymerase II transcription elongation. *Mol Cell Biol* **31:** 1848–1860.

Sayani S, Chanfreau GF. 2012. Sequential RNA degradation pathways provide a fail-safe mechanism to limit the accumulation of unspliced transcripts in *Saccharomyces cerevisiae*. *RNA* **18:** 1563–1572.

Schwartz S, Meshorer E, Ast G. 2009. Chromatin organization marks exon–intron structure. *Nat Struct Mol Biol* **16:** 990–995.

Semlow DR, Blanco MR, Walter NG, Staley JP. 2016. Spliceosomal DEAH-Box ATPases remodel pre-mRNA to activate alternative splice sites. *Cell* **164:** 985–998.

Sims RJ III, Millhouse S, Chen CF, Lewis BA, Erdjument-Bromage H, Tempst P, Manley JL, Reinberg D. 2007. Recognition of trimethylated histone H3 lysine 4 facilitates the recruitment of transcription postinitiation factors and pre-mRNA splicing. *Mol Cell* **28:** 665–676.

Sorenson MR, Stevens SW. 2014. Rapid identification of mRNA processing defects with a novel single-cell yeast reporter. *RNA* **20:** 732–745.

Sorenson MR, Jha DK, Ucles SA, Flood DM, Strahl BD, Stevens SW, Kress TL. 2016. Histone H3K36 methylation regulates pre-mRNA splicing in *Saccharomyces cerevisiae*. *RNA Biol* **13:** 412–426.

Spingola M, Ares M Jr. 2000. A yeast intronic splicing enhancer and Nam8p are required for Mer1p-activated splicing. *Mol Cell* **6:** 329–338.

Subramanian V, Fields PA, Boyer LA. 2015. H2A.Z: a molecular rheostat for transcriptional control. *F1000Prime Rep* **7:** 01.

Tang J, Abovich N, Rosbash M. 1996. Identification and characterization of a yeast gene encoding the U2 small nuclear ribonucleoprotein particle B″ protein. *Mol Cell Biol* **16:** 2787–2795.

Tardiff DF, Rosbash M. 2006. Arrested yeast splicing complexes indicate stepwise snRNP recruitment during in vivo spliceosome assembly. *RNA* **12:** 968–979.

Tolstorukov MY, Goldman JA, Gilbert C, Ogryzko V, Kingston RE, Park PJ. 2012. Histone variant H2A.Bbd is associated with active transcription and mRNA processing in human cells. *Mol Cell* **47:** 596–607.

Tramantano M, Sun L, Au C, Labuz D, Liu Z, Chou M, Shen C, Luk E. 2016. Constitutive turnover of histone H2A.Z at yeast promoters requires the preinitiation complex. *Elife* **5:** e14243.

Wan Y, Saleem RA, Ratushny AV, Roda O, Smith JJ, Lin CH, Chiang JH, Aitchison JD. 2009. Role of the histone variant H2A.Z/Htz1p in TBP recruitment, chromatin dynamics, and regulated expression of oleate-responsive genes. *Mol Cell Biol* **29:** 2346–2358.

Weber CM, Henikoff JG, Henikoff S. 2010. H2A.Z nucleosomes enriched over active genes are homotypic. *Nat Struct Mol Biol* **17:** 1500–1507.

Weber CM, Ramachandran S, Henikoff S. 2014. Nucleosomes are context-specific, H2A.Z-modulated barriers to RNA polymerase. *Mol Cell* **53:** 819–830.

Zhang H, Roberts DN, Cairns BR. 2005. Genome-wide dynamics of Htz1, a histone H2A variant that poises repressed/basal promoters for activation through histone loss. *Cell* **123:** 219–231.

Zlatanova J, Thakar A. 2008. H2A.Z: view from the top. *Structure* **16:** 166–179.

The histone variant H2A.Z promotes efficient co-transcriptional splicing in *S. cerevisiae*

Lauren T. Neves[1,2], Stephen Douglass[1], Roberto Spreafico[4], Srivats Venkataramanan[1], Tracy L. Kress[5] and Tracy L. Johnson, Ph.D.[1,3]*

Supplemental Materials and Methods

RNA-seq minimum-read filters: Raw reads for two biological replicate samples of wild-type, *xrn1*Δ, and *upf1*Δ cells were normalized based on read depth. The geometric mean of both spliced and unspliced reads was calculated for each gene in each pair of biological replicates. The minimum-read threshold was defined as a geometric mean of 10 counts. Any genes with a geometric mean of <10 spliced counts or <10 unspliced counts (Figure S3, in orange) were deemed noise and disregarded in the analysis. Due to the high number of unusual isoforms, YKL186C was omitted for this study. Thresholds for *xrn1*Δ samples were applied to *prp43*^{DAmP} sample analysis (Figures 7 and S9). Number of genes that passed threshold: WT background: RPG n = 90, non-RPG n =129; *xrn1*Δ, *prp43*^{DAmP} background: RPG n=92, non-RPG n=164; *upf1*Δ background: RPG n=92, non-RPG n=141.

qRT-PCR analysis and quantification: For qRT-PCR analysis of *mud1*Δ and *isy1*Δ mutants: RNA isolation, cDNA synthesis and qPCR was performed as previously described (Kress et. al, 2008). Yeast cultures were grow at 30°C n to OD 0.35-0.5 and shifted to 37°C for 30 minutes. RNA was isolated using hot phenol chloroform extraction. Prior to conversion to cDNA, 10 ug RNA was treated with 5 units of RQ1 DNase I (Promega) for 40 min. at 37°C and cDNA was then generated using 1ug dN_9

oligo. The reverse transcription reaction was stopped with 1.0 mL of water. QPCR was performed using a Stratagene MX3500) with 58°C annealing for 35 cycles (20 uL of cDNA and 0.5 uL Taq DNA polymerase (NEB standard Taq). cDNA was analyzed by qPCR with primers that detect the intron levels or the total levels of the mRNA. Percent unspliced RNA (pre-mRNA) was determined by dividing the relative amounts of the intron product (pre-mRNA) by the relative amount of the total product (total mRNA) and multiplying by 100. A standard curve was generated using 100 ng of genomic DNA isolated from WT cells titrated 2-fold down to 1.25 ng.

Whole cell extract and immunoblot: Cells were grown in YPD media to an OD_{600} between 0.5-0.7 and lysed using FA-1 Lysis buffer (50mM HEPES-KOH pH 7.5, 140 mM NaCl, 1 mM EDTA pH 8.0, 1% Triton-X, .1% Deoxycholate, plus protease inhibitors) and .3 mm glass beads with 5 minutes of vortexing at 4°C. The supernated was cleared by centrifugation and protein concentration was determined by spectrophotometer. Total protein was resolved by a 15% SDS-PAGE and transferred to a PVDF membrane for immunoblotting with a 1:4000 dilution of anti-PGK (Molecular Probes) and a 1:10,000 dilution of anti-HA 12CA5 (Roche), 1:5000 dilution of anti-Rpb3 (BioLegend) or a 1:5000 dilution of anti-phospho S2 (Abcam). Signal was detected using Pierce ECL Western Blotting Solution (ThermoScientific).

Supplemental Figure Legends

Figure S1: Splicing of non-consensus splice sites

A. Distribution of changes in splicing in groups of intron-containing genes characterized by RPGs or nonRPGs, and any consensus or non-consensus splice sites.

   c5'ss: consensus 5' splice site. cBP: consensus branch point. c3'SS: consensus 3' splice site. nc5'ss: non-consensus 5' splice site. ncBP: non-consensus branch point. nc3'SS: non-consensus 3' splice

B. Venn diagram representing overlap of intron-containing genes with ≥10% splicing defect in WT, *xrn1*Δ, and *upf1*Δ cells.

Figure S2: Genetic interactions and splicing profile of *swr1*Δ cells resembles those of *htz1*Δ cells.

A. Serial dilution assay of double mutants, *mud1*Δ *swr1*Δ and *isy1*Δ *swr1*Δ. Cells were grown at 30°C in YPD liquid media until desired OD_{600} was obtained. Cells were spotted as a ten-fold dilution onto YPD plates and incubated at 30°C or 37°C for two days.

B. Distribution in splicing efficiencies of all intron-containing genes upon deletion of *SWR1* in either WT (left), *xrn1*Δ (middle) or *upf1*Δ (right) cells, represented as an X-Y plot. RPGs are denoted in orange.

C. Comparison of splicing efficiencies of all intron-containing genes upon deletion of *HTZ1* or *SWR1* in WT(left), *xrn1*Δ (middle) or *upf1*Δ (right) cells, represented as an X-Y plot.

D. Comparison of change in splicing efficiencies of all intron-containing genes in the WT background upon deletion of *HTZ1* or *SWR1*, represented as an X-Y plot. There is strong overlap in the subset of genes whose splicing is negatively affected in *htz1*Δ cells and *swr1*Δ cells (3rd quadrant).

Figure S3: Analysis of RNA-seq samples removed by minimum-read filter.

A. As in Figures 2A and 2B, but including genes removed by filtering process. Distribution in splicing efficiencies of all intron-containing genes upon deletion of *HTZ1*, represented as an X-Y plot, in WT (left), *xrn1*Δ (middle), or *upf1*Δ (right) cells. Genes that did not pass our minimum-read filter are indicated by open circles.

B. As in Figure 2C, but including genes removed by filtering process. Distribution of changes in splicing efficiency upon deletion of *HTZ1* compared to RPKM in WT (top), *xrn1*Δ (middle) and *upf1*Δ (bottom) cells. Vertical dotted line represents RPKM of 150. Horizontal lines represent 10% change in splicing efficiency. Genes that did not pass our minimum-read filter are indicated by open circles. Changes in splicing of removed points are evenly distributed between increased and decreased splicing (Chi-square test, p-values indicated).

Figure S4: H2A.Z affects splicing of ribosomal protein genes when the spliceosome is compromised.

A. RT-qPCR analysis of levels of unspliced (pre-mRNA) products of nonRPGs in WT, *mud1*Δ, and *isy1*Δ cells ± *HTZ1*. cDNA was collected after temperature shift

to 37°C for 30 minutes. Graphs represent average of three to four independent experiments and error bars represent the SEM.

B. Top: Analysis of intron-containing RPGs by RT-PCR in the presence and absence of HTZ1. Products were analyzed on 6% PAGE gels. Pre-mRNA size indicated by genomic DNA size. Bottom: Quantification of intron-containing RPG RT-PCR products. pre-mRNA denoted in grey and spliced mRNA denoted in black. Graphs represent the average of two independent experiments and error bars represent the SD.

C. RT-qPCR analysis of levels of unspliced (pre-mRNA) products of RPGs in WT, *mud1*Δ, and *isy1*Δ cells ± *HTZ1*. cDNA was collected after temperature shift to 37°C for 30 minutes. Graphs represent average of three to four independent experiments and error bars represent the SEM.

Figure S5: H2A.Z-mediated splicing changes are not due to changes in spliceosome availability

A. Log-2 fold change in RPKM for all genes, general splicing factor genes (Table S1), and spliceosomal snRNAs upon deletion of *HTZ1* in WT (left), *xrn1*Δ (middle), or *upf1*Δ (right) cells. Less than 2-fold change was observed for all splicing factors and snRNAs.

B. Log-2 fold change in RPKM for all genes, and intron-containing RPGs upon deletion of *HTZ1* in WT (left), *xrn1*Δ (middle), or *upf1*Δ (right) cells. Less than 2-fold change was observed for all RPGs.

Figure S6: Deletion of *HTZ1* does not affect protein expression of ChIP splice factors or RNAPII core protein

A. Protein immunoblot of Msl1-HA and Lea1-HA strains used for ChIP assays in Figure 5D. WT and htz1Δ cultures were grown in YPD liquid media and whole cell extracts were prepared and probed with anti-HA 12CA5 (Roche) (top), and anti-PGK1 as a loading control (Molecular Probes) (bottom).
B. Protein immunoblot for Prp42-HA used for ChIP assays in Figure 5E. Samples prepared as in figure S5A.
C. Protein immunoblot for Snu114-HA used for ChIP assays in Figure 5F. Samples prepared as in figure S5A.
D. Protein immunoblot for Rpb3 and serine2-P used for ChIP assays in Figure 6B. Samples prepared as in figure S5A. Whole cell extracts were probed with anti-Rpb3 (BioLegend) (top), anti-phospho S2 (Abcam) (middle), and anti-PGK1 as a loading control (Molecular Probes) (bottom).

Figure S7: RNAPII CTD Ser-2 is phosphorylated earlier in gene body.

A. Schematic of intron-containing genes, *YCL002C, ECM33, RPL13A,* and intronless gene *PMA1*. Underlined numbers represent amplicons generated by each primer set used in this experiment.
B. Percent change in Rpb3 occupancy and Ser2-P enrichment (normalized to Rpb3) in *htz1*Δ cells as compared to WT.

Figure S8: Deletion of *DST1* exacerbates polymerase kinetics defect in cells lacking *HTZ1.*

A. Serial dilution assay of double mutant *dst1*Δ *htz1*Δ. Cells were grown at 30°C in YPD liquid media until desired OD_{600} was obtained. Cells were spotted as a ten-fold dilution onto YPD plates and incubated at 25°C, 30°C, or 37°C for two days.

B. Left: Analysis of candidate genes by RT-PCR in WT, and *dst1*Δ cells ± *HTZ1.* Products were analyzed on 6% PAGE gels (8% for *SUS1*). Pre-mRNA size indicated by genomic DNA size. Middle: Quantification of RT-PCR pre-mRNA products. Right: Quantification of *SUS1* RT-PCR pre-mRNA and splicing intermediate containing only the second *SUS1* intron. Quantification graphs represent the average of three independent experiments (four for *YCL002C* in WT) and error bars represent the SD.

C. Schematic of intron-containing genes, *YCL002C, ECM33,* and *RPL13A*. Underlined numbers represent amplicons generated by each primer set used in this experiment.

D. Occupancy of Msl1 at each region of *YCL002C* (left), *ECM33* (middle), or *RPL13A* (right) relative to the non-transcribed region in WT or *dst1*Δ. Graphs represent the average of six (WT) or three (*dst1*Δ) independent experiments and error bars represent the standard error of the means. P-values for each primer set determined by students t-test. Significant values indicated.

gDNA: genomic DNA. s: spliced mRNA product. *: p-value < .01 **: p-value < .001. ***: p-value < .0001.

Figure S9: *prp43*^{DAmP} decreases *PRP43* RNA levels and suppresses H2A.Z-mediated splice defects.

A. RT-qPCR analysis of levels of Prp43 RNA in WT and *prp43*^{DAmP} cells, normalized to *SCR1*, a RNAPIII transcript. Graphs represent average of three independent experiments and error bars represent the SD.

B. Analysis of candidate genes by RT-PCR in WT and *prp43*^{DAmP} cells ± *HTZ1.* Products were analyzed on 6% PAGE gels (8% for *SUS1*). Pre-mRNA size indicated by genomic DNA size.

C. Distribution in splicing efficiencies of all intron-containing genes in *prp43*^{DAmP} cells compared to WT cells.

D. Distribution of changes in splicing in groups of intron-containing genes characterized by RPGs or nonRPGs, and any consensus or non consensus splice sites.

c5'ss: consensus 5' splice site. cBP: consensus branch point. c3'SS: consensus 3' splice site. nc5'ss: non-consensus 5' splice site. ncBP: non-consensus branch point. nc3'SS: non-consensus 3' splice

Supplemental Table Legends

Supplemental Table S1: Splicing factors

List of all genes encoding splicing factors as defined by Chen & Cheng, 2012 [49].

Supplemental Table S2: Splicing factors

List of all strains described in this paper.

Supplemental Table S3: Plasmids

List of all plasmids used in this paper.

Supplemental Table S4: Primers

List of all primers used in this paper.

Supplemental Table S5: RNA-Seq Count Data

Splicing efficiency, unspliced and spliced counts, RPKMs for all genes. Replicate 2 data only pertains to figure S3.

Supplemental Figures

Neves_FigS1

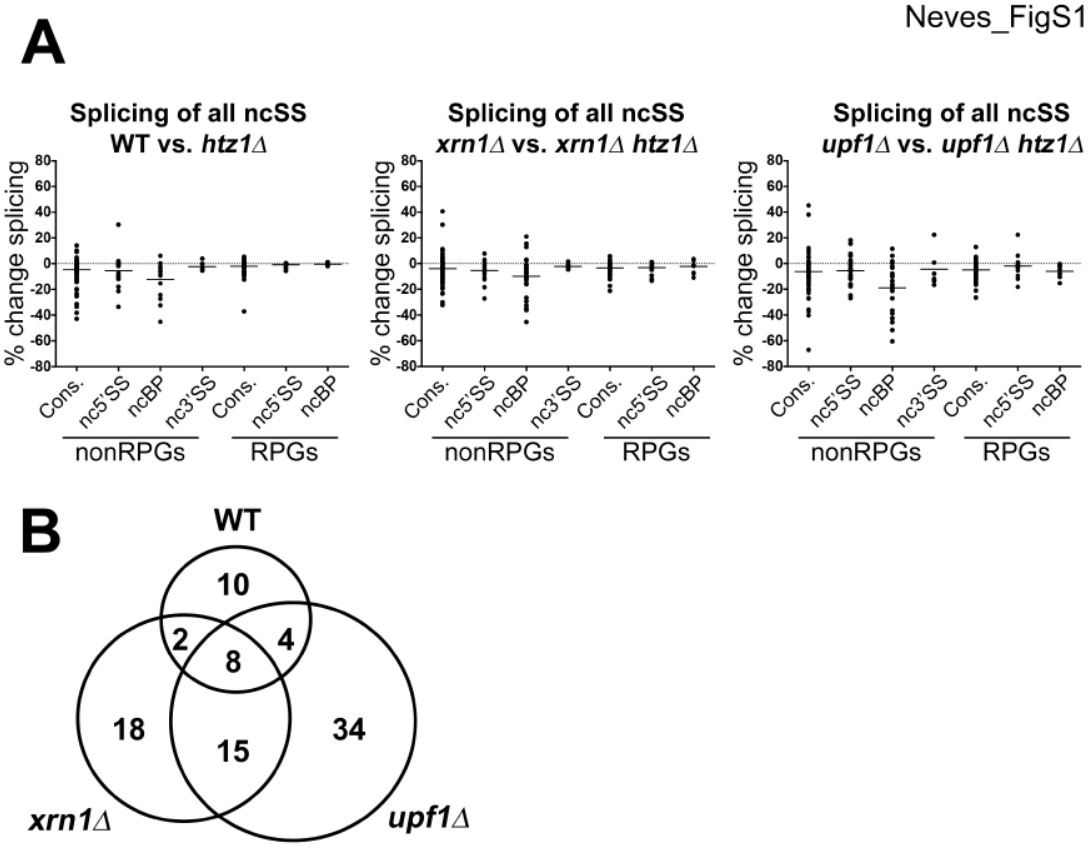

Neves_FigS2

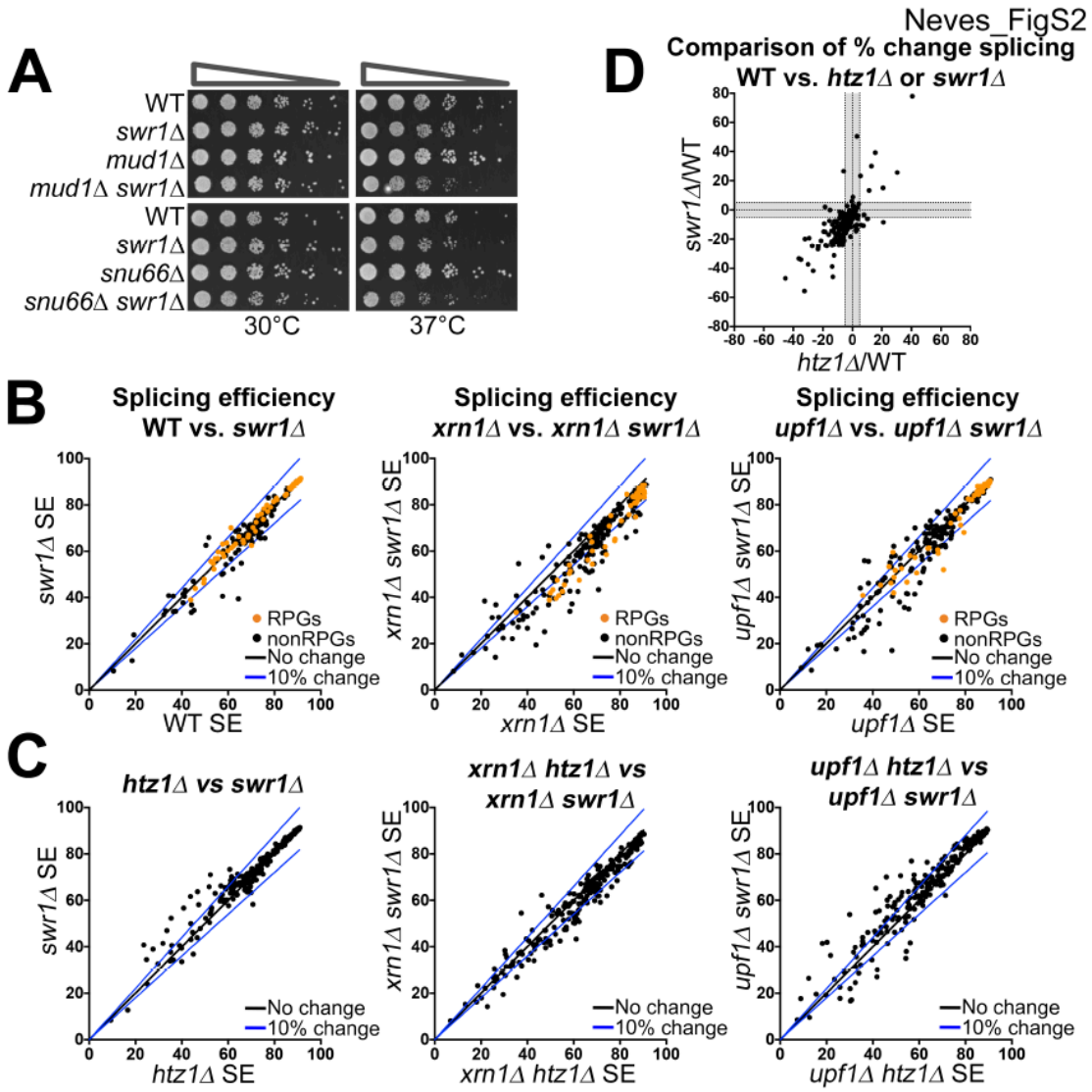
A
WT
swr1Δ
mud1Δ
mud1Δ swr1Δ
WT
swr1Δ
snu66Δ
snu66Δ swr1Δ
30°C
37°C
D
Comparison of % change splicing
WT vs. htz1Δ or swr1Δ
swr1Δ/WT
htz1Δ/WT
B
Splicing efficiency
WT vs. swr1Δ
swr1Δ SE
WT SE
Splicing efficiency
xrn1Δ vs. xrn1Δ swr1Δ
xrn1Δ swr1Δ SE
xrn1Δ SE
Splicing efficiency
upf1Δ vs. upf1Δ swr1Δ
upf1Δ swr1Δ SE
upf1Δ SE
RPGs
nonRPGs
No change
10% change
C
htz1Δ vs swr1Δ
swr1Δ SE
htz1Δ SE
xrn1Δ htz1Δ vs
xrn1Δ swr1Δ
xrn1Δ swr1Δ SE
xrn1Δ htz1Δ SE
upf1Δ htz1Δ vs
upf1Δ swr1Δ
upf1Δ swr1Δ SE
upf1Δ htz1Δ SE

Neves_FigS3

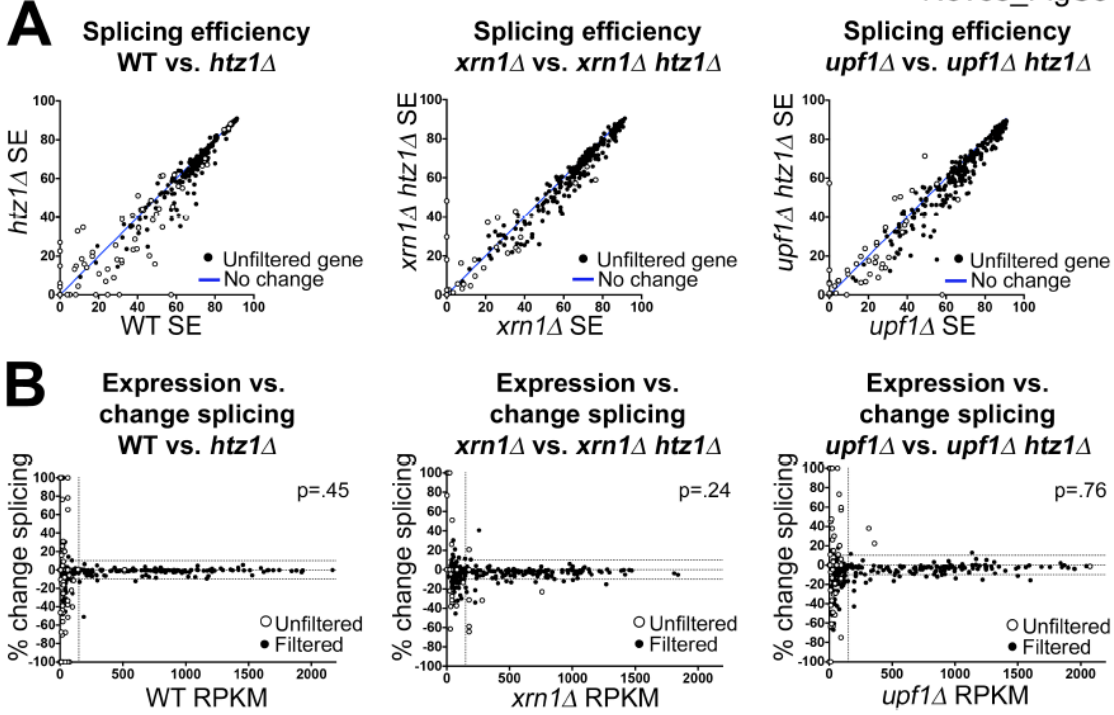
A
Splicing efficiency
WT vs. htz1Δ
htz1Δ SE
WT SE
Unfiltered gene
No change
Splicing efficiency
xrn1Δ vs. xrn1Δ htz1Δ
xrn1Δ htz1Δ SE
xrn1Δ SE
Unfiltered gene
No change
Splicing efficiency
upf1Δ vs. upf1Δ htz1Δ
upf1Δ htz1Δ SE
upf1Δ SE
Unfiltered gene
No change
B
Expression vs.
change splicing
WT vs. htz1Δ
% change splicing
WT RPKM
p=.45
Unfiltered
Filtered
Expression vs.
change splicing
xrn1Δ vs. xrn1Δ htz1Δ
% change splicing
xrn1Δ RPKM
p=.24
Unfiltered
Filtered
Expression vs.
change splicing
upf1Δ vs. upf1Δ htz1Δ
% change splicing
upf1Δ RPKM
p=.76
Unfiltered
Filtered

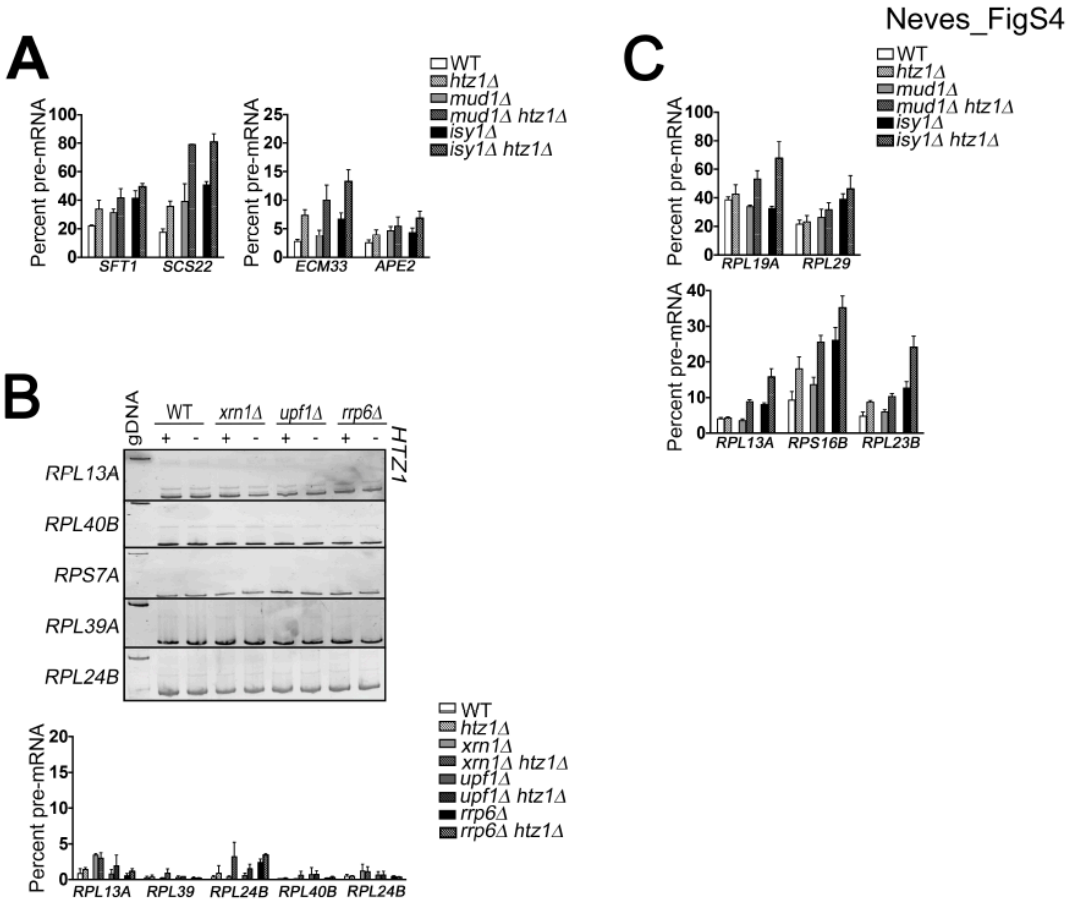
Neves_FigS4
A
Percent pre-mRNA
SFT1
SCS22
ECM33
APE2
WT
htz1Δ
mud1Δ
mud1Δ htz1Δ
isy1Δ
isy1Δ htz1Δ
B
gDNA
WT
xrn1Δ
upf1Δ
rrp6Δ
HTZ1
RPL13A
RPL40B
RPS7A
RPL39A
RPL24B
RPL13A
RPL39
RPL24B
RPL40B
RPL24B
xrn1Δ htz1Δ
upf1Δ
upf1Δ htz1Δ
rrp6Δ
rrp6Δ htz1Δ
C
RPL19A
RPL29
RPL13A
RPS16B
RPL23B

Neves_FigS5

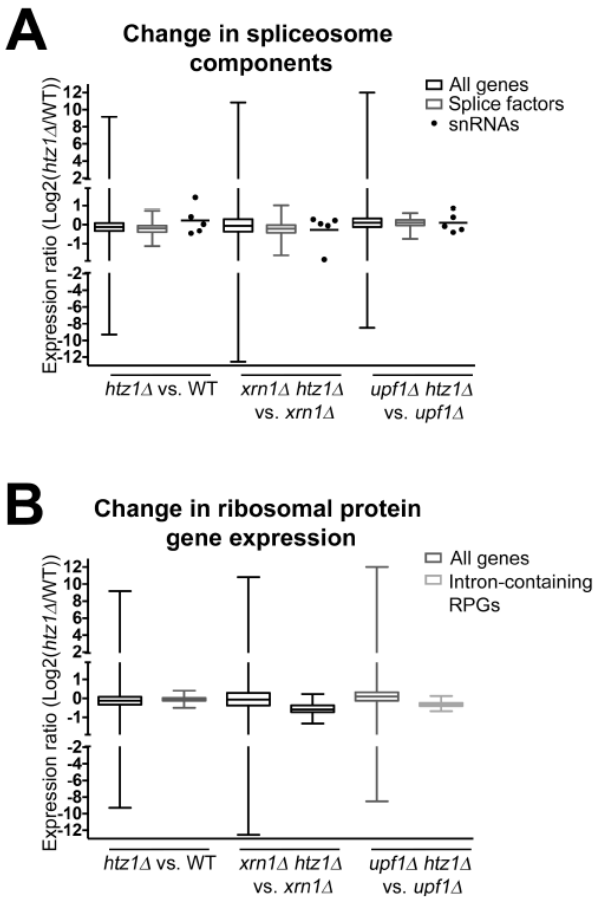
A
Change in spliceosome components
All genes
Splice factors
snRNAs
Expression ratio (Log2(htz1Δ/WT))
12
10
8
6
4
2
1
0
-1
-2
-4
-6
-8
-10
-12
htz1Δ vs. WT
xrn1Δ htz1Δ vs. xrn1Δ
upf1Δ htz1Δ vs. upf1Δ
B
Change in ribosomal protein gene expression
All genes
Intron-containing RPGs
Expression ratio (Log2(htz1Δ/WT))
htz1Δ vs. WT
xrn1Δ htz1Δ vs. xrn1Δ
upf1Δ htz1Δ vs. upf1Δ

Neves_FigS6

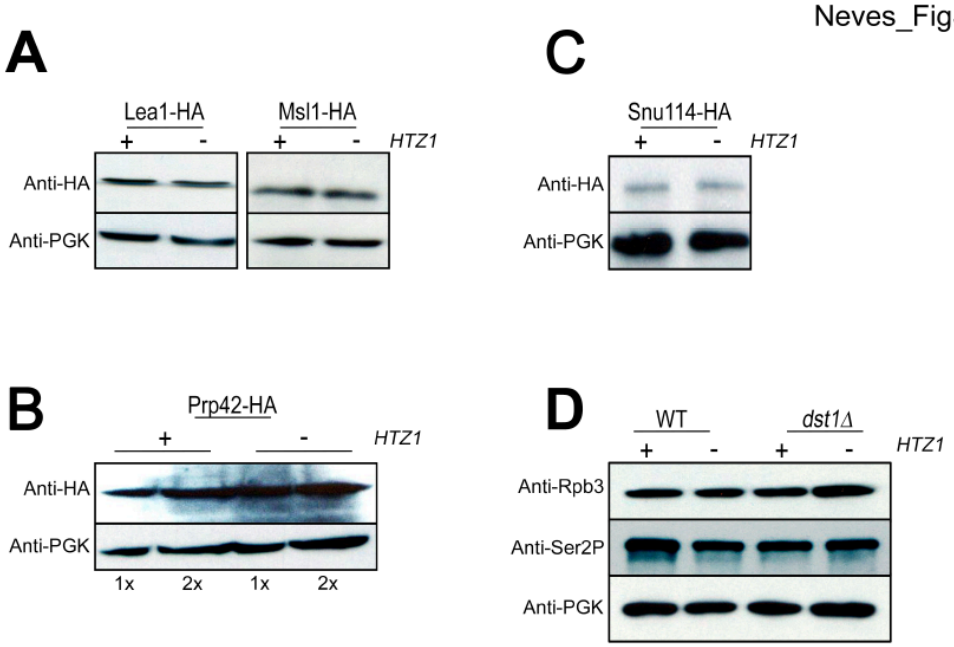
A
Lea1-HA
Msl1-HA
+
-
+
-
HTZ1
Anti-HA
Anti-PGK
C
Snu114-HA
+
-
HTZ1
Anti-HA
Anti-PGK
B
Prp42-HA
+
-
HTZ1
Anti-HA
Anti-PGK
1x
2x
1x
2x
D
WT
dst1Δ
+
-
+
-
HTZ1
Anti-Rpb3
Anti-Ser2P
Anti-PGK

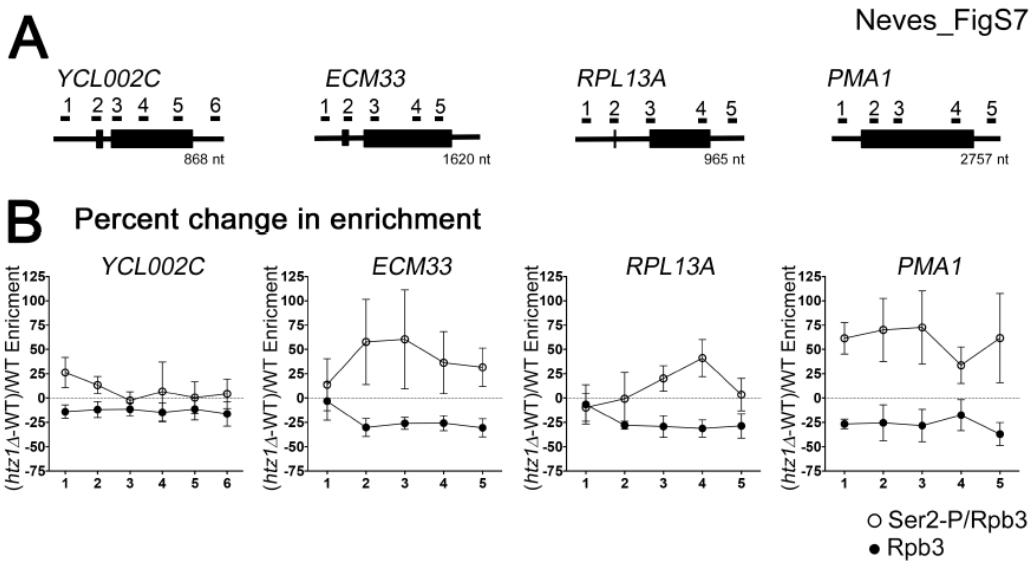
A
Neves_FigS7
YCL002C
1 2 3 4 5 6
868 nt
ECM33
1 2 3 4 5
1620 nt
RPL13A
1 2 3 4 5
965 nt
PMA1
1 2 3 4 5
2757 nt
B
Percent change in enrichment
YCL002C
ECM33
RPL13A
PMA1
(htz1Δ-WT)/WT Enricment
125
100
75
50
25
0
-25
-50
-75
1 2 3 4 5 6
1 2 3 4 5
Ser2-P/Rpb3
Rpb3

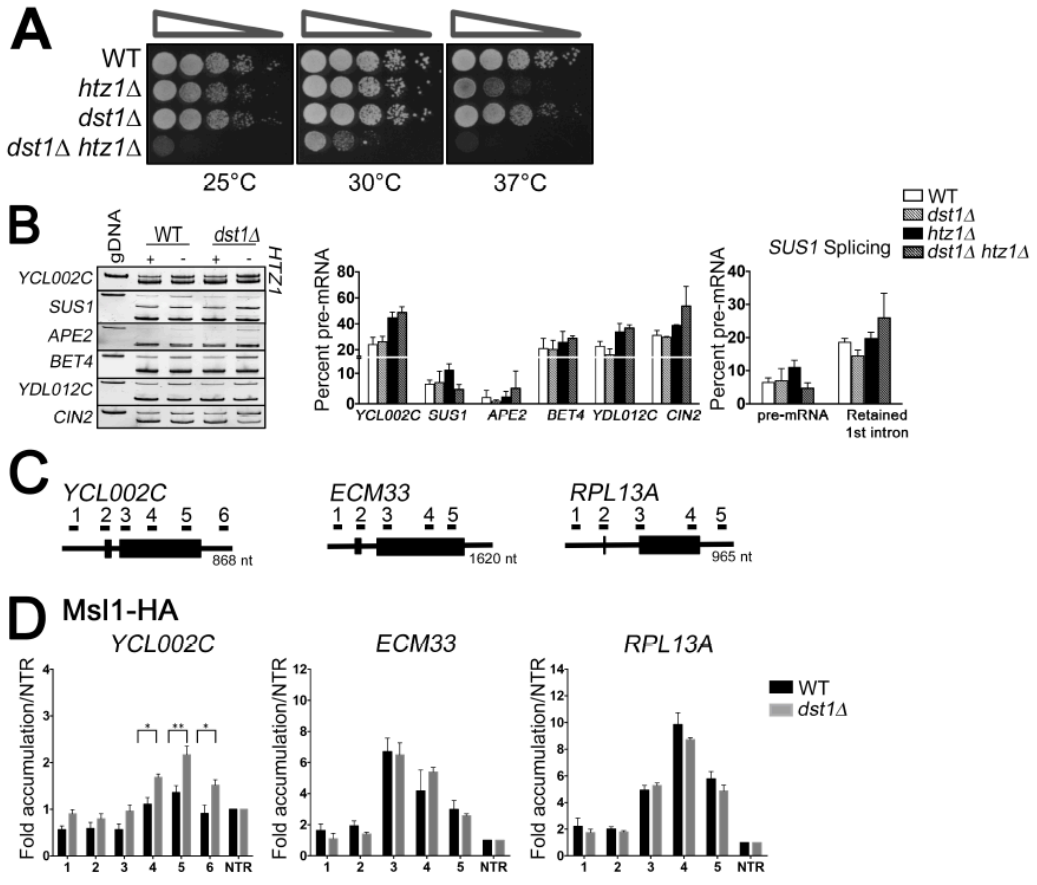
A
WT
htz1Δ
dst1Δ
dst1Δ htz1Δ
25°C
30°C
37°C
B
gDNA
WT
dst1Δ
+
-
+
-
HTZ1
YCL002C
SUS1
APE2
BET4
YDL012C
CIN2
Percent pre-mRNA
YCL002C
SUS1
APE2
BET4
YDL012C
CIN2
WT
dst1Δ
htz1Δ
dst1Δ htz1Δ
SUS1 Splicing
Percent pre-mRNA
pre-mRNA
Retained 1st intron
C
YCL002C
1 2 3 4 5 6
868 nt
ECM33
1 2 3 4 5
1620 nt
RPL13A
1 2 3 4 5
965 nt
D
Msl1-HA
YCL002C
ECM33
RPL13A
Fold accumulation/NTR
1 2 3 4 5 6 NTR
1 2 3 4 5 NTR
1 2 3 4 5 NTR
WT
dst1Δ

Neves_FigS9

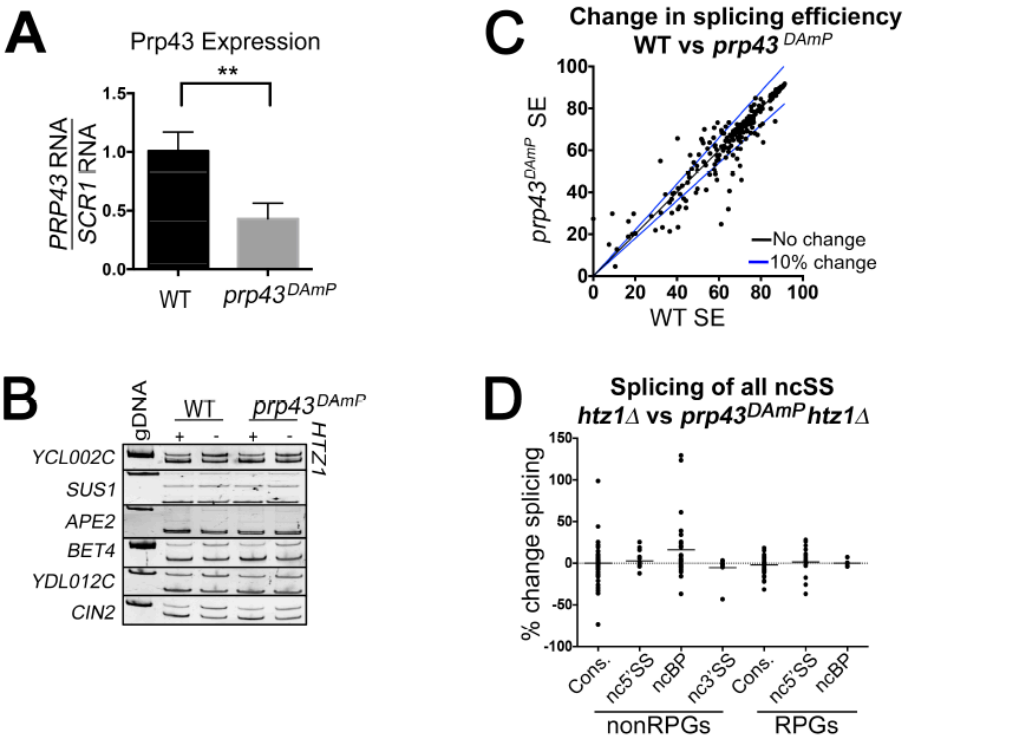
A
Prp43 Expression
**
PRP43 RNA / SCR1 RNA
1.5
1.0
0.5
0.0
WT
prp43DAmP
B
gDNA
WT
prp43DAmP
+ - + -
HTZ1
YCL002C
SUS1
APE2
BET4
YDL012C
CIN2
C
Change in splicing efficiency
WT vs prp43 DAmP
prp43DAmP SE
100
80
60
40
20
0
0 20 40 60 80 100
WT SE
No change
10% change
D
Splicing of all ncSS
htz1Δ vs prp43DAmP htz1Δ
% change splicing
150
100
50
0
-50
-100
Cons.
nc5'SS
ncBP
nc3'SS
Cons.
nc5'SS
ncBP
nonRPGs
RPGs

CHAPTER 3

Chromatin-remodeling SWI/SNF complex regulates Coenzyme Q_6 synthesis and a metabolic shift to respiration in yeast.

Chromatin-remodeling SWI/SNF complex regulates coenzyme Q_6 synthesis and a metabolic shift to respiration in yeast

Received for publication, May 23, 2017, and in revised form, July 17, 2017 Published, Papers in Press, July 24, 2017, DOI 10.1074/jbc.M117.798397

Agape M. Awad[‡§1], Srivats Venkataramanan[§¶1], Anish Nag[‡§], Anoop Raj Galivanche[¶], Michelle C. Bradley[‡§], Lauren T. Neves[§¶], Stephen Douglass[¶], Catherine F. Clarke[‡§2], and Tracy L. Johnson[§¶3]

From the [‡]Department of Chemistry and Biochemistry, the [§]Molecular Biology Institute, and the [¶]Department of Molecular Cell and Developmental Biology, UCLA, Los Angeles, California 90095

Edited by Dennis R. Voelker

Despite its relatively streamlined genome, there are many important examples of regulated RNA splicing in *Saccharomyces cerevisiae*. Here, we report a role for the chromatin remodeler SWI/SNF in respiration, partially via the regulation of splicing. We find that a nutrient-dependent decrease in Snf2 leads to an increase in splicing of the *PTC7* transcript. The spliced *PTC7* transcript encodes a mitochondrial phosphatase regulator of biosynthesis of coenzyme Q_6 (ubiquinone or CoQ_6) and a mitochondrial redox-active lipid essential for electron and proton transport in respiration. Increased splicing of *PTC7* increases CoQ_6 levels. The increase in *PTC7* splicing occurs at least in part due to down-regulation of ribosomal protein gene expression, leading to the redistribution of spliceosomes from this abundant class of intron-containing RNAs to otherwise poorly spliced transcripts. In contrast, a protein encoded by the nonspliced isoform of *PTC7* represses CoQ_6 biosynthesis. Taken together, these findings uncover a link between Snf2 expression and the splicing of *PTC7* and establish a previously unknown role for the SWI/SNF complex in the transition of yeast cells from fermentative to respiratory modes of metabolism.

Similar to other eukaryotic genomes, genes in *Saccharomyces cerevisiae* may be interrupted by non-coding sequences, called introns. Introns are removed from the pre-mRNA through the action of the spliceosome, a macromolecular machine composed of five small nuclear ribonucleoproteins. The spliceosome recognizes consensus sequence signals on the pre-mRNA, termed splice sites, by which it subsequently binds to the intron and catalyzes its removal via two transesterification reactions (1). Pre-mRNA splicing is critical for accurate gene expression in all eukaryotes, and there is significant evidence that alterations in microenvironments, such as changes in the chromatin state or chromatin-modifying factors, can affect splicing outcomes (1). However, the mechanisms for how chromatin and chromatin factors influence splicing are not completely understood.

Although the genome of *S. cerevisiae* contains a smaller number of introns than metazoan genomes, there are, nonetheless, numerous examples of intron-dependent gene regulation (2). The largest functional class of intron-containing genes (ICGs)[4] in budding yeast is ribosomal protein genes (RPGs) that encode the protein components of the ribosome. Therefore, the energy-intensive process of translation is under the heavy regulatory control of the spliceosome, such that splicing of RPGs can be finely tuned to the cells' environmental conditions and to nutrient availability (3).

Interestingly, this enrichment of introns within RPGs impacts the splicing of, as well as provides an opportunity for the regulation of, other ICGs within the yeast genome. About a third of yeast introns occur in RPGs, and the high transcription levels of these genes means that about 90% of the intron load encountered by the spliceosome is from this one functional class of genes (4). Indeed, the prevalence of RPG introns functions to titrate spliceosomes away from other introns, especially those containing suboptimal splice sites. Conversely, down-regulating RPG expression promotes the splicing of transcripts harboring suboptimal splice sites. This effect is perhaps best described during the process of yeast meiosis. Under conditions of vegetative growth, a number of meiosis-specific ICGs are expressed, but they possess suboptimal splice sites and are therefore poorly recognized by the spliceosome and suboptimally spliced. However, upon the down-regulation of RPGs during meiosis, increased availability of the previously limiting pool of spliceosomes leads to improved splicing efficiency of introns in meiosis-specific transcripts (5, 6).

This work was supported by National Science Foundation Grants MCB-1330803 and 1518316, and by NIGMS, National Institutes of Health, Grant GM-085474; the Whitcome Pre-doctoral Fellowship in Molecular Biology (to S. V.); and Ruth L. Kirschstein National Service Award GM-007185 (to M. B). The authors declare that they have no conflicts of interest with the contents of this article. The content is solely the responsibility of the authors and does not necessarily represent the official views of the National Institutes of Health.

RNA-seq data are available in the Gene Expression Omnibus (GEO) under accession number GSE94404.

[1] Both authors contributed equally to this work.

[2] To whom correspondence may be addressed: UCLA Dept. of Chemistry and Biochemistry, 607 Charles E. Young Dr. E., Box 156905, Los Angeles, CA 90095. Tel. 310-825-0771; Fax: 310-206-5213; E-mail: cathy@chem.ucla.edu.

[3] To whom correspondence may be addressed: UCLA Dept. of Molecular Cell and Developmental Biology, 610 Charles E. Young Dr. S., Los Angeles, CA 90095. Tel.: 310-206-2416; E-mail: tljohnson@ucla.edu.

[4] The abbreviations used are: ICG, intron-containing gene; RPG, ribosomal protein gene; ns, non-spliced; s, spliced; CoQ, coenzyme Q; DMQ_6, 5-demethoxy-Q_6; 4HB, 4-hydroxybenzoic acid; HHB, 3-hexaprenyl-4-hydroxybenzoic acid; qPCR, quantitative PCR; TOR, target of rapamycin.

There are other important examples of intron-based regulation in *S. cerevisiae*, especially among ICGs with non-consensus splice sites (7, 8). One such gene is *PTC7*, which encodes a Mg^{2+}/Mn^{2+}-dependent, type 2C serine/threonine protein phosphatase (9). The intron within *PTC7* is particularly intriguing because it contains a non-consensus branch-point sequence, rendering its splicing relatively inefficient under logarithmic growth conditions. The *PTC7* intron lacks a premature termination codon and is translated in-frame. The longer, non-spliced (ns) form of the *PTC7* RNA encodes a longer protein ($Ptc7_{ns}$) that contains a single trans-membrane helix located near the N terminus but is otherwise identical to the protein isoform derived from the spliced *PTC7* RNA ($Ptc7_s$). The read-through nature of the *PTC7* intron is conserved across yeast species, indicating potential functionality for both $Ptc7_s$ and $Ptc7_{ns}$ protein isoforms (10). $Ptc7_{ns}$ has been localized to the nuclear membrane, whereas $Ptc7_s$ is located within mitochondria (10). $Ptc7_s$ has been implicated in regulation of coenzyme Q (also termed ubiquinone or CoQ) biosynthesis via its phosphatase activity (11, 12). However, mechanisms of regulation of Ptc7 itself and the role of the evolutionarily conserved $Ptc7_{ns}$ isoform remain outstanding questions.

CoQ is a redox-active lipid composed of a fully substituted benzoquinone ring and a polyisoprenoid tail and is required for mitochondrial electron transport. The length of the polyisoprenoid group is species-specific; humans produce CoQ_{10}, and *S. cerevisiae* produce CoQ_6, with 10 and 6 isoprene units, respectively. The primary role of CoQ in the inner mitochondrial membrane is to accept the electrons from complex I and complex II and pass those electrons to complex III. Several other metabolic pathways, such as pyrimidine synthesis, sulfide oxidation, and fatty acid β-oxidation, rely on CoQ as an electron carrier (13). CoQ is present in all intracellular membranes, where it may function as a lipid-soluble antioxidant. Several human syndromes, including encephalomyopathy, ataxia, cerebellar atrophy, myopathy, and steroid-resistant nephrotic syndrome, are linked to primary deficiencies in CoQ biosynthesis (14–17).

Mitochondrial proteins are responsible for facilitating the biosynthesis of CoQ_6 in *S. cerevisiae* and include Coq1–Coq11 (18). Many of the Coq proteins necessary for the biosynthesis of CoQ_6 associate in a high-molecular weight complex (termed the "CoQ-synthome"), a multisubunit complex that is peripherally associated with the inner mitochondrial membrane on the matrix side (18). $Ptc7_s$ has been shown to localize to the mitochondria, where it is thought to regulate the phosphorylation state of Coq7 (11) and/or influence mitochondrial respiratory metabolism (12). In the former case, Ptc7s is believed to control, at least in part, the phosphorylation state of the Coq7 polypeptide, which modulates its hydroxylase activity. Coq7 catalyzes the hydroxylation of 5-demethoxy-Q_6 (DMQ_6), the penultimate step in the biosynthesis of CoQ_6 in yeast (19, 20).

The conserved SWI/SNF complex utilizes ATP hydrolysis by Snf2, the catalytic subunit, to disrupt specific histone–DNA contacts, resulting in the sliding or eviction of nucleosomes from the locus. As a result, Snf2 activity contributes to transcriptional regulation (21, 22). The genome-wide distribution of SWI/SNF is responsive to conditions of stress, and the complex is required for transcription of a number of stress response genes (23, 24). We have previously reported that levels of Snf2 change in response to nutrient conditions. We have also reported that the change in Snf2 leads to changes in levels of RPG transcripts, thereby regulating splicing outcomes (6). Here, we show that changes in levels of Snf2 modulate the CoQ_6 biosynthetic pathway in *S. cerevisiae*. First, we show that deletion of Snf2 alters the relative levels of $Ptc7_s$ and $Ptc7_{ns}$ isoforms in yeast and increases both the rate of synthesis and steady-state levels of CoQ_6. This is due to down-regulation of RPG transcripts and an increase in the available pool of spliceosomes. Moreover, we find that the Snf2 protein is down-regulated over time under batch growth conditions and nutrient depletion, and together with a concomitant increase in the splicing of *PTC7*, this leads to higher CoQ_6 levels in preparation for the transition from a fermentative mode of metabolism to a respiratory mode. Furthermore, we show that the two Ptc7 isoforms have opposing effects on the CoQ_6 biosynthetic pathway, which may explain contradictory reports in the literature about the effects of Ptc7 on CoQ_6 levels (11, 12). Importantly, although Snf2 is down-regulated in response to nutrient-depleted conditions, it is nonetheless required for growth on nonfermentable carbon sources, suggesting that dynamic control of Snf2 levels is crucial for the transition from fermentation to respiration.

Results

Deletion of Snf2 leads to enhanced splicing of PTC7 and a shift in the ratios of Ptc7 protein isoforms

Previously published RNA sequencing data for yeast lacking Snf2, the core ATPase component of the SWI/SNF complex (GEO accession number GSE94404), revealed an increase in splicing of a number of introns (6). Satisfyingly, the greatest improvement in splicing upon deletion of Snf2 is experienced by *RPL22B*, via a previously described mechanism consistent with down-regulation of RPG expression (25). The next two largest improvements in splicing efficiency are experienced by *YBR062C* (an ORF of unknown function) and *PTC7*, a previously described type 2C serine-threonine mitochondrial phosphatase that contains all 11 canonical motifs of the PPM family (type 2C) protein phosphatases, previously reported to play a role in CoQ_6 biosynthesis in yeast (11) (Fig. 1*A*). This increase in splicing of *PTC7* RNA was verified by RT-PCR (Fig. 1*B*). In addition, the results from the RNA-seq and RT-PCR were also independently verified by qPCR (data not shown). It has previously been demonstrated that increased splicing of poorly recognized introns can be achieved by decreased expression of competing, highly expressed RPGs (5). Furthermore, we have shown that deletion of Snf2 causes *en masse* down-regulation of RPGs and consequent improvement in splicing of a large number of introns (6). RPG down-regulation in the absence of Snf2 was validated by RT-PCR analysis. For example, expression of RPS16A and RPL34B, two intron-containing RPGs, is down-regulated in *snf2*Δ yeast compared with WT (Fig. 1*C*).

The *PTC7* transcript makes two distinct protein isoforms, one from the nonspliced and one from the spliced RNA. The spliced isoform ($Ptc7_s$) localizes to the mitochondria, whereas

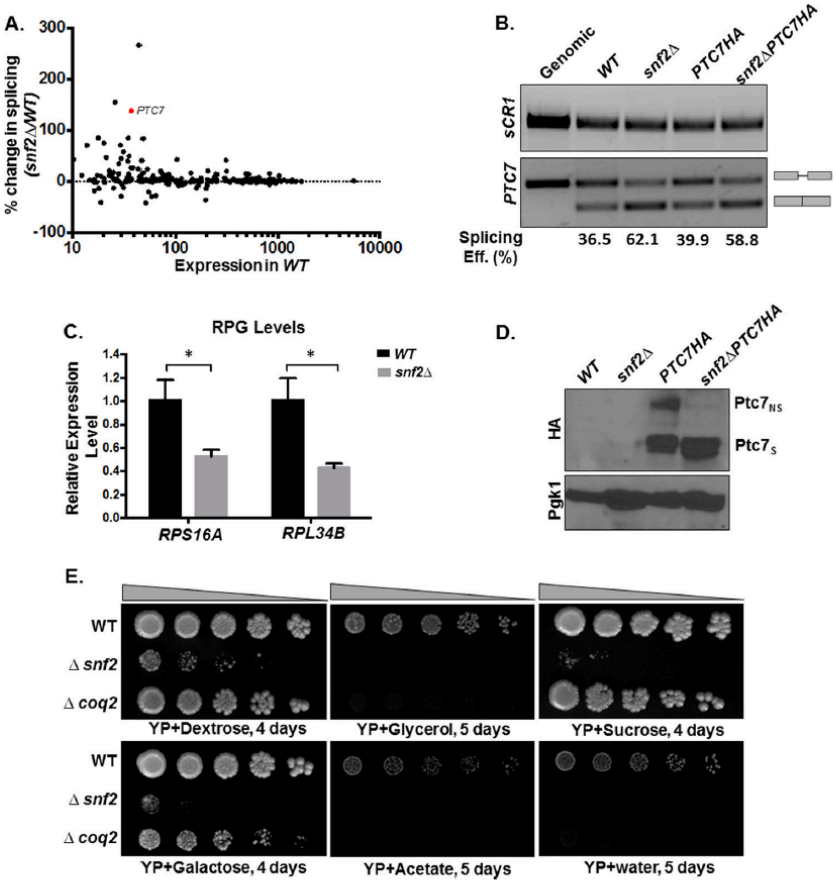

Figure 1. Deletion of *SNF2* enhances splicing of *PTC7* and the steady-state levels of the short Ptc7 protein isoform. *A*, deletion of *SNF2* enhances splicing of a subset of yeast RNAs, including *PTC7*. The scatter plot shows changes in splicing of individual introns in *snf2*Δ yeast over WT plotted against expression in WT. Percentage change in splicing is calculated as 100 × (S.E. in *snf2*Δ − S.E. in WT)/(S.E. in WT). *PTC7* is represented by the *red dot*. *B*, expression and splicing of *PTC7* in *WT* and *snf2*Δ yeast with HA-tagged and untagged Ptc7. Semiquantitative analysis of splicing efficiency of *PTC7* mRNA is indicated *below* each *lane*. *sCR1* served as an internal control. *Gray bars*, exons of the RNA; *thin gray line*, intron. *C*, RT-qPCR measurement of selected intron-containing RPG transcripts between WT and *snf2*Δ yeast strains. Shown is the mean of three biological replicates (unpaired Student's *t* test; *, $p < 0.05$). *Error bars*, S.D. *D*, deletion of *SNF2* affects steady-state levels of HA-tagged Ptc7 proteins. Proteins derived from the nonspliced and spliced forms of the *PTC7*-HA RNA are denoted as $Ptc7_{ns}HA$ and $Ptc7_sHA$, respectively. Pgk1 (phosphoglycerate kinase 1) served as a loading control. *E*, serial dilutions (5-fold) of WT BY4741, *snf2*Δ, and *coq2*Δ (negative respiratory-deficient control; W303 background, because the deletion is unstable in the BY background) on YP agar plates with the indicated carbon sources.

the nonspliced isoform ($Ptc7_{ns}$) has been reported to localize to the nuclear envelope (10). The *PTC7* gene was endogenously HA-tagged, and Western blot analysis demonstrated that deletion of Snf2 leads to an increase in the levels of $Ptc7_s$ compared with $Ptc7_{ns}$ (Fig. 1*D*). It is noteworthy that the increase in the ratio of $Ptc7_s/Ptc7_{ns}$ polypeptides in the WT and *snf2*Δ cells appears to be greater than the increased ratio of spliced/unspliced RNA.

It has previously been demonstrated that yeast strains lacking Snf2 fail to grow on non-fermentable carbon sources, such as glycerol or acetate (26). However, *snf2*Δ mutants frequently incur secondary mutations, and the growth of such strains can resemble WT. Therefore, growth on fermentable and non-fermentable carbon sources was used as a quality control for the assessment of the *bona fide* phenotype (24) of *snf2*Δ prior to each experiment (Fig. 1*E*).

Deletion of Snf2 leads to increased CoQ_6 synthesis in yeast and improves the flux from DMQ_6 to CoQ_6

$Ptc7_s$ has previously been described as playing a role in regulating CoQ_6 synthesis in *S. cerevisiae* (11). A schematic of the entire CoQ_6 biosynthetic pathway with 4-hydroxybenzoic acid as the ring precursor and the role of Ptc7 is detailed in Fig. 2*A*. $Ptc7_s$ is thought to enhance CoQ_6 biosynthesis via its activation of Coq7 and subsequent catalysis of the hydroxylation of DMQ_6, the penultimate step of CoQ_6 biosynthesis (Fig. 2*B*) (11, 27).

$^{13}C_6$-Labeled 4-hydroxybenzoic acid ($^{13}C_6$-4HB), a ring precursor for Q biosynthesis, was used to determine the levels of $^{13}C_6$-CoQ_6 biosynthesis in WT *versus* *snf2*Δ yeast grown to similar culture densities. The absence of Snf2 causes increased steady-state levels of CoQ_6 and increased *de novo* biogenesis of $^{13}C_6$-CoQ_6 (Fig. 3*A*). Additionally, there are significant changes in the levels of *de novo* synthesized DMQ_6, as well as 3-hexa-

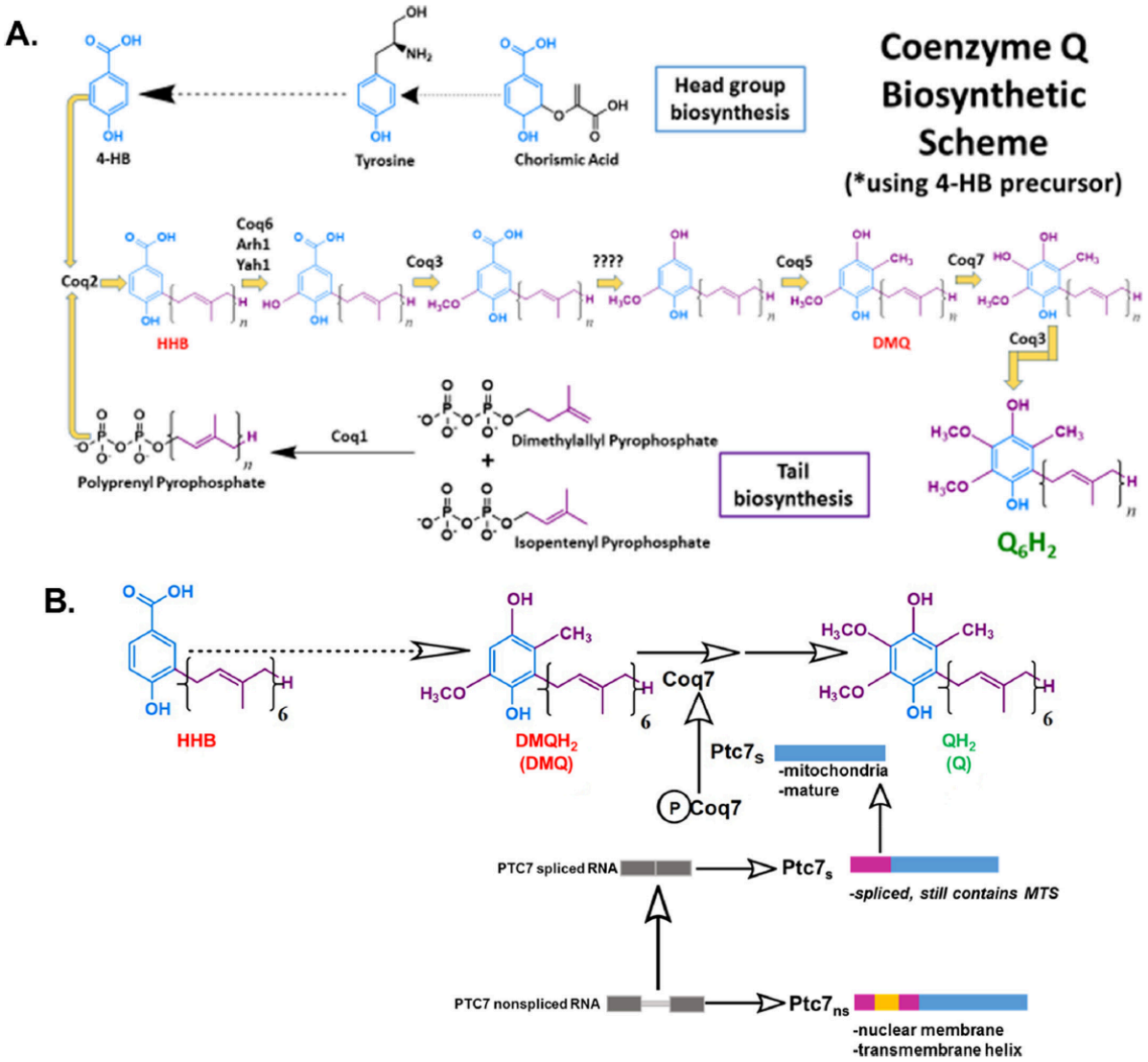

Figure 2. CoQ_6 biosynthetic pathway in *S. cerevisiae* and role of $Ptc7_s$ isoform on Coq7 phosphorylation and function. *A*, schematic of CoQ_6 biosynthetic pathway in yeast using 4HB as a ring precursor, ultimately forming the reduced CoQ_6H_2 product *in vivo*. The *question marks above* the decarboxylation and second hydroxylation steps denote that the enzyme(s) responsible is still unknown. *B*, schematic of the CoQ_6 biosynthetic pathway in yeast. The proposed function of $Ptc7_s$ as a mitochondrial phosphatase modulating Coq7 activity is indicated. $Ptc7_{ns}$ has been localized to nuclear membrane. The *gray bars* represent the exon regions of the RNA, and the *thin gray line* represents the intron region of the RNA. The *pink-colored regions* represent the predicted 38-amino acid mitochondrial targeting sequence (*MTS*) of the protein, the *yellow region* represents the 31-amino acid intron of the protein (which interrupts the MTS after amino acid 19, hence spanning from amino acid 20 to 50), and the *blue region* depicts the mature and spliced polypeptide, which spans from amino acid 51 to 374 (47).

prenyl-4-hydroxybenzoic acid (HHB), an early CoQ_6 biosynthetic intermediate (Fig. 3, *B* and *D*). Consistent with the increased synthesis of CoQ_6 being a consequence of Ptc7 action, the *snf2*Δ yeast show significantly lower ratios of $^{13}C_6$-DMQ_6 level to $^{13}C_6$-CoQ_6 content, indicating a significant increase in the efficiency of conversion of DMQ_6 to CoQ_6, namely the step catalyzed by Coq7, a target of $Ptc7_s$ (Fig. 3*C*) (11). Strikingly, we also observe that the levels of both steady-state and *de novo* synthesized HHB are significantly lower in *snf2*Δ than in the WT yeast (Fig. 3*D*). This suggests that the deletion of Snf2 not only causes higher CoQ_6 production by regulating catalysis from DMQ_6 but that it also funnels the early precursors more efficiently than WT, thus allowing a more streamlined conversion of intermediates of the pathway to the overall product of CoQ_6. This is reinforced by the observation that *snf2*Δ yeast show significantly lower ratios of $^{13}C_6$-HHB to $^{13}C_6$-CoQ_6 content (Fig. 3*E*).

Depletion of Snf2 during batch growth is associated with increased PTC7 splicing and increased CoQ_6 production

Because *snf2*Δ yeast have a significantly slower growth rate than WT, we considered the possibility that the increased CoQ_6

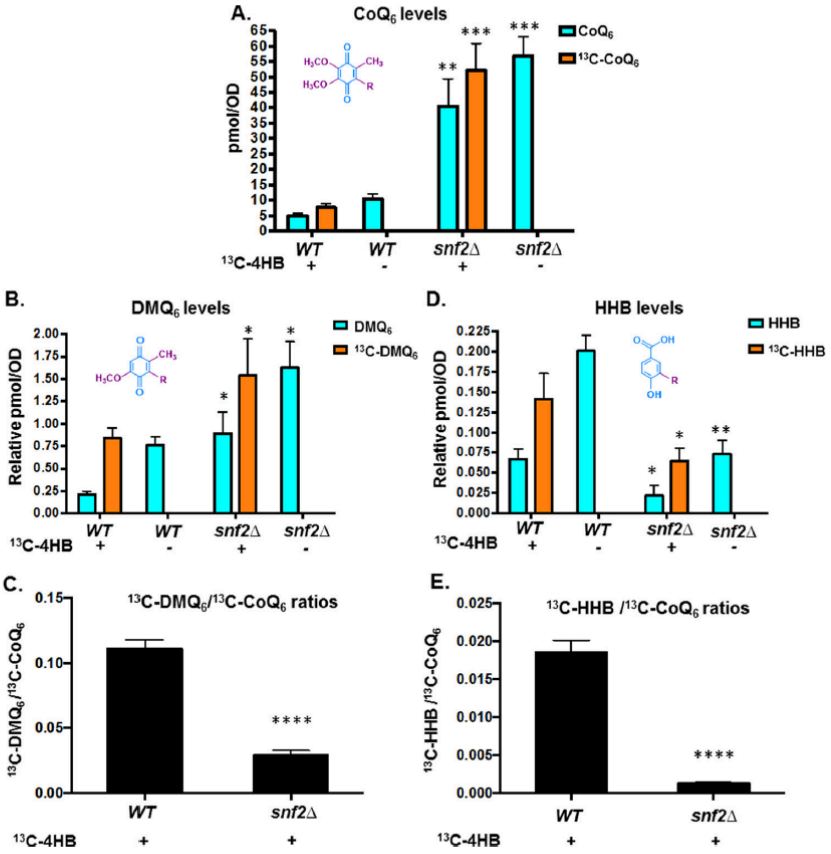

Figure 3. Deletion of *SNF2* leads to increased steady state levels and *de novo* CoQ_6 biosynthesis in yeast and improves the flux from DMQ_6 to CoQ_6. *A*, levels of steady-state CoQ_6 (^{12}C-CoQ_6, *blue bars*) and *de novo* synthesized CoQ_6 ($^{13}C_6$-CoQ_6, *orange bars*) were determined in WT and *snf2*Δ yeast. $^{13}C_6$-4HB was added during midlog phase (A_{600} = 0.5), and labeling was allowed to proceed until a cell density of A_{600} ~1.75 was reached by both strains. ^{12}C-CoQ_6 and $^{13}C_6$-CoQ_6 present in yeast cell pellets were quantified by HPLC-MS/MS, as described under "Experimental procedures." *Error bars*, S.D. of $n = 3$ biological replicates (unpaired Student's *t* test between *corresponding bars* for *snf2*Δ and WT; **, $p < 0.005$; ***, $p < 0.0005$). *B*, levels of steady-state (^{12}C-DMQ_6, *blue bars*) and *de novo* synthesized DMQ_6 ($^{13}C_6$-DMQ_6, *orange bars*) were determined in WT and *snf2*Δ yeast. DMQ_6 was determined from the same cultures as in *A*. *Error bars*, S.D. of $n = 3$ biological replicates (unpaired Student's *t* test between corresponding bars for *snf2*Δ and *WT*; *, $p < 0.05$). *C*, ratios of $^{13}C_6$-DMQ_6/$^{13}C_6$-CoQ_6 in WT and *snf2*Δ yeast, depicting flux of conversion of $^{13}C_6$-DMQ_6 to $^{13}C_6$-CoQ_6. *Error bars*, S.D. of $n = 3$ biological replicates (unpaired Student's *t* test between corresponding bars for *snf2*Δ and WT; ****, $p < 0.00005$). *D*, levels of steady-state HHB (^{12}C-HHB, *blue bars*) and *de novo* synthesized HHB ($^{13}C_6$-HHB, *orange bars*) were determined in WT and *snf2*Δ yeast. HHB was determined from the same cultures as in *A*. *Error bars*, S.D. of $n = 3$ biological replicates (unpaired Student's *t* test between *corresponding bars* for *snf2*Δ and WT; *, $p < 0.05$; **, $p < 0.005$). *E*, ratios of ^{13}C-HHB/^{13}C-CoQ_6 in WT and *snf2*Δ yeast, depicting flux of conversion of $^{13}C_6$-HHBto $^{13}C_6$-CoQ_6. *Error bars*, S.D. of $n = 3$ biological replicates (unpaired Student's *t* test between *corresponding bars* for *snf2*Δ and WT; ****, $p <$ 0.00005).

synthesis was a consequence of the increased time in culture required to achieve equal cell density. To address this, rates of CoQ_6 biosynthesis in WT and *snf2*Δ yeast were determined at timed intervals of culture. First, measurements of steady-state and *de novo* synthesis rates of CoQ_6 between 2 and 12 h of batch growth in YPD revealed that whereas there is indeed an increased rate of synthesis in the *snf2*Δ yeast strain, the steady-state levels of CoQ_6 plateau within 4–6 h of labeling (Fig. 4*A*). We also observe decreasing levels of Snf2 as the time course progresses and nutrients are depleted (Fig. 4*B*). Consistent with the role of Snf2 in RPG transcription, RPG levels decrease with time in batch cultures of yeast, in a manner that tracks well with decreasing levels of Snf2 (Fig. 4*C*). This decrease also coincides with a concomitant increase in the splicing of *PTC7* (Fig. 4, *D* and *E*). Notably, splicing of the *PTC7* transcript in *snf2*Δ yeast starts off higher than in WT yeast, but as Snf2 is depleted from the WT strain, splicing of the *PTC7* transcript approaches the levels of splicing in the *snf2*Δ strain (Fig. 4*F*).

To better understand the kinetics of CoQ_6 synthesis, a shorter time course was performed to capture points preceding the plateau, between 0 and 5 h of labeling. Within 4 h after labeling with ^{13}C-4HB precursor, significant down-regulation in the levels of Snf2 protein is evident (Fig. 5*A*). The decrease in the level of Snf2 protein is mirrored in the increase in splicing efficiency of *PTC7* transcript in the WT strain (Fig. 5, *B–E*). It is interesting to note that the *PTC7* transcript is initially better spliced in the *snf2*Δ strain than in WT, but as the levels of Snf2 in the WT yeast decrease, splicing improves to a degree comparable with the *snf2*Δ strain (Fig. 5, *D* and compare *C* and *F*).

Additionally, there is a striking increase in the overall CoQ_6 product and its *de novo* biosynthesis in the *snf2*Δ yeast within 0–5 h of labeling, as compared with CoQ_6 levels of the WT

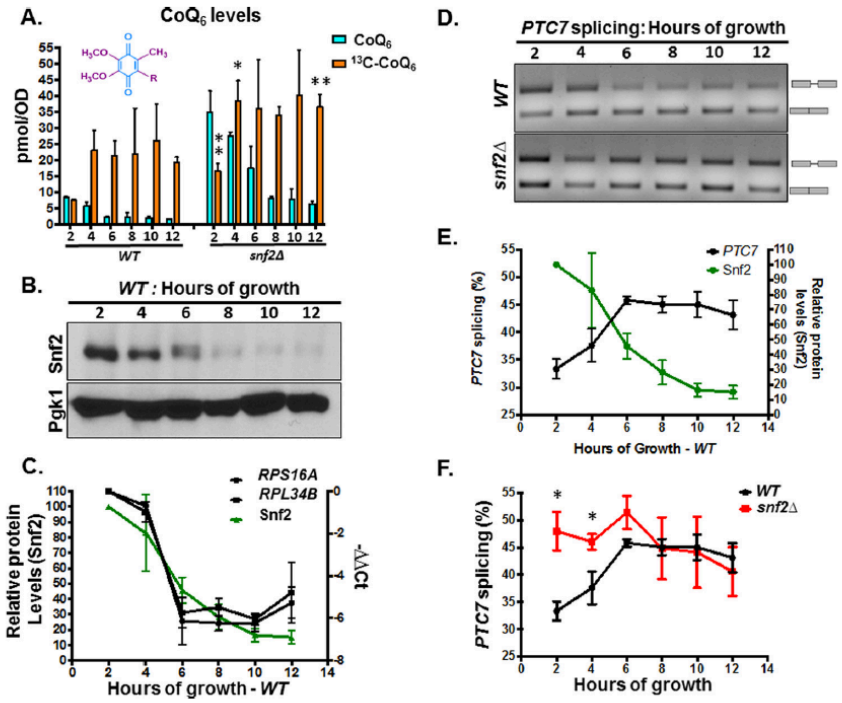

Figure 4. Snf2 levels decrease during batch growth, coinciding with increased *PTC7* splicing and increased CoQ_6 synthesis. *A*, levels of steady-state CoQ_6 (^{12}C-CoQ_6, *blue bars*) and *de novo* synthesized CoQ_6 ($^{13}C_6$-CoQ_6, *orange bars*) in WT and *snf2*Δ yeast were determined at the designated hours after labeling with $^{13}C_6$-4HB. *Error bars*, S.D. of $n = 3$ biological replicates (unpaired Student's *t* test between *corresponding bars* for *snf2*Δ and WT; *, $p < 0.05$; **, $p < 0.005$). *B*, steady-state levels of Snf2 protein in WT cells corresponding to samples from *A* were determined by immunoblot. Pgk1 served as a loading control. *C*, RT-qPCR measurement of selected intron-containing RPG transcripts (*black lines*) and Snf2 protein levels (*green line*) in WT yeast cells were determined at the designated hours after labeling with $^{13}C_6$-4HB as indicated in *A*. Shown is the mean of three biological replicates. *Error bars*, S.D. *D*, expression and splicing of *PTC7* in WT and *snf2*Δ yeast cells corresponding to samples from *A*. PCR products representing the spliced and nonspliced forms are indicated. *E*, quantification of splicing of *PTC7* transcript (*black line*) and Snf2 protein levels (*green line*) in WT yeast cells corresponding to samples from *D*. Snf2 protein levels were previously depicted in *C* and are shown here again for purposes of comparison. Shown is the mean of three biological replicates. *Error bars*, S.D. *F*, quantification of splicing of *PTC7* transcripts in WT and *snf2*Δ yeast cells corresponding to samples from *D*. The splicing of WT *PTC7* shown in *D* is depicted again here for purposes of comparison. Shown is the mean of three biological replicates. *Error bars*, S.D. (unpaired Student's *t* test; *, $p < 0.05$.

during the same time course (Fig. 6, compare *A* and *F*). Furthermore, the gradual increase in CoQ_6 biosynthesis observed in the WT strain plateaus at 3–4 h after labeling (Fig. 6*A*), by which point the significant down-regulation in the levels of Snf2 protein is also evident (Fig. 5*A*). The steady-state and *de novo* synthesized levels of DMQ_6 and HHB were also measured in the 5-h time course of WT and *snf2*Δ yeast (Fig. 6, *B*, *C*, *G*, and *H*). Strikingly, the conversion of *de novo* DMQ_6 to CoQ_6 increases (as shown by the decreased ratio of $^{13}C_6$-DMQ_6 to $^{13}C_6$-CoQ_6) in a manner concurrent with the decrease in Snf2 levels and increase in *PTC7* splicing in WT (compare Fig. 6*D* with Fig. 5 (*A* and *B*)). In fact, as the levels of Snf2 in WT yeast decrease, the conversion efficiency of DMQ_6 to CoQ_6 approaches the low ratio of DMQ_6 to CoQ_6 in *snf2*Δ yeast (Fig. 6, compare *D* and *I*). The role of $Ptc7_s$ in the increased synthesis of CoQ_6 in the absence of Snf2 can be inferred from the observation that whereas the conversion efficiency from DMQ_6 to CoQ_6 is higher in the absence of Snf2, the level of DMQ_6 itself does not change appreciably between WT and *snf2*Δ yeast over the 5-h time course (Fig. 6, compare *B* and *G*). However, the *snf2*Δ cells also show significantly lower rates of HHB synthesis (Fig. 6, compare *C* and *H*), as well as lower ratios of $^{13}C_6$-HHB to $^{13}C_6$-CoQ_6 content (Fig. 6, compare *E* and *J*), consistent with the observation that deletion of Snf2 markedly accelerates the synthesis of CoQ_6, presumably by expediting the conversion of these intermediates to the final product.

RPG down-regulation in general leads to increased PTC7 splicing

Our previous work showed that Snf2-dependent down-regulation of ribosomal protein genes enhances splicing, particularly of genes with nonconsensus splice sites. To determine whether the observed increase in *PTC7* splicing is a consequence of RPG down-regulation *per se*, rapamycin was used to inhibit target of rapamycin (TOR)-dependent RPG transcription in a Snf2-independent manner (28) (Fig. 7*A*). It has also been previously published that rapamycin mitigates certain mitochondrial disorders in *Drosophila* and improves lifespan in response to TOR inhibition, purportedly by modulating carbon metabolism (29). In our work, rapamycin treatment led to a significant increase in the splicing of the *PTC7* transcript (Fig. 7, *B* and *C*). As previously observed, the change in the ratio of $Ptc7_s$/$Ptc7_{ns}$ protein (Fig. 1*D*) is greater than the change in the ratio of spliced to nonspliced transcript upon the deletion of Snf2 (Fig. 1*B*). This suggests that whereas Snf2-dependent RPG down-regulation changes the splicing of the *PTC7* transcript,

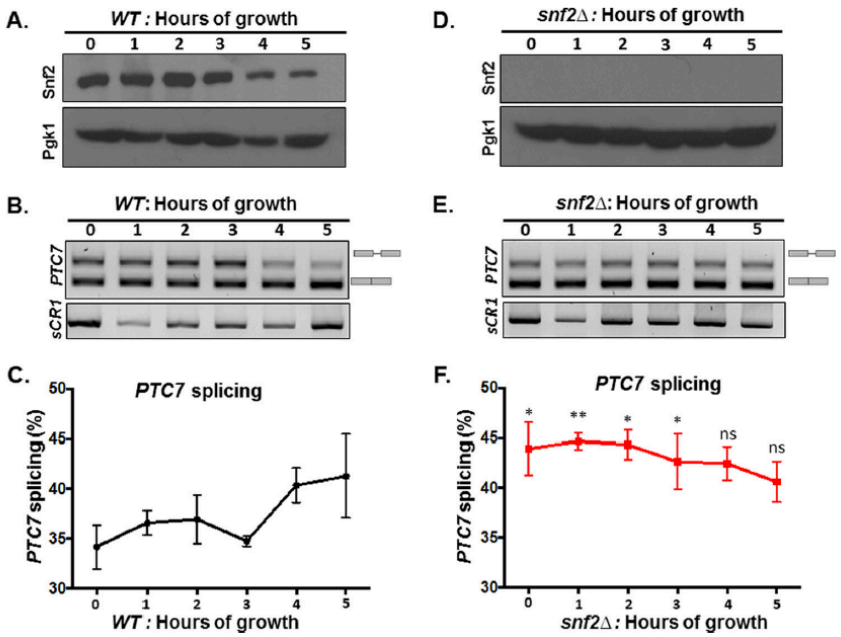

Figure 5. The decrease in Snf2 levels over time in batch cultures of WT yeast correlates with enhanced splicing of *PTC7* RNA. *A*, steady-state levels of Snf2 protein in WT cells corresponding to samples from indicated time points were determined by immunoblot. Pgk1 (phosphoglycerate kinase 1) served as a loading control. *B*, expression and splicing of *PTC7* in WT yeast cells corresponding to samples from *A*; PCR products represent the spliced and nonspliced forms, as indicated. *C*, quantification of splicing of *PTC7* transcript (*black line*) in WT yeast cells corresponding to samples from *B*. Shown is the mean of three biological replicates. *Error bars*, S.D. *D*, the Snf2 protein is absent in *snf2*Δ cells corresponding to samples from the indicated time points as determined by immunoblot. Pgk1 served as a loading control. *E*, expression and splicing of *PTC7* in *snf2*Δ yeast cells corresponding to samples from *D*; PCR products representing the spliced and nonspliced forms are indicated. *F*, quantification of splicing of *PTC7* transcript (*red line*) in *snf2*Δ yeast cells corresponding to samples from *E*. Shown is the mean of three biological replicates. *Error bars*, S.D. (unpaired Student's *t* test between *corresponding bars* for *snf2*Δ and WT in *C*; *, $p < 0.05$; **, $p < 0.005$).

there are probably additional layers of gene regulation that control the relative levels of the $Ptc7_s$ and $Ptc7_{ns}$ protein isoforms. Experiments probing these mechanisms are currently ongoing. Nonetheless, these results are consistent with a model whereby down-regulation of RPG expression redirects spliceosomes from these abundant transcripts to otherwise poorly spliced transcripts, such as *PTC7* (5, 6). In light of the role of Snf2 in RPG expression, changes in Snf2 levels allow fine-tuning of splicing in response to the cell's metabolic needs.

Ptc7 isoforms have differing and opposing effects on CoQ_6 synthesis

The predicted structures of the two isoforms of Ptc7, $Ptc7_s$ and $Ptc7_{ns}$, have been modeled (Fig. 8, *A* and *B*). In fact, the $Ptc7_{ns}$ contains a transmembrane helix, encoded for by the *PTC7* intron, which is capable of spanning the nuclear membrane. Overall, the presence of this transmembrane helix is not predicted to influence the folding of the rest of the protein, thus potentially retaining its phosphatase activity (Fig. 8).

To determine the effect of each Ptc7 isoform on CoQ_6 synthesis, we assayed CoQ_6 levels in cells expressing both forms of Ptc7, $Ptc7_s$ only, $Ptc7_{ns}$ only, or neither (*ptc7*Δ). As reported previously, there is no significant change in CoQ_6 synthesis levels in the *ptc7*Δ mutant (12, 30). However, exclusive expression of $Ptc7_s$ leads to an increase in CoQ_6 synthesis, whereas exclusive expression of $Ptc7_{ns}$ leads to a decrease in CoQ_6 synthesis (Fig. 9*A*). The relative RNA levels from each strain are shown (Fig. 9*B*). Moreover, there are no significant changes observed in the protein levels of Snf2 or Coq7, the target of Ptc7 activity (Fig. 9*C*), in these strains. Whereas each of these isoforms was expressed within the endogenous context and from the endogenous *PTC7* promoter, protein levels of the $Ptc7_{ns}$ appeared to be increased relative to the other isoforms (Fig. 9, *B* and *C*), perhaps due to a cellular feedback mechanism that increases expression or enhances stability of $Ptc7_{ns}$.

The steady-state and *de novo* synthesized levels of CoQ_6 were also measured in a 5-h time course with the yeast strains expressing either $Ptc7_{ns}$ or $Ptc7_s$. Both steady-state and *de novo* CoQ_6 biosynthesis are significantly lower in $Ptc7_{ns}$ strain than in the $Ptc7_s$ and in fact appear to be actively repressed, suggesting that the two isoforms of Ptc7 have differing and opposing effects on CoQ_6 biosynthesis (Fig. 9*D*). In addition, the exclusive presence of $Ptc7_s$ causes increased *de novo* biogenesis of ^{13}C-CoQ_6 as compared with the exclusive presence $Ptc7_{ns}$ (Fig. 9*D*). Whereas the positive effect of $Ptc7_s$ on CoQ_6 biosynthesis is consistent with the mechanisms of Ptc7 action described previously, it is clear that $Ptc7_{ns}$ has a repressive effect on CoQ_6 biosynthesis (compare $Ptc7_{ns}$ and *ptc7*Δ in Fig. 9*A*). To begin to elucidate the mechanism of this repression, we assayed the mRNA transcript levels of genes encoding components of the CoQ_6 biosynthetic complex (*viz. COQ1–11* and *PTC7*). On average, there is little change in the expression of the complex upon deletion of Snf2 (Fig. 9, *G* and *H*) or with the exclusive expression of $Ptc7_s$ or *ptc7*Δ. However, exclusive expression of $Ptc7_{ns}$ is associated with pronounced down-regulation of every

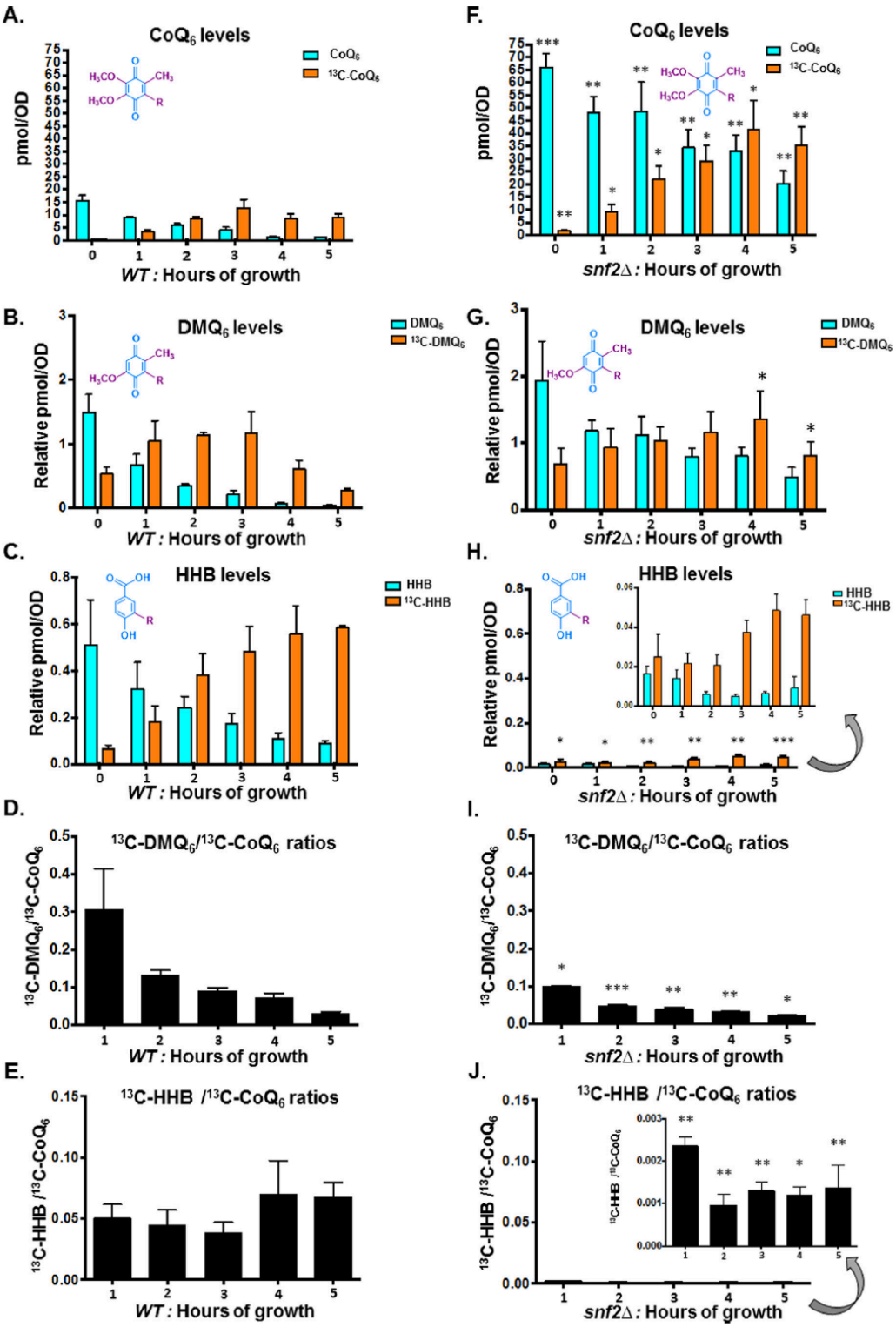
A.
CoQ6 levels
CoQ6
13C-CoQ6
pmol/OD
WT : Hours of growth
F.
CoQ6 levels
snf2Δ : Hours of growth
B.
DMQ6 levels
Relative pmol/OD
WT : Hours of growth
G.
DMQ6 levels
snf2Δ : Hours of growth
C.
HHB levels
HHB
13C-HHB
WT : Hours of growth
H.
HHB levels
snf2Δ : Hours of growth
D.
13C-DMQ6/13C-CoQ6 ratios
WT : Hours of growth
I.
13C-DMQ6/13C-CoQ6 ratios
snf2Δ : Hours of growth
E.
13C-HHB /13C-CoQ6 ratios
WT : Hours of growth
J.
13C-HHB /13C-CoQ6 ratios
snf2Δ : Hours of growth

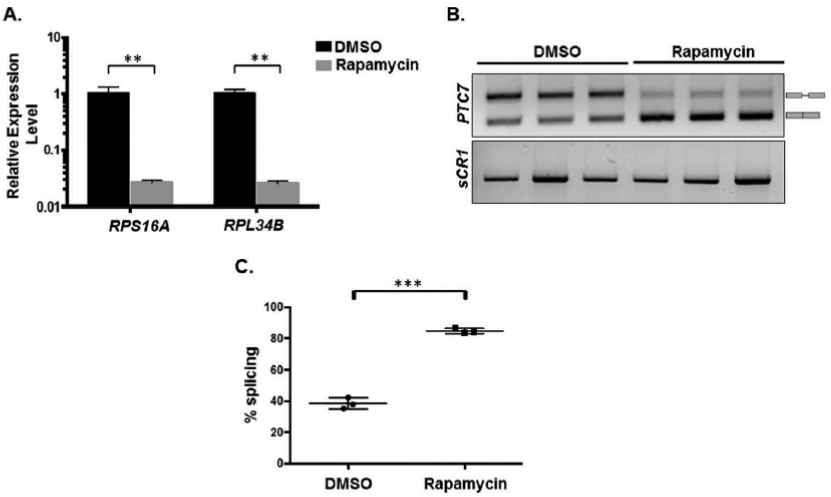

Figure 7. RPG down-regulation and redistribution of spliceosomes result in increased *PTC7* splicing. *A*, RT-qPCR measurement of selected intron-containing RPG transcripts between WT yeast treated with rapamycin and a vehicle control. Mean of three biological replicates (unpaired Student's *t* test, $^{**}p < 0.005$). *Error bars*, S.D. *B*, expression and splicing of *PTC7* in WT yeast treated with rapamycin and a vehicle control (DMSO). PCR products representing the spliced and nonspliced forms are indicated. *C*, quantification of three independent biological replicates of *B* (unpaired Student's *t* test; ***, $p < 0.0005$). *Error bars*, S.D.

member of the CoQ-synthome (Fig. 9, *E* and *F*). Although the mechanism by which these components are down-regulated is unclear, it is interesting that $Ptc7_{ns}$ has previously been localized to the nuclear membrane (10), hinting at a novel role for this isoform in expression of the RNAs encoding the CoQ-synthome. Two possible mechanisms by which nucleus-localized $Ptc7_{ns}$ may affect synthesis of the CoQ-synthome are via direct action on nucleus-localized Coq7 or via indirect effects on gene expression. It is important to mention here that to the best of our knowledge, no reports have demonstrated nuclear localization of, or a nuclear role for, Coq7 in *S. cerevisiae*.

Interestingly, yeast strains engineered to express either $Ptc7_s$ or $Ptc7_{ns}$ still retain the ability to grow on medium containing a non-fermentable carbon source, as do *ptc7*Δ null mutants (data not shown). This is consistent with our prior observations that ~1–10% of CoQ_6 levels are sufficient for comparable growth on medium containing a nonfermentable carbon source. It has been postulated that residual CoQ_6 levels are observed due to the overlapping activities of Ptc5 and/or Ptc6, and in fact the *ptc5*Δ*ptc7*Δ double null mutant has impaired growth under conditions of temperature stress (11, 31). It is also worth noting that unlike the deletion of *SNF2*, the conversion efficiencies or ratios between the early components of the pathway (DMQ_6 or HHB) and CoQ_6 do not vary between strains exclusively expressing either Ptc7 isoform (Fig. 10, *C* and *D*). This is because although there are significant changes in the levels of *de novo* synthesized DMQ_6 as well as HHB when comparing $Ptc7_s$ to $Ptc7_{ns}$ (Fig. 10, *A* and *B*), $Ptc7_s$ is synthesizing higher levels of *de novo* CoQ_6, DMQ_6, and HHB, compared with overall lower levels of these same lipids in $Ptc7_{ns}$ (Fig. 10, *C* and *D*). Thus, the overall conversion efficiencies (ratios) between both isoforms are comparable (Fig. 10, *C* and *D*). This is consistent with our interpretation that the absence of Snf2 contributes to the metabolic state of the cell in other ways in addition to its role in regulation of the Ptc7 isoforms.

Figure 6. Overall conversion efficiency of the CoQ_6 biosynthetic pathway increases upon depletion of Snf2, with increased conversions of both DMQ_6 to Q_6 and HHB to Q_6. *A*, levels of steady-state CoQ_6 (^{12}C-CoQ_6, *blue bars*) and *de novo* synthesized CoQ_6 ($^{13}C_6$-CoQ_6, *orange bars*) in WT yeast cells were determined at the designated hours after labeling with $^{13}C_6$-4HB. *Error bars*, S.D. of $n = 3$ biological replicates. *B*, levels of steady-state DMQ_6 (^{12}C-DMQ_6, *blue bars*) and *de novo* synthesized DMQ_6 ($^{13}C_6$-DMQ_6, *orange bars*) in WT yeast were determined at the designated hours after labeling with $^{13}C_6$-4HB. *Error bars*, S.D. of $n = 3$ biological replicates. *C*, levels of steady-state HHB (^{12}C-HHB, *blue bars*) and *de novo* synthesized ($^{13}C_6$-HHB, *orange bars*) in WT and *snf2*Δ yeast were determined at the designated hours after labeling with $^{13}C_6$-4HB. *Error bars*, S.D. of $n = 3$ biological replicates. *D*, the ratio of $^{13}C_6$-DMQ_6/$^{13}C_6$-CoQ_6 in WT yeast was determined at the designated hours after labeling with $^{13}C_6$-4HB. *Error bars*, S.D. of $n = 3$ biological replicates. The 0-h time point is excluded, because the ratio is not indicative of pathway conversion. *E*, the ratio of $^{13}C_6$-HHB/$^{13}C_6$-CoQ_6 in WT yeast was determined at the designated hours after labeling with $^{13}C_6$-4HB. *Error bars*, S.D. of $n = 3$ biological replicates. The 0-h time point is excluded, because the ratio is not indicative of pathway conversion. *F*, levels of steady-state CoQ_6 (^{12}C-CoQ_6, *blue bars*) and *de novo* synthesized ($^{13}C_6$-CoQ_6, *orange bars*) in *snf2*Δ yeast cells were determined at the designated hours after labeling with $^{13}C_6$-4HB. *Error bars*, S.D. of $n = 3$ biological replicates (unpaired Student's *t* test between *corresponding bars* for *snf2*Δ and WT in *A*; *, $p < 0.05$; **, $p < 0.005$; ***, $p < 0.0005$). *G*, levels of steady-state DMQ_6 (^{12}C-DMQ_6, *blue bars*) and *de novo* synthesized DMQ_6 ($^{13}C_6$-DMQ_6, *orange bars*) in *snf2*Δ yeast were determined at the designated hours after labeling with $^{13}C_6$-4HB. *Error bars*, S.D. of $n = 3$ biological replicates. (unpaired Student's *t* test between *corresponding bars* for *snf2*Δ and WT in *B*; *, $p < 0.05$). *H*, levels of steady-state HHB (^{12}C-HHB, *blue bars*) and *de novo* synthesized HHB ($^{13}C_6$-HHB, *orange bars*) in *snf2*Δ yeast were determined at the designated hours after labeling with ^{13}C-4HB. *Error bars*, S.D. of $n = 3$ biological replicates (unpaired Student's *t* test between corresponding bars for *snf2*Δ and WT in *C*; *, $p < 0.05$; **, $p < 0.005$; ***, $p < 0.0005$). *I*, the ratio of $^{13}C_6$-DMQ_6/$^{13}C_6$-CoQ_6 in *snf2*Δ yeast cells was determined at the designated hours after labeling with $^{13}C_6$-4HB. *Error bars*, S.D. of $n = 3$ biological replicates (unpaired Student's *t* test between corresponding bars for *snf2*Δ and WT in *D*; *, $p < 0.05$; **, $p < 0.005$; ***, $p < 0.0005$). The 0-h time point is excluded, because the ratio is not indicative of pathway conversion. *J*, the ratio of $^{13}C_6$-HHB/$^{13}C_6$-CoQ_6 in *snf2*Δ yeast cells was determined at the designated hours after labeling with $^{13}C_6$-4HB. *Error bars*, S.D. of $n = 3$ biological replicates (unpaired Student's *t* test between *corresponding bars* for *snf2*Δ and WT in *E*; *, $p < 0.05$; **, $p < 0.005$). The 0-h time point is excluded, because the ratio is not indicative of pathway conversion.

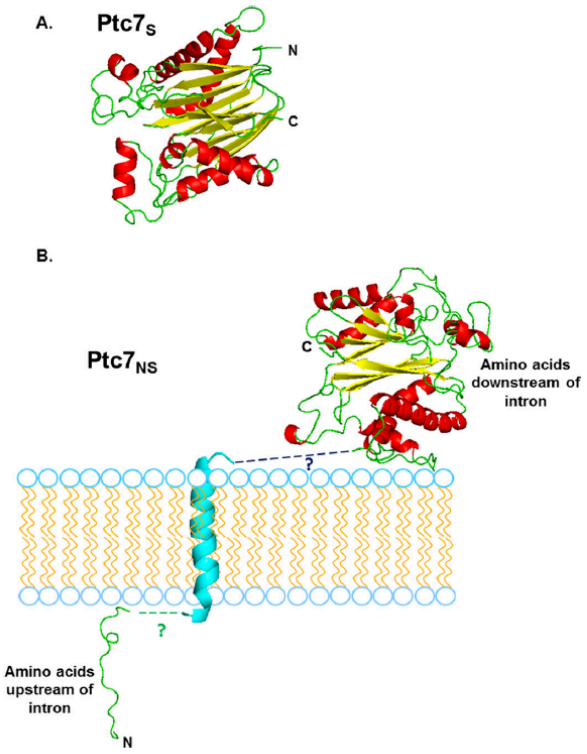

Figure 8. Structural predictions of mitochondrial $Ptc7_s$ and nuclear membrane traversing $Ptc7_{ns}$. *A*, PHYRE2 homology modeling of mature mitochondrial $Ptc7_s$, which is experimentally determined to start at amino acid Gly^{39} (46). 85% of residues modeled at >90% confidence (15% of residues modeled *ab initio*). The N terminus and C terminus of the protein are shown. *B*, PHYRE2 homology modeling of nuclear membrane $Ptc7_{ns}$. The predicted trans-membrane helix encoded by the intron is shown in *cyan*. 86% of residues modeled at >90% confidence (14% of residues modeled *ab initio*. To show the interaction with the nuclear membrane, the N-terminal loop residing on the one side of the nuclear membrane is proposed to be linked to the modeled transmembrane helix, which is then proposed to be linked to the rest of the Ptc7 protein that is predicted to reside on the alternate side of the nuclear membrane. The *nine black dashes* connecting the helix to the larger portion of the protein represent nine amino acids in the intron that were in an unmodeled region.

These data reveal a novel role for Snf2 in respiration and specifically in the transition from a largely fermentative mode of metabolism to a largely respiratory one in *S. cerevisiae*, as shown by the model in Fig. 11. Under conditions of high nutrient availability, Snf2-dependent transcription of intron-rich RPGs sequesters spliceosomes away from transcripts with weak splice sites, such as *PTC7.* As a consequence, both isoforms of the Ptc7 protein are expressed at appreciable levels, and their opposing effects on CoQ_6 synthesis ensure that CoQ_6 is maintained at a relatively low level. As the nutrients in the medium are depleted, the levels of Snf2 and, consequently, RPG transcripts, decrease concurrently, freeing up spliceosomes to act on *PTC7.* This leads to better splicing of *PTC7* and a shift in the relative abundances of the two protein isoforms, which eventually leads to an increase in CoQ_6 synthesis.

Discussion

Whereas it has been broadly acknowledged that chromatin states and chromatin factors influence splicing outcomes in various organisms, identifying the functional importance of such regulation under biologically relevant conditions remains a challenge. We have shown previously that down-regulation of Snf2, the core ATPase component of the SWI/SNF chromatin-remodeling complex, in response to nutrient depletion leads to a change in cellular splicing outcomes due to down-regulation of RPGs and subsequent redistribution of spliceosomes (5, 6). We show here that Snf2-dependent changes in splicing of *PTC7* during yeast growth, combined with the general conditions in the cell in the absence of Snf2, causes a shift in the ratio of two distinct isoforms of the Ptc7 protein that have distinct and opposing effects on CoQ_6 biosynthesis. This change in the ratio of the isoforms is concomitant with an increase in CoQ_6 levels in the cell, preparing for the transition from a largely fermentative to a respiratory mode of metabolism.

Previous studies have presented contradictory evidence regarding the involvement of *PTC7* in CoQ_6 biosynthesis. Ptc7 is required for the dephosphorylation of Coq7, thus transitioning Coq7 to its "active" form, which is able to catalyze the penultimate step of the CoQ_6 pathway. This led to the prediction that the *ptc7*Δ strain would demonstrate decreased CoQ_6 synthesis, as assayed by quantification of lipids from purified mitochondria (11). Surprisingly, although Ptc7 supports general respiratory function, the absence of *PTC7* does not lead to a deficiency in CoQ_6 levels, as assayed in lipid extracts of whole cells (12) (Fig. 9*A*). The studies here help to resolve this apparent contradiction. Studies with the *ptc7*Δ cells fail to address the opposing roles that the two Ptc7 isoforms have in the cell under WT conditions. Only cells with the capacity to express both $Ptc7_s$ and $Ptc7_{ns}$ can accurately reflect the full extent of Ptc7 function. We demonstrate that exclusive expression of $Ptc7_{ns}$ has a significant repressive effect on CoQ_6 biosynthesis (Fig. 9, *A* and *D*). Notably, the rates of conversions from precursors in the pathway to the final product remained unchanged, indicating down-regulation of the entire pathway (Fig. 10, *C* and *D*). Consistent with this, we observe down-regulation of almost all of the components of the CoQ_6 biosynthetic complex upon exclusive expression of $Ptc7_{ns}$ (Fig. 9*F*). The mechanism by which $Ptc7_{ns}$ affects RNA expression is as yet unknown, and investigations to understand the same are ongoing.

PTC7 is not the only known example of a gene in *S. cerevisiae* encoding functional proteins from both the nonspliced pre-mRNA as well as the "mature" spliced mRNA (10). We recently reported translation of unspliced *GCR1* pre-mRNA leading to a functional Gcr1 protein, although in this case, translation starts from within the retained intron (7). Whereas the read-through nature of the intron is conserved across most *Saccharomycetaceae* species, the intron is excised in the same species (analysis of publicly available RNA-seq data sets; data not shown), rendering it likely that both forms of the protein are necessary and functional. This is illustrated in the case of *Tetrapisispora blattae*, which, like *S. cerevisiae*, underwent a whole genome duplication event; but unlike *S. cerevisiae*, which lost the duplications of most of its genes, *T. blattae* retains two copies of the *PTC7* gene. Interestingly, the two *PTC7* genes in *T. blattae* subfunctionalized into a gene that encodes a mitochondrial PP2C ($Ptc7_b$, from a spliced transcript of *PTC7b* con-

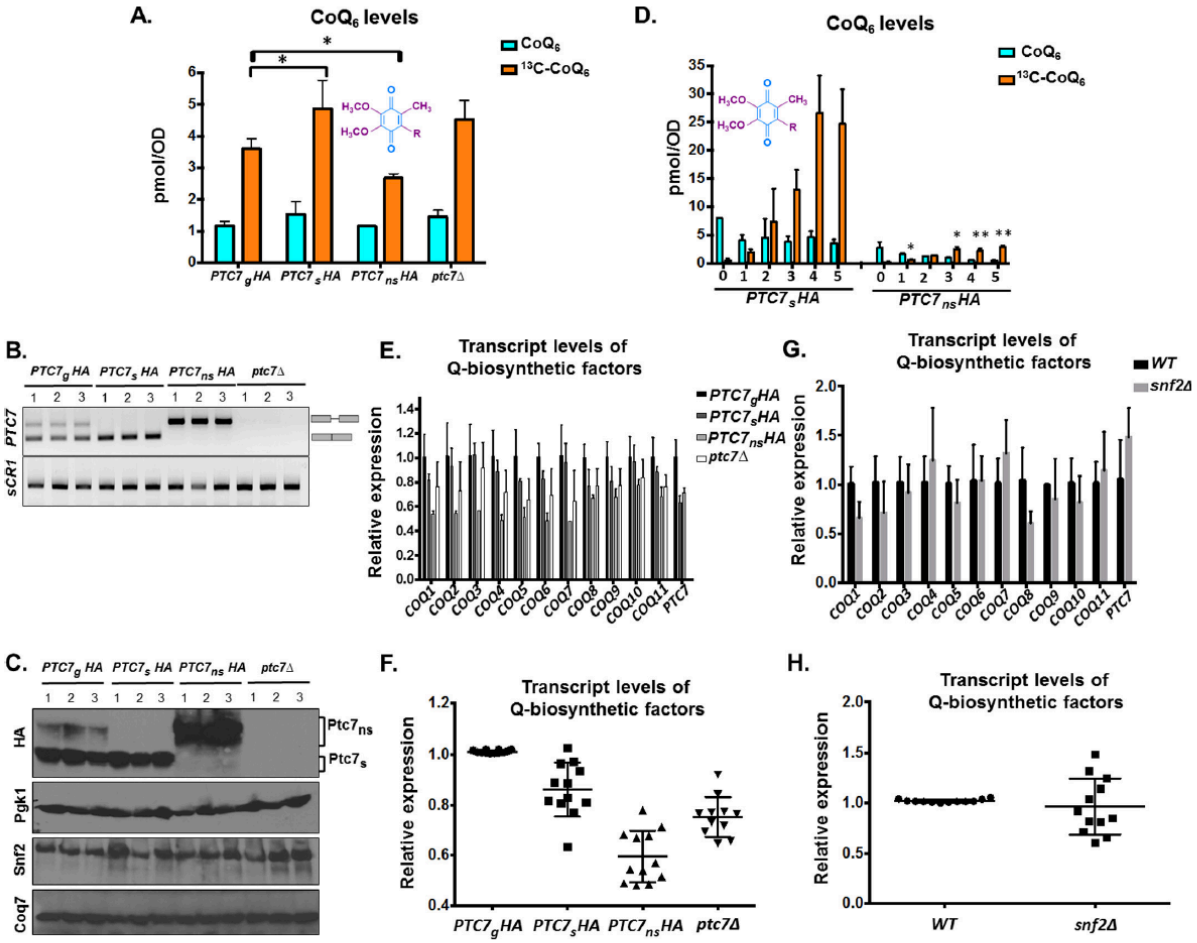

Figure 9. Ptc7 isoforms have differing and opposing effects on CoQ_6 synthesis. *A*, levels of steady-state CoQ_6 (^{12}C-CoQ_6, *blue bars*) and *de novo* synthesized CoQ_6 ($^{13}C_6$-CoQ_6, *orange bars*) in strains expressing distinct Ptc7 isoforms (*$PTC7_gHA$*, genomic, both isoforms expressed; *$PTC7_sHA$*, exclusively expresses the isoform from spliced mRNA; *$PTC7_{ns}HA$*, exclusively expresses the isoform from nonspliced pre-mRNA) and *ptc7*Δ. Labeling with $^{13}C_6$-4HB was allowed to proceed for 3 h. *Error bars*, S.D. of $n = 3$ biological replicates (unpaired Student's *t* test; *, $p < 0.05$). *B*, expression and splicing of *PTC7* for samples corresponding to *A*. PCR products representing the spliced and nonspliced forms are indicated. *C*, steady-state levels of HA-tagged Ptc7 proteins were determined by immunoblotting for samples corresponding to *A*. Proteins derived from the nonspliced and spliced forms of the *PTC7* RNA are denoted as $Ptc7_{ns}$ and $Ptc7_s$, respectively. Pgk1 (phosphoglycerate kinase 1) served as a loading control. Immunoblots for Snf2 and Coq7 are also included. *D*, levels of steady-state (^{12}C-CoQ_6, *blue bars*) and *de novo* synthesized ($^{13}C_6$-CoQ_6, *orange bars*) CoQ_6 in *$PTC7_sHA$* and *$PTC7_{ns}HA$* yeast cells were determined at the designated hours after labeling with $^{13}C_6$-4HB. *Error bars*, S.D. of $n = 3$ biological replicates (unpaired Student's *t* test between corresponding bars for *$PTC7_sHA$* and *$PTC7_{ns}HA$*; *, $p < 0.05$; **, $p < 0.005$). *E*, RT-qPCR measurement of *COQ1–COQ11* and *PTC7* transcript levels between strains expressing different Ptc7 isoforms (*$PTC7_gHA$*, genomic, both isoforms expressed; *$PTC7_sHA$*, exclusively expresses the isoform from spliced mRNA; *$PTC7_{ns}HA$*, exclusively expresses the isoform from non-spliced pre-mRNA) and *ptc7*Δ. Shown is the mean of three biological replicates. *Error bars*, S.D. *F*, summary analysis of transcript levels of Q-biosynthetic factors from *E*. *G*, RT-qPCR measurement of *COQ1-COQ11* and *PTC7* transcript levels between WT and *snf2*Δ yeast. Shown is the mean of three biological replicates. *Error bars*, S.D. *H*, summary analysis of transcript levels of Q-biosynthetic factors from *G*.

taining a stop codon within its intron) and a second gene encoding a PP2C predicted to localize to the nuclear envelope ($Ptc7_a$, from an nonspliced transcript of *PTC7a* (32). This conservation further suggests that both protein isoforms derived from the *PTC7* transcript in *S. cerevisiae* are functional. Cells lacking $Ptc7_{ns}$ show increased sensitivity to latrunculin A treatment, compared with strains expressing both isoforms of Ptc7 or lacking $Ptc7_s$ (10). Such sensitivity might suggest a distinct role for $Ptc7_{ns}$ in actin filament formation.

It is noteworthy that nuclear roles for numerous metabolic enzymes have been described previously. The ability of metabolic enzymes to "moonlight" in the nucleus, affecting gene regulation at various steps, appears to be crucial for the ability of cells to sense and adapt to their potentially distinct nutrient environments (33). Numerous mitochondrial enzymes, such as succinate dehydrogenase, fumarase, aconitase, and malate dehydrogenase (all components of the Krebs cycle), have been shown to have significant nuclear roles in the regulation of gene expression (34–38). In some of these cases, enzymatic activity of these enzymes has been shown to be crucial to their nuclear roles (39). This precedence, combined with the evolutionarily conserved presence of an isoform of Ptc7 in the nuclear membrane, raises the possibility that a nucleus-localized phosphatase is crucial to regulation of components of the CoQ_6 biosyn-

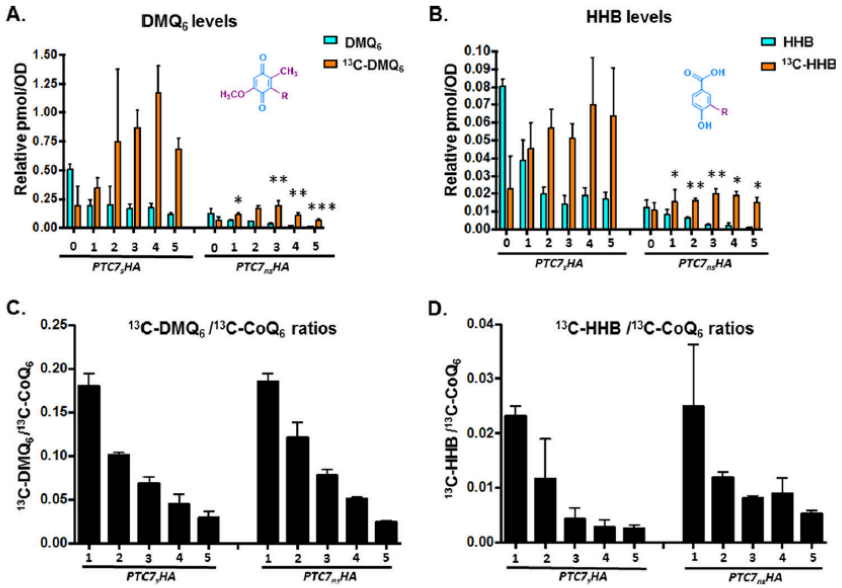

Figure 10. Exclusive expression of Ptc7 isoforms dramatically alters levels of CoQ_6 biosynthetic pathway intermediates DMQ_6 and HHB, yet overall conversion efficiency between both isoforms is comparable. *A*, levels of steady-state DMQ_6 (^{12}C-DMQ_6, *blue bars*) and *de novo* synthesized DMQ_6 ($^{13}C_6$-DMQ_6, *orange bars*) in *$PTC7_s$HA* and *$PTC7_{ns}$HA* yeast cells were determined at the designated hours after labeling with $^{13}C_6$-4HB. *Error bars*, S.D. of $n = 3$ biological replicates (unpaired Student's *t* test between *corresponding bars* for *$PTC7_s$HA* and *$PTC7_{ns}$HA*; *, $p < 0.05$; **, $p < 0.005$; ***, $p < 0.0005$). *B*, levels of steady-state HHB (^{12}C-HHB, *blue bars*) and *de novo* synthesized HHB ($^{13}C_6$-HHB, *orange bars*) in *$PTC7_s$HA* and *$PTC7_{ns}$HA* yeast cells were determined at the designated hours after labeling with $^{13}C_6$-4HB. *Error bars*, S.D. of $n = 3$ biological replicates (unpaired Student's *t* test between *corresponding bars* for *$PTC7_s$HA* and *$PTC7_{ns}$HA*; *, $p < 0.05$; **, $p < 0.005$). *C*, ratio of $^{13}C_6$-DMQ_6/$^{13}C_6$-CoQ_6 in *$PTC7_s$HA* and *$PTC7_{ns}$HA* yeast cells were determined at the designated hours after labeling with $^{13}C_6$-4HB. Ratios were derived from levels of $^{13}C_6$-CoQ_6, as shown in Fig. 7*D*. *Error bars*, S.D. of $n = 3$ biological replicates. The 0-h time point is excluded, because the ratio is not indicative of pathway conversion. *D*, ratio of $^{13}C_6$-HHB/$^{13}C_6$-CoQ_6 in *$PTC7_s$HA* and *$PTC7_{ns}$HA* yeast cells were determined at the designated hours after labeling with $^{13}C_6$-4HB. Ratios were derived from levels of $^{13}C_6$-CoQ_6, as shown in Fig. 7*D*. *Error bars*, S.D. of $n = 3$ biological replicates. The 0-h time point is excluded, because the ratio is not indicative of pathway conversion.

thetic pathway. Intriguingly, CLK-1 and COQ7, the *C. elegans* and human homologs of Coq7, which is a target for Ptc7 in *S. cerevisiae* (11), have been demonstrated to localize to the nucleus and are postulated to have roles independent of CoQ biosynthesis (40). COQ7 has also been shown to associate with chromatin in HeLa cells (40), although recently this has been attributed to a transformed cell phenomenon (41). Whereas nuclear localization of Coq7 in *S. cerevisiae* has not been demonstrated, we suggest a potential role in nuclear gene regulation for Ptc7 via phosphatase activity on Coq7 or other unidentified targets, including conventionally nuclear and other "moonlighting" mitochondrial enzymes.

It is also possible that Ptc7 has a substrate other than Coq7 that affects expression of the CoQ_6-synthome. In fact, a recent study identified with high confidence numerous differentially phosphorylated proteins in a *ptc7*Δ strain (12). Notably, this proteomic analysis does not distinguish between the potential effects of the two Ptc7 isoforms globally. In fact, rescue using plasmid-based expression of *PTC7* (full-length) does not restore dephosphorylation levels for a number of nuclear proteins, although the increased phosphorylation of mitochondrial proteins upon deletion of *PTC7* is almost completely reversed by exogenous expression of Ptc7 (12). Furthermore, it is possible that the mitochondrial role for $Ptc7_s$ is in fact covered by multiple redundancies. Ptc5 and Ptc6, two other PP2C protein phosphatases, also localize to the mitochondrial membrane, and *PTC5* demonstrates a negative genetic interaction with *PTC7*, indicating the possibility of overlapping functions (11, 31).

Interestingly, the effect of Snf2 deletion on CoQ_6 biosynthesis does not perfectly mirror the exclusive expression of $Ptc7_s$. We postulate that this is partially due to the Snf2 affecting the flux of the entire CoQ_6 biosynthetic pathway, as demonstrated by the increased conversion of early precursors. Whereas deletion of Snf2 does not, on average, change the expression of the components of the CoQ_6-synthome (Fig. 9, *G* and *H*), it is possible the Snf2 may have other effects of CoQ_6 flux. We are exploring these possibilities.

Intriguingly, although the absence of Snf2 enhances levels of CoQ_6, yeast strains lacking Snf2 have a severe growth defect on non-fermentable carbon sources, such as glycerol or acetate (26) (Fig. 1*E*). However, Snf2 protein is undetectable by immunoblotting during growth in medium containing glycerol or acetate as the only carbon source (data not shown). This leads us to hypothesize that before Snf2 protein is down-regulated in response to glucose depletion, it is required for the transition from a fermentative metabolic state to one that is predominantly respiratory in nature. The molecular details of the requirement for Snf2 in this transition are the subject of ongoing investigation. However, it is probably at least in part due to its reported role in the activation (de-repression) of genes whose transcription had previously been subject to glucose-mediated catabolite repression. This activation occurs once the glucose has been depleted or the yeast have been shifted to a

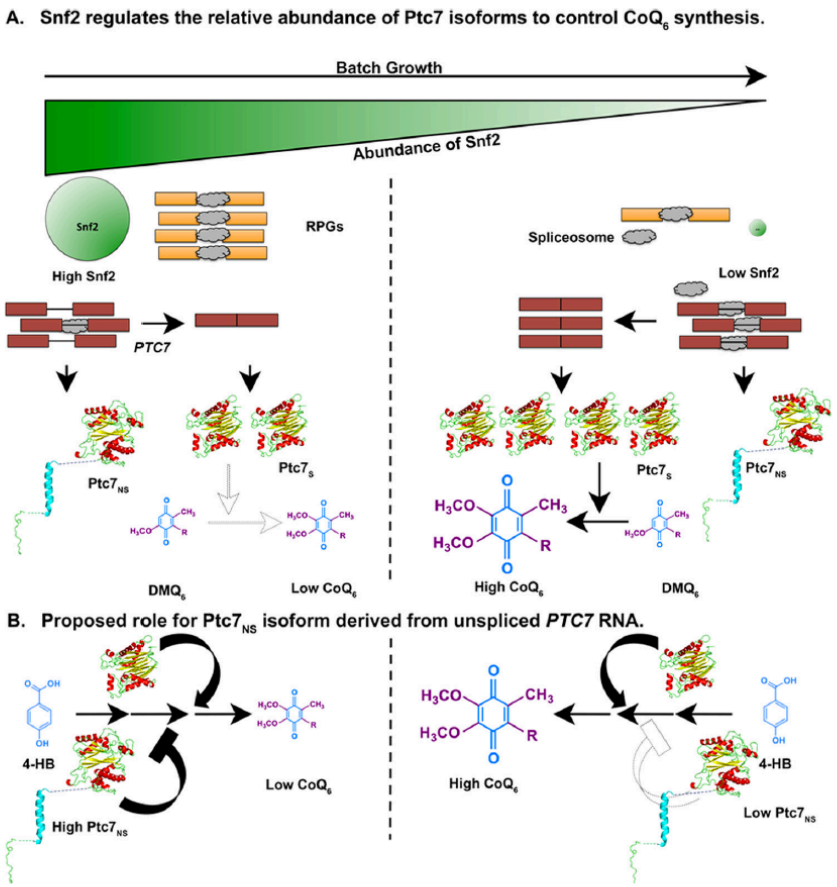

Figure 11. Model for a novel role for Snf2 in respiration, and in the transition from a primarily fermentative mode of metabolism to a primarily respiratory mode of metabolism. *A*, during *S. cerevisiae* batch growth, the abundance of Snf2 decreases in conjunction with depletion of nutrients in the medium. RPGs under the control of Snf2 are down-regulated, allowing redistribution of spliceosomes to other poorly spliced transcripts. Splicing of the *PTC7* transcript increases, enhancing the ratio of $Ptc7_s/Ptc7_{ns}$ and overall levels of $Ptc7_s$. These changes in Ptc7 isoform levels lead to increased conversion of DMQ_6 and increased synthesis of CoQ_6. The *darker arrow* represents a greater effect or reaction conversion, whereas a *lighter arrow* represents a smaller effect or reaction conversion. *B*, $Ptc7_{ns}$ has a repressive effect on CoQ_6 biosynthesis. CoQ_6 levels are low or high, depending on the levels of the $Ptc7_{ns}$ isoform relative to $Ptc7_s$. Similar to *A*, *darker arrows* and *bars* denote a larger effect, whereas *lighter arrows* and *bars* denote a smaller effect.

different, non-fermentable carbon source (26). We postulate that once the gene expression profile required for adaptation to the new nutrient environment has been initiated and/or established, the requirement for Snf2 is relieved, and in fact, the down-regulation of Snf2 enhances splicing of *PTC7*. This transient requirement for Snf2 bears striking similarities to a previous report detailing the role of Snf2 in reversing Ume6-mediated repression at certain meiotic genes early in meiosis, before it is itself down-regulated to enable splicing of meiotic transcripts (6).

This work reveals a mechanism by which SWI/SNF acts as a nexus point in the fermentation–respiratory transition in *S. cerevisiae*. We also demonstrate opposing effects of isoforms of a single gene, *PTC7*, on the process of CoQ_6 biosynthesis, via distinct mechanisms. Numerous aspects of these mechanisms remain to be studied, as well as their potential roles in the gene regulation response to other physiological conditions that yeast might experience.

Experimental procedures

Yeast strains and culture conditions

The yeast strains used in this study are listed in Table 1. All strains except W303Δcoq2 are derived from the BY background. Yeast strains were grown in YPD (1% yeast extract, 2% peptone, 2% dextrose) medium at 30 °C. Snf2 and Ptc7 null strains were maintained with a backup expression plasmid (pRS316 backbone harboring either *SNF2* or *PTC7*). The plasmid was shuffled out by growth on 5-fluoroorotic acid before using the strains in experiments. Strains with tagged isoforms of Ptc7 were a kind gift from Dr. Ron Davis (10). These strains were back-crossed against WT or *snf2*Δ strains, and daughter strains used for this study are listed in Table 1. The *snf2*Δ strain was observed to spontaneously mutate if grown on YPD for longer than 7–8 days, acquiring suppressor mutations that made it difficult to distinguish from WT. Hence, for all experiments with *snf2*Δ, the plasmid contain-

Table 1
Genotype and source of yeast strains

Strain number	Name	Genotype	Source/reference
TJY6724	WT	*MATa his3Δ leu2Δ LYS2 met15Δ ura3Δ*	Ref. 6
TJY6727	*snf2Δ*	*MATα his3Δ leu2Δ ura3Δ snf2Δ::NatMX*	Ref. 6
TJY7114	*$PTC7_gHA$*	*MATa his3Δ leu2Δ ura3Δ $PTC7_g$HA:KanMX*	This study
TJY7115	*snf2Δ$PTC7_gHA$*	*MATa his3Δ leu2Δ ura3Δ snf2Δ::NatMX $PTC7_g$HA:KanMX*	This study
W303Δ*coq2*	*coq2Δ*	*MATa ade2-1 his3-1,15 leu2-3,112 trp1-1 ura3-1 coq2::HIS3*	Ref. 47
TJY7116	*$PTC7_sHA$*	*MATa his3Δ leu2Δ ura3Δ $PTC7_s$HA:KanMX*	This study
TJY7118	*$PTC7_{ns}HA$*	*MATa his3Δ leu2Δ ura3Δ $PTC7_{ns}$HA:KanMX*	This study
TJY7142	*ptc7Δ*	*MATa his3Δ leu2Δ ura3Δ ptc7Δ:KanMX*	This study
BY4741Δ*coq9*	*coq9Δ*	*MATα his3Δ0 leu2Δ0 met15Δ0 ura3Δ0 coq9::KANMX4*	Ref. 48

ing *SNF2* was shuffled out prior to each experiment, allowing a fresh *snf2Δ* strain with each experiment, to avoid these suppressor mutants. We found that this was absolutely instrumental to observe the proper phenotype and behavior of the *snf2Δ* strain.

RNA-sequencing analyses

The RNA-sequencing data reported in this study were generated previously (6). Briefly, RNA sequencing libraries were prepared using the Illumina Truseq® V3 kit and ribosomal RNA depletion (Ribo-Zero, Illumina). Single-end, 50-nucleotide sequence reads (HiSeq 2000) were aligned to SacCer3 and spliced transcripts from the Ares Lab Yeast Intron Database version 3 (42) in a single step using STAR (43). Only the highest scoring alignments for each read were kept, allowing for at most a single tie. Reads/kb/million were computed for each gene by dividing the total number of reads that aligned entirely within the gene's exon boundaries by the gene's total exon length in kilobase pairs per million mapped reads. Reads within ICGs were categorized as exonic, spliced, or unspliced. Exonic reads map entirely within an exon, as defined by the Ares Lab Yeast Intron Database. Introns with annotated small nucleolar RNAs within the defined intron boundaries were disregarded in this analysis. Spliced reads are those that align with a gap that corresponds to an annotated intron, and unspliced reads map partially within an exon and partially within an intron with no gap. Spliced and unspliced read counts were normalized by dividing total spliced counts by the number of potential unique alignment positions that contribute to the total. For spliced reads, this is read length minus one for every intron. For unspliced read counts, this is the length of the intron plus the read length minus one. Splicing efficiency for each intron was calculated as normalized spliced counts divided by the sum of the normalized spliced and normalized unspliced counts. Changes in splicing efficiency were calculated as percentage difference over WT efficiency and plotted against expression levels (reads/kb/million) in WT. Data are available under GEO accession number GSE94404, and detailed methods were described previously (6).

RT-PCR and real-time PCR analysis

RNA was isolated from a 5-ml aliquot of cell culture corresponding to time points described in each experiment. After DNase treatment (Roche Applied Science), equal quantities of total RNA from each sample were used to make cDNA using a cDNA synthesis kit (Fermentas). To detect *PTC7* splicing isoforms, primers flanking the intronic sequences were used for PCR using 1 μl of cDNA diluted 1:20. PCR products were then separated on a 2% agarose gel and imaged. RT-qPCR was done in a 10-μl reaction volume with gene-specific primers using 1 μl of cDNA diluted 1:20 using Perfecta SYBR Green Fastmix (Quanta Biosciences) and a CFX96 Touch System (Bio-Rad). All samples were analyzed in triplicate for each independent experiment. RT-qPCR was also performed for the *scR1* (cytoplasmic signal recognition particle RNA subunit) RNA from each cDNA sample. Gene expression analysis was done by $2^{-\Delta Ct}$ methods using *scR1* as a reference. -Fold expression of mRNA was measured compared with WT by $2^{-\Delta\Delta Ct}$ methods (44).

Immunoblots

Protein was isolated from cell pellets with FA-1 lysis buffer (50 mM HEPES, pH 7.5, 150 mM NaCl, 1 mM EDTA, 1% Triton X-100, 0.1% sodium deoxycholate, 1 mM PMSF, and protease inhibitors) with bead beating. The buffer was supplemented with protease inhibitor mixture tablet (Roche Applied Science). Total protein was resolved by SDS-PAGE. The gel was transferred to PVDF membrane, and proteins were detected with the following antibodies at the stated dilutions: anti-SNF2 antibody (yN-20, Santa Cruz Biotechnology) at a 1:200 dilution in 2% milk, anti-HA antibody (901514, BioLegend) at a 1:2000 dilution in 5% milk, anti-Pgk1 antibody (459250, Invitrogen) at a 1:3000 dilution in 5% milk, or anti-Coq7 antibody (described previously (16) at a 1:2000 dilution in 3% milk. Signal was detected with enhanced chemiluminescence (Thermo Scientific) as described by the manufacturer.

Metabolic labeling of CoQ_6 with $^{13}C_6$-labeled precursors

Yeast strains were grown overnight in 25 ml of YPD in a shaking incubator (30 °C, 250 rpm) and diluted to an A_{600} of 0.1 in 60 ml of fresh YPD the next morning. The cultures were incubated as before to an A_{600} of 0.5 (midlog phase) and subsequently treated with $^{13}C_6$-4HB at 10 μg/ml (600 μg total) or ethanol vehicle control (0.015%, v/v). At designated time periods, cells were harvested by centrifugation at 3000 × *g* for 5 min, from 50-ml aliquots (used for lipid extraction) or 10-ml aliquots (used for RNA and protein analysis). Cell pellets were stored at −20 °C.

Analysis of CoQ_6 and CoQ_6 intermediates

Lipid extraction of cell pellets was conducted as described (18) with methanol and petroleum ether and CoQ_4 as the internal standard. Lipid measurements were performed by HPLC-

MS/MS and normalized to total OD. Prior to mass spectrometry analysis, all samples were treated with 1.0 mg/ml benzoquinone to oxidize hydroquinones to quinones. Mass spectrometry analyses utilized a 4000 QTRAP linear MS/MS spectrometer (Applied Biosystems), and data were acquired and analyzed using Analyst version 1.4.2 and 1.5.2 software (Applied Biosystems). Separation of lipid quinones was performed with a binary HPLC delivery system and a Luna 5μ phenyl-hexyl column (100 × 4.6 mm, 5 μm; Phenomenex). The mobile phase consisted of a 95:5 methanol/isopropyl alcohol solution with 2.5 mM ammonium formate as solution A and a 100% isopropyl alcohol solution with 2.5 mM ammonium formate as solution B. The percentage of solution B was increased linearly from 0 to 5% over 6 min, whereby the flow rate was increased from 600 to 800 μl. Initial flow rate and mobile phase conditions were changed back to initial phase conditions linearly over 3.5 min. Each sample was analyzed using multiple-reaction monitoring mode. The following precursor-to-product ion transitions were detected as well as the +17 *m/z* ammoniated adducts for each of the metabolic products: $^{13}C_6$-HHB *m/z* 553.4/157.0 (ammoniated: 570.4/157.0), ^{12}C-HHB *m/z* 547.4/151.0 (ammoniated: 564.4/151.0), $^{13}C_6$-DMQ_6 *m/z* 567.6/173.0 (ammoniated: 584.6/173.0), ^{12}C-DMQ_6 *m/z* 561.6/167.0 (ammoniated: 578.6/167.0), $^{13}C_6$-CoQ_6 *m/z* 597.4/203.1 (ammoniated: 614.4/203.1), ^{12}C-CoQ_6 *m/z* 591.4/197.1 (ammoniated: 608.4/197.1), and ^{12}C-CoQ_4 *m/z* 455.4/197.0 (ammoniated: 472.4/197.0).

Plate dilution assays

Strains were grown overnight in 5 ml of YPD and diluted to an A_{600} of 0.2 in sterile PBS. A 5-fold serial dilution in PBS was performed, after which 2 μl of each dilution (1×, 5×, 25×, 125×, and 625×) were spotted onto the designated carbon sources. The final A_{600} of the aforementioned dilution series are 0.2, 0.04, 0.008, 0.0016, and 0.00032, respectively.

PHYRE homology modeling

Phyre2 is a modeling program designed to analyze protein structure, function, and mutations (45). It is used to analyze the primary sequence of a protein and, with homology detection methods, constructs a structure that compares the protein of interest with other proteins (or motifs of proteins) with known structure. In regard to Ptc7, the full nonspliced version of the protein ($Ptc7_{ns}$), which is composed of 374 amino acids and retains its 31-amino acid intron (amino acids 19–50), was analyzed. The resulting structure and alignment coverage contained 86% of residues modeled at >90% confidence, with 14% of residues modeled *ab initio*. Additionally, the spliced isoform of Ptc7 ($Ptc7_s$), which is localized and processed in the mitochondria, comprised of 305 amino acids, resulting from the removal of the 31-amino acid intron and the excision of the predicted mitochondrial targeting sequence (the 38 N-terminal amino acids of $Ptc7_s$) (46), was also modeled using the PHYRE2 intensive modeling mode. The resulting structure and alignment coverage contains 85% of residues modeled at >90% confidence, with 15% of residues modeled *ab initio*.

Author contributions—A. M. A. and S. V. contributed equally to this work (both conducted the majority of the experiments, analyzed the results, and wrote the paper together). A. N. and M. C. B. assisted A. M. A. in conducting experiments; A. N. assisted A. M. A. in analyzing mass spectrometry results. A. R. G. and L. N. assisted S. V. in experiments, with A. R. G. also having assisted in the background research relating to PTC7 differential splicing in the snf2Δ strain shown in Fig. 1*A*. S. D. aligned the RNA-sequencing data and calculated splicing efficiencies. M. C. B. and L. N. thoroughly read and edited the working draft of the paper. C. F. C. and T. L. J. oversaw all details related to the project and provided guidance on experiments, data analysis, and the writing of this paper.

Acknowledgments—We thank Dr. James Bowie (UCLA) for advice and guidance in generating the PHYRE models and in the depiction of the spliced and nonspliced versions of Ptc7. We acknowledge the UCLA Molecular Instrumentation Core proteomics facility for the use of the QTRAP4000. We thank the laboratory of Dr. Ronald W. Davis (Stanford) for generously providing the Ptc7 spliced and nonspliced isoforms.

References

1. Naftelberg, S., Schor, I. E., Ast, G., and Kornblihtt, A. R. (2015) Regulation of alternative splicing through coupling with transcription and chromatin structure. *Annu. Rev. Biochem.* **84,** 165–198
2. Johnson, T. L., and Vilardell, J. (2012) Regulated pre-mRNA splicing: the ghostwriter of the eukaryotic genome. *Biochim. Biophys. Acta* **1819,** 538–545
3. Pleiss, J. A., Whitworth, G. B., Bergkessel, M., and Guthrie, C. (2007) Rapid, transcript-specific changes in splicing in response to environmental stress. *Mol. Cell* **27,** 928–937
4. Ares, M., Jr., Grate, L., and Pauling, M. H. (1999) An handful of intron-containing genes produces the lion's share of yeast mRNA. *RNA* **5,** 1138–1139
5. Munding, E. M., Shiue, L., Katzman, S., Donohue, J. P., and Ares, M., Jr. (2013) Competition between pre-mRNAs for the splicing machinery drives global regulation of splicing. *Mol. Cell* **51,** 338–348
6. Venkataramanan, S., Douglass, S., Galivanche, A. R., and Johnson, T. L. (2017) The chromatin remodeling complex Swi/Snf regulates splicing of meiotic transcripts in *Saccharomyces cerevisiae*. *Nucleic Acids Res.* 10.1093/nar/gkx373
7. Hossain, M. A., Claggett, J. M., Edwards, S. R., Shi, A., Pennebaker, S. L., Cheng, M. Y., Hasty, J., and Johnson, T. L. (2016) Posttranscriptional regulation of Gcr1 expression and activity is crucial for metabolic adjustment in response to glucose availability. *Mol. Cell* **62,** 346–358
8. Hossain, M. A., Rodriguez, C. M., and Johnson, T. L. (2011) Key features of the two-intron *Saccharomyces cerevisiae* gene *SUS1* contribute to its alternative splicing. *Nucleic Acids Res.* **39,** 8612–8627
9. Jiang, L., Whiteway, M., Ramos, C. W., Rodriguez-Medina, J. R., and Shen, S.-H. (2002) The YHR076W gene encodes a type 2C protein phosphatase and represents the seventh PP2C gene in budding yeast. *FEBS Lett.* **527,** 323–325
10. Juneau, K., Nislow, C., and Davis, R. W. (2009) Alternative splicing of *PTC7* in *Saccharomyces cerevisiae* determines protein localization. *Genetics* **183,** 185–194
11. Martín-Montalvo, A., González-Mariscal, I., Pomares-Viciana, T., Padilla-López, S., Ballesteros, M., Vazquez-Fonseca, L., Gandolfo, P., Brautigan, D. L., Navas, P., and Santos-Ocaña, C. (2013) The phosphatase Ptc7 induces coenzyme Q biosynthesis by activating the hydroxylase Coq7 in yeast. *J. Biol. Chem.* **288,** 28126–28137
12. Guo, X., Niemi, N. M., Hutchins, P. D., Condon, S. G., Jochem, A., Ulbrich, A., Higbee, A. J., Russell, J. D., Senes, A., Coon, J. J., and Pagliarini, D. J. (2017) Ptc7p dephosphorylates select mitochondrial proteins to enhance metabolic function. *Cell Rep.* **18,** 307–313

13. Turunen, M., Olsson, J., and Dallner, G. (2004) Metabolism and function of coenzyme Q. *Biochim. Biophys. Acta* **1660,** 171–199
14. Doimo, M., Desbats, M. A., Cerqua, C., Cassina, M., Trevisson, E., and Salviati, L. (2014) Genetics of coenzyme Q10 deficiency. *Mol. Syndromol.* **5,** 156–162
15. Quinzii, C. M., Emmanuele, V., and Hirano, M. (2014) Clinical presentations of coenzyme Q10 deficiency syndrome. *Mol. Syndromol.* **5,** 141–146
16. Tran, U. C., and Clarke, C. F. (2007) Endogenous synthesis of coenzyme Q in eukaryotes. *Mitochondrion* **7,** S62–S71
17. González-Mariscal, I., García-Testón, E., Padilla, S., Martín-Montalvo, A., Pomares Viciana, T., Vazquez-Fonseca, L., Gandolfo Domínguez, P., and Santos-Ocaña, C. (2014) The regulation of coenzyme Q biosynthesis in eukaryotic cells: all that yeast can tell us. *Mol. Syndromol.* **5,** 107–118
18. Allan, C. M., Awad, A. M., Johnson, J. S., Shirasaki, D. I., Wang, C., Blaby-Haas, C. E., Merchant, S. S., Loo, J. A., and Clarke, C. F. (2015) Identification of Coq11, a new coenzyme Q biosynthetic protein in the CoQ-synthome in *Saccharomyces cerevisiae*. *J. Biol. Chem.* **290,** 7517–7534
19. Padilla, S., Jonassen, T., Jiménez-Hidalgo, M. A., Fernández-Ayala, D. J., López-Lluch, G., Marbois, B., Navas, P., Clarke, C. F., and Santos-Ocaña, C. (2004) Demethoxy-Q, an intermediate of coenzyme Q biosynthesis, fails to support respiration in Saccharomyces cerevisiae and lacks antioxidant activity. *J. Biol. Chem.* **279,** 25995–26004
20. Padilla, S., Tran, U. C., Jiménez-Hidalgo, M., López-Martín, J. M., Martín-Montalvo, A., Clarke, C. F., Navas, P., and Santos-Ocaña, C. (2009) Hydroxylation of demethoxy-Q6 constitutes a control point in yeast coenzyme Q6 biosynthesis. *Cell Mol. Life Sci.* **66,** 173–186
21. Whitehouse, I., Flaus, A., Cairns, B. R., White, M. F., Workman, J. L., and Owen-Hughes, T. (1999) Nucleosome mobilization catalysed by the yeast SWI/SNF complex. *Nature* **400,** 784–787
22. Liu, X., Li, M., Xia, X., Li, X., and Chen, Z. (2017) Mechanism of chromatin remodelling revealed by the Snf2-nucleosome structure. *Nature* **544,** 440–445
23. Dutta, A., Gogol, M., Kim, J. H., Smolle, M., Venkatesh, S., Gilmore, J., Florens, L., Washburn, M. P., and Workman, J. L. (2014) Swi/Snf dynamics on stress-responsive genes is governed by competitive bromodomain interactions. *Genes Dev.* **28,** 2314–2330
24. Dutta, A., Sardiu, M., Gogol, M., Gilmore, J., Zhang, D., Florens, L., Abmayr, S. M., Washburn, M. P., and Workman, J. L. (2017) Composition and function of mutant Swi/Snf complexes. *Cell Rep.* **18,** 2124–2134
25. Gabunilas, J., and Chanfreau, G. (2016) Splicing-mediated autoregulation modulates Rpl22p expression in *Saccharomyces cerevisiae*. *PLoS Genet.* **12,** e1005999
26. Neigeborn, L., and Carlson, M. (1984) Genes affecting the regulation of SUC2 gene expression by glucose repression in *Saccharomyces cerevisiae*. *Genetics* **108,** 845–858
27. Martín-Montalvo, A., González-Mariscal, I., Padilla, S., Ballesteros, M., Brautigan, D. L., Navas, P., and Santos-Ocaña, C. (2011) Respiratory-induced coenzyme Q biosynthesis is regulated by a phosphorylation cycle of Cat5p/Coq7p. *Biochem. J.* **440,** 107–114
28. Martin, D. E., Soulard, A., and Hall, M. N. (2004) TOR regulates ribosomal protein gene expression via PKA and the Forkhead transcription factor FHL1. *Cell* **119,** 969–979
29. Wang, A., Mouser, J., Pitt, J., Promislow, D., and Kaeberlein, M. (2016) Rapamycin enhances survival in a *Drosophila* model of mitochondrial disease. *Oncotarget* **7,** 80131–80139
30. González-Mariscal, I., Martín-Montalvo, A., Ojeda-González, C., Rodríguez-Eguren, A., Gutiérrez-Rios, P., Navas, P., and Santos-Ocaña, C. (2017) Balanced CoQ6 biosynthesis is required for lifespan and mitophagy in yeast. *Microb. Cell* **4,** 38–51
31. Sharmin, D., Sasano, Y., Sugiyama, M., and Harashima, S. (2014) Effects of deletion of different PP2C protein phosphatase genes on stress responses in *Saccharomyces cerevisiae*. *Yeast* **31,** 393–409
32. Marshall, A. N., Montealegre, M. C., Jiménez-Lopez, C., Lorenz, M. C., and van Hoof, A. (2013) Alternative splicing and subfunctionalization generates functional diversity in fungal proteomes. *PLoS Genet.* **9,** e1003376
33. Boukouris, A. E., Zervopoulos, S. D., and Michelakis, E. D. (2016) Metabolic enzymes moonlighting in the nucleus: metabolic regulation of gene transcription. *Trends Biochem. Sci.* **41,** 712–730
34. De, P., and Chatterjee, R. (1962) Evidence of nucleolar succinic dehydrogenase activity. *Exp. Cell Res.* **27,** 172–173
35. De, P., and Chatterjee, R. (1962) Nucleolar localization of succinic dehydrogenase in human malignant cells with MTT. *Experientia* **18,** 562
36. Yogev, O., Yogev, O., Singer, E., Shaulian, E., Goldberg, M., Fox, T. D., and Pines, O. (2010) Fumarase: a mitochondrial metabolic enzyme and a cytosolic/nuclear component of the DNA damage response. *PLoS Biol.* **8,** e1000328
37. Jung, S. J., Seo, Y., Lee, K. C., Lee, D., and Roe, J. H. (2015) Essential function of Aco2, a fusion protein of aconitase and mitochondrial ribosomal protein bL21, in mitochondrial translation in fission yeast. *FEBS Lett.* **589,** 822–828
38. Lee, S. M., Kim, J. H., Cho, E. J., and Youn, H. D. (2009) A nucleocytoplasmic malate dehydrogenase regulates p53 transcriptional activity in response to metabolic stress. *Cell Death Differ.* **16,** 738–748
39. McEwen, B. S., Allfrey, V. G., and Mirsky, A. E. (1963) Studies on energy-yielding reactions in thymus nuclei. *J. Biol. Chem.* **238,** 2571–2578
40. Monaghan, R. M., Barnes, R. G., Fisher, K., Andreou, T., Rooney, N., Poulin, G. B., and Whitmarsh, A. J. (2015) A nuclear role for the respiratory enzyme CLK-1 in regulating mitochondrial stress responses and longevity. *Nat Cell Biol.* **17,** 782–792
41. Liu, J. L., Yee, C., Wang, Y., and Hekimi, S. (2017) A single biochemical activity underlies the pleiotropy of the aging-related protein CLK-1. *Sci. Rep.* **7,** 859
42. Grate, L., and Ares, M., Jr. (2002) Searching yeast intron data at Ares lab Web site. *Methods Enzymol.* **350,** 380–392
43. Dobin, A., Davis, C. A., Schlesinger, F., Drenkow, J., Zaleski, C., Jha, S., Batut, P., Chaisson, M., and Gingeras, T. R. (2013) STAR: ultrafast universal RNA-seq aligner. *Bioinformatics* **29,** 15–21
44. Livak, K. J., and Schmittgen, T. D. (2001) Analysis of relative gene expression data using real-time quantitative PCR and the $2(-\Delta\Delta C(T))$ method. *Methods* **25,** 402–408
45. Kelley, L. A., Mezulis, S., Yates, C. M., Wass, M. N., and Sternberg, M. J. (2015) The Phyre2 web portal for protein modeling, prediction and analysis. *Nat. Protoc.* **10,** 845–858
46. Vögtle, F. N., Wortelkamp, S., Zahedi, R. P., Becker, D., Leidhold, C., Gevaert, K., Kellermann, J., Voos, W., Sickmann, A., Pfanner, N., and Meisinger, C. (2009) Global analysis of the mitochondrial N-proteome identifies a processing peptidase critical for protein stability. *Cell* **139,** 428–439
47. Ashby, M. N., Kutsunai, S. Y., Ackerman, S., Tzagoloff, A., and Edwards, P. A. (1992) COQ2 is a candidate for the structural gene encoding para-hydroxybenzoate:polyprenyltransferase. *J. Biol. Chem.* **267,** 4128–4136
48. Winzeler, E. A., Shoemaker, D. D., Astromoff, A., Liang, H., Anderson, K., Andre, B., Bangham, R., Benito, R., Boeke, J. D., Bussey, H., Chu, A. M., Connelly, C., Davis, K., Dietrich, F., Dow, S. W., *et al.* (1999) Functional characterization of the *S. cerevisiae* genome by gene deletion and parallel analysis. *Science* **285,** 901–906

CHAPTER 4

Coordination of transcription elongation and spliceosome assembly and a role for H2A.Z

INTRODUCTION

Co-transcriptional recruitment of the spliceosome to nascent mRNA occurs in a stepwise fashion via a series of highly regulated rearrangements (Johnson and Vilardell 2012). Intriguingly, H2A.Z deletion leads to persistent occupancy of the U2 snRNP-associated protein Msl1 on the nascent RNA (Neves et al. 2017), indicating a defect in spliceosomal rearrangements (Gunderson et al. 2011). Additionally, recruitment of a downstream splicing factor Snu114 is significantly decreased, suggesting that H2A.Z loss causes defective spliceosome rearrangements that prevent binding of downstream spliceosome components (Neves et al. 2017). Given the reported roles of H2A.Z in transcription (Santisteban et al. 2011), we hypothesized that H2A.Z affects transcriptional elongation in such a way that alters spliceosome rearrangement kinetics. Indeed, H2A.Z deletion leads to decreased RNA polymerase II (RNAPII) occupancy throughout the gene body of tested genes (Neves et al. 2017), suggesting that transcription elongation is defective in cells lacking H2A.Z. Moreover, deletion of the well-characterized elongation factor Dst1 (TFIIS), which leads to persistent U2 snRNP association in a similar manner to H2A.Z deletion, can exacerbate H2A.Z-mediated splicing defects (Neves et al. 2017). Stalled spliceosomes are normally recognized and disassembled by Prp43 (Arenas and Abelson 1997). Satisfyingly, our previous work has shown that, in the absence of H2A.Z, depletion of Prp43 improves splicing of a number of intron-containing genes (ICGs), particularly those containing a non-consensus branchpoint (BP) sequence (Neves et al. 2017). This is likely because Prp43 depletion allows more time for rearrangements to occur before spliceosome disassembly takes place. Our work suggests that H2A.Z is required for maintaining an optimal transcription elongation rate and, in absence of H2A.Z, elongation is slowed, altering the availability of nascent pre-mRNA and delaying

spliceosome rearrangements. Decreased availability of disassembly machinery slows the kinetics of spliceosome disassembly and allows more time for rearrangements to take place (Figure 4.1).

It is clear that H2A.Z affects the kinetics of transcription elongation and the outcomes of co-transcriptional splicing. However, the way in which H2A.Z coordinates these processes remains ambiguous. While splicing of non-consensus BP containing introns is most affected by H2A.Z deletion, it is not clear if H2A.Z specifically affects the step of branchpoint recognition. Here we show that not only mutation of the BP sequence, but also mutation of the 5' or 3' splice site (SS), renders introns susceptible to loss of H2A.Z. Additionally, aberrant spliceosome recruitment and rearrangements upon H2A.Z deletion (Neves et al. 2017) indicate that H2A.Z likely affects the conversion to the catalytically competent B* splicing complex. Additionally, we attempt to elucidate the relationship between the rate of transcription elongation, the rate of spliceosome rearrangements, and the "molecular clocks" that drive those rearrangements. Our data suggests that the disassembly machinery interactions with the co-transcriptional spliceosome occur weakly or very transiently. Interestingly, we find that cells containing a hypomorphic allele of the DEAH-box helicase Prp22 are incapable of growth under transcriptional stress, providing further evidence for the need for precise kinetic coordination of transcription and splicing. Finally, we show that deletion of Dst1 in cells lacking H2A.Z may affect splicing outcomes in two distinct and opposing manners.

RESULTS

Mutation of splice sites renders introns sensitive to H2A.Z presence for efficient splicing.

We previously observed strong genetic interactions of H2A.Z with U2 snRNP factors and splicing defects, particularly in introns containing non-consensus BP sequences (Neves et al.

2017), leading us to predict that H2A.Z potentially affects the step of branch point recognition. However, it is unclear whether changes to the branch point specifically, render introns sensitive to H2A.Z loss or if any weak splice site, or, indeed, factors beyond splice site sequences, can confer sensitivity to H2A.Z. In order to compare splicing of introns with a suboptimal BP sequence to those containing consensus sequences or a suboptimal 5' or 3' SS in an otherwise identical context, we employed the *ACT1-CUP1* reporter system. In this assay, *cup1*Δ cells were transformed with a plasmid encoding the *CUP1* gene interrupted by the *ACT1* intron. Cup1 is essential for copper toxicity resistance in yeast and, therefore, growth in copper-containing media is a readout for the efficiency of splicing of the *ACT1-CUP* construct (Lesser and Guthrie 1993). As the splice sites in yeast are very well conserved, *ACT1-CUP1* constructs containing mutations in the 5' SS, BP sequence, or 3' SS allow us to determine how well the spliceosome can utilize suboptimal splice sites (Lesser and Guthrie 1993) (Figure 4.2 A). We compared the splicing of mutated *ACT1-CUP1* in *cup1*Δ and *htz1*Δ*cup1*Δ cells. Notably, the consensus *ACT1-CUP1* construct is spliced efficiently, even in the absence of *HTZ1*. Surprisingly, we find that when any splice site is mutated, cells grow poorly in the presence of copper (Figure 4.2 B), suggesting that any suboptimal splice site renders introns dependent on H2A.Z presence. However, this is consistent with our previous genetic observations that, in destabilizing conditions, H2A.Z is required for growth when any component of the spliceosome is compromised (Neves et al. 2017).

Deletion of H2A.Z decreases co-transcriptional recruitment of the NineTeen Complex.

Previously we observed that spliceosome rearrangements are defective in the absence of H2A.Z, and, in particular, there is persistent association of the U2 snRNP factor Msl1 with the

nascent RNA and concomitant decreased association of the downstream U5 snRNP factor Snu114 (Neves et al. 2017). Because co-transcriptional recruitment of the spliceosome to the nascent pre-mRNA occurs in a predictable and stepwise fashion, chromatin immunoprecipitation of splicing factors can be used to determine at what point in spliceosome assembly defects occur when H2A.Z is lost. We further analyzed changes in spliceosome rearrangements upon *HTZ1* deletion by examining the recruitment profile of the NineTeen Complex (NTC) factor Prp19 across three ICGs (*YCL002C, ECM33, RPL13A*)(Figure 4.3 A). Consistent with decreased U5 snRNP recruitment, Prp19 recruitment across *ECM33* and *RPL13A* is significantly reduced in cells lacking H2A.Z (Figure 4.3 B). Prp19 recruitment was slightly decreased through the middle of exon 2 of *YCL002C* (Figure 4.3 B, left). However, because Prp19 recruitment to *YCL002C* is very low in wild type cells, differences in Prp19 enrichment are difficult to resolve. The extremely low recruitment of the NTC may, in part, account for poor splicing of *YCL002C* even under optimal conditions. Decreased Prp19 occupancy cannot be attributed to changes in protein expression (Figure 4.3 C). These results are consistent with our model in which loss of H2A.Z increases the association of the U2 snRNP and reduces association of downstream splicing factors. These findings are similar to spliceosome rearrangement defects observed upon loss of histone deacetylases Hos2 or Hos3, suggesting that H2A.Z and histone H3 acetylation may have overlapping roles in co-transcriptional splicing (Gunderson et al. 2011).

Association of disassembly factors with nascent RNA is very transient.

Prp43 is a DEAH-box helicase that has functions in ribosome biogenesis as well as spliceosome disassembly (Arenas and Abelson 1997; Leeds et al. 2006). Prp43 not only catalyzes disassembly upon completion of splicing (Arenas and Abelson 1997), but can also

disassemble spliceosomes when splicing is slowed (Koodathingal et al. 2010; Koodathingal and Staley 2013a).

Because we have shown that, while spliceosome rearrangements are defective in cells lacking H2A.Z, depletion of Prp43 can suppress defects in splicing outcomes, we suspect that Prp43 disassembles stalled spliceosomes that occur when H2A.Z is absent (Neves et al. 2017). We therefore predicted that we would observe increased Prp43 enrichment on the nascent RNA of poorly spliced ICGs in cells lacking H2A.Z. Surprisingly, Prp43 showed no enrichment across candidate genes *YCL002C* or *ECM33* compared to a non-transcribed region in wild-type or *htz1*Δ cells (Figure 4.4 A, B). Because Prp43 is highly abundant, has roles outside of splicing, and may physically interact with histones (Lebaron et al. 2005; Lambert et al. 2009; Banerjee et al. 2015), it is possible that Prp43 occupancy is difficult capture at specific genes. We therefore focused on Ntr1, a spliceosome disassembly factor that forms the nineteen-related (NTR) complex with Ntr2 and Prp43 in order to recruit Prp43 to the spliceosome (Tsai et al. 2005). However, similar to Prp43, no enrichment of Ntr1 could be observed at candidate genes compared to a non-transcribed region (Figure 4.4 C).

While it is conceivable that Prp43 disassembles stalled spliceosomes post-transcriptionally, because Prp43 helicase targets the U2 snRNP-intron interaction (Fourmann et al. 2016) and we have shown that, despite prolonged association, U2 snRNP enrichment decreases to wild-type levels at the 3' end of the RNA in *htz1*Δ cells (Neves et al. 2017), there is a strong possibility that Prp43 association is very transient. Interactions between the spliceosome and disassembly machinery may also be too weak to capture through traditional methods of chromatin immunoprecipitation and so we cannot conclude that Prp43 is not present at the gene locus in *htz1*Δ cells without further examination.

DAmP alleles do not change RNA abundance of DEAH-box helicases Prp16 and Prp22 but can cause sensitivity to defects in transcription elongation.

A subset of DEAD- and DEAH-box helicases that drive spliceosomal rearrangements and disassembly have been proposed to act as 'molecular clocks' (Koodathingal and Staley 2013a). In particular DEAH-box helicases Prp16 and Prp22, along with disassembly factor Prp43, may act as an intrinsic timing mechanism that can recognize stalled spliceosomes and target them for splice-site resampling or disassembly and pre-mRNA release (Mayas et al. 2006; Koodathingal et al. 2010; Chen et al. 2013; Semlow et al. 2016). Therefore, changes in expression of these proteins may allow for decreased (in the case of elevated Prp16/Prp22) or increased (reduced Prp16/Prp22) reliance on H2A.Z to provide precise coordination of splicing with transcription elongation.

Surprisingly, we were unable to detect any sporulation of a heterozygous diploid strain containing a *prp16*^{DAmP} allele (data not shown). In this strain, the 3'UTR of *PRP16* is disrupted with an antibiotic resistance cassette, a modification that is expected to RNA expression (Breslow et al. 2008), although we were unable to detect an appreciable change in *PRP16* RNA levels (Figure 4.5 A). However, sporulation could not be induced even when the *prp16*^{DAmP} heterozygous diploid was supplemented with a plasmid containing a wild type *PRP16* copy (data not shown), suggesting that this allele may in fact cause overexpression of Prp16 at the translational level and/or have a dominant-negative effect on Prp16 function. Because we were unable to attain haploid cells from the heterozygous diploid strain, we constructed *prp16*^{DAmP} alleles in both wild-type and *htz1*Δ cells (as described in Breslow et al. 2008). Unexpectedly, neither the *prp16*^{DAmP} nor *prp22*^{DAmP} construct significantly altered *PRP16* or *PRP22* RNA levels (respectively) in wild-type or cells lacking H2A.Z (Figure 4.5 B). Additionally, while *prp22*^{DAmP}

confers a slight growth defect that is exacerbated at lower temperatures (25°C), deletion of H2A.Z does not appear to affect growth of either *prp16*^{DAmP} or *prp22*^{DAmP} cells in rich media (Figure 4.5 C). Curiously, and despite no apparent change in *PRP22* RNA expression, *prp22*^{DAmP} cells are highly intolerant to defects in transcription elongation as they are incapable of growth in the presence of 6-azauracil (6AU) (Figure 4.5 D). Mutants with known defects in transcription elongation (such as *DST1*) are highly susceptible to 6AU (Mason and Struhl 2005), which inhibits inosine 5' monophosphate (IMP) dehydrogenase leading to a decrease in the pool of available ribonucleotides (Archambault et al. 1992). This suggests that the DAmP allele may alter Prp22 expression at the protein level and provides further evidence for the kinetic coordination of splicing and transcription elongation.

Deletion of transcription elongation factor Dst1 in cells lacking H2A.Z affects splicing by two distinct mechanisms.

Dst1 (TFIIS) is a well characterized transcription elongation factor that prevents backtracking of stalled polymerase elongation complexes (Reviewed in Freedman et al. 2013). We previously found that, similar to H2A.Z, Dst1 is important for efficient rearrangements of the U2 snRNP and deletion of *DST1* not only exacerbates growth defects, but can also further decrease splicing efficiency of non-consensus BP containing introns of *CIN2* and *SUS1* in cells lacking H2A.Z (Neves et al. 2017).

In the absence of Dst1, RNAPII is less processive and polymerase pause sites shift, particularly during transcriptional stress (Mason and Struhl 2005; Churchman and Weissman 2011). We therefore asked how deletion of Dst1 affects polymerase occupancy patterns in cells lacking H2A.Z. Satisfyingly, loss of Dst1 in *htz1*Δ cells further decreases Rpb3 occupancy on

our candidate genes *ECM33* and *PMA1* (Figure 4.6 A, B), suggesting that H2A.Z and Dst1 have overlapping, but not identical, roles in transcription elongation. Increased perturbation to transcription elongation kinetics by Dst1 deletion in *htz1*Δ cells may further disrupt spliceosome rearrangements and lead to decreased splicing.

We next analyzed splicing genome-wide to determine to what extent Dst1 deletion enhances H2A.Z-mediated splice defects. We repeated our comparison of the splicing efficiency in wild-type and *htz1*Δ cells (Figure 4.6 C, left), and, as expected, deletion of H2A.Z decreases splicing of a subset of genes. In contrast, deletion of Dst1 has little to no affect on the majority of ICGs (Figure 4.6 C, middle), indicating that the affect of Dst1 alone on co-transcriptional splicing is more subtle than that of H2A.Z. There are notable exceptions, such as decreased splicing of *NBL1* or increased splicing of *MCO13* (Figure 4.6 C, middle: *NBL1* in green, *MCO13* in blue), that suggest that splicing of these genes are particularly susceptible to Dst1 presence. Although we expected to largely find decreased splicing, we also observed subsets of genes in which splicing was increased by deletion of Dst1 in *htz1*Δ cells (Figure 4.6 C, right). Interestingly, splicing of ICGs with generally poor splicing (<40% in wild-type cells) is most improved by the deletion of Dst1 in *htz1*Δ cells (Figure 4.6 D).

It has been shown that competition between RNAs for spliceosome components alters splicing efficiency. In *S. cerevisiae*, due to the large number of intron-containing ribosomal protein genes (RPGs), perturbations to RPG expression alters the availability of the spliceosome to non-RPG pre-mRNAs (Munding et al. 2013). Specifically, down-regulation of intron-containing RPGs, which typically account for 90% of all spliced transcripts, leads to a global increase of non-RPG splicing, especially of poorly spliced genes such as intron-containing meiotic transcripts (Munding et al. 2013; Venkataramanan et al. 2017). We therefore considered

the possibility that splicing improvement due to *DST1* deletion was due to altered RPG abundance. In fact, although deletion of *HTZ1* or *DST1* alone does not significantly alter RPG expression, there is a general decrease in RPG expression in *dst1*Δ *htz1*Δ double mutants (Figure 4.6, E). While the general down-regulation is modest (1.3 fold decrease on average), past studies have shown that even small changes in RPG expression are enough to improve splicing globally (Munding et al. 2013). Deletion of Dst1 may not only affect transcription elongation, but may also increase the available pool of spliceosomes, and therefore may alter splicing in two distinct and opposing ways in cells lacking H2A.Z.

DISCUSSION

While spatial and temporal coordination of the processes of RNA synthesis and RNA processing has been established (Reviewed in Herzel et al. 2017), the mechanisms by which such kinetic coordination occurs have not been well characterized. A growing body of recent evidence indicates that the local chromatin environment plays a role in establishing and maintaining coordination between transcription elongation and pre-mRNA splicing. In particular, our past studies demonstrate that H2A.Z promotes transcription elongation and ensures optimal splicing, particularly of slowly spliced weak introns. Depletion of spliceosome disassembly machinery in cells lacking H2A.Z allows for more time for the completion of splicing catalysis and therefore can help restore appropriate splicing (Neves et al. 2017). In this chapter, we demonstrate that H2A.Z is important for splicing of weak splice sites at any position (5' SS, BP, or 3' SS) and likely influences spliceosome rearrangements that drive the transition to the catalytically competent B* complex. Disassembly of spliceosomes stalled prior to catalysis in *htz1*Δ cells likely takes place rapidly through very transient or weak association of Prp43. Additionally,

supporting the fine-tuned coordination of transcription and splicing, we show that changes in DEAH-box helicase genes that potential alter RNA stability render cells extremely sensitive to changes in transcription elongation. However, we find such coordination of the chromatin with transcription elongation and spliceosome machinery may be multivariable and perturbations to one process may have consequences that affect the overall balance in multiple ways.

Does H2A.Z influence a specific step of splicing?

Our mutational analysis of splicing of the *ACT1-CUP1* reporter gene demonstrates that mutation of any splice site renders cells lacking H2A.Z unable to produce enough functional Cup1 to survive in the presence of copper (Figure 4.2). While these results suggest that weak splice sites alone can confer sensitivity to H2A.Z in an otherwise identical context, there are important caveats to this experiment that must be addressed. As growth is the readout, this assay only indirectly measures changes in splicing efficiency of the *ACT1* intron. It will be interesting in the future to directly assay changes in splicing in *htz1*Δ*cup1*Δ cells grown in copper-containing using RT-PCR. Additionally, because the *ACT1-CUP1* construct is introduced on a plasmid, rather than integrated at an endogenous promoter, it is difficult to assay for a direct role of a histone on *ACT1* splicing with high confidence. It has been shown that plasmid DNA is packaged in to nucleosome-like structures (Mladenova et al. 2009), but it will be important to determine if, and where, H2A.Z occupies the *ACT1-CUP1* plasmid.

Chromatin immunoprecipitation reveals that, similar to Snu114 (Neves et al. 2017), loss of H2A.Z leads to decreased association of the NineTeen Complex protein Prp19 with nascent RNA (Figure 4.3). In summary, we have found that U2 snRNP occupancy is prolonged and downstream U5 snRNP and NTC recruitment is greatly decreased, but U1 snRNP occupancy is

unchanged in the absence of H2A.Z (Neves et al. 2017). Together, these findings indicate that H2A.Z influences spliceosome rearrangements just downstream of U1 snRNP ejection as the NTC is recruited, potentially during conversion to the catalytically competent B* complex (Hoskins and Moore 2012). The DEAH-box helicase Prp2 mediates this transition by catalyzing ATP-dependent rearrangements that dissociate SF3 from the branch point to allow for the first step of splicing catalysis (Lardelli et al. 2010). Mutation of Prp2 blocks the first step of splicing by arresting SF3-containing spliceosomes, which are targeted for Prp43-mediated disassembly (Lardelli et al. 2010; Chen et al. 2013). Changes in association of SF3 factors, such as Hsh155 or Prp9, with nascent RNA in cells lacking H2A.Z, such as persistent enrichment as observed with Msl1, may indicate that H2A.Z is required for Prp2 functions.

How does disassembly machinery respond to spliceosomes stalled in the absence of H2A.Z?

Because Prp43 disassembles stalled spliceosomes, we expected to find increased Prp43 enrichment on the nascent RNA of poorly spliced ICGs in cells lacking H2A.Z, but, surprisingly, no Prp43 enrichment could be observed across candidate genes (Figure 4.4). Prp43 normally disassembles the intron-lariat complex after catalysis is complete and the mature mRNA has been released (Arenas and Abelson 1997; Martin et al. 2002) and so it is possible that, under optimal splicing conditions, Prp43 acts upon the spliceosome post-transcriptionally. However, this is unlikely to be true in the case of spliceosomes stalled before either of the two catalytic steps. It has been shown that Prp43 helicase activity mediates disassembly through disruption of the U2 snRNP-intron interaction (Fourmann et al. 2016). Our previous studies show that, while the temporal association of the U2 snRNP factor Msl1 with nascent RNA is aberrantly extended in cells lacking H2A.Z, Msl1 enrichment decreases to wild-type levels near the end of our

candidate gene indicating that the U2 snRNP is removed from the RNA before transcription is complete (Neves et al. 2017). Therefore, during disassembly of stalled or suboptimal spliceosomes, disassembly machinery likely interacts with the spliceosome very transiently. Intriguingly, it was recently shown that Ntr2, the third protein component of NTR complex, is not strictly required for spliceosome disassembly but may have a role in discriminating between optimal and suboptimal/stalled spliceosomes (Fourmann et al. 2017). Increased occupancy of Ntr2, rather than Prp43 or Ntr1, may be more indicative of disassembly of stalled spliceosomes that occur in H2A.Z. Additionally, it will be of interest to determine if deletion or depletion of Ntr2 is sufficient to suppress H2A.Z mediated splicing defects.

How does H2A.Z coordinate the kinetics of splicing catalysis and transcription elongation?

DEAH-box helicases Prp16 and Prp22 have been proposed to act as 'molecular clocks' because they can recognize and reversibly reject suboptimal, slowly spliced substrates to either activate alternative splice sites or reject substrates to trigger spliceosome disassembly and subsequent degradation of unspliced transcripts (Mayas et al. 2006; Koodathingal et al. 2010; Koodathingal and Staley 2013b; Semlow et al. 2016). Interestingly, the presence of Prp16 or Prp22 prevents binding of the NTR complex and subsequent Prp43 recruitment (Chen et al. 2013). The balance of Prp16 and Prp22 with Prp43 therefore helps determine the fate of the nascent mRNA. It was recently demonstrated that Prp16 overexpression suppresses defective splicing caused by H2A.Z deletion (Nissen et al. 2017), likely because, although Prp16 normally antagonizes stalled spliceosomes, excess Prp16 can protect nascent mRNA by outcompeting disassembly factors and promoting resampling of weak splice sites (Chen et al. 2013; Semlow et al. 2016).

We find that *prp22*^{DAmP} cells are highly intolerant to treatment with 6-azauracil (Figure 4.5), which inhibits inosine 5' monophosphate (IMP) dehydrogenase leading to a decrease in the pool of available ribonucleotides (Archambault et al. 1992). As mutants with known defects in transcription elongation (such as *DST1*) are highly susceptible to 6AU (Mason and Struhl 2005), 6AU treatment likely inhibits or slows elongation. Because *PRP22* RNA abundance is unchanged in *prp22*^{DAmP} cells, the DAmP allele may alter Prp22 expression at the protein level. The 3'UTR has long been known to have an important role in translational regulation (Day and Tuite 1998) and, because the *prp22*^{DAmP} allele confers a clear growth disadvantage, is likely that DAmP allele to changes in Prp22 protein expression. Therefore, in order to determine the nature of the relationship between defects in transcription elongation and changes in Prp22 abundance, it will be important to determine the protein expression of Prp22 using a specific antibody. Alternatively, a 'degron' allele, in which the DAmP allele has been combined with a short C-terminally fused degradation tag, could be used (Breslow et al. 2008). Not only can protein produced from a *PRP22* degron allele be visualized and quantified, but also this tag is reported to target the protein for proteasomal degradation, thus producing a stronger hypomorphic allele (Breslow et al. 2008).

Our data supports a model by which H2A.Z coordinates the kinetics of transcription elongation and spliceosome rearrangements (Figure 4.1). We therefore expected that perturbation to transcription elongation machinery would exacerbate splicing defects in *htz1*Δ cells. Surprisingly, although loss of Dst1 further decreased RNAPII occupancy in *htz1*Δ cells, we find that *DST1* deletion can both exacerbate and suppress of H2A.Z-mediated splicing defects (Figure 4.6). Interestingly, loss of both Dst1 and H2A.Z leads to a general down-regulation of intron-containing ribosomal protein genes, which typically account for the vast majority of all

transcripts engaged by the spliceosome (Munding et al. 2013). Therefore, loss of both H2A.Z and Dst1 may affect splicing outcomes in at least two opposing ways. Loss of Dst1 exacerbates transcription elongation defects in *htz1*Δ cells, which can perturb downstream spliceosome rearrangements and further decrease splicing efficiency of a number of H2A.Z-sensitive ICGs. However, through an as-yet unknown mechanism, deletion of both *DST1* and *HTZ1* causes generally decreased expression of intron-containing RPGs, which relieves competition for the limited spliceosome and improves splicing of normally poorly spliced genes (Munding et al. 2013).

Because decreases in global RPG levels may lead to increased splicing efficiency, it will be necessary to uncouple effects of spliceosome availability and transcription elongation on splicing outcomes to determine to what extent deletion of *DST1* in cells lacking H2A.Z exacerbates splicing defects through transcriptional defects. As increased spliceosome availability due to decreased RPG expression may enhance splicing of non-RPGs and mask splicing defects due to transcriptional changes in *dst1*Δ *htz1*Δ, restoring competition for spliceosomes in these cells may reveal splicing defects due to exacerbated transcription elongation defects. Decreased expression of splicing factors (as through the DAmP method described previously) will limit spliceosome availability and likely lead to strong splicing defects in cells lacking both H2A.Z and Dst1. Due to the compounded transcription elongation defects we observed in *dst1*Δ *htz1*Δ cells (Figure 4.6 A,B), we expect to observe more unspliced pre-mRNA in double mutants expressing DAmP alleles than in either of the single mutants (*htz1*Δ or *dst1*Δ) alone. Due to the multivariate coordination of the chromatin with transcription elongation and spliceosome machinery, in which perturbations to one process may have multiple and

opposing consequences, more work is necessary to elucidate the mechanisms by which the chromatin influences and maintains the kinetic balance of transcription and splicing.

MATERIALS AND METHODS

Yeast strains, media, and plasmids: All *S. cerevisiae* strains used in this study are listed in Table 4.1. Strains described in Table 4.1 are in the BY4743 strain background with the exception of Prp19-HA, provided by Karla Neugebauer, and *cup1*Δ strains, provided by Christine Guthrie. All strains were propagated according to standard procedures in either YPD (1% yeast extract, 2% peptone, 2% dextrose) or appropriate selective media. Deletion of *HTZ1* in *cup1*Δ strains was as described in (Neves et al. 2017). The $prp16^{DAmP}$ strains were constructed as described in (Breslow et al. 2008).

TABLE 4.1: Yeast strains used in this chapter

Name	Parent	Relevant Phenotype	Reference
TJY1977	BY 4743	leu2Δ0 ura3Δ0	Open Biosystems
TJY1900	BY 4743	htz1Δ::kanMX4	Open Biosystems
TJY7101	BY4743	leu2Δ0 ura3Δ0 kanMX4	This study
TJY6906	BY 4741	htz1Δ::natMX4	This study
TJY6907	BY 4742	htz1Δ::natMX4	This study
TJY7193	LG1/BY 4742	PRP19-HA3::TRP1	This study
TJY7194	LG1/BY 4742	PRP19-HA3::TRP1 htz1Δ::natMX4 htz1Δ::kanMX4	This study
TJY7084	BY 4743	PRP43-HA3::HIS3	Calvin Leung
TJY7085	BY 4743	PRP43-HA3::HIS3 htz1Δ::natMX4	This study
TJY7173	BY 4743	NTR1-MYC::kanMX3	Calvin Leung
TJY7174	BY 4743	NTR1-MYC::kanMX3 htz1Δ::natMX4	This study
TJY3983	YTV311	cup1Δ::URA3-52	Christine Guthrie
TJY6824	YTV311	cup1Δ::URA3-52 htz1Δ::kanMX4	This study
TJY1271	BY 4341	dst1Δ::kanMX4	Open Biosystems
TJY7093	BY 4743	dst1Δ::kanMX4 htz1Δ::natMX4	This study
TJY7175	BY 4741	prp22DAmP::kanMX4	Open Biosystems
TJY7176	BY 4743	prp22DAmP::kanMX4 htz1Δ::natMX4	This study
TJY7196	BY 4741	prp16DAmP::kanMX4	This study
TJY7178	BY 4741	prp16DAmP::kanMX4 htz1Δ::natMX4	This study

Viability assay/dilution series: For growth analysis of *cup1*Δ strains containing a centromeric *ACT1-CUP1* (*URA3*) plasmid, strains were grown overnight in SC-LEU liquid media at 30°C. Cells were diluted to an OD_{600} of .1 in 5 ml of SC-LEU media and incubated at 30°C until all strains reached early-log phase. A ten-fold serial dilution of each strain was spotted on to SC-LEU plates with indicated $CuSO_4$ concentrations and incubated 30°C for 3 days. *ACT1-CUP1* plasmids are as described in (Lesser and Guthrie 1993).

For growth analysis of DAmP mutants: strains were grown overnight in YPD+G418 liquid media at 30°C. Cells were diluted to an OD_{600} of .1 in 5 ml of YPD+G418 and incubated at 30°C until all strains reached early-log phase. A ten-fold serial dilution of each strain was spotted on to YPD, CSM or selective plates (+/- 6 azauracil) and incubated for 2 to 3 days at 30°C unless otherwise noted.

Chromatin immunoprecipitation (ChIP) and qPCR: Cells were grown in YPD to an OD_{600} between 0.5-0.7 and then crosslinked at room temperature for 15 minutes with formaldehyde to a final concentration of 1%. Crosslinking was quenched at room temperature for 5 minutes with glycine to a final concentration of 125mM. Cells were disrupted with glass beads (0.5mm) for 40 minutes at 4°C. Lysates were sonicated for a total of 2:30 minutes at 15% intensity (10 seconds on, 15 seconds off and on ice). After sonication, lysates were cleared by centrifugation. For Prp19 and Prp43, samples were then used for immunoprecipitation with anti-HA Y11 (Santa Cruz). For Ntr1, samples were used for immunoprecipitation with anti-Myc 9E10 (Roche). After immunoprecipitation, samples were washed and incubated overnight at 65°C to reverse crosslinking. All samples were incubated with Proteinase K (Sigma) and RNAse A (Ambion), followed by purification using a PCR product purification kit (Qiagen).

DNA samples were then analyzed by real-time PCR. Input DNA was diluted 1:10 and 1 µl of this was used in a 10 ul reaction volume. For ChIP DNA, samples were diluted 1:2 and 1 µl of this was used in a 20 µl or 10ul reaction volume. Reactions consisted of 1x Perfecta SYBR GREEN Master Mix (Quanta Biosciences) and .5 µl primers. Real-time PCR was performed using a CFX96 Touch System (BioRad). All samples were run in technical duplicate for each independent experiment. Primers used are as described in (Neves et al. 2017).

For quantification, standard curves were generated for each primer set, and DNA concentration for each INPUT and ChIP sample was calculated. ChIP values were divided by the INPUT, and these values were divided by the non-transcribed control and expressed as fold accumulation over the non-transcribed control. Reported values are averages of three or more independent experiments and error bars represent the standard error of the mean.

Whole cell extract and immunoblot: Cells were grown in YPD media to an OD_{600} between 0.5-0.7 and lysed using FA-1 Lysis buffer (50mM HEPES-KOH pH 7.5, 140 mM NaCl, 1 mM EDTA pH 8.0, 1% Triton-X, .1% Deoxycholate, plus protease inhibitors) and .3 mm glass beads with 5 minutes of vortexing at 4°C. The supernatant was cleared by centrifugation and total protein was resolved by a 15% SDS-PAGE and transferred to a PVDF membrane for immunoblotting with a 1:4000 dilution of anti-PGK (Molecular Probes) and a 1:10,000 dilution of anti-HA 12CA5 (Roche). Signal was detected using Pierce ECL Western Blotting Solution (ThermoScientific).

RT-qPCR analysis and quantification: For quantification of *PRP16* and *PRP22* cells were grown in YPD+G418 media to an OD_{600} between 0.4 and 0.7. Total RNA was isolated from

10 ml of cells using a hot-phenol extraction method and dissolved in 100 µl water. 15 ug of RNA was DNAse treated (Roche) and treated RNA concentration was measured by spectrophotometer. 2-4 ug of RNA was used to make cDNA using the Maxima^{TM} First Strand cDNA Synthesis Kit (Fermentas). qRT-PCR was done in a 10 µl reaction volume with gene specific primers using 1 µl of cDNA diluted 1:20 using Perfecta Sybr Green Fastmix (Quanta Biosciences) and a CFX96 Touch System (BioRad). All samples were analyzed in triplicate for each independent experiment. qRT-PCR was also performed for the *scR1* RNA from each cDNA sample. Gene expression analysis was done by 2-ΔCt methods using *scR1* cytoplasmic RNA as reference. Primers for each gene assayed are listed in Table 4.2. Fold-expression of mRNA was measured compared to WT by 2-ΔΔCt methods (Livak and Schmittgen 2001)

TABLE 4.2: qPCR primers

PRP16 qPCR F	ACTAACGCCTGGGTTGCTTT
PRP16 qPCR R	TCGGATTGTTGCTGCTGAGT
PRP22 qPCR F	AAGGCGTGCTTTGACTTCAC
PRP22 qPCR R	ACTGCCGTCATCTCTTTTCG
sCR1 F	TTTCTGGTGGGATGGGATAC
sCR1 R	TTTACGACGGAGGAAAGACG

RNA-seq library preparation, alignment and splicing efficiency calculation: RNA-seq libraries for WT, *htz1*Δ, *dst1*Δ, and *dst1*Δ*htz1*Δ strains were constructed in conjunction with *prp43*^{DAmP} strain libraries described in (Neves et al. 2017). Library preparation, sequence alignment and splicing efficiency calculation were performed as described in (Neves et al. 2017).

RNA-seq minimum-read filters: The minimum-read threshold for RNA-seq analysis for Figure 4.4 was defined as a 10 raw counts of spliced reads in at least one sample. Due to the high

number of unusual isoforms, YKL186C was omitted for this study. Number of genes that passed threshold: RPG n = 92, non-RPG n = 159. RPKM values are unfiltered.

ACKNOWLEDGEMENTS

Prp43-HA and Ntr1-Myc strains were constructed by Calvin Leung and RNA-seq alignment and splicing efficiency calculations were carried out by Dr. Stephen Douglass. Thank you for your time and expertise.

Figure 4.1

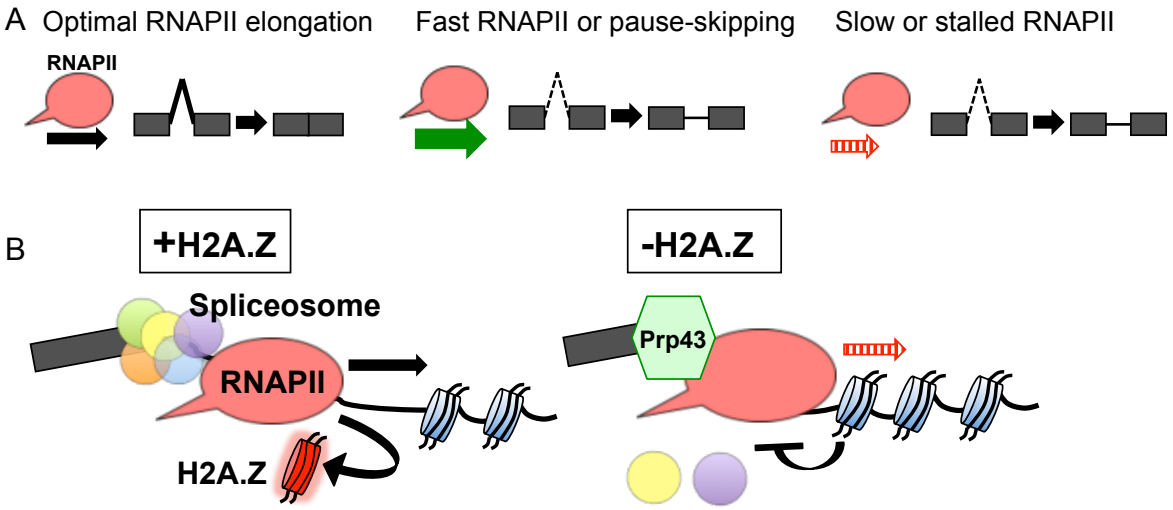

Figure 4.1 Model of H2A.Z coordination of transcription elongation and splicing

A. Transcription and splicing are kinetically coupled via a 'Goldilocks' model; an optimal elongation rate is required for efficient splicing. Adapted from (Fong et al. 2014)

B. H2A.Z promotes kinetic coordination between transcription elongation and splicing. H2A.Z-nucleosomes are more readily evicted by RNAPII than canonical H2A-nucleosomes and loss of H2A.Z results in elongation defects that alter spliceosome rearrangements. In the absence of H2A.Z, the DEAH-box helicase Prp43 recognizes and disassembles stalled spliceosomes before splicing is complete.

Figure 4.2

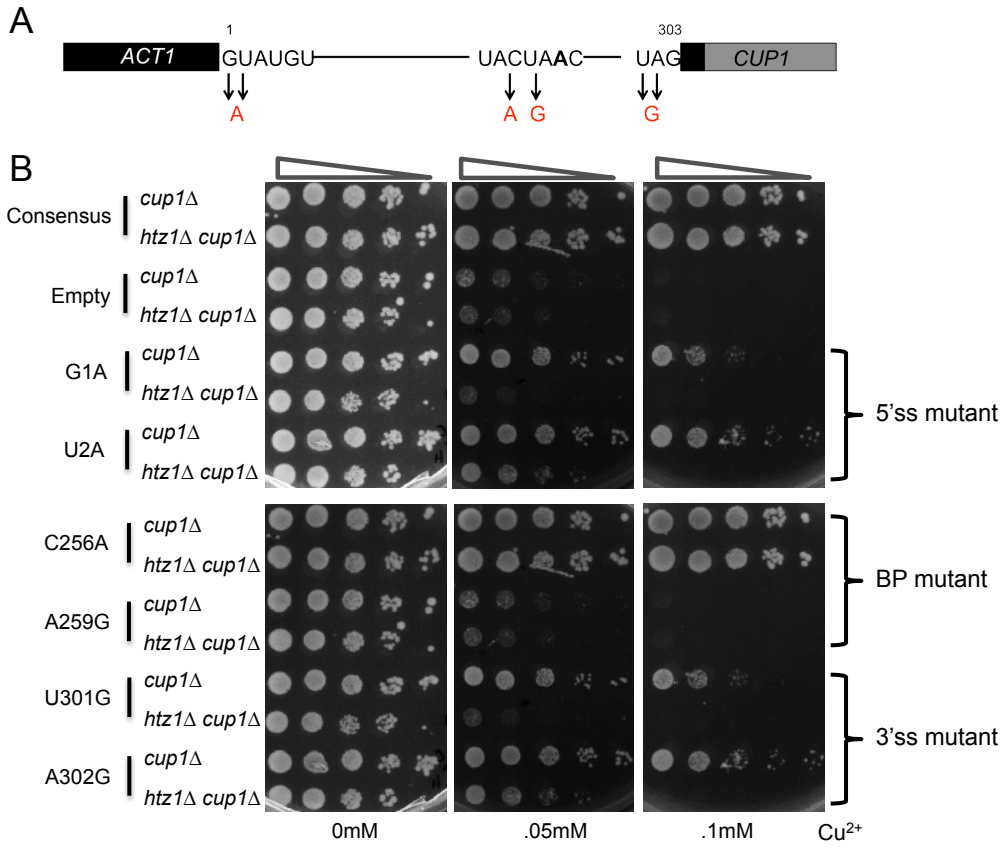

Figure 4.2 Introns containing mutated splice sites are sensitive to H2A.Z presence

A. Schematic of *ACT1-CUP1* hybrid construct. Splice site mutations indicated in red. Adapted from (Lesser and Guthrie 1993)

B. Serial dilution assay of *cup1*Δ and *htz1*Δ *cup1*Δ mutants. Cells were transformed with empty pRS315 LEU plasmid or pRS315 containing the *ACT1-CUP1* construct with consensus or mutated splice sites (as indicated). Cells were grown at 30°C in CSM-LEU selective liquid media until desired OD600 was obtained. Cells were spotted as a ten-fold dilution onto CSM-LEU plates containing increasing concentrations of $CuSO_4$ and incubated at 30°C for three days.

Figure 4.3

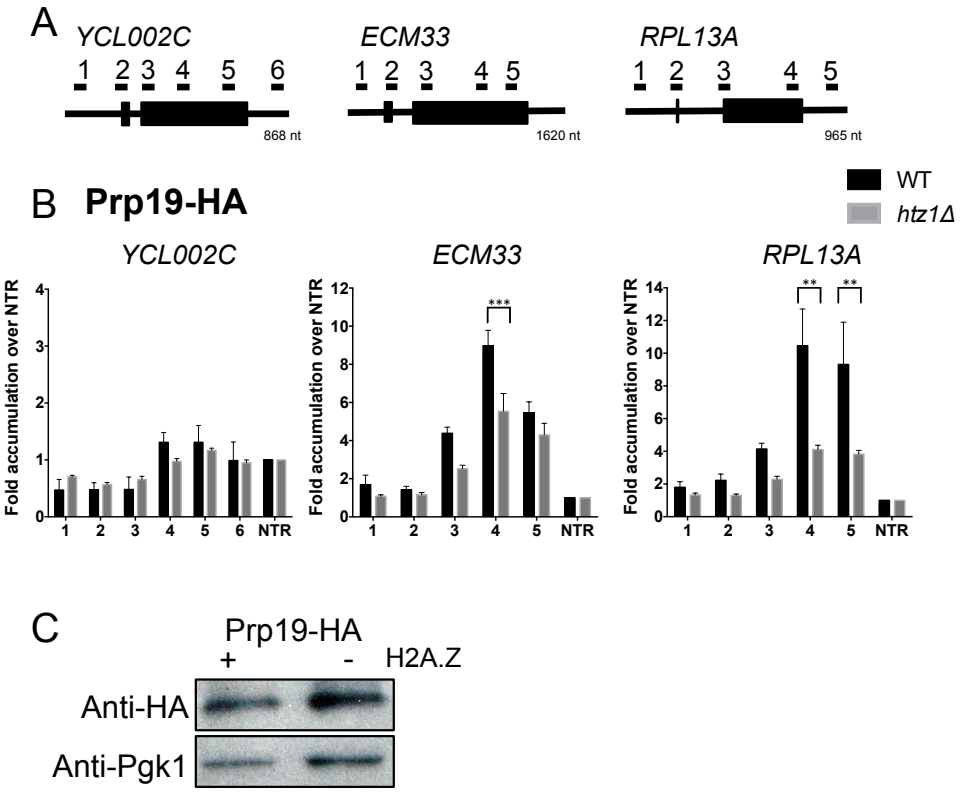

Figure 4.3 Co-transcriptional NineTeen Complex recruitment is decreased in the absence of H2A.Z Introns containing mutated splice sites are sensitive to H2A.Z presence

A. Schematic of intron-containing genes, *YCL002C, ECM33,* and *RPL13A*. Underlined numbers represent amplicons generated by each primer set used in this experiment.

B. Occupancy of Prp19 at each region of *YCL002C* (left), *ECM33* (middle), or *RPL13A* (right) relative to the non-transcribed region in WT or *htz1*Δ. Graphs represent the average of three independent experiments and error bars represent the standard error of the means. P-values for each primer set determined by students t-test. Significant values indicated. *: p-value < .01 **: p-value < .001. ***: p-value < .0001.

C. Protein immunoblot of Prp19-HA strains used for ChIP assay. WT and *htz1*Δ whole cell extracts probed with anti-HA 12CA5 (top), and anti-PGK1 as a loading control (bottom)

Figure 4.4

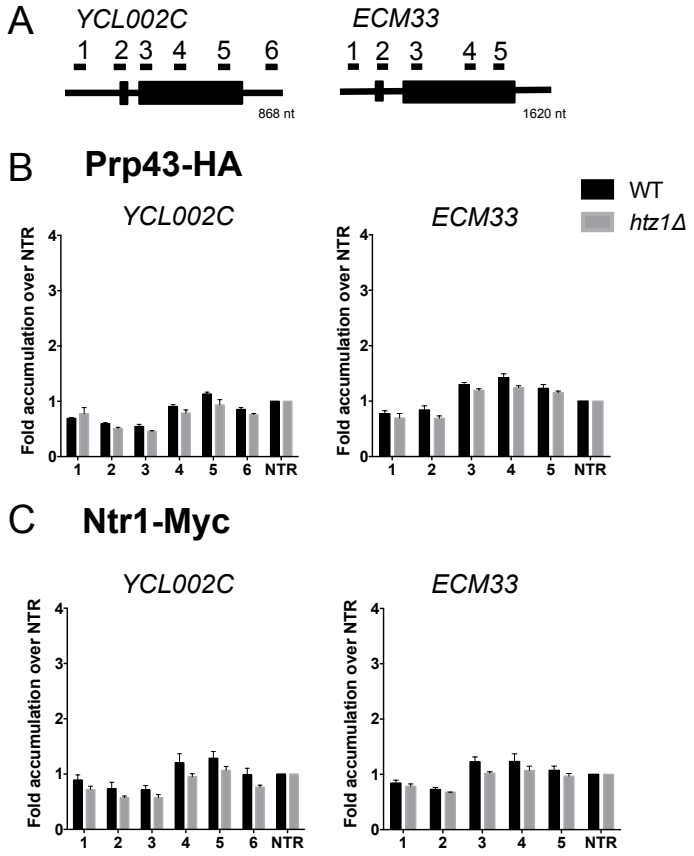

Figure 4.4 Enrichment of disassembly factor Prp43 or cofactor Ntr1 at candidate genes could not be determined using chromatin immunoprecipitation

A. Schematic of intron-containing genes, *YCL002C,* and *ECM33*. Underlined numbers represent amplicons generated by each primer set used in this experiment.

B. Occupancy of Prp43 at each region of *YCL002C* (left), or *ECM33* (right) relative to the non-transcribed region in WT or *htz1*Δ.

C. Occupancy of Ntr1 at each region of *YCL002C* (left), or *ECM33* (right) relative to the non-transcribed region in WT or *htz1*Δ.

Graphs represent the average of three independent experiments and error bars represent the standard error of the means.

Figure 4.5

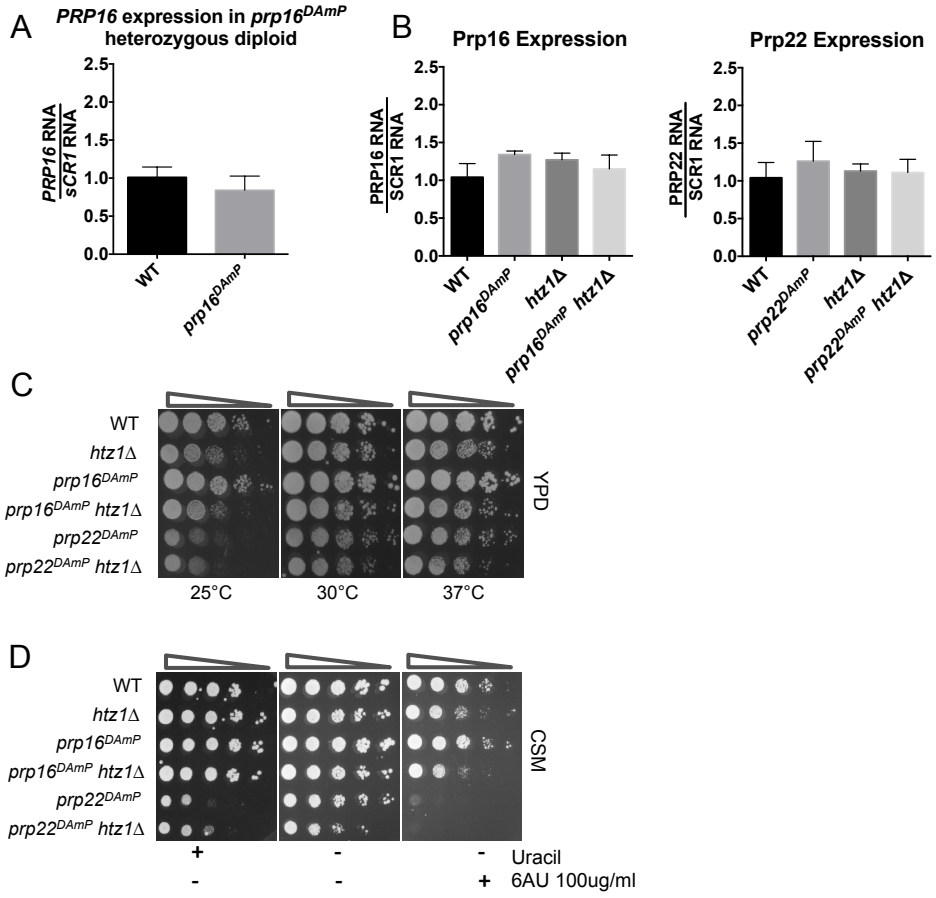

Figure 4.5 DAmP alleles do not alter *PRP16* or *PRP22* RNA levels but *prp22^{DAmP}* renders cells highly susceptible to transcription defects

A. RT-qPCR analysis of levels of RNA in diploid WT and heterozygous diploid *prp16^{DAmP}*, normalized to *sCR1*, an RNAPIII transcript. Graphs represent average of three independent experiments and error bars represent the SD.

B. RT-qPCR analysis of levels of RNA in WT and *prp16^{DAmP}* (right) or *prp22^{DAmP}* (left) cells ± *HTZ1*, normalized to *sCR1*, an RNAPIII transcript. Graphs represent average of three independent experiments and error bars represent the SD.

C. Serial dilution assay of *prp16^{DAmP} htz1*Δ and *prp22^{DAmP} htz1*Δ mutants. Cells were grown at 30°C in YPD+G418 liquid media until desired OD_{600} was obtained. Cells were spotted

as a ten-fold dilution onto YPD+G418 plates and incubated at 25°C, 30°C, or 37°C for two days.

D. Serial dilution assay of *prp16*^{DAmP} *htz1*Δ and *prp22*^{DAmP} *htz1*Δ mutants under transcriptional stress. Cells were grown at 30°C in YPD+G418 liquid media until desired OD_{600} was obtained. Cells were spotted as a ten-fold dilution onto CSM-URA plates with or without 6-azauracil (6AU) and incubated at 30°C for two to three days.

Figure 4.6

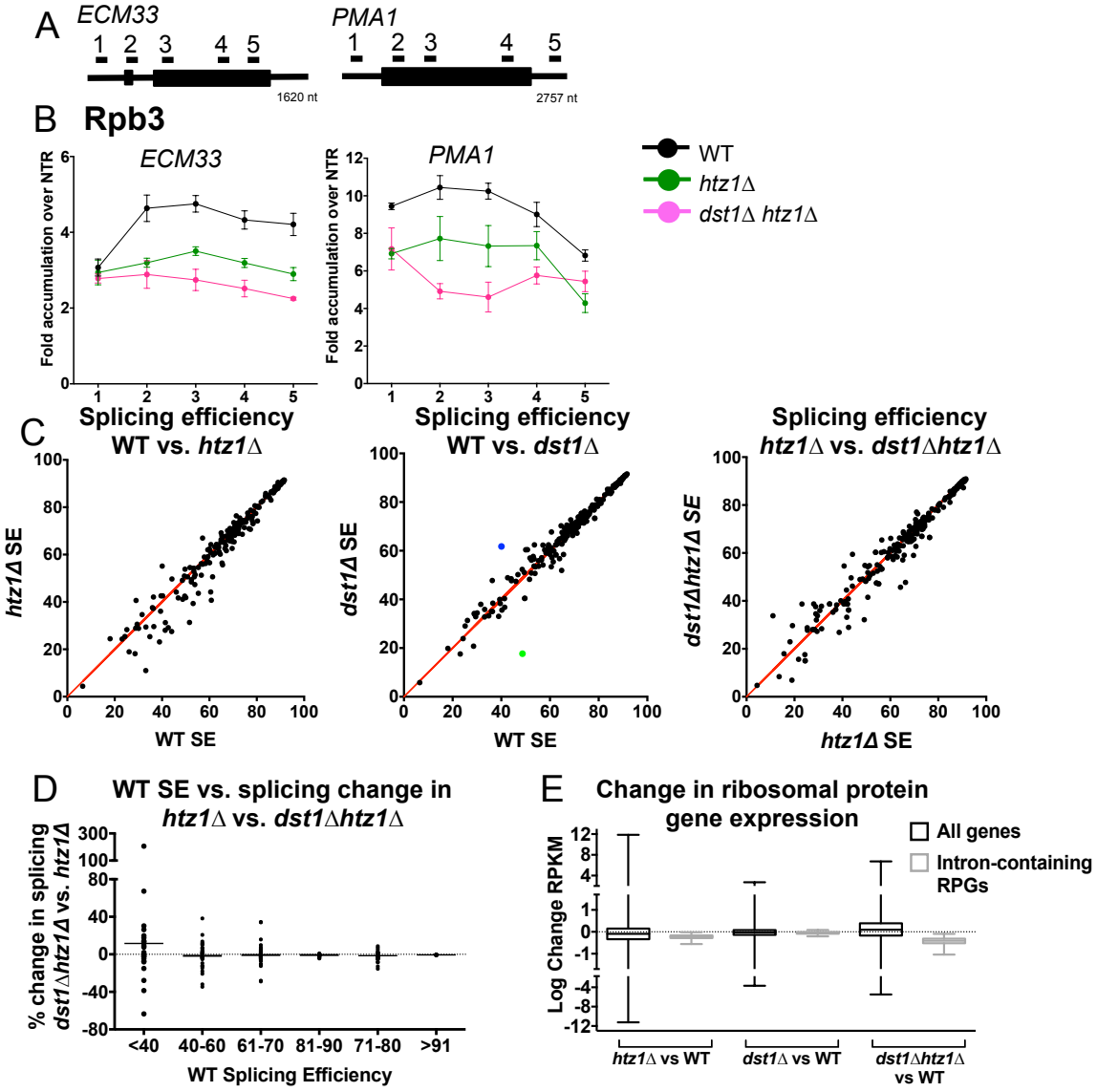

Figure 4.6 Deletion of *DST1* can both exacerbate and indirectly suppress H2A.Z-mediated splicing defects

A. Schematic of intron-containing genes, *ECM33,* and *PMA1*. Underlined numbers represent amplicons generated by each primer set used in this experiment.

B. Occupancy of Rpb3 at each region of *ECM33* (left), or *PMA1* (right) relative to the non-transcribed region in WT, *htz1*Δ, or *dst1*Δ *htz1*Δ.

C. Distribution in splicing efficiencies of all intron-containing genes upon deletion of *HTZ1* in WT cells (left), deletion of *DST1* in WT cells (middle), or deletion of *DST1* in *htz1*Δ cells (right), represented as an X-Y plot.

D. Distribution of changes in splicing efficiency upon deletion of *DST1* in *htz1*Δ cells compared to binned WT percent splicing efficiency (spliced mRNA over spliced plus unspliced RNA).

E. Log-2 fold change in RPKM for all genes, and intron-containing RPGs deletion of *HTZ1* in WT cells (left), deletion of *DST1* in WT cells (middle), or deletion of *DST1* in *htz1*Δ cells (right). Deletion of *DST1* in *htz1*Δ cells leads to an average of 1.3 fold decrease for intron-containing RPGs.

REFERENCES

Archambault J, Lacroute F, Ruet A, Friesen JD. 1992. Genetic interaction between transcription elongation factor TFIIS and RNA polymerase II. *Molecular and cellular biology* **12**: 4142-4152.

Arenas JE, Abelson JN. 1997. Prp43: An RNA helicase-like factor involved in spliceosome disassembly. *P Natl Acad Sci USA* **94**: 11798-11802.

Banerjee D, McDaniel PM, Rymond BC. 2015. Limited portability of G-patch domains in regulators of the Prp43 RNA helicase required for pre-mRNA splicing and ribosomal RNA maturation in Saccharomyces cerevisiae. *Genetics* **200**: 135-147.

Breslow DK, Cameron DM, Collins SR, Schuldiner M, Stewart-Ornstein J, Newman HW, Braun S, Madhani HD, Krogan NJ, Weissman JS. 2008. A comprehensive strategy enabling high-resolution functional analysis of the yeast genome. *Nat Methods* **5**: 711-718.

Chen HC, Tseng CK, Tsai RT, Chung CS, Cheng SC. 2013. Link of NTR-mediated spliceosome disassembly with DEAH-box ATPases Prp2, Prp16, and Prp22. *Mol Cell Biol* **33**: 514-525.

Churchman LS, Weissman JS. 2011. Nascent transcript sequencing visualizes transcription at nucleotide resolution. *Nature* **469**: 368-+.

Day DA, Tuite MF. 1998. Post-transcriptional gene regulatory mechanisms in eukaryotes: an overview. *J Endocrinol* **157**: 361-371.

Fong N, Kim H, Zhou Y, Ji X, Qiu J, Saldi T, Diener K, Jones K, Fu XD, Bentley DL. 2014. Pre-mRNA splicing is facilitated by an optimal RNA polymerase II elongation rate. *Genes Dev* **28**: 2663-2676.

Fourmann JB, Dybkov O, Agafonov DE, Tauchert MJ, Urlaub H, Ficner R, Fabrizio P, Luhrmann R. 2016. The target of the DEAH-box NTP triphosphatase Prp43 in Saccharomyces cerevisiae spliceosomes is the U2 snRNP-intron interaction. *Elife* **5**.

Fourmann JB, Tauchert MJ, Ficner R, Fabrizio P, Luhrmann R. 2017. Regulation of Prp43-mediated disassembly of spliceosomes by its cofactors Ntr1 and Ntr2. *Nucleic Acids Res* **45**: 4068-4080.

Freedman MS, Kaplan JM, Markovic-Plese S. 2013. Insights into the Mechanisms of the Therapeutic Efficacy of Alemtuzumab in Multiple Sclerosis. *J Clin Cell Immunol* **4**.

Gunderson FQ, Merkhofer EC, Johnson TL. 2011. Dynamic histone acetylation is critical for cotranscriptional spliceosome assembly and spliceosomal rearrangements. *Proc Natl Acad Sci U S A* **108**: 2004-2009.

Herzel L, Ottoz DSM, Alpert T, Neugebauer KM. 2017. Splicing and transcription touch base: co-transcriptional spliceosome assembly and function. *Nat Rev Mol Cell Biol* **18**: 637-650.

Hoskins AA, Moore MJ. 2012. The spliceosome: a flexible, reversible macromolecular machine. *Trends in Biochemical Sciences* **37**: 179-188.

Johnson TL, Vilardell J. 2012. Regulated pre-mRNA splicing: the ghostwriter of the eukaryotic genome. *Biochim Biophys Acta* **1819**: 538-545.

Koodathingal P, Novak T, Piccirilli JA, Staley JP. 2010. The DEAH Box ATPases Prp16 and Prp43 Cooperate to Proofread 5 ' Splice Site Cleavage during Pre-mRNA Splicing. *Mol Cell* **39**: 385-395.

Koodathingal P, Staley JP. 2013a. Splicing fidelity DEAD/H-box ATPases as molecular clocks. *Rna Biol* **10**: 1073-1079.

-. 2013b. Splicing fidelity: DEAD/H-box ATPases as molecular clocks. *RNA Biol* **10**: 1073-1079.

Lambert JP, Mitchell L, Rudner A, Baetz K, Figeys D. 2009. A novel proteomics approach for the discovery of chromatin-associated protein networks. *Mol Cell Proteomics* **8**: 870-882.

Lardelli RM, Thompson JX, Yates JR, 3rd, Stevens SW. 2010. Release of SF3 from the intron branchpoint activates the first step of pre-mRNA splicing. *RNA* **16**: 516-528.

Lebaron S, Froment C, Fromont-Racine M, Rain JC, Monsarrat B, Caizergues-Ferrer M, Henry Y. 2005. The splicing ATPase prp43p is a component of multiple preribosomal particles. *Mol Cell Biol* **25**: 9269-9282.

Leeds NB, Small EC, Hiley SL, Hughes TR, Staley JP. 2006. The splicing factor Prp43p, a DEAH box ATPase, functions in ribosome biogenesis. *Molecular and cellular biology* **26**: 513-522.

Lesser CF, Guthrie C. 1993. Mutational analysis of pre-mRNA splicing in Saccharomyces cerevisiae using a sensitive new reporter gene, CUP1. *Genetics* **133**: 851-863.

Livak KJ, Schmittgen TD. 2001. Analysis of relative gene expression data using real-time quantitative PCR and the 2(-Delta Delta C(T)) Method. *Methods* **25**: 402-408.

Martin A, Schneider S, Schwer B. 2002. Prp43 is an essential RNA-dependent ATPase required for release of lariat-intron from the spliceosome. *J Biol Chem* **277**: 17743-17750.

Mason PB, Struhl K. 2005. Distinction and relationship between elongation rate and processivity of RNA polymerase II in vivo. *Mol Cell* **17**: 831-840.

Mayas RM, Maita H, Staley JP. 2006. Exon ligation is proofread by the DExD/H-box ATPase Prp22p. *Nat Struct Mol Biol* **13**: 482-490.

Mladenova V, Mladenov E, Russev G. 2009. Organization of Plasmid DNA into Nucleosome-Like Structures after Transfection in Eukaryotic Cells. *Biotechnol Biotec Eq* **23**: 1044-1047.

Munding EM, Shiue L, Katzman S, Donohue JP, Ares M, Jr. 2013. Competition between pre-mRNAs for the splicing machinery drives global regulation of splicing. *Mol Cell* **51**: 338-348.

Neves LT, Douglass S, Spreafico R, Venkataramanan S, Kress TL, Johnson TL. 2017. The histone variant H2A.Z promotes efficient cotranscriptional splicing in S. cerevisiae. *Genes Dev* **31**: 702-717.

Nissen KE, Homer CM, Ryan CJ, Shales M, Krogan NJ, Patrick KL, Guthrie C. 2017. The histone variant H2A.Z promotes splicing of weak introns. *Genes Dev* **31**: 688-701.

Santisteban MS, Hang M, Smith MM. 2011. Histone variant H2A.Z and RNA polymerase II transcription elongation. *Mol Cell Biol* **31**: 1848-1860.

Semlow DR, Blanco MR, Walter NG, Staley JP. 2016. Spliceosomal DEAH-Box ATPases Remodel Pre-mRNA to Activate Alternative Splice Sites. *Cell* **164**: 985-998.

Tsai RT, Fu RH, Yeh FL, Tseng CK, Lin YC, Huang YH, Cheng SC. 2005. Spliceosome disassembly catalyzed by Prp43 and its associated components Ntr1 and Ntr2. *Genes Dev* **19**: 2991-3003.

Venkataramanan S, Douglass S, Galivanche AR, Johnson TL. 2017. The chromatin remodeling complex Swi/Snf regulates splicing of meiotic transcripts in Saccharomyces cerevisiae. *Nucleic Acids Res*.

CHAPTER 5

Swr1 presence impedes appropriate alkaline stress response pathways in the absence of H2A.Z.

INTRODUCTION

Organisms in their natural environment are continuously exposed to changing conditions, including, but certainly not limited to, fluctuations in temperature, salt concentration, pH, nutrient availability, toxic substances. In order to survive and grow, cells must be capable of responding and adapting to such stresses. While cells within multicellular organisms are often able to avoid the effects of a suboptimal environment due to their location or interdependence among specialized cells, unicellular organisms must possess multiple signaling mechanisms to respond to changing conditions. Perhaps the most well studied example is that of the budding yeast *Saccharomyces cerivisiae*, which is capable of growing under a broad range of conditions. In these organisms, remodeling of gene expression pathways underlies all responses to environmental change (Causton et al. 2001). Often diverse signaling pathways and gene expression patterns are coordinated into an integrated stress response. This can clearly be observed in the alkaline pH stress response in yeast (Reviewed in Serra-Cardona et al. 2015). A major component of the yeast alkaline stress response is the conserved Rim101 pathway, named for the Rim101 Cys_2His_2 zinc-finger transcriptional repressor. Under alkaline conditions, Rim101 is activated and regulates expression of a set of target response genes including several encoding ion pumps (Lamb et al. 2001). However, the alkaline stress response involves not only the Rim101 pathway, but also a number of additional gene expression pathways that regulate nutrient homeostasis including Snf1-regulated carbon metabolism, copper and iron uptake, and phosphate-starvation response pathways (Reviewed in Serra-Cardona et al. 2015) (Figure 5.1).

Because regulation of transcription is influenced by the structure of chromatin, the chromatin environment plays an important role in regulated gene expression patterns in response and adaptation to stress. Chromatin consists of an array of nucleosomes made up of DNA

wrapped around two copies each of the four core histone proteins, H2A, H2B, H3, and H4. The N-terminal tails of these histones can be dynamically modified in response to environmental cues and frequently reflect changes in gene expression patterns. For example, approximately 60% of all nucleosomes undergo at least one histone modification change upon diamide stress (Weiner et al. 2015), which is known to induce rapid and massive transcriptional reprogramming of stress-response pathways in yeast (Gasch et al. 2000). Importantly, the timing and location of these modifications correlates strongly with induced transcriptional changes (Weiner et al. 2015).

H2A.Z, an H2A variant encoded by *HTZ1* in *S. cerevisiae*, has been shown to have important roles in the regulation of transcription initiation and elongation, as well as co-transcriptional splicing (Malagon et al. 2004; Zhang et al. 2005; Santisteban et al. 2011; Weber et al. 2014; Subramanian et al. 2015; Rudnizky et al. 2016; Neves et al. 2017; Nissen et al. 2017). However, the biological relevance of the role of H2A.Z in these processes has not been fully characterized. In most metazoans, including *Xenopus, Drosophila,* and mice, H2A.Z is essential and may have roles in cell differentiation and cancer progression (Marques et al. 2010; Domaschenz et al. 2017; Punzeler et al. 2017). Particularly in plants, H2A.Z is required for regulation of stress response pathways (Coleman-Derr and Zilberman 2012; Sura et al. 2017) and, in yeast, while non-essential under optimal conditions, H2A.Z loss renders cells highly sensitive to a number of stressors including genotoxic substances, temperature changes, and increased pH (Serrano et al. 2004; Sinha et al. 2008; Neves et al. 2017). In both yeast and plant cells, H2A.Z has also been shown to be important for growth in phosphate-limiting conditions (Smith et al. 2010; Rosonina et al. 2014). Specifically in yeast, loss of H2A.Z causes slow growth in low-phosphate media, likely due to decreased expression of a phosphate starvation response gene (Rosonina et al. 2014).

However, the manner by which pathways and mechanisms influenced by the histone variant underlie the biological functions of H2A.Z remain poorly understood. Sensitivity to DNA damaging reagents in the absence of H2A.Z suggests that H2A.Z is involved in genome stability. Indeed, H2A.Z is a structural component of centromeres (Greaves et al. 2007), is required for proper chromosome segregation (Krogan et al. 2004), and is transiently recruited to double-stranded breaks (DSBs) (Kalocsay et al. 2009), although its precise role in DNA damage repair are unclear (Gursoy-Yuzugullu et al. 2016). In addition to potential roles in maintaining DNA stability, recent studies in plant cells indicate that H2A.Z is enriched in and important for transcriptional regulation of stress response genes (March-Diaz et al. 2008; Hu et al. 2011; Coleman-Derr and Zilberman 2012).

Unlike canonical histones, H2A.Z may be inserted into chromatin at any point throughout the cell cycle (Zlatanova and Thakar 2008). The SWR-C remodeling complex is a multisubunit complex that catalyzes displacement of H2A/H2B dimers in exchange for H2A.Z/H2B dimers (Krogan et al. 2003; Kobor et al. 2004; Mizuguchi et al. 2004). SWR-C is composed of the catalytic core protein Swr1 as well as 12 additional subunits, including Swc2, which is responsible for targeting SWR-C to the chromatin (Mizuguchi et al. 2004; Morillo-Huesca et al. 2010). Intriguingly, deletion of *SWR1* suppresses growth defects of *htz1*Δ cells in a variety of stress conditions, particularly in the presence DNA-damaging reagents (Collins et al. 2007; Halley et al. 2010; Morillo-Huesca et al. 2010). Indeed, in the absence of H2A.Z, the SWR-C complex remains intact and is recruited to DSBs, where it is proposed to interfere with DNA damage checkpoint activity (Morillo-Huesca et al. 2010). Notably, deletion of *SWC2* also suppresses sensitivity of *htz1*Δ cells to DNA-damaging reagents (Halley et al. 2010; Morillo-Huesca et al. 2010), suggesting a model by which continued SWR-C chromatin binding and

histone-replacement activity transiently destabilize nucleosomes when H2A.Z is not present and cannot be inserted in to the chromatin. This Swr1 activity and subsequent chromatin instability may also lead to transcriptional misregulation (Halley et al. 2010; Morillo-Huesca et al. 2010).

Here we show that the loss of H2A.Z renders cells sensitive to alkaline pH conditions, likely due to numerous changes in gene expression, particularly of those genes involved in the phosphate-starvation response pathway. Increased expression of genes involved in copper and iron uptake, as well as potential changes in copper utilization, may reflect compensatory activation of alternative alkaline stress response pathways. Finally we show that transcription misregulation and alkaline sensitivity are likely not due to loss of H2A.Z per se, but rather due to continued Swr1 activity in the absence of H2A.Z. When H2A.Z is lost, the presence of Swr1 leads to aberrant RNA polymerase II (RNAPII) phosphorylation and decreased expression of phosphate-starvation response genes.

RESULTS

H2A.Z affects expression of stress response genes.

H2A.Z is involved in transcriptional regulation and gene expression (Santisteban et al. 2000; Zhang et al. 2005; Morillo-Huesca et al. 2010) and, particularly in plants, has been shown to affect the expression of stress-response genes (Coleman-Derr and Zilberman 2012; Sura et al. 2017). In order to determine whether H2A.Z affects the expression of distinct classes of genes, we re-analyzed our previous RNA-sequencing data to determine genome-wide expression changes upon deletion of *HTZ1* (Neves et al. 2017). We compared differential expression of all genes between wild-type (n=3) and *htz1*Δ (n=2) cells (Figure 5.2 A). Because differences in biological replicate number lower the statistical significance of differential expression algorithm

outputs, we widened our downstream analyses to include genes whose expression is statistically significantly altered as determined by both an adjusted p-value <.05 and an un-adjusted p-value <.01 (Figure 5.2 A).

Of the significantly altered genes whose expression is increased upon loss of H2A.Z, the largest classes are cell wall stress responsive genes (p = .003) (Boorsma et al. 2004) and copper/iron uptake genes (GO Terms: Copper ion transport, iron ion homeostasis) (Figure 5.2 B). The regulation of copper and iron uptake genes has been linked not only to low cation starvation but also to respiratory conditions and alkaline stress (Serrano et al. 2004; Arredondo and Nunez 2005; Serra-Cardona et al. 2015). Consistent with findings in Arabidopsis (Smith et al. 2010), down-regulated genes are enriched for genes involved in the phosphate starvation response ($p = 8.734*10^{-12}$) (Vardi et al. 2014), as well as genes encoding vacuolar proteins (GO Term: Vacuole, p = .018) (Figure 5.2 B). As the yeast vacuolar compartment stores a large polyphosphate pool, the vacuole is important for intracellular phosphate homeostasis (Shirahama et al. 1996). Similar to the copper and iron uptake pathway, dynamic regulation of phosphate uptake is also involved in alkaline stress responses (Reviewed in Serra-Cardona et al. 2015).

H2A.Z is normally enriched only in genes down-regulated in the absence of H2A.Z.

H2A.Z is enriched around the transcription start site (TSS) of the majority of yeast genes, typically in the +1 and -1 nucleosome flanking the nucleosome free region (Ranjan et al. 2013; Gu et al. 2015). Using previously published ChIP-seq data, we confirmed that H2A.Z occupies the nucleosomes near the 5' end of the majority of genes whose expression decreases in *htz1*Δ cells (Figures 5.3 A and C). Strikingly, the population of genes whose expression increases upon

H2A.Z loss appears to be largely deplete of H2A.Z and enrichment around the ATG start site is far lower than that of down-regulated genes (Figures 5.3 B and C).

A number of studies find that highly transcribed ribosomal protein genes (RPGs) are deplete of H2A.Z-containing nucleosomes in yeast (Raisner et al. 2005; Zhang et al. 2005; Ranjan et al. 2013; Gu et al. 2015). As depletion of RNAPII components leads to H2A.Z accumulation in RPGs, low ChIP-seq enrichment signal is likely due to an inability to capture H2A.Z occupancy as it is rapidly turned over during transcription (Tramantano et al. 2016). However, the average wild-type expression of genes whose expression increases in *htz1*Δ cells is similar to average genome-wide expression (Average RPKM: up-regulated genes = 132, all genes = 149). Therefore, high levels of transcription cannot account for low H2A.Z occupancy in these genes. It is possible that up-regulation of these genes is not directly due to loss of H2A.Z at the gene locus, but rather, may secondary effects downstream of immediate expression changes in *htz1*Δ cells.

Copper uptake and/or utilization may be altered upon loss of H2A.Z.

Due to its ability to donate and accept electrons, copper is an important nutrient and an essential ion in the mitochondrial electron transport chain. While cells are unable to respire in the absence of copper, copper is also toxic because its electron transfer properties can lead to ROS generation (Reviewed in De Freitas et al. 2003). We therefore suspected that up-regulation of copper uptake genes, which potentially increases intracellular copper levels, in *htz1*Δ cells would lead to decreased tolerance to increasing levels of environmental copper. Surprisingly, loss of H2A.Z does not affect cell viability in the presence of copper (Figure 5.4 A). Yeast produce several metallothionein proteins capable of binding heavy metals including Cup1, which plays a

dominant role in copper detoxification (Fogel and Welch 1982; Fogel et al. 1988). Therefore, we considered the possibility that potent Cup1 activity could mask copper sensitivity of cells lacking H2A.Z. However, similar to wild-type cells, *HTZ1* deletion in *cup1*Δ cells does not increase copper sensitivity (Figure 5.4 A).

In the presence of copper sulfate, yeast typically produce rust-colored colonies which, while the mechanism is unclear, is thought to be due precipitation of hydrogen sulfide and copper ions at the cell surface (Fay et al. 2004). Interestingly, although we observe no change in copper sensitivity, loss of H2A.Z suppresses production of rust colored colonies, indicating that H2A.Z may affect copper uptake/utilization and/or hydrogen sulfide production (Figure 5.4 B).

Because copper import is absolutely required for respiration and mutations to mitochondrial genes have been found to suppress rust coloration (Kim et al. 2009; Schlecht et al. 2014), we next asked if loss of H2A.Z affected cell viability on a non-fermentable carbon source. Although deletion of *HTZ1* alone does not affect growth on glycerol-containing media, loss of both H2A.Z and Cup1 renders cells incapable of respiratory growth (Figure 5.4 C). Therefore H2A.Z may affect the balance between copper utility and toxicity.

H2A.Z and Prp43 interactions affect alkaline stress resistance in unexpected ways.

Yeast are capable of living in a relatively wide range of environment pH conditions and adaptation to alkaline conditions requires coordination of a variety of gene expression pathways including, but not limited to, cell wall remodeling, phosphate starvation response, and copper and iron uptake (Reviewed in Serra-Cardona et al. 2015). Because H2A.Z affects the expression of a number of genes involved in increased pH stress responses, it is likely that *HTZ1* deletion alters the cell's ability to adapt to alkaline conditions. Indeed, consistent with previous reports,

while WT cells are capable of growing in a wide pH range, cells lacking H2A.Z grow very poorly in alkaline media (Figure 5.5 A) (Serrano et al. 2004). This phenotype may reflect an inability to appropriately express phosphate starvation response genes that are normally up-regulated under alkaline stress (Figures 5.2 B) (Serrano et al. 2004). Intriguingly, decreased expression of the spliceosome disassembly factor Prp43 causes strong sensitivity to both acidic and alkaline growth conditions (Figure 5.5 A). Because Prp43 has multiple cellular roles including splicesome disassembly and ribosome biogenesis, the underlying mechanisms driving sensitivity to non-optimal pH conditions is still unclear. Consistent with past genetic studies (Neves et al. 2017), deletion of *HTZ1* only suppresses sensitivity to both high and low pH conditions (Figure 5.5 A).

Pho5 is a secreted acid phosphatase that is highly expressed under low-phosphate conditions (Oshima 1997), as well as in response to elevated pH conditions (Casado et al. 2011; Casamayor et al. 2012). Because *PHO5* expression is highly correlated to intracellular ortho- and polyphosphate levels, it is frequently used as a readout for the phosphate starvation response pathway (Auesukaree et al. 2004; Thomas and O'Shea 2005; Rosonina et al. 2014; Desfougeres et al. 2016). Similar to *htz1*Δ cells, expression of *PHO5* RNA is reduced by more than 2-fold in $prp43^{DAmP}$ cells, but, consistent with genetic interactions, *PHO5* expression is restored to wild-type levels in the $prp43^{DAmP}$ *htz1*Δ (Figure 5.5 B).

PHO85 is an intron-containing gene that codes for cyclin-dependent kinase that negatively regulates phosphate-starvation genes under high phosphate conditions (O'Neill et al. 1996). However, counter-intuitively, mutations to *PHO85* confer alkaline sensitivity, suggesting that Pho85 affects pH stress response pathways in diverse ways (Serrano et al. 2004; Arino 2010). We have previously shown that down-regulation of Prp43 can suppress splicing defects in

cells lacking H2A.Z (Neves et al. 2017), and so we considered the possibility that changes in *PHO5* expression, and subsequent alkaline sensitivity, in *prp43*^{DAmP} and *htz1*Δ cells is due to changes in *PHO85* splicing. Consistent with previous findings (Neves et al. 2017), deletion of *HTZ1* leads to increased *PHO85* pre-mRNA, and Prp43 depletion partially restores this defect (Figure 5.5 C). However, the level of *PHO85* pre-mRNA in *prp43*^{DAmP} cells does not differ significantly from wild-type levels (Figure 5.5 C) and so the way in which Prp43 down-regulation affects *PHO5* expression remains unclear. Together these data suggest that H2A.Z and Prp43 interactions are important for adaptation to alkaline conditions and, while defects in *PHO85* splicing may be partially responsible, they cannot fully explain the alkaline sensitivity of H2A.Z and Prp43 mutants.

Alkaline stress sensitivity and inhibition of phosphate gene expression is due to the presence of Swr1 in the absence of H2A.Z.

Swr1, a Swi2/Snf2-related ATPase, catalyzes the deposition of H2A.Z into the chromatin in place of H2A (Krogan et al. 2003; Kobor et al. 2004; Mizuguchi et al. 2004). Loss of Swr1, which catalyzes the deposition of H2A.Z into the chromatin, leads to a global decrease in H2A.Z occupancy, particularly at promoters, and affects splicing outcomes similarly to loss of H2A.Z (Mizuguchi et al. 2004; Zhang et al. 2005; Sadeghi et al. 2011). We therefore asked if Swr1 affects cell viability in alkaline conditions similarly to H2A.Z. Surprisingly, deletion of *SWR1* not only had no affect on growth on high pH media, but also suppressed alkaline sensitivity of *htz1*Δ cells (Figure 5.6 A).

Differences in alkaline sensitivity could be, at least in part, explained by differences in the expression of phosphate starvation genes (Serra-Cardona et al. 2015). Consistent with growth

analysis results, past RNA-sequencing (Neves et al. 2017) reveals that, in contrast to deletion of *HTZ1*, *SWR1* deletion does not significantly alter expression of phosphate starvation genes, high-affinity phosphate transporters, or vacuolar polyphosphate transporters (Figure 5.6 B). In fact, deletion of *SWR1* in a wild-type background not only results in increased *PHO5* expression, but also restores *PHO5* expression in *htz1*Δ cells to above wild-type levels (Figure 5.6 C). Therefore, decreased phosphate-starvation gene abundance may not be due to H2A.Z loss itself, but rather, is likely due to Swr1 activity interference with appropriate phosphate gene expression.

Deletion of *SWR1* restores appropriate polymerase phosphorylation in *htz1*Δ cells.

We, and others, have shown that H2A.Z has roles in regulation of both transcription initiation and elongation (Santisteban et al. 2000; Zhang et al. 2005; Wan et al. 2009; Santisteban et al. 2011; Li et al. 2012; Weber et al. 2014; Subramanian et al. 2015; Rudnizky et al. 2016; Neves et al. 2017). RNAPII contains a unique C-terminal domain (CTD) consisting of sequence repeats that are phosphorylated in a predictable manner during transcription elongation. Typically the polymerase is hypo-phosphorylated at the promoter and, upon initiation, becomes phosphorylated at serine 5 (Ser5-P). Ser5-P declines near the 3' end of the transcript in favor of serine 2 phosphorylation (Ser2-P) (Komarnitsky et al. 2000; Alexander et al. 2010). In particular, we have shown that H2A.Z promotes efficient transcription elongation in part by ensuring appropriately time serine 2 phosphorylation and, in the absence of H2A.Z, Ser2-P increases through the gene body and accumulates earlier in transcription (Neves et al. 2017). Because phosphate responsive genes have been shown to be sensitive to perturbations in CTD phosphorylation (Rosonina et al. 2014), we asked whether expression changes upon loss of H2A.Z or Swr1 reflect changes in RNAPII phosphorylation status.

In order to determine if deletion of *HTZ1* or *SWR1* affects CTD phosphorylation in a manner that correlates with expression of *PHO5* we analyzed the abundance of Rpb3, the core RNAPII subunit, or phosphorylated Rpb1, the CTD-containing subunit of RNAPII. Rpb3 abundance is slightly decreased in *htz1*Δ cells (Figure 5.7 A, B and C) likely reflecting previous observations that RNAPII occupancy decreases across gene bodies upon H2A.Z loss (Neves et al. 2017). Also consistent with past findings (Neves et al. 2017), deletion of *HTZ1* leads to increased serine 2 phosphorylation relative to total RNAPII (Figure 5.7 A and C). Satisfyingly, deletion of *SWR1* restores Rpb3 abundance and suppresses Ser2-P accumulation defects in *htz1*Δ cells (Figure 5.6 A and C), indicating that the presence of Swr1 in the absence of H2A.Z may interfere with proper RNAPII activity and drive aberrant serine 2 phosphorylation.

In addition to phosphorylation of serines 2 and 5, the CTD is also dynamically phosphorylated at tyrosine 1, threonine 4, and serine 7 throughout transcription (Reviewed in Heidemann and Eick 2012). Similar to Ser2-P, threonine 4 phosphorylation (Thr4-P) increases toward the 3' end of transcribed genes and is proposed to have roles in transcription elongation (Hintermair et al. 2012). A recent study showed that Thr4-P is required for repression of phosphate starvation response genes and mutation of threonine 4 residues to valines results in overexpression of phosphate genes including *PHO5* (Rosonina et al. 2014). Interestingly, relative Thr4-P abundance increases more than 6-fold upon loss of H2A.Z (Figure 5.7 B and C), suggesting that changes in threonine 4 phosphorylation may underlie changes in phosphate gene expression. As decreased or abolished Thr4-P results in phosphate gene overexpression, increased Thr4-P is expected to result in decreased phosphate gene abundance. As observed with serine 2 phosphorylation, deletion of *SWR1* suppresses aberrant phosphorylation of threonine 4, restoring relative Thr4-P abundance to wild-type levels (Figure 5.7 B and C).

RNAPII is hypophosphorylated prior to transcription initiation and actively dephosphorylated at the transcription termination site (Mayfield et al. 2016), and, therefore, Ser2-P and Thr4-P abundances reflect transcriptionally active polymerase machinery. While we cannot rule out the possibility that defects in RNAPII occupancy and phosphorylation are due to changes in total Rpb3 abundance, our past comparisons of CTD phosphorylation to polymerase enrichment have revealed that serine 2 phosphorylation specifically of transcriptionally engaged polymerase machinery is increased across candidate genes (Neves et al. 2017). We therefore asked whether loss of H2A.Z affects threonine 4 phosphorylation of the polymerase while actively engaged with phosphate-sensitive genes. While *HTZ1* deletion has little affect on polymerase occupancy across the *PHO5*, Thr4-P abundance increases near the 3' end of the gene as compared to wild type cells (Figure 5.7 E). Consistent with a model in which persistent Swr1 activity impairs appropriate CTD phosphorylation, deletion of *SWR1* suppresses hyperphosphorylation of threonine 4 in cells lacking H2A.Z (Figure 5.7 E). Interestingly, deletion of *SWR1* in both wild-type and *htz1*Δ cells leads to increased polymerase abundance and slightly decreased Thr4-P levels across the *PHO5* gene as compared to wild-type cells in both (Figure 5.7 E). High polymerase engagement and low Thr4-P likely explain *PHO5* overexpression observed in *swr1*Δ and *swr1*Δ *htz1*Δ cells (Figure 5.6 C).

Together, these results are consistent with a model in which loss of H2A.Z leads to changes in polymerase dynamics that affects expression of phosphate responsive genes, resulting in a decreased ability to adapt to alkaline conditions. However, polymerase defects and phosphate gene expression changes are not directly due to the loss of the H2A.Z histone itself, but rather because activity of its exchange factor Swr1 interferes with appropriate polymerase phosphorylation.

DISCUSSION

It has been demonstrated that H2A.Z has roles in many cellular processes including chromosome segregation and maintenance, transcription initiation and elongation (Reviewed in Zlatanova and Thakar 2008), and, most recently, splicing (Neves et al. 2017; Nissen et al. 2017). H2A.Z has been implicated in plant cell stress response (Boden et al. 2013; Sura et al. 2017), early metazoan embryo development (Reviewed in Zlatanova and Thakar 2008), and a number of human cancers (Reviewed in Buschbeck and Hake 2017). Yet, it remains unclear as to how the various roles of H2A.Z affect the cell's overall viability and ability to adapt to its environment. Here we demonstrate that H2A.Z is required for viability in high pH growth conditions and expression of genes involved in alkaline stress response pathways. Additionally, we demonstrate the presence of the histone exchange factor Swr1, rather than the absence of H2A.Z, is responsible for aberrant gene expression and alkaline sensitivity in *htz1*Δ cells. When H2A.Z is lost, the presence of Swr1 leads to aberrant transcription elongation and decreased stress-response gene expression.

Swr1 interferes with the alkaline stress response pathway in the absence of H2A.Z

In yeast, adaptation to alkaline growth conditions requires extensive remodeling of multiple gene expression pathways, including the activation of high-affinity phosphate and copper/iron uptake genes (Reviewed in Serra-Cardona et al. 2015). Consistent with past findings that cells lacking H2A.Z cannot induce *PHO5* when phosphate is limiting (Santisteban et al. 2000; Rosonina et al. 2014), we find that H2A.Z is required for expression of many phosphate-starvation response genes (Figure 5.2 B), likely accounting for alkaline sensitivity of *htz1*Δ cells. In contrast, H2A.Z loss leads to up-regulation of copper and iron uptake genes and possible

changes in copper utilization (Figures 5.2 B and 5.4). This was surprising to us because H2A.Z occupancy in up-regulated genes is very low (Figure 5.3). However, due to crosstalk between phosphate and copper acquisition pathways (Perea-Garcia et al. 2013), this may represent a secondary affect due an inability to activate phosphate-starvation response genes.

Depletion of the spliceosome disassembly factor Prp43 renders cells extremely sensitive to both increased and decreased pH, and deletion of *HTZ1* suppresses these growth defects (Figure 5.5 A). Because Prp43 and H2A.Z have been shown to coordinate spliceosome assembly and disassembly (Neves et al. 2017), it was possible that these growth phenotypes reflect defects in pre-mRNA splicing. Indeed, an intron-containing gene encodes Pho85, a cyclin-dependent kinase that has roles regulating the phosphate homeostasis pathway (O'Neill et al. 1996). However, *PHO85* splicing outcomes are not sufficient to explain the alkaline sensitivity of $prp43^{DAmP}$ strains (Figure 5.5 C). Prp43 and H2A.Z have diverse functions and, while we cannot rule out the possibility that co-transcriptional splicing is important for growth in high pH conditions, these results suggest the alkaline stress response requires interactions beyond spliceosomal functions Prp43 and H2A.Z.

Surprisingly, cells lacking Swr1, which is required for H2A.Z insertion into the chromatin, are not sensitive to increased pH and show no change in phosphate-starvation response gene expression (Figure 5.6). This is consistent with previous reports that deletion of *HTZ1*, but not *SWR1*, negatively impacts *PHO5* expression (Barbaric et al. 2007). Interestingly, deletion of *SWR1* suppresses alkaline sensitivity of and restores *PHO5* expression in cells lacking H2A.Z (Figure 5.6). We, and others, have shown that H2A.Z is important for efficient transcription elongation as well as appropriate serine 2 phosphorylation of the RNAPII C-terminal domain (Santisteban et al. 2011; Rudnizky et al. 2016; Neves et al. 2017). Here we find

that not only serine 2, but also threonine 4, is hyperphosphorylated upon H2A.Z loss (Figure 5.7). Intriguingly, a recent study showed Thr4-P is coordinated with H2A.Z and is required for repression of phosphate-regulated genes (Rosonina et al. 2014), suggesting that hyperphosphorylation of threonine 4 in the absence H2A.Z could decrease *PHO5* expression. Consistent with genetic and *PHO5* expression analysis, deletion of *SWR1* restores total, as well as *PHO5* gene body specific, threonine 4 phosphorylation to at, or even below, wild-type levels in *htz1*Δ cells (Figure 5.7). While questions remain as to how Swr1 impedes appropriate gene expression, RNAPII hyperphosphorylation in the absence of H2A.Z suggests that continued Swr1 activity interferes with transcription elongation machinery.

How does Swr1 affect stress response in the absence of H2A.Z?

To characterize the roles of Swr1 and H2A.Z in adaptation to changing environments it will be important to establish their influence on stress response pathways. Because the alkaline stress response requires activation of numerous coordinate gene expression pathways, to determine the affect of Swr1 on phosphate homeostasis in the absence of H2A.Z, it will be necessary to assay the growth of *htz1*Δ cells with and without Swr1 in low phosphate conditions. Cells lacking H2A.Z have been shown to grow poorly when phosphate is limiting (Rosonina et al. 2014), and if Swr1 activity activation of the phosphate-starvation response, deletion of *SWR1* is expected to restore viability of *htz1*Δ cells. While we have shown that loss of H2A.Z leads to *PHO5* down-regulation in phosphate-replete media (Figure 5.6), it will be important to verify that *HTZ1* deletion compromises *PHO5* induction (Rosonina et al. 2014) and to determine whether deletion of *SWR1* can restore appropriate activation of *PHO5* when phosphate is low. Additionally, RNA-sequencing followed by differential expression analysis of *htz1*Δ cells with

and without *SWR1* in high and low phosphate conditions will allow us to expand our analysis to all phosphate-regulated genes.

Viability and colony color analyses of *swr1*Δ cells (with and without H2A.Z) in copper-containing media, followed by the RNA-seq analyses describe above, can help elucidate the role of Swr1 in copper uptake and utilization pathways. If, similar to cells lacking H2A.Z, *swr1*Δ and *swr1*Δ *htz1*Δ cells fail to change color in the presence of copper and up-regulate copper/iron genes, effects of Swr1 on these gene expression pathways are likely due to a loss of H2A.Z exchange. However, increased copper/iron uptake gene expression in *htz1*Δ cells may be due to persistent Swr1 activity or, because heavy metal ion and phosphate uptake gene expression are well coordinated (Perea-Garcia et al. 2013), may be a secondary to an impaired phosphate-starvation response. In both cases, *swr1*Δ cells are expected to resemble wild-type, but, if up-regulation is a secondary effect, ectopic expression of phosphate-regulated genes in *htz1*Δ cells should restore appropriate copper/iron uptake gene expression levels.

The RNA-seq analysis described above will not only elucidate the affects of Swr1 and H2A.Z on phosphate-starvation and copper/iron-uptake expression, but can also reveal changes in other stress pathways and determine if the role of H2A.Z in splicing is important for stress response. In yeast, genes involved in the secretory pathway, which is critical for the unfolded protein response (UPR) (Tsvetanova 2013), make up the second largest class of intron-containing genes (Spingola et al. 1999). Decreased splicing of secretory genes may impair the UPR pathway when H2A.Z is lost. Splicing analysis in *swr1*Δ *htz1*Δ double mutants will also reveal if persistent Swr1 activity also impedes splicing in the absence of H2A.Z. Our past analysis has shown that, although there is considerable overlap between the splicing efficiency, a number of genes display better splicing in *swr1*Δ cells as compared to *htz1*Δ cells (Neves et al.

2017). It is possible that, while the effect of Swr1 on splicing is largely due to the subsequent lack of H2A.Z in the chromatin, persistent Swr1 activity may exacerbate splicing defects.

How does Swr1 impede stress response gene expression in the absence of H2A.Z?

In order to determine if Swr1 directly affects transcription of phosphate-starvation genes it will first be important to demonstrate that Swr1 is recruited to the chromatin in the absence of H2A.Z. Indeed, previous reports have shown that Swr1 can be found on the chromatin in *htz1*Δ cells (Morillo-Huesca et al. 2010; Ranjan et al. 2013), however, genome-wide chromatin immunoprecipitation analyses will verify that Swr1 is recruited to the *PHO5* and other phosphate-starvation gene loci in the absence of H2A.Z in both phosphate replete and limiting conditions. If Swr1 does impede transcription machinery, we expect to find greater or more wide-spread Swr1 enrichment at affected genes when H2A.Z is lost.

We suspect that, when H2A.Z is not present to be inserted in to the chromatin, persistent Swr1 activity impairs phosphate-starvation gene expression by impairing efficient transcription elongation and promoting hyperphosphorylation of RNAPII CTD serine 2 and threonine 4. We show that deletion of *SWR1* reverses threonine hyperphosphorylation across the *PHO5* gene body in *htz1*Δ cells, but it will be useful to elucidate phosphorylation patterns across other affected phosphate-sensitive genes (such as those described in Figure 5.6 B). Additionally, it will be necessary to determine Thr4-P levels across phosphate-sensitive genes in *htz1*Δ cells with and without Swr1 in low phosphate growth conditions.

Although the mechanism by which Swr1 impedes the transcription machinery is unclear, it is possible that Swr1 interacts with and recruits kinases that could drive hyperphosphorylation of the CTD. In yeast, two kinases, Bur1 and Ctk1, are responsible for serine 2 phosphorylation

(Reviewed in Heidemann et al. 2013). Interestingly, the gene encoding Ctk1 negatively interacts with *HTZ1* but positively interacts with *SWR1* (Zheng et al. 2010), suggesting that Swr1 may functionally oppose the roles of Ctk1 and H2A.Z. Although no threonine 4 kinase has been identified in yeast, polo-like kinases Plk1 and Plk3 have been demonstrated to phosphorylate threonine 4 in humans (Hintermair et al. 2012; Hintermair et al. 2016). Intriguingly, Cdc5, the only known polo-like kinase in yeast, can be complemented by human Plk1 or Plk3 (Lee and Erikson 1997; Archambault and Glover 2008) and physically interacts with the SWR-C subunit Swc5 (Ptacek et al. 2005). Therefore, further characterization of physical interactions between the SWR-C machinery and CTD kinases can indicate how Swr1 drives hyperphosphorylation in the absence of H2A.Z. Additionally, identification of mutations that disrupt such physical interactions and restore appropriate elongation could help verify that recruitment of kinases to the transcription machinery by persistent Swr1 occupancy drives gene expression defects in the absence of H2A.Z.

Here we show that defects in cells lacking H2A.Z are likely not only be due to loss of the histone itself, but may caused by deleterious consequences of an incomplete SWR-C complex. Therefore, this work highlights the importance of tight regulation of chromatin remodeling complexes and indicates that phenotypes that arise as a result of chromatin mutations must be evaluated from multiple perspectives.

MATERIALS AND METHODS

Yeast strains, media, and plasmids: All *S. cerevisiae* strains used in this study are listed in Table 5.1. Strains described in Table 5.1 are in the BY4743 strain background with the exception *cup1*Δ, provided by Christine Guthrie. All strains were propagated according to standard procedures in either YPD (1% yeast extract, 2% peptone, 2% dextrose) or appropriate selective media. Deletion of *HTZ1* in *cup1*Δ strains was as described in (Neves et al. 2017).

TABLE 5.1: Yeast strains used in this chapter

Name	Parent	Relevant Phenotype	Reference
TJY1977	BY 4743	leu2Δ0 ura3Δ0	Open Biosystems
TJY1900	BY 4743	htz1Δ::kanMX4	Open Biosystems
TJY7101	BY 4743	leu2Δ0 ura3Δ0 kanMX4	This study
TJY6906	BY 4741	htz1Δ::natMX4	This study
TJY6907	BY 4742	htz1Δ::natMX4	This study
TJY3983	YTV311	cup1Δ::URA3-52	Christine Guthrie
TJY6824	YTV311	cup1Δ::URA3-52 htz1Δ::kanMX4	This study
TJY7100	BY 4741	prp43DAmP::kanMX4	Open Biosystems
TJY7101	BY 4743	prp43DAmP::kanMX4 htz1Δ::natMX4	This study
TJY5852	BY 4341	swr1Δ::kanMX4	Open Biosystems
TJY7080	BY 4743	swr1Δ::kanMX4 htz1Δ::natMX4	This study

RNA-sequencing and differential expression analysis: RNA-seq libraries WT, *htz1*Δ, *swr1*Δ, and *swr1*Δ*htz1*Δ strains were constructed in (Neves et al. 2017). Library preparation and STAR sequence alignment were performed as described in (Neves et al. 2017). Read counts obtained from the alignment were utilized to identify differentially expressed transcripts and calculate the fold change in expression using the DESeq2 package (reference). For Figure 5.6, RPKM values from above data sets were obtained from (Neves et al. 2017).

ChIP-seq analysis: ChIP-seq reads were obtained from Gu et al. and converted to FastQ format using the NCBI SRA Toolkit (Gu et al. 2015). Sequence alignment, normalization, and BigWig file generation was performed as described in (Neves et al. 2017). After normalizing input and

immunoprecipitation pileup tracks for differential read count, a ratio track was created by dividing the normalized immunoprecipitation track by the normalized input track.

Metagenes and heatmaps were plotted using the R package 'seqPlots' (Stempor 2014). Heatmaps were plotted of fixed distances upstream and downstream of the translation start site, and clustered via k-means (n = 5) separately for genes up-regulated or down-regulated in *htz1*Δ cells. Metagenes were plotted of fixed distances upstream and downstream of the translation start site and scaled 1:1.

Viability assay/dilution series: For copper sensitivity growth analysis of *htz1*Δ strains, strains were grown overnight in CSM (+2% glucose) liquid media at 30°C. Cells were diluted to an OD_{600} of .1 in 5 ml of CSM (+2% glucose) media and incubated at 30°C until all strains reached early-log phase. A ten-fold serial dilution of each strain was spotted on to CSM +2% glucose or +3% glycerol plates with indicated $CuSO_4$ concentrations and incubated 30°C for 2 to 3 days.

For pH sensitivity growth analysis of *htz1*Δ, *prp43*^{DAmP}, and *swr1*Δ strains, strains were grown overnight in YPD+G418 liquid media at 30°C. Cells were diluted to an OD_{600} of .1 in 5 ml of YPD+G418 and incubated at 30°C until all strains reached early-log phase. A ten-fold serial dilution of each strain was spotted on to YPD+G418 with indicated pH. and incubated for 2 days at 30°C unless otherwise noted. YPD pH was adjusted with NaOH or HCl prior to sterilization.

RT-PCR splicing analysis, RT-qPCR analysis and quantification: Cells were grown in YPD+G418 media to an OD_{600} between 0.4 and 0.7. Total RNA was isolated from 10 ml of cells using a hot-phenol extraction method and dissolved in 100 µl of diethylpyrocarbonate (DEPC)-treated water. 10-20 ug of RNA was DNAse treated (Roche) and treated RNA concentration was

measured by spectrophotometer. 2-4 ug of RNA was used to make cDNA using the Maxima^{TM} First Strand cDNA Synthesis Kit (Fermentas). cDNA was diluted 1:20 and used for PCR.

To detect splicing isoforms of *PHO85*, primers flanking the intronic sequences were used for 27-cycle PCR using 1ul of diluted cDNA. PCR products were diluted 1:5 and run on a 6% TBE polyacrylamide gel. Gels were stained with SYBR green (Sigma) and image was captured using Image Lab (Bio-Rad). Bands were quantified as percent total of band intensity using Image Lab software.

For quantification of *PHO5* abundance, qRT-PCR was done in a 10 µl reaction volume with gene specific primers using 1 µl of diluted cDNA using Perfecta Sybr Green Fastmix (Quanta Biosciences) and a CFX96 Touch System (BioRad). All samples were analyzed in triplicate for each independent experiment. qRT-PCR was also performed for the *scR1* RNA from each cDNA sample. Gene expression analysis was done by 2-ΔCt methods using *scR1* cytoplasmic RNA as reference. Fold-expression of mRNA was measured compared to WT by 2-ΔΔCt methods (Livak and Schmittgen 2001).

All samples were analyzed in triplicate for each independent experiment. Primers for each gene assayed are listed in Table 5.2. For Figures 5.5 and 5.6, primers PHO5 653 F and PHO5 799 R were used for *PHO5* abundance.

Whole cell extract and immunoblot: Cells were grown in YPD+G418 media to an OD_{600} between 0.3-0.5 and lysed using FA-1 Lysis buffer (50mM HEPES-KOH pH 7.5, 140 mM NaCl, 1 mM EDTA pH 8.0, 1% Triton-X, .1% Deoxycholate, plus protease inhibitors) and .3 mm glass beads with 5 minutes of vortexing at 4°C. The supernatant was cleared by centrifugation and total protein was resolved by a 6% - 12% SDS-PAGE and transferred to a PVDF membrane for immunoblotting with 1:500 dilution anti-phospho S2 (Abcam), 1:2000 anti-

phospho T4 (Novus), 1:4000 anti-Rpb3 (BioLegend) and 1:4000 dilution of anti-PGK (Molecular Probes). Signal was detected using ProSignal Dura ECL (Genesee Scientific). Bands were quantified as percent total of band intensity using Image Lab software and normalized to wild-type values.

Chromatin immunoprecipitation (ChIP) and qPCR: Cells were grown in YPD to an OD_{600} between 0.5-0.7 and then crosslinked at room temperature for 15 minutes with formaldehyde to a final concentration of 1%. Crosslinking was quenched at room temperature for 5 minutes with glycine to a final concentration of 125mM. Cells were disrupted with glass beads (0.5mm) for 40 minutes at 4°C in lysis buffer containing phosphatase inhibitor (Sigma cocktails 2 and 3). Lysates were sonicated for a total of 2:30 minutes at 15% intensity (10 seconds on, 15 seconds off and on ice). After sonication, lysates were cleared by centrifugation. For Rpb3, samples were then used for immunoprecipitation with anti-RPB3 (BioLegend). For threonine 4-phosphorylation, samples were used for immunoprecipitation with anti-p Thr4 (Novus). After immunoprecipitation, samples were washed and incubated overnight at 65°C to reverse crosslinking. All samples were incubated with Proteinase K (Sigma) and RNAse A (Ambion), followed by purification using a PCR product purification kit (Qiagen).

DNA samples were then analyzed by real-time PCR. Input DNA was diluted 1:10 and 1 µl of this was used in a 10 ul reaction volume. For ChIP DNA, samples were diluted 1:2 and 1 µl of this was used in a 20 µl or 10ul reaction volume. Reactions consisted of 1x Perfecta SYBR GREEN Master Mix (Quanta Biosciences) and .5 µl primers. Real-time PCR was performed using a CFX96 Touch System (BioRad). All samples were run in technical duplicate for each independent experiment. Primers used are as described in Table 5.2 or (Neves et al. 2017).

For quantification, standard curves were generated for each primer set, and DNA concentration for each INPUT and ChIP sample was calculated. ChIP values were divided by the INPUT, and these values were divided by the non-transcribed control and expressed as fold accumulation over the non-transcribed control. Reported values are averages of three or more independent experiments and error bars represent the standard error of the mean.

TABLE 5.2: PCR primers

PHO85 F	GATCTCACGGATGGCCGTAGA
PHO85 R	GGGCAAACTTGAGCAATACCAATG
PHO5 2 F	GTTTAAATCTGTTGTTTATTCA
PHO5 95 R	CCAATCTTGTCGACATCGGCTA
PHO5 131 F	CGGACCATACTACTCTTTCCCT
PHO5 253 R	CCAGACTGACAGTAGGGTATCT
PHO5 653 F	GGACTACGATGCCAATGATG
PHO5 799 R	CTTCAAATGCACACCACGAG
PHO5 1037 F	CACCGCTGGTATAATTGACG
PHO5 1116 R	GGATCTGTGGAAAGTGTTGC
sCR1 F	TTTCTGGTGGGATGGGATAC
sCR1 R	TTTACGACGGAGGAAAGACG

ACKNOWLEDGEMENTS

RNA-seq alignment and RPKM calculations were carried out by Dr. Stephen Douglass. DESeq2 ChIP-seq analyses were carried out in conjunction with Dr. Srivats Venkataramanan. Thank you for your time and expertise.

Figure 5.1

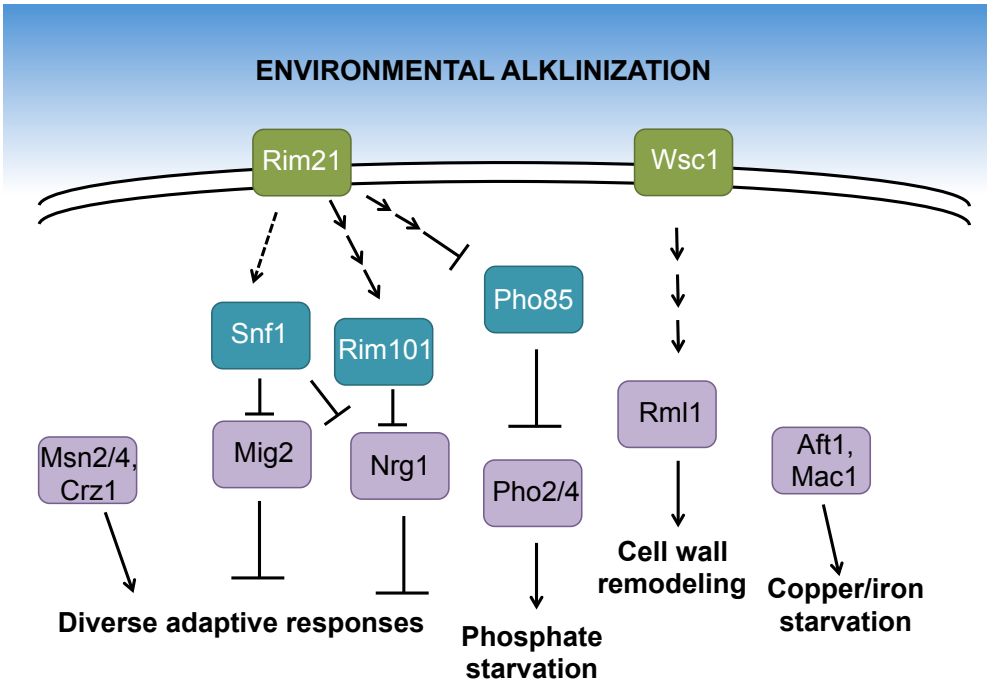

Figure 5.1 Known signaling pathways in alkaline pH response

Non-exhaustive representation of signaling pathways involved in alkaline pH response. Dashed lines represent uncharacterized links. Figure adapted from (Serra-Cardona et al. 2015).

Figure 5.2

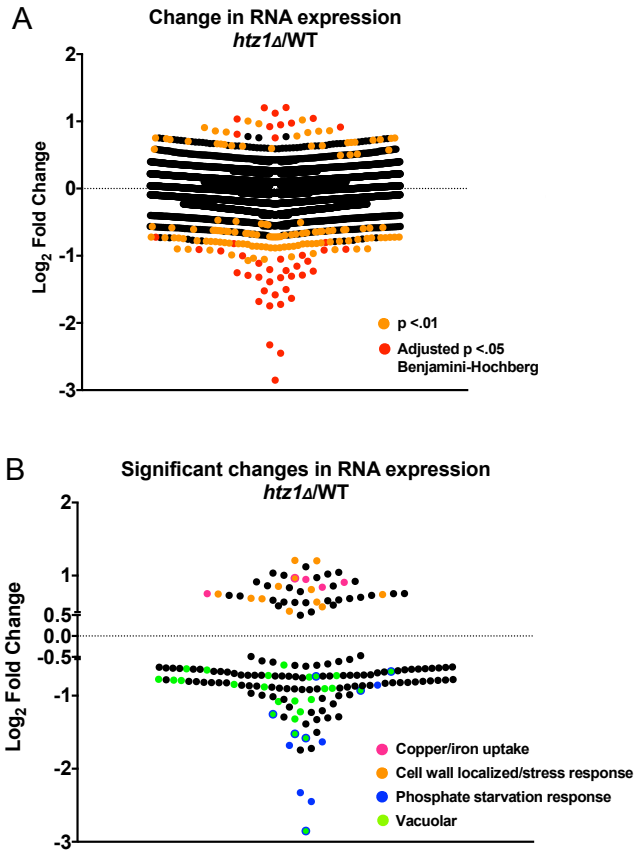

Figure 5.2 Expression of stress response genes is altered in cells lacking H2A.Z

A. Distribution of differential expression values for all genes in *htz1*Δ versus wild-type (WT) cells. Log_2 Fold Change values calculated by DESeq2 and significant values are denoted in red or orange. Significant differential expression was determined by an adjusted p-value <.05 (Benjamini-Hochberg for multi-testing) or a p-value <.01 (unadjusted).

B. Distribution of significant differential expression values (red and orange values from A). Log_2 Fold Change values >0: increased expression in *htz1*Δ (n = 45). Log_2 Fold Change values <0: decreased expression in *htz1*Δ (n = 128). Gene classes are denoted: copper and iron uptake genes in pink, cell wall genes in orange, phosphate starvation genes in blue, vacuolar genes in green.

Figure 5.3

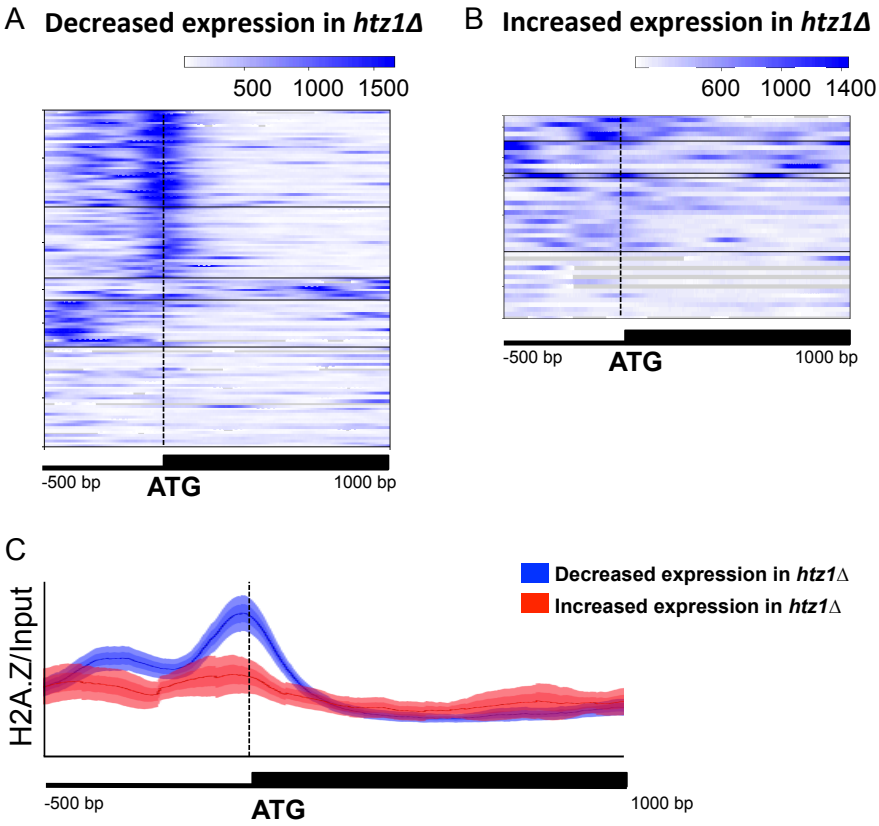

Figure 5.3 H2A.Z is normally enriched in genes down-regulated in *htz1*Δ cells

A. K-means clustering (n = 5) of H2A.Z ChIP-seq occupancy over input profile of 500 nucleotides upstream and 1000 nucleotides downstream of the translation start site (ATG) of genes significantly down-regulated in *htz1*Δ (n = 128). Vertical line indicates the ATG.

B. H2A.Z ChIP-seq occupancy profile, as in Figure 5.3 A (K-means n = 5), of genes significantly up-regulated in *htz1*Δ (n = 45). Vertical line indicates the ATG.

C. Comparison of Metagene analysis of H2A.Z ChIP-seq occupancy over input profile for genes down-regulated (in blue) versus up-regulated (in red) in *htz1*Δ cells. Lines represent the average fold enrichment of two biological replicates and 95% CI. Y-axis represents 0-1000 mapped ChIP reads normalized to input.

Analysis of data by Gu et al., 2015 and includes average two biological replicates.

Figure 5.4

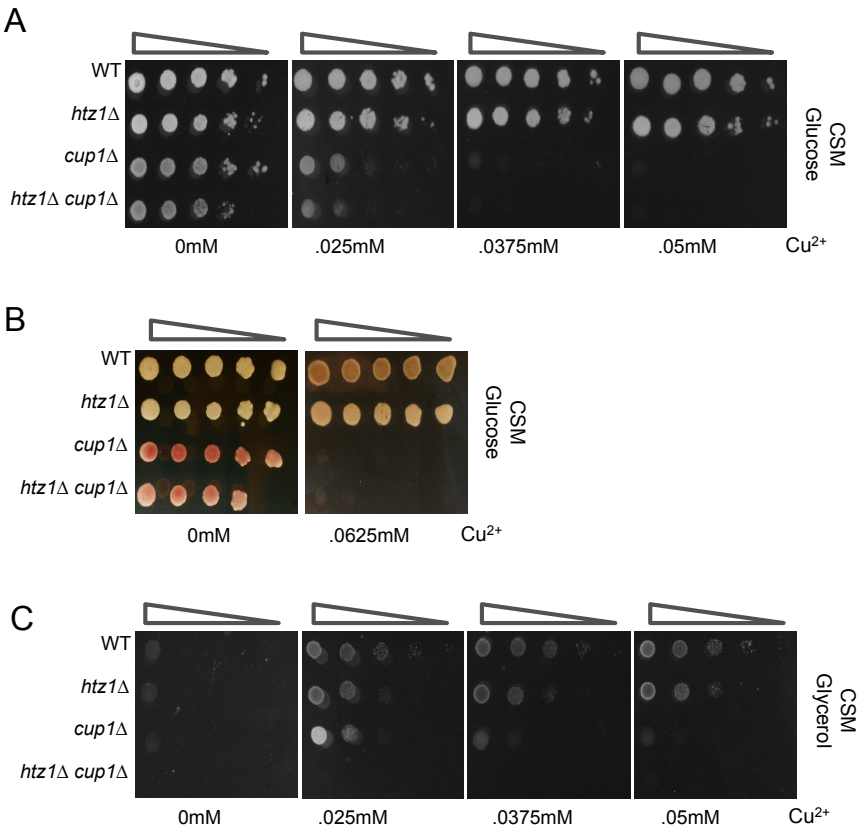

Figure 5.4 H2A.Z alters copper uptake and/or utilization

C. Serial dilution assay of *htz1*Δ and *cup1*Δ *htz1*Δ mutants. Cells were grown at 30°C in CSM liquid media until desired OD600 was obtained. Cells were spotted as a ten-fold dilution onto CSM + 2% glucose plates containing increasing concentrations of $CuSO_4$ and incubated at 30°C for two days.

D. Color image of serial dilution assay of *htz1*Δ and *cup1*Δ *htz1*Δ mutants grown in the presence of absence of copper. Cells were grown at 30°C in CSM liquid media until desired OD600 was obtained. Cells were spotted as a ten-fold dilution onto CSM + 2% glucose plates with or without $CuSO_4$ and incubated at 30°C for two (0mM) or four (.0675mM) days.

E. Serial dilution assay of *htz1*Δ and *cup1*Δ *htz1*Δ mutants in respiratory conditions. Cells were grown at 30°C in CSM liquid media until desired OD600 was obtained. Cells were spotted as a ten-fold dilution onto CSM + 3% glycerol plates containing increasing concentrations of $CuSO_4$ and incubated at 30°C for four days.

Figure 5.5

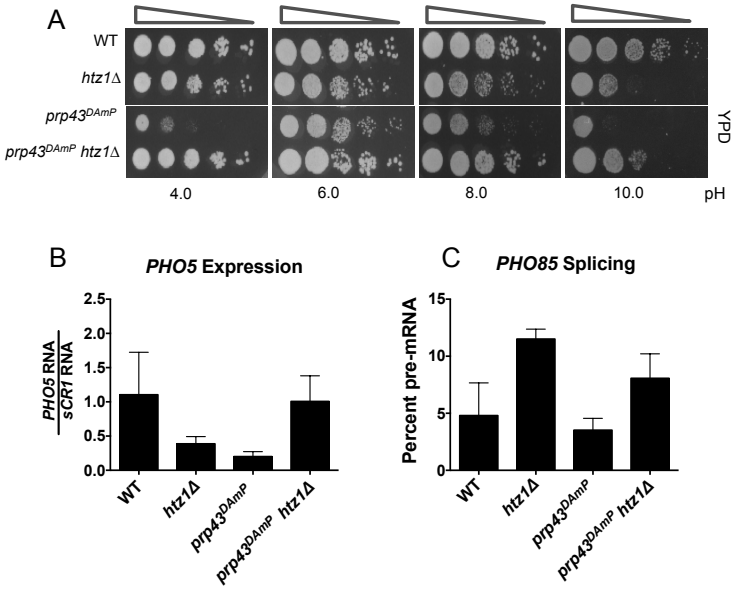

Figure 5.5 H2A.Z and Prp43 interactions affect alkaline stress resistance

A. Serial dilution assay of *prp43*^{DAmP} *htz1*Δ mutants. Cells were grown at 30°C in YPD+G418 liquid media until desired OD600 was obtained. Cells were spotted as a ten-fold dilution onto YPD+G418 plates of increasing pH values and incubated at 30°C for two or six (for pH 10) days.

B. RT-qPCR analysis of levels of *PHO5* RNA in WT or *prp43*^{DAmP} cells ± *HTZ1*, normalized to *sCR1*, an RNAPIII transcript. Graphs represent average of three independent experiments and error bars represent the SD.

C. Quantification of unspliced (pre-mRNA) products of *PHO85* in WT or *prp43*^{DAmP} cells ± *HTZ1* as determined by splicing analysis RT-PCR. Products were analyzed on 6% PAGE gels and pre-mRNA size was determined by genomic DNA size.

Figure 5.6

A

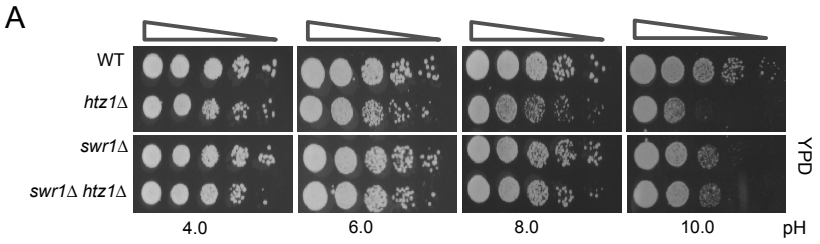

B

	Average RPKM		
	WT (n=3)	*htz1Δ* (n=2)	*swr1Δ* (n=1)
PHO11	64.83	5.36	71.23
PHO12	72.25	6.71	90.70
PHO5	76.37	17.56	87.08
PHO84	678.96	33.85	1063.80
PHO89	20.84	0.57	21.76
SPL2	54.43	2.75	91.04
VTC1	481.63	213.12	647.79
VTC2	116.87	56.70	115.85
VTC3	190.04	32.88	219.48
VTC4	225.06	64.46	253.13

	Fold change	
	htz1Δ/WT	*swr1Δ*/WT
PHO11	-3.60	0.14
PHO12	-3.43	0.33
PHO5	-2.12	0.19
PHO84	-4.33	0.65
PHO89	-5.20	0.06
SPL2	-4.31	0.74
VTC1	-1.18	0.43
VTC2	-1.04	-0.01
VTC3	-2.53	0.21
VTC4	-1.80	0.17

C

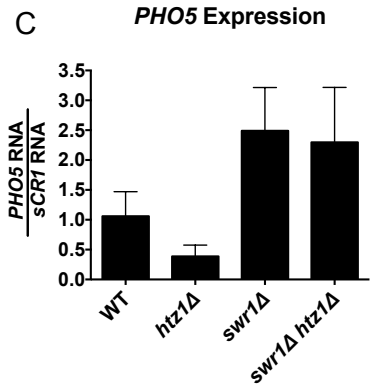

Figure 5.6 Swr1 impedes alkaline stress resistance and phosphate starvation response genes in the absence of H2A.Z

A. Serial dilution assay of *swr1*Δ *htz1*Δ mutants. Cells were grown at 30°C in YPD+G418 liquid media until desired OD600 was obtained. Cells were spotted as a ten-fold dilution onto YPD+G418 plates of increasing pH values and incubated at 30°C for two or six (for pH 10) days. Dilution series performed in parallel to Figure 5.5 A and WT and *htz1*Δ dilution series is reprinted for comparison.

B. Top: List of average RPKM values for phosphate starvation response genes in WT, *htz1*Δ, and *swr1*Δ cells. Bottom: Log^2 (fold change of RPKM) values for *htz1*Δ or *swr1*Δ versus WT cells.

C. RT-qPCR analysis of levels of *PHO5* RNA in WT or *swr1*Δ cells ± *HTZ1*, normalized to *sCR1*, an RNAPIII transcript. Graphs represent average of three independent experiments and error bars represent the SD.

Figure 5.7

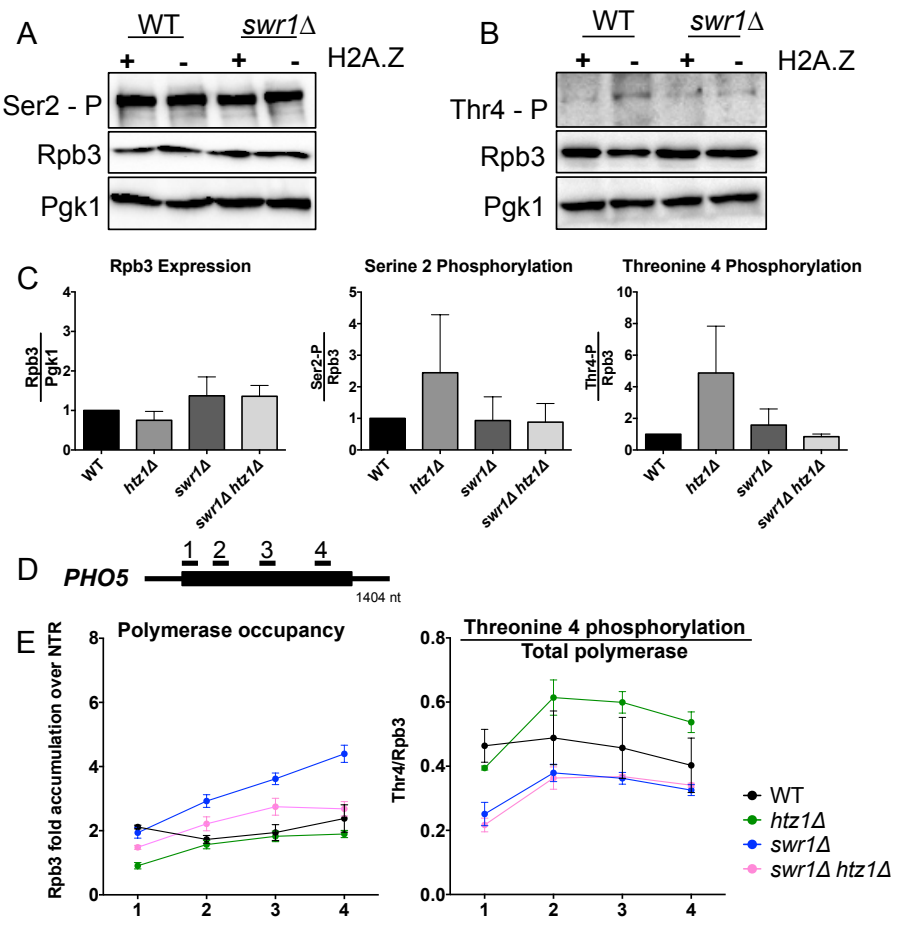

Figure 5.7 Deletion of *SWR1* restores appropriate RNAPII phosphorylation that occurs in the absence of H2A.Z

A. Protein immunoblot of RNAPII C-terminal domain phosphorylated at serine 2 (Ser2) compared to RNAPII core component Rpb3. WT and *swr1*Δ ± *HTZ1* cultures were grown in YPD+G418 liquid media and whole cell extracts were prepared and probed with anti-phospho S2 (Abcam), anti-Rpb3 (BioLegend), and anti-PGK1 as a loading control (Molecular Probes).

B. Protein immunoblot of RNAPII C-terminal domain phosphorylated at threonine 4 (Thr4) compared to RNAPII core component Rpb3, as in Figure 5.7 A. Whole cell extracts were probed with anti-phospho T4 (Novus), anti-Rpb3, and anti-PGK1.

C. Quantification of Figure 5.7 A immunoblot. Left: Quantification of Rpb3 relative to WT and normalized to loading control Pgk1. Middle: Quantification of Ser2-P relative to Rpb3. Right: Quantification of Thr4-P relative to Rpb3. Graphs represent the average of two (Ser2-P) to three (Rpb3 and Thr4-P) independent experiments and error bars represent the standard deviation.

D. Schematic of *PHO5* gene and qPCR amplicons.

E. Left: Occupancy of Rpb3 at each region of *PHO5* relative to the non-transcribed region in WT, *htz1*Δ*, swr1*Δ*,* or *swr1*Δ *htz1*Δ. Right: Threonine 4 phosphorylation state of RNAPII C-terminal domain relative to the non-transcribed region and then normalized to Rpb3 occupancy at each region of *PHO5* in WT, *htz1*Δ*, swr1*Δ*,* or *swr1*Δ *htz1*Δ. Graphs represent the average of three independent experiments and error bars represent the SEM.

REFERENCES

Alexander RD, Innocente SA, Barrass JD, Beggs JD. 2010. Splicing-Dependent RNA Polymerase Pausing in Yeast. *Molecular Cell* **40**: 582-593.

Archambault V, Glover DM. 2008. Yeast Polo-like kinase substrates are nailed with the right tools. *Genome Biol* **9**: 203.

Arino J. 2010. Integrative responses to high pH stress in S. cerevisiae. *OMICS* **14**: 517-523.

Arredondo M, Nunez MT. 2005. Iron and copper metabolism. *Mol Aspects Med* **26**: 313-327.

Auesukaree C, Homma T, Tochio H, Shirakawa M, Kaneko Y, Harashima S. 2004. Intracellular phosphate serves as a signal for the regulation of the PHO pathway in Saccharomyces cerevisiae. *J Biol Chem* **279**: 17289-17294.

Barbaric S, Luckenbach T, Schmid A, Blaschke D, Horz W, Korber P. 2007. Redundancy of chromatin remodeling pathways for the induction of the yeast PHO5 promoter in vivo. *J Biol Chem* **282**: 27610-27621.

Boden SA, Kavanova M, Finnegan EJ, Wigge PA. 2013. Thermal stress effects on grain yield in Brachypodium distachyon occur via H2A.Z-nucleosomes. *Genome Biol* **14**: R65.

Boorsma A, de Nobel H, ter Riet B, Bargmann B, Brul S, Hellingwerf KJ, Klis FM. 2004. Characterization of the transcriptional response to cell wall stress in Saccharomyces cerevisiae. *Yeast* **21**: 413-427.

Buschbeck M, Hake SB. 2017. Variants of core histones and their roles in cell fate decisions, development and cancer. *Nat Rev Mol Cell Biol* **18**: 299-314.

Casado C, Gonzalez A, Platara M, Ruiz A, Arino J. 2011. The role of the protein kinase A pathway in the response to alkaline pH stress in yeast. *Biochem J* **438**: 523-533.

Casamayor A, Serrano R, Platara M, Casado C, Ruiz A, Arino J. 2012. The role of the Snf1 kinase in the adaptive response of Saccharomyces cerevisiae to alkaline pH stress. *Biochem J* **444**: 39-49.

Causton HC, Ren B, Koh SS, Harbison CT, Kanin E, Jennings EG, Lee TI, True HL, Lander ES, Young RA. 2001. Remodeling of yeast genome expression in response to environmental changes. *Mol Biol Cell* **12**: 323-337.

Coleman-Derr D, Zilberman D. 2012. Deposition of histone variant H2A.Z within gene bodies regulates responsive genes. *PLoS Genet* **8**: e1002988.

Collins SR, Miller KM, Maas NL, Roguev A, Fillingham J, Chu CS, Schuldiner M, Gebbia M, Recht J, Shales M et al. 2007. Functional dissection of protein complexes involved in yeast chromosome biology using a genetic interaction map. *Nature* **446**: 806-810.

De Freitas J, Wintz H, Kim JH, Poynton H, Fox T, Vulpe C. 2003. Yeast, a model organism for iron and copper metabolism studies. *Biometals* **16**: 185-197.

Desfougeres Y, Gerasimaite RU, Jessen HJ, Mayer A. 2016. Vtc5, a Novel Subunit of the Vacuolar Transporter Chaperone Complex, Regulates Polyphosphate Synthesis and Phosphate Homeostasis in Yeast. *J Biol Chem* **291**: 22262-22275.

Domaschenz R, Kurscheid S, Nekrasov M, Han S, Tremethick DJ. 2017. The Histone Variant H2A.Z Is a Master Regulator of the Epithelial-Mesenchymal Transition. *Cell Rep* **21**: 943-952.

Fay JC, McCullough HL, Sniegowski PD, Eisen MB. 2004. Population genetic variation in gene expression is associated with phenotypic variation in Saccharomyces cerevisiae. *Genome Biol* **5**: R26.

Fogel S, Welch JW. 1982. Tandem gene amplification mediates copper resistance in yeast. *Proceedings of the National Academy of Sciences of the United States of America* **79**: 5342-5346.

Fogel S, Welch JW, Maloney DH. 1988. The molecular genetics of copper resistance in Saccharomyces cerevisiae--a paradigm for non-conventional yeasts. *J Basic Microbiol* **28**: 147-160.

Gasch AP, Spellman PT, Kao CM, Carmel-Harel O, Eisen MB, Storz G, Botstein D, Brown PO. 2000. Genomic expression programs in the response of yeast cells to environmental changes. *Mol Biol Cell* **11**: 4241-4257.

Greaves IK, Rangasamy D, Ridgway P, Tremethick DJ. 2007. H2A.Z contributes to the unique 3D structure of the centromere. *Proceedings of the National Academy of Sciences of the United States of America* **104**: 525-530.

Gu M, Naiyachit Y, Wood TJ, Millar CB. 2015. H2A.Z marks antisense promoters and has positive effects on antisense transcript levels in budding yeast. *BMC Genomics* **16**: 99.

Gursoy-Yuzugullu O, House N, Price BD. 2016. Patching Broken DNA: Nucleosome Dynamics and the Repair of DNA Breaks. *J Mol Biol* **428**: 1846-1860.

Halley JE, Kaplan T, Wang AY, Kobor MS, Rine J. 2010. Roles for H2A.Z and its acetylation in GAL1 transcription and gene induction, but not GAL1-transcriptional memory. *PLoS biology* **8**: e1000401.

Heidemann M, Eick D. 2012. Tyrosine-1 and threonine-4 phosphorylation marks complete the RNA polymerase II CTD phospho-code. *RNA Biol* **9**: 1144-1146.

Heidemann M, Hintermair C, Voss K, Eick D. 2013. Dynamic phosphorylation patterns of RNA polymerase II CTD during transcription. *Biochim Biophys Acta* **1829**: 55-62.

Hintermair C, Heidemann M, Koch F, Descostes N, Gut M, Gut I, Fenouil R, Ferrier P, Flatley A, Kremmer E et al. 2012. Threonine-4 of mammalian RNA polymerase II CTD is targeted by Polo-like kinase 3 and required for transcriptional elongation. *EMBO J* **31**: 2784-2797.

Hintermair C, Voss K, Forne I, Heidemann M, Flatley A, Kremmer E, Imhof A, Eick D. 2016. Specific threonine-4 phosphorylation and function of RNA polymerase II CTD during M phase progression. *Sci Rep* **6**: 27401.

Hu Y, Shen Y, Conde ESN, Zhou DX. 2011. The role of histone methylation and H2A.Z occupancy during rapid activation of ethylene responsive genes. *PLoS One* **6**: e28224.

Kalocsay M, Hiller NJ, Jentsch S. 2009. Chromosome-wide Rad51 spreading and SUMO-H2A.Z-dependent chromosome fixation in response to a persistent DNA double-strand break. *Mol Cell* **33**: 335-343.

Kim HS, Huh J, Fay JC. 2009. Dissecting the pleiotropic consequences of a quantitative trait nucleotide. *FEMS Yeast Res* **9**: 713-722.

Kobor MS, Venkatasubrahmanyam S, Meneghini MD, Gin JW, Jennings JL, Link AJ, Madhani HD, Rine J. 2004. A protein complex containing the conserved Swi2/Snf2-related ATPase Swr1p deposits histone variant H2A.Z into euchromatin. *PLoS biology* **2**: E131.

Komarnitsky P, Cho EJ, Buratowski S. 2000. Different phosphorylated forms of RNA polymerase II and associated mRNA processing factors during transcription. *Gene Dev* **14**: 2452-2460.

Krogan NJ, Baetz K, Keogh MC, Datta N, Sawa C, Kwok TC, Thompson NJ, Davey MG, Pootoolal J, Hughes TR et al. 2004. Regulation of chromosome stability by the histone H2A variant Htz1, the Swr1 chromatin remodeling complex, and the histone acetyltransferase NuA4. *Proceedings of the National Academy of Sciences of the United States of America* **101**: 13513-13518.

Krogan NJ, Keogh MC, Datta N, Sawa C, Ryan OW, Ding H, Haw RA, Pootoolal J, Tong A, Canadien V et al. 2003. A Snf2 family ATPase complex required for recruitment of the histone H2A variant Htz1. *Mol Cell* **12**: 1565-1576.

Lamb TM, Xu W, Diamond A, Mitchell AP. 2001. Alkaline response genes of Saccharomyces cerevisiae and their relationship to the RIM101 pathway. *J Biol Chem* **276**: 1850-1856.

Lee KS, Erikson RL. 1997. Plk is a functional homolog of Saccharomyces cerevisiae Cdc5, and elevated Plk activity induces multiple septation structures. *Mol Cell Biol* **17**: 3408-3417.

Li Z, Gadue P, Chen K, Jiao Y, Tuteja G, Schug J, Li W, Kaestner KH. 2012. Foxa2 and H2A.Z mediate nucleosome depletion during embryonic stem cell differentiation. *Cell* **151**: 1608-1616.

Livak KJ, Schmittgen TD. 2001. Analysis of relative gene expression data using real-time quantitative PCR and the 2(-Delta Delta C(T)) Method. *Methods* **25**: 402-408.

Malagon F, Tong AH, Shafer BK, Strathern JN. 2004. Genetic interactions of DST1 in Saccharomyces cerevisiae suggest a role of TFIIS in the initiation-elongation transition. *Genetics* **166**: 1215-1227.

March-Diaz R, Garcia-Dominguez M, Lozano-Juste J, Leon J, Florencio FJ, Reyes JC. 2008. Histone H2A.Z and homologues of components of the SWR1 complex are required to control immunity in Arabidopsis. *Plant J* **53**: 475-487.

Marques M, Laflamme L, Gervais AL, Gaudreau L. 2010. Reconciling the positive and negative roles of histone H2A.Z in gene transcription. *Epigenetics* **5**: 267-272.

Mayfield JE, Burkholder NT, Zhang YJ. 2016. Dephosphorylating eukaryotic RNA polymerase II. *Biochim Biophys Acta* **1864**: 372-387.

Mizuguchi G, Shen X, Landry J, Wu WH, Sen S, Wu C. 2004. ATP-driven exchange of histone H2AZ variant catalyzed by SWR1 chromatin remodeling complex. *Science (New York, NY)* **303**: 343-348.

Morillo-Huesca M, Clemente-Ruiz M, Andujar E, Prado F. 2010. The SWR1 histone replacement complex causes genetic instability and genome-wide transcription misregulation in the absence of H2A.Z. *PLoS One* **5**: e12143.

Neves LT, Douglass S, Spreafico R, Venkataramanan S, Kress TL, Johnson TL. 2017. The histone variant H2A.Z promotes efficient cotranscriptional splicing in S. cerevisiae. *Genes Dev* **31**: 702-717.

Nissen KE, Homer CM, Ryan CJ, Shales M, Krogan NJ, Patrick KL, Guthrie C. 2017. The histone variant H2A.Z promotes splicing of weak introns. *Genes Dev* **31**: 688-701.

O'Neill EM, Kaffman A, Jolly ER, O'Shea EK. 1996. Regulation of PHO4 nuclear localization by the PHO80-PHO85 cyclin-CDK complex. *Science* **271**: 209-212.

Oshima Y. 1997. The phosphatase system in Saccharomyces cerevisiae. *Genes Genet Syst* **72**: 323-334.

Perea-Garcia A, Garcia-Molina A, Andres-Colas N, Vera-Sirera F, Perez-Amador MA, Puig S, Penarrubia L. 2013. Arabidopsis copper transport protein COPT2 participates in the cross talk between iron deficiency responses and low-phosphate signaling. *Plant Physiol* **162**: 180-194.

Ptacek J, Devgan G, Michaud G, Zhu H, Zhu X, Fasolo J, Guo H, Jona G, Breitkreutz A, Sopko R et al. 2005. Global analysis of protein phosphorylation in yeast. *Nature* **438**: 679-684.

Punzeler S, Link S, Wagner G, Keilhauer EC, Kronbeck N, Spitzer RM, Leidescher S, Markaki Y, Mentele E, Regnard C et al. 2017. Multivalent binding of PWWP2A to H2A.Z regulates mitosis and neural crest differentiation. *EMBO J* **36**: 2263-2279.

Raisner RM, Hartley PD, Meneghini MD, Bao MZ, Liu CL, Schreiber SL, Rando OJ, Madhani HD. 2005. Histone variant H2A.Z marks the 5' ends of both active and inactive genes in euchromatin. *Cell* **123**: 233-248.

Ranjan A, Mizuguchi G, FitzGerald PC, Wei D, Wang F, Huang Y, Luk E, Woodcock CL, Wu C. 2013. Nucleosome-free region dominates histone acetylation in targeting SWR1 to promoters for H2A.Z replacement. *Cell* **154**: 1232-1245.

Rosonina E, Yurko N, Li W, Hoque M, Tian B, Manley JL. 2014. Threonine-4 of the budding yeast RNAP II CTD couples transcription with Htz1-mediated chromatin remodeling. *Proceedings of the National Academy of Sciences of the United States of America* **111**: 11924-11931.

Rudnizky S, Bavly A, Malik O, Pnueli L, Melamed P, Kaplan A. 2016. H2A.Z controls the stability and mobility of nucleosomes to regulate expression of the LH genes. *Nat Commun* **7**: 12958.

Sadeghi L, Bonilla C, Stralfors A, Ekwall K, Svensson JP. 2011. Podbat: a novel genomic tool reveals Swr1-independent H2A.Z incorporation at gene coding sequences through epigenetic meta-analysis. *PLoS Comput Biol* **7**: e1002163.

Santisteban MS, Hang M, Smith MM. 2011. Histone variant H2A.Z and RNA polymerase II transcription elongation. *Molecular and cellular biology* **31**: 1848-1860.

Santisteban MS, Kalashnikova T, Smith MM. 2000. Histone H2A.Z regulats transcription and is partially redundant with nucleosome remodeling complexes. *Cell* **103**: 411-422.

Schlecht U, Suresh S, Xu W, Aparicio AM, Chu A, Proctor MJ, Davis RW, Scharfe C, St Onge RP. 2014. A functional screen for copper homeostasis genes identifies a pharmacologically tractable cellular system. *BMC genomics* **15**: 263.

Serra-Cardona A, Canadell D, Arino J. 2015. Coordinate responses to alkaline pH stress in budding yeast. *Microb Cell* **2**: 182-196.

Serrano R, Bernal D, Simon E, Arino J. 2004. Copper and iron are the limiting factors for growth of the yeast Saccharomyces cerevisiae in an alkaline environment. *J Biol Chem* **279**: 19698-19704.

Shirahama K, Yazaki Y, Sakano K, Wada Y, Ohsumi Y. 1996. Vacuolar function in the phosphate homeostasis of the yeast Saccharomyces cerevisiae. *Plant Cell Physiol* **37**: 1090-1093.

Sinha H, David L, Pascon RC, Clauder-Munster S, Krishnakumar S, Nguyen M, Shi G, Dean J, Davis RW, Oefner PJ et al. 2008. Sequential elimination of major-effect contributors

identifies additional quantitative trait loci conditioning high-temperature growth in yeast. *Genetics* **180**: 1661-1670.

Smith AP, Jain A, Deal RB, Nagarajan VK, Poling MD, Raghothama KG, Meagher RB. 2010. Histone H2A.Z regulates the expression of several classes of phosphate starvation response genes but not as a transcriptional activator. *Plant Physiol* **152**: 217-225.

Spingola M, Grate L, Haussler D, Ares M, Jr. 1999. Genome-wide bioinformatic and molecular analysis of introns in Saccharomyces cerevisiae. *RNA* **5**: 221-234.

Stempor P. 2014. seqplots: An interactive tool for visualizing NGS signals and sequence motif densities along genomic features using average plots and heatmaps. *R package version 1102* http://github.com/przemol/seqplots**.**

Subramanian V, Fields PA, Boyer LA. 2015. H2A.Z: a molecular rheostat for transcriptional control. *F1000Prime Rep* **7**: 01.

Sura W, Kabza M, Karlowski WM, Bieluszewski T, Kus-Slowinska M, Paweloszek L, Sadowski J, Ziolkowski PA. 2017. Dual Role of the Histone Variant H2A.Z in Transcriptional Regulation of Stress-Response Genes. *Plant Cell* **29**: 791-807.

Thomas MR, O'Shea EK. 2005. An intracellular phosphate buffer filters transient fluctuations in extracellular phosphate levels. *Proc Natl Acad Sci U S A* **102**: 9565-9570.

Tramantano M, Sun L, Au C, Labuz D, Liu Z, Chou M, Shen C, Luk E. 2016. Constitutive turnover of histone H2A.Z at yeast promoters requires the preinitiation complex. *Elife* **5**.

Tsvetanova NG. 2013. The secretory pathway in control of endoplasmic reticulum homeostasis. *Small GTPases* **4**: 28-33.

Vardi N, Levy S, Gurvich Y, Polacheck T, Carmi M, Jaitin D, Amit I, Barkai N. 2014. Sequential feedback induction stabilizes the phosphate starvation response in budding yeast. *Cell Rep* **9**: 1122-1134.

Wan Y, Saleem RA, Ratushny AV, Roda O, Smith JJ, Lin CH, Chiang JH, Aitchison JD. 2009. Role of the histone variant H2A.Z/Htz1p in TBP recruitment, chromatin dynamics, and regulated expression of oleate-responsive genes. *Molecular and cellular biology* **29**: 2346-2358.

Weber CM, Ramachandran S, Henikoff S. 2014. Nucleosomes are context-specific, H2A.Z-modulated barriers to RNA polymerase. *Mol Cell* **53**: 819-830.

Weiner A, Hsieh TH, Appleboim A, Chen HV, Rahat A, Amit I, Rando OJ, Friedman N. 2015. High-resolution chromatin dynamics during a yeast stress response. *Mol Cell* **58**: 371-386.

Zhang H, Roberts DN, Cairns BR. 2005. Genome-wide dynamics of Htz1, a histone H2A variant that poises repressed/basal promoters for activation through histone loss. *Cell* **123**: 219-231.

Zheng W, Zhao H, Mancera E, Steinmetz LM, Snyder M. 2010. Genetic analysis of variation in transcription factor binding in yeast. *Nature* **464**: 1187-1191.

Zlatanova J, Thakar A. 2008. H2A.Z: view from the top. *Structure* **16**: 166-179.

CONCLUDING REMARKS

Early studies of pre-mRNA splicing have largely been carried out *in vitro* and have been critically important in elucidating the mechanism by which the spliceosome removes introns. However, it has become abundantly clear that the process of pre-mRNA splicing does not occur in isolation and is influenced by many factors including transcription dynamics, chromatin states, and environmental cues (Reviewed in Herzel et al. 2017). Recent growth in new and powerful technologies have made it possible to study the intricate coordination and regulation of gene expression processes in far more depth than ever before.

The recent observation that splicing is often complete soon after the intron emerges from the polymerase not only indicates that the splicing cycle takes place very rapidly, but also provides more evidence of the need for tight coordination of the timing of transcription and splicing (Oesterreich et al. 2016). The kinetics of RNA polymerase II elongation are dynamic and influenced by a number of factors such as activity of elongation factors (such as Dst1) or local chromatin architecture (such as histone modifications or variants) (Reviewed in Herzel et al. 2017). Although a common model suggests that slow elongation provides a greater "window of opportunity" for splicing to occur, recent studies have shown that co-transcriptional splicing may rely on a "Goldilocks-like" relationship between elongation rate and pre-mRNA splicing (Fong et al. 2014).

While it has become a well-accepted hypothesis that the local chromatin architecture can influence splicing outcomes of a particular gene by modulating recruitment of spliceosome machinery and/or directing RNA polymerase II dynamics, the mechanisms by which the chromatin establishes such coordination remained unclear. In this dissertation, I have sought to elucidate the role of a histone variant in coordinating the timing of RNA transcription and

splicing. In Chapter 2, I have established a role for H2A.Z, a variant of the canonical H2A, in coordinating RNA polymerase II elongation dynamics with spliceosome rearrangements in order to promote splicing of weak introns (Neves et al. 2017). Splicing outcomes are not only dependent on the kinetics of spliceosome assembly but also disassembly, and the requirement for H2A.Z is decreased when disassembly machinery is less abundant (Neves et al. 2017). Interestingly, Prp43, the catalytic spliceosome disassembly factor, has roles in ribosome biogenesis as well as pre-mRNA splicing (Leeds et al. 2006), indicating that there is likely crosstalk between co-transcriptional splicing and translation.

Not only does chromatin structure and composition influence splicing locally, but there is also precedent for more global regulation of splicing mediated by the chromatin environment through competition for spliceosome machinery (Venkataramanan et al. 2017). In fact, in Chapter 3, we demonstrate that levels of the chromatin remodeling protein, Snf2, decrease as glucose is depleted in the medium (Geng and Laurent 2004; Biddick et al. 2008; Awad et al. 2017), which leads to downregulation of RPG transcript levels and spliceosome redistribution that permits the splicing of *PTC7,* a gene required for optimal mitochondrial activity during respiration (Awad et al. 2017). The two *PTC7* isoforms are conserved across fungal species indicating that alternative splicing functionally expands the yeast proteome in order to adapt to a changing environment (Marshall et al. 2013)

The local and global effects on splicing demonstrated in Chapters 2 and 3 are not necessarily mutually exclusive. In fact, in Chapter 4, I show that perturbations to transcription elongation can lead to dynamic and gene-specific changes in splicing outcomes due to the opposing effects of local changes in polymerase and spliceosome kinetics and global changes in spliceosome availability. Because splicing is facilitated by optimal polymerase elongation and

loss of the elongation factor Dst1 exacerbates growth and transcription defects of cells lacking H2A.Z, we expected to find strong splicing defects in double mutants. However, to our surprise, splicing changes are gene specific and splicing efficiency of many genes improves. Interestingly, upon further examination, we found that expression of intron-enriched ribosomal protein genes, which typically account for 90% of the spliceosomal load (Ares et al. 1999; Warner 1999), are down-regulated in double mutants. This indicates that, while local spliceosome rearrangements are likely strongly perturbed, competition for the limiting spliceosome is relieved in cells lacking both Dst1 and H2A.Z, promoting splicing of weak introns. Therefore, regulated splicing not only requires local input from transcription and chromatin but may also be influenced by environmental cues that affect global changes in protein synthesis and availability.

Because H2A.Z is at the nexus of coordinated transcription and pre-mRNA splicing, in Chapter 5 we asked what role H2A.Z plays in adapting to stress. We find that H2A.Z is necessary for appropriate copper utilization and adaptation to alkaline pH conditions, potentially due to role in promoting expression of phosphate-starvation response genes. Intriguingly, deletion of Swr1, which inserts H2A.Z in to the chromatin (Krogan et al. 2003; Mizuguchi et al. 2012), suppresses these effects and restores appropriate phosphate gene expression, suggesting that continued SWR-C activity in the absence of H2A.Z is deleterious to the cell. It will be of important to determine if H2A.Z-mediated splicing defects are also due, at least in part, to incomplete chromatin remodeling machinery. It is of interest to note that, while H2A.Z structure and localization are highly conserved (Zlatanova and Thakar 2008), the Swc2 homologue YL1, rather than Swr1, is responsible for H2A.Z deposition in metazoans(Latrick et al. 2016; Liang et al. 2016). While Swr1 is able to bind both H2A.Z and H2A-containing dimers (Hong et al. 2014), YL1 has no affinity for H2A (Latrick et al. 2016; Liang et al. 2016). It is therefore

possible that the preference for YL1 over Swr1 in H2A.Z deposition in metazoans evolved to minimize potential deleterious effects of incomplete SWR-C activity at the chromatin.

Overall, the work presented in this dissertation establishes a novel relationship between chromatin and the regulation of pre-mRNA splicing. I demonstrate that a variant histone affects the splicing of intron-containing genes by modulating the relative kinetics of RNA synthesis and processing factors. However, it is clear that this coordination does not take place in isolation but rather occurs amongst a multitude of inputs that influence global effects on splicing and begin to build an intriguing picture of nuclear environments dynamically and coordinately changing in response to cellular requirements.

REFERENCES

Ares M, Jr., Grate L, Pauling MH. 1999. A handful of intron-containing genes produces the lion's share of yeast mRNA. *RNA* **5**: 1138-1139.

Awad AM, Venkataramanan S, Nag A, Galivanche AR, Bradley MC, Neves L, Douglass S, Clarke CF, Johnson TL. 2017. Chromatin-remodeling SWI/SNF complex regulates coenzyme Q6 synthesis and a metabolic shift to respiration in yeast. *Journal of Biological Chemistry*.

Biddick RK, Law GL, Chin KK, Young ET. 2008. The transcriptional coactivators SAGA, SWI/SNF, and mediator make distinct contributions to activation of glucose-repressed genes. *J Biol Chem* **283**: 33101-33109.

Fong N, Kim H, Zhou Y, Ji X, Qiu J, Saldi T, Diener K, Jones K, Fu XD, Bentley DL. 2014. Pre-mRNA splicing is facilitated by an optimal RNA polymerase II elongation rate. *Genes Dev* **28**: 2663-2676.

Geng F, Laurent BC. 2004. Roles of SWI/SNF and HATs throughout the dynamic transcription of a yeast glucose-repressible gene. *EMBO J* **23**: 127-137.

Herzel L, Ottoz DSM, Alpert T, Neugebauer KM. 2017. Splicing and transcription touch base: co-transcriptional spliceosome assembly and function. *Nat Rev Mol Cell Biol* **18**: 637-650.

Hong J, Feng H, Wang F, Ranjan A, Chen J, Jiang J, Ghirlando R, Xiao TS, Wu C, Bai Y. 2014. The catalytic subunit of the SWR1 remodeler is a histone chaperone for the H2A.Z-H2B dimer. *Mol Cell* **53**: 498-505.

Krogan NJ, Keogh MC, Datta N, Sawa C, Ryan OW, Ding H, Haw RA, Pootoolal J, Tong A, Canadien V et al. 2003. A Snf2 family ATPase complex required for recruitment of the histone H2A variant Htz1. *Mol Cell* **12**: 1565-1576.

Latrick CM, Marek M, Ouararhni K, Papin C, Stoll I, Ignatyeva M, Obri A, Ennifar E, Dimitrov S, Romier C et al. 2016. Molecular basis and specificity of H2A.Z-H2B recognition and deposition by the histone chaperone YL1. *Nat Struct Mol Biol* **23**: 309-316.

Leeds NB, Small EC, Hiley SL, Hughes TR, Staley JP. 2006. The splicing factor Prp43p, a DEAH box ATPase, functions in ribosome biogenesis. *Mol Cell Biol* **26**: 513-522.

Liang X, Shan S, Pan L, Zhao J, Ranjan A, Wang F, Zhang Z, Huang Y, Feng H, Wei D et al. 2016. Structural basis of H2A.Z recognition by SRCAP chromatin-remodeling subunit YL1. *Nat Struct Mol Biol* **23**: 317-323.

Marshall AN, Montealegre MC, Jimenez-Lopez C, Lorenz MC, van Hoof A. 2013. Alternative splicing and subfunctionalization generates functional diversity in fungal proteomes. *PLoS Genet* **9**: e1003376.

Mizuguchi G, Wu WH, Alami S, Luk E. 2012. Biochemical assay for histone H2A.Z replacement by the yeast SWR1 chromatin remodeling complex. *Methods Enzymol* **512**: 275-291.

Neves LT, Douglass S, Spreafico R, Venkataramanan S, Kress TL, Johnson TL. 2017. The histone variant H2A.Z promotes efficient cotranscriptional splicing in S. cerevisiae. *Genes Dev* **31**: 702-717.

Oesterreich FC, Herzel L, Straube K, Hujer K, Howard J, Neugebauer KM. 2016. Splicing of Nascent RNA Coincides with Intron Exit from RNA Polymerase II. *Cell* **165**: 372-381.

Venkataramanan S, Douglass S, Galivanche AR, Johnson TL. 2017. The chromatin remodeling complex Swi/Snf regulates splicing of meiotic transcripts in Saccharomyces cerevisiae. *Nucleic Acids Res* **45**: 7708-7721.

Warner JR. 1999. The economics of ribosome biosynthesis in yeast. *Trends Biochem Sci* **24**: 437-440.

Zlatanova J, Thakar A. 2008. H2A.Z: view from the top. *Structure* **16**: 166-179.